

For Reference

NOT TO BE TAKEN FROM THIS ROOM

Ex libris
UNIVERSITATIS
ALBERTAENSIS



T H E U N I V E R S I T Y O F A L B E R T A

RELEASE FORM

NAME OF AUTHOR Dennis Lyle Oracheski
TITLE OF THESIS Influence of the Cordillera on Crossing
 Frontal Cloud Bands
DEGREE FOR WHICH THESIS WAS PRESENTED Master of Science
YEAR THIS DEGREE GRANTED 1978

Permission is hereby granted to THE UNIVERSITY OF ALBERTA LIBRARY to reproduce single copies of this thesis and to lend or sell such copies for private, scholarly, or scientific research purposes only.

The author reserves all other publication rights, and neither the thesis nor extensive extracts from it may be printed or otherwise reproduced in any manner.

THE UNIVERSITY OF ALBERTA

INFLUENCE OF THE CORDILLERA ON
CROSSING FRONTAL CLOUD BANDS

by



DENNIS LYLE ORACHESKI

A THESIS

SUBMITTED TO THE FACULTY OF GRADUATE STUDIES AND RESEARCH
IN PARTIAL FULFILMENT OF THE REQUIREMENTS FOR THE DEGREE OF
MASTER OF SCIENCE

IN

METEOROLOGY

DEPARTMENT OF GEOGRAPHY

EDMONTON, ALBERTA

SPRING, 1978

18-82

THE UNIVERSITY OF ALBERTA
FACULTY OF GRADUATE STUDIES AND RESEARCH

The undersigned certify that they have read, and recommend to the Faculty of Graduate Studies and Research, for acceptance, a thesis entitled "Influence of the Cordillera on Crossing Frontal Cloud Bands" submitted by Dennis Lyle Oracheski in partial fulfilment of the requirements for the degree of Master of Science in Meteorology.

ABSTRACT

The introductory chapters contain a review of mountain-wave theory and cloud physics. Mountain barriers affect three scales of atmospheric motion:

(a) Long-wavelength Rossby waves. In the northern hemisphere, semi-permanent troughs in the upper atmosphere occur to the lee of the major barriers, the response increasing with height. The lower troposphere reflects the seasonal thermal contrast between land and ocean. Mean cloud is determined more by the greater evaporation over the ocean.

(b) Synoptic-scale waves associated with cyclones. A maximum of cyclogenesis occurs to the lee of mountain barriers while cyclones undergo cyclolysis upwind of a barrier. Cloud is formed by the horizontal advection of air through vertical motion fields, ascent saturating the air and vice versa.

(c) Meso-scale gravity (lee or mountain) waves. The synoptic-scale cloud pattern is modified by the formation of wave clouds, lenticular clouds, and cirrus plumes and the clearing of existing cloud in the upper troposphere. The mountain waves are a function of the vertical profile of wind speed and temperature, and barrier height and width.

Surface boundary conditions produce

(a) orographic vertical motion. Ascent produces a crest cloud over the barrier while descent gives subsidence clearing and a pressure trough to the lee. The loss of moisture through precipitation over the barrier gives a rain shadow and decreased cloud to the lee.

(b) frictional vergences. The ageostrophic winds slowly alter the synoptic flow at higher levels.

Mountains also affect the stability of the troposphere. Forced ascent over a barrier may release potential instability. Convection due to solar heating is enhanced, especially to the lee of a barrier.

The last chapters illustrate the effect of mountains on cloud systems moving in from the Pacific; three cases of frontal bands crossing the Cordillera are examined in detail. Case 1 occurs during the summer season (May); cases 2 and 3 during early winter (November). Cloud patterns are analyzed using:

(a) weather satellite images from ESSA 8 and NOAA 2/3;

(b) synoptic charts at the surface, 700 mb, and 500 mb;

(c) vertical time-sections (and cloud time-sections) at stations in the Pacific Ocean, along the coast, in the interior plateau, and to the lee of the mountains.

TABLE OF CONTENTS

	Page
ABSTRACT	iv
TABLE OF CONTENTS	vi
LIST OF TABLES	ix
LIST OF FIGURES	x
LIST OF OVERLAYS	xiii
LIST OF PHOTOGRAPHIC PLATES	xv
CHAPTER	
A AIRFLOW OVER MOUNTAINS	1
A.1 Scales of Perturbation from Zonal Flow	1
A.2 Planetary Waves	1
A.3 Synoptic-scale Waves	12
A.4 Mesoscale Waves	20
A.5 Blocking	29
B CLOUDS AND VERTICAL MOTION	34
B.1 Introduction	34
B.2 Formation of Clouds	34
B.3 Precipitation	38
B.4 Dissipation of Clouds	39
B.5 Methods of Computing Omega	40
B.6 Boundary Conditions	46

CHAPTER		Page
C	OBSERVED CLOUD PATTERNS	49
C.1	Planetary Waves	49
C.2	Synoptic-scale Waves	50
C.3	Mesoscale Waves	54
C.4	Boundary Conditions	57
C.5	Convection	60
C.6	Summary	61
D	CASE STUDIES DATA	66
D.1	Case Selection	66
D.2	Storm Tracks	67
D.3	Satellite Data	69
D.4	Conventional Maps	77
D.5	Vertical Time-sections	80
E	CASE HISTORIES: CASE 1: 19-22MAY72	85
E.1	Synoptic Situation	85
E.2	19MAY72: Notes, Comments, and Observations ..	88
E.3	20MAY72: Notes, Comments, and Observations ..	93
E.4	21MAY72: Notes, Comments, and Observations ..	98
E.5	22MAY72: Notes, Comments, and Observations ..	105
F	CASE HISTORIES: CASE 2: 07-10NOV72	139
F.1	Synoptic Situation	139
F.2	07NOV72: Notes, Comments, and Observations ..	142
F.3	08NOV72: Notes, Comments, and Observations ..	147
F.4	09NOV72: Notes, Comments, and Observations ..	153
F.5	10NOV72: Notes, Comments, and Observations ..	161

CHAPTER	Page
G CASE HISTORIES: CASE 3: 19-20NOV72	186
G.1 Synoptic Situation	186
G.2 19NOV73: Notes, Comments, and Observations ..	189
G.3 20NOV73: Notes, Comments, and Observations ..	198
H SUMMARY AND CONCLUSIONS	220
REFERENCES	229
APPENDIX 1. LIST OF SYMBOLS	239
APPENDIX 2. LIST OF ABBREVIATIONS	242

LIST OF TABLES

Table		Page
A.1	Wavelength and zonal wind speed of Rossby waves at latitude 45°N for 'n' waves around the Earth.	10
D.1	Observed frontal cloud bands for 1972.	68
D.2	Schallert's classification of surface lows by trajectory and intensity.	69
D.3	Orbital parameters for weather satellites ESSA 8, NOAA 2, and NOAA 3.	72
E.1	Afternoon dew-point depressions.	113
E.2	Hours of southerly winds ahead of cold front.	113
F.1	Winds at Ship PAPA ahead and behind passage of TROWAL.	158

LIST OF FIGURES

Figure		Page
A.1	Mean monthly 500-mb heights in summer (August) and winter (February).	2
A.2	Normal pressure distribution at sea level in summer (August) and winter (February). ..	3
A.3	Constant absolute vorticity trajectories of a fluid passing over a barrier.	7
A.4	Streamlines giving total response of all resonance waves over the mountain barrier on 68-10-10-1200Z.	25
A.5	Streamlines over mountain barrier on 69-01-08-0000Z.	26
A.6	Dominant horizontal wavenumber in the tropospheric duct as a function of K_0 and α_0	27
C.1	Classification of orographic clouds.	55
E.1	Track and 1200Z position of 500-mb troughs and lows for the period 10-31MAY72.	86
E.2	Track, intensity, and 1200Z position of surface lows for the period 10-31MAY72.	87
E.3	Vertical time-section for Ocean Station (Ship) PAPA.	114
E.4	Vertical time-section for Annette Island (ANN) and cloud time-sections for Prince Rupert (PR) and Sandspit (ZP).	115
E.5	Vertical time-section for Port Hardy (ZT) and cloud time-sections for Port Hardy (ZT) and Vancouver (VR).	116
E.6	Vertical time-section for Quillayute (UIL) and cloud time-section for Estevan Point (EP).	117

Figure		Page
E.7	Vertical time-section for Prince George (XS) and cloud time-sections for Prince George (XS) and Williams Lake (WL).	118
E.8	Vertical time-section for Vernon (WVK) and cloud time-section for Penticton (YF).	119
E.9	Vertical time-section for Fort Nelson (YE) and cloud time-sections for Fort Nelson (YE) and Fort St. John (XJ).	120
E.10	Vertical time-section for Edmonton (Stony Plain) and cloud time-sections for Edmonton International (EG) and Calgary (YC).	121
F.1	Track and 1200Z position of 500-mb troughs and lows for the period 01-19NOV72.	140
F.2	Track, intensity, and 1200Z position of surface lows for the period 01-19NOV72.	141
F.3	Vertical time-section for Ocean Station (Ship) PAPA.	167
F.4	Vertical time-section for Port Hardy (ZT).	167
F.5	Vertical time-section for Prince George (XS).	168
F.6	Vertical time-section for Vernon (WVK).	168
F.7	Vertical time-section for Edmonton (Stoney Plain) and cloud time-section for Edmonton city (XD).	169
G.1	Track and 1200Z position of 500-mb troughs and lows for the period 09NOV-02DEC73.	187
G.2	Track, intensity, and 1200Z position of surface lows for the period 09NOV-02DEC73.	188
G.3	Diagrams showing the air flow over the Coast Mountains of California and the downstream change in cirrus clouds.	200

Figure		Page
G.4	Vertical time-section for Ocean Station (Ship) PAPA.	207
G.5	Vertical time-section for Port Hardy (ZT). .	207
G.6	Vertical time-section for Prince George (XS).	208
G.7	Vertical time-section for Vernon (WVK).	208
G.8	Vertical time-section for Edmonton (Stony Plain) and cloud time-sections for Edmonton International (EG) and Edmonton City (XD).	209

LIST OF OVERLAYS

Overlay		Page
1a	19MAY (72) SFC analysis.	124
1b	19MAY 700MB analysis.	123
1c	19MAY 500MB analysis.	122
2a	20MAY (72) SFC analysis.	128
2b	20MAY 700MB analysis.	127
2c	20MAY 500MB analysis.	126
3a	21MAY (72) SFC analysis.	133
3b	21MAY 700MB analysis.	132
3c	21MAY 500MB analysis.	131
3d	21MAY W600MB chart.	130
4a	22MAY (72) SFC analysis.	137
4b	22MAY 700MB analysis.	136
4c	22MAY 500MB analysis.	135
5a	07NOV (72) SFC analysis.	172
5b	07NOV 700MB analysis.	171
5c	07NOV 500MB analysis.	170
6a	08NOV (72) SFC analysis.	176
6b	08NOV 700MB analysis.	175
6c	08NOV 500MB analysis.	174
7a	09NOV (72) SFC analysis.	180
7b	09NOV 700MB analysis.	179
7c	09NOV 500MB analysis.	178
8a	10NOV (72) SFC analysis.	184

Overlay		Page
8b	10NOV 700MB analysis.	183
8c	10NOV 500MB analysis.	182
9a	19NOV(73) SFC analysis.	212
9b	19NOV 700MB analysis.	211
9c	19NOV 500MB analysis.	210
10a	20NOV(73) SFC analysis.	217
10b	20NOV 700MB analysis.	216
10c	20NOV 500MB analysis.	215

LIST OF PHOTOGRAPHIC PLATES

Plate		Page
1	19MAY72 ESSA 8 VIDICON MOSAIC orbits(frames) = 15719(2,3), 15720(2)	125
2	20MAY72 ESSA 8 VIDICON MOSAIC orbits(frames) = 15706(2,3), 15707(2,3) . . .	129
3	21MAY72 ESSA 8 VIDICON MOSAIC orbits(frames) = 15731(2,3), 15732(2,3) . . .	134
4	22MAY72 ESSA 8 VIDICON MOSAIC orbits(frames) = 15743(2,3), 15744(2,3), 15745(2)	138
5	07NOV72 ESSA 8 VIDICON MOSAIC orbits(frames) = 17865(1,2,3), 17866(1,3) . .	173
6	08NOV72 ESSA 8 VIDICON MOSAIC orbits(frames) = 17878(1,2), 17879(1,2) . . .	177
7	09NOV72 ESSA 8 VIDICON MOSAIC orbits(frames) = 17890(1,2,3), 17891(1,2), 17892(1)	181
8	10NOV72 ESSA 8 VIDICON MOSAIC orbit(frames) = 17903(1,2,3)	185
9a	19NOV73 NOAA SRIR MOSAIC infra-red channel of NOAA 2 orbits 5009, 5010.	213
9b	19NOV73 NOAA SRVIS MOSAIC visible channel.	214
10a	20NOV73 NOAA SRIR MOSAIC infra-red channel of NOAA 2 orbit 5021 (right) and NOAA 3 orbit 0741 (left).	218
10b	20NOV73 NOAA SRVIS MOSAIC visible channel.	219

CHAPTER A

AIRFLOW OVER MOUNTAINS

A.1 Scales of Perturbation from Zonal Flow

A first approximation for the air flow at mid-latitudes is a zonal current resulting from the differential heating between polar and equatorial regions and the rotation of the Earth. This flow does not provide the necessary meridional heat exchange since there is no transport of heat from equator to pole. Perturbing the zonal flow with a longitudinal component will cause sensible and latent heat to be transported poleward, tending to establish a thermally-driven, steady-state circulation. Mountains affect the airflow on all scales of motion: they profoundly influence the configuration of the long, planetary (Rossby) waves; they often strongly modify synoptic-scale waves associated with cyclones; they produce a large class of mesoscale waves such as gravity and lee waves; and ultimately, on the micro-scale, mountains act on the airflow through friction.

A.2 Planetary Waves

From mean upper-air charts (refer to Figure A.1), trough positions are found to be unaffected by the seasonal change of winter to summer. This is in marked contrast to

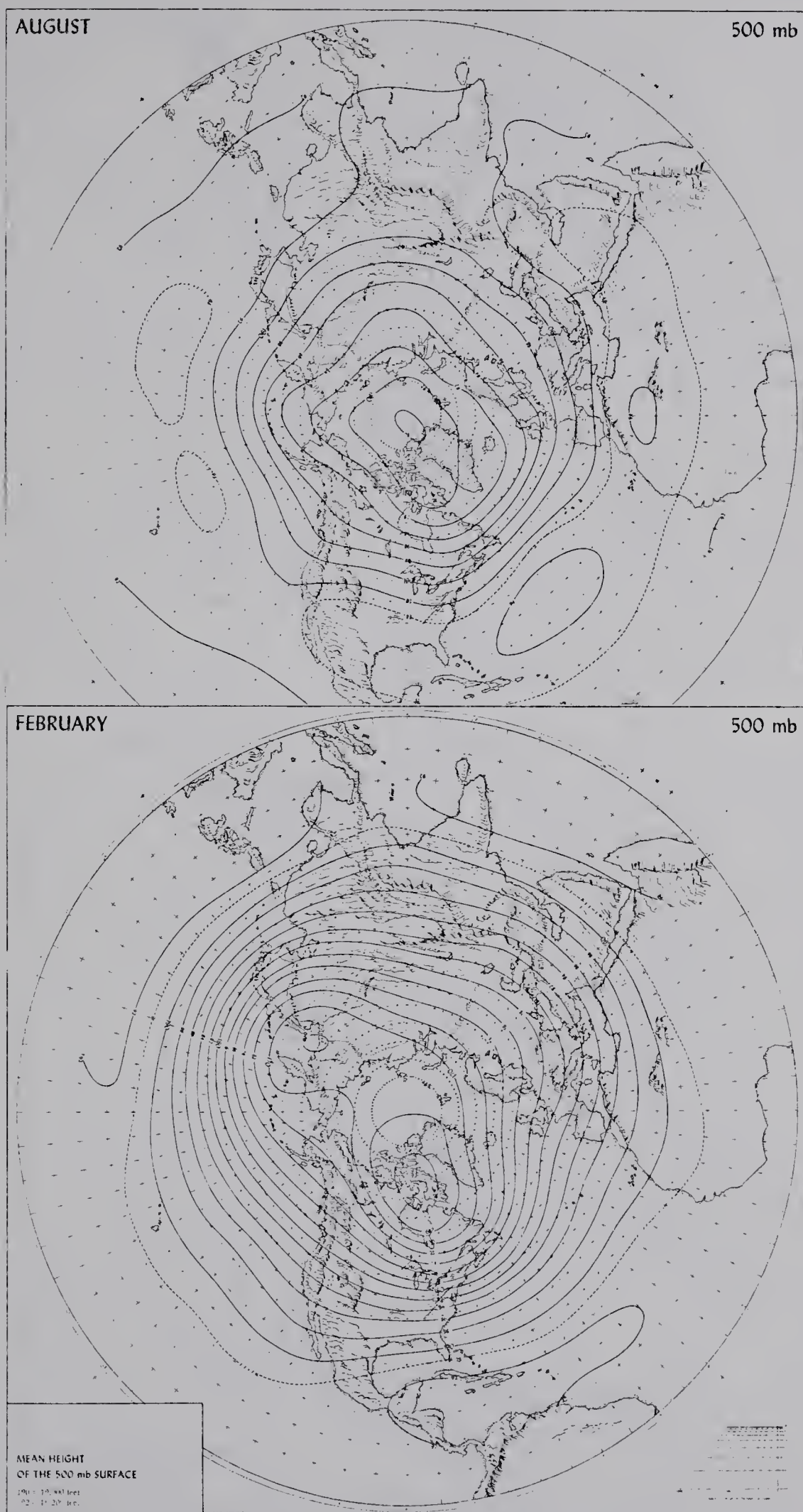


Figure A.1. Mean monthly 500-mb heights (in hundreds of feet) in summer (August, top) and winter (February, bottom). [from Lahey, et al., 1958]

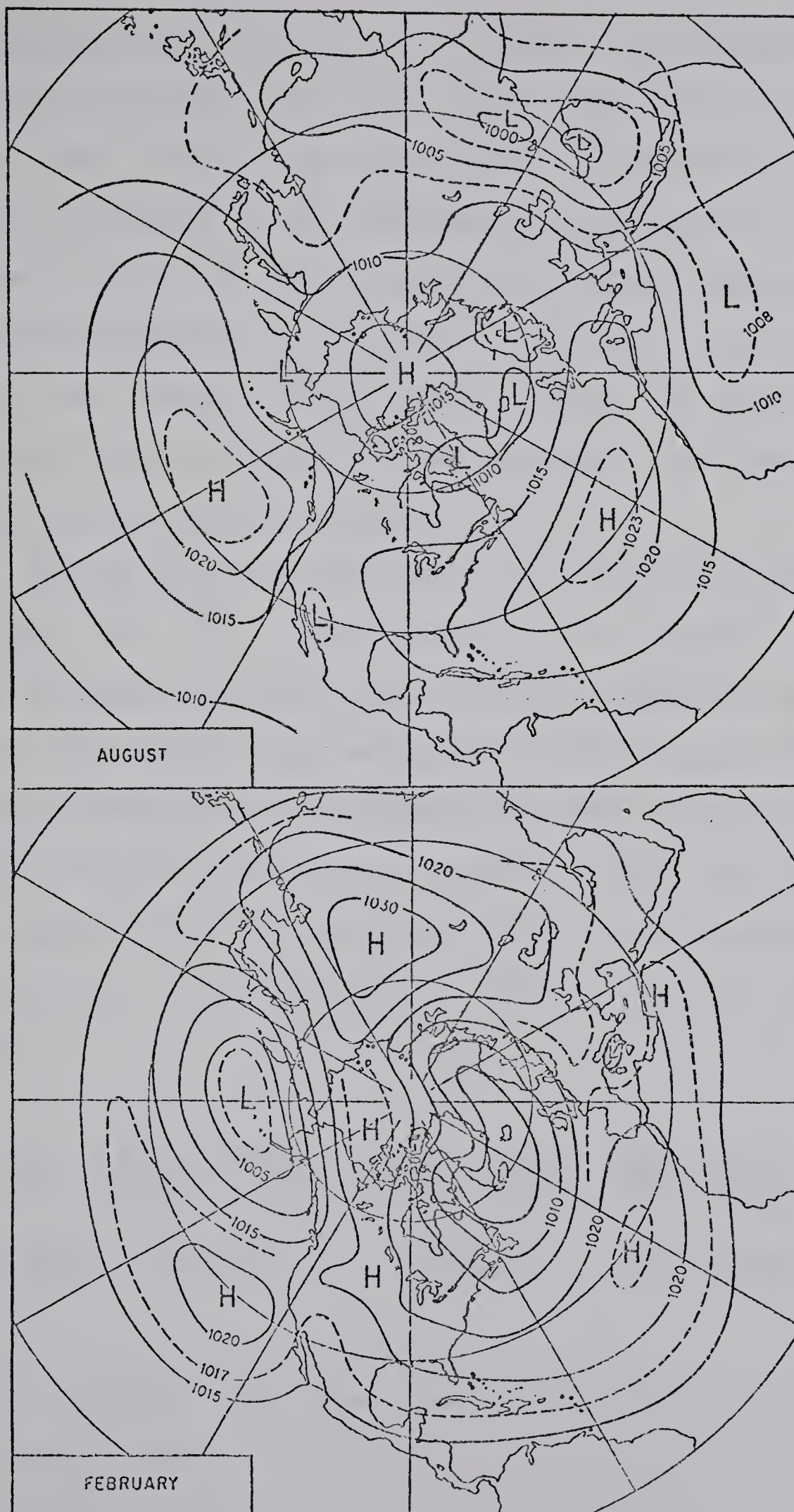


Figure A.2. Normal pressure distribution at sea level in summer (August, top) and winter (February, bottom). [from Petterssen, 1956, Figures 12.6.2 & 12.6.1]

the sea-level mean charts --- in winter, low pressure areas occur over the oceans and highs over continental areas; in summer, the reverse is true (refer to Figure A.2). This reversal is created by the differential heating and cooling of water and land from winter to summer. This seasonal variation decreases with height. At 500 mb (approximately 5.5 km), the major change from winter to summer is the increase in the height of the isobaric surface and a decrease in the height gradient.

During all seasons, two mean trough positions exist along 150W and 70W, approximately 60° downwind of the Tibetan Plateau and the North American Cordillera, respectively. The effect of an orographic barrier on air flow can be demonstrated using the theorem of the conservation of absolute vorticity derived by Rossby in 1940 [see e.g. Hess (1959), Section 16.4]. Combining the vorticity equation for level surfaces (see Appendix 1 for a complete list of symbols)

$$\frac{dQ}{dt} = -QD - \left[\frac{\partial w}{\partial x} \frac{\partial v}{\partial z} - \frac{\partial w}{\partial y} \frac{\partial u}{\partial z} \right] - \left[\frac{\partial \alpha}{\partial x} \frac{\partial p}{\partial y} - \frac{\partial \alpha}{\partial y} \frac{\partial p}{\partial x} \right] - \left[\frac{\partial F_y}{\partial x} - \frac{\partial F_x}{\partial y} \right] \quad (\text{A. 1})$$

(divergence) (tilting) (solenoid) (other forces)

and the equation for the horizontal divergence 'D' of a fluid of depth 'H'

$$D = \nabla_2 \cdot \vec{V} = -\frac{1}{H} \frac{dH}{dt} \quad (\text{A. 2})$$

gives, neglecting the small tilting, solenoid, and other forces terms in the vorticity equation

$$\frac{dQ}{dt} = \frac{Q}{H} \frac{dH}{dt}$$

whence

$$\frac{d}{dt} \left[\frac{Q}{H} \right] = \frac{d}{dt} \left[\frac{q+f}{H} \right] = 0 \quad (\text{A. 3})$$

Assuming the atmosphere to be a fluid of depth $H_0=8$ km, for air flowing over a barrier of height 2 km, the depth 'H' will be reduced to 6 km and the absolute vorticity 'Q' must decrease correspondingly. Using the definition of relative vorticity 'q' in terms of the curvature of the streamlines K_s and the wind shear $\frac{\partial V}{\partial n}$

$$q = V K_s - \frac{\partial V}{\partial n}$$

$$Q = f + q = f + V K_s - \frac{\partial V}{\partial n} \quad (\text{A. 4})$$

then, if 'Q' decreases at constant 'f', either the product $V K_s$ decreases or the wind shear increases.

Mean charts show ridges over the Tibetan Plateau and the Cordillera, and Namias & Clapp (1949) found that jet-stream maximum wind speeds decrease over mountain complexes.

For a ridge, the curvature is negative. If it is assumed that the relative vorticity ' q ' is only a function of curvature K_s , not wind speed and shear, then for ' q ' to decrease, the wind speed must increase if the curvature is kept constant. Since this contradicts the observed flow, the curvature K_s must vary significantly as the air flows over a mountain barrier.

The curvature of a streamline decreases for air flowing over a barrier, giving an anticyclonic component to the flow. For initially zonal flow with zero relative vorticity, the air will be south of its original latitude after passing over the barrier. The Coriolis parameter ' f ' is now less, ' q ' must be greater than zero and the air will acquire cyclonic curvature. The flow is controlled only by the latitude effect in ' f ' and will oscillate north and south in constant absolute vorticity trajectories.

A better understanding of cross-barrier flow may be obtained by modelling the flow using numerical techniques. Figure A.3 shows several trajectories using the theorem of conservation of absolute vorticity. A fluid of depth 10 km and speed $30 \text{ m}\cdot\text{s}^{-1}$ flows over a equator-to-pole barrier of height 2 km and half-width 10° longitude. With upstream ridge positions 10° , 20° , and 40° from the crest of the barrier, a trough is produced directly over the barrier and a ridge immediately downstream. This configuration is similar to the ridge observed in the Gulf of Alaska and the cold low in a trough over the southwestern United States. The 30° -

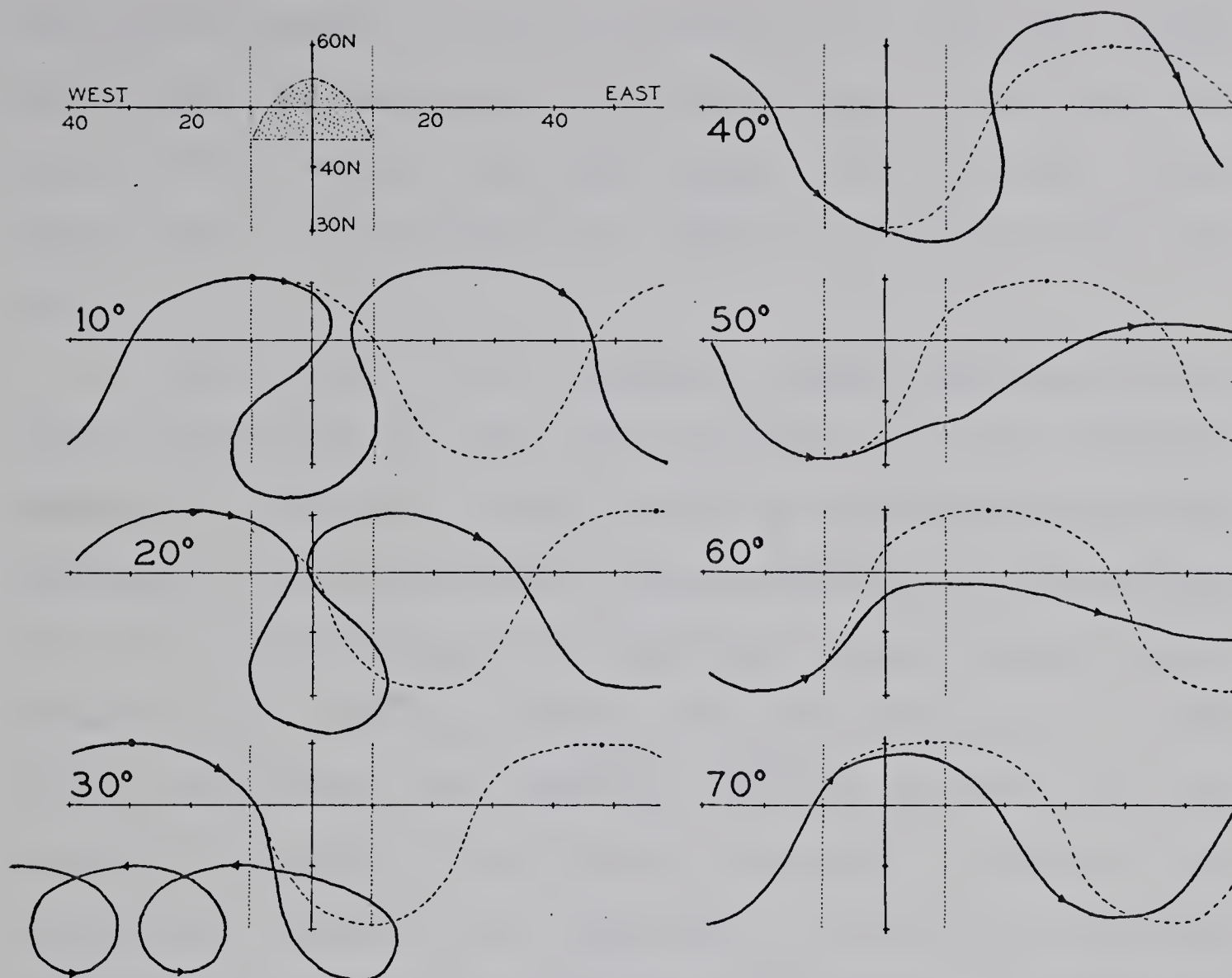


Figure A.3. Constant absolute vorticity trajectories of a fluid of 10-km depth passing over a barrier of 2-km height and 10°-longitude half-width for upstream ridge positions of 10° to 70°. Dashed lines give the trajectory of the fluid with no barrier.

upstream ridge position produces a physically unlikely flow --- individual particle trajectories cross themselves and the ridge position must shift. For the 50° to 60° upstream ridge position, the trough is upstream of the barrier. The amplitude of the down-barrier waves are significantly reduced and the wavelengths increased. At 70°, the downstream ridge occurs over the barrier. The only result produced by the barrier is a small decrease in the cross-

barrier wavelength. A south-to-north flow along the ridge, often observed on upper air charts, cannot exist in a one-layer fluid. Using a two-layer model, south-to-north flows could exist if the boundary was above the height of the barrier.

The cause of the permanent trough positions in the upper troposphere has been the subject of many studies. Charney & Eliassen (1949) using a one-dimensional model concluded "the large-scale quasi-stationary disturbances of the mid-latitudes are produced mainly by the forced ascent of the westerly currents over the mountains". Döös (1962) concluded that thermal effects account for the essential features of the observed sea-level pressure distribution, whereas the importance of mountains increases with height. This is in contrast to Kasahara & Washington (1969). Using a two-level general circulation model, they showed that thermal forcing without topography simulates the observed climatology of both hemispheres, summer and winter, rather well, whereas orographic forcing alone does not, particularly in summer.

The theoretical studies referred to above involve many simplifying assumptions. Using more realistic boundary conditions at the Earth's surface may change the flow pattern significantly. The simplest model assumes the atmosphere to be a fluid in a channel. Kasahara (1966) shows that a westerly flow past an obstacle representing a mountain produces, on the lee side, a train of long waves

characteristic of planetary waves. The number of waves generated agrees with that expected from the Rossby-Haurwitz wave formula [see Haltiner (1971), Section 2.7]

$$U - c = \beta \left(\frac{L}{2\pi} \right)^2 \left(1 - \frac{L^2}{d^2} \right)^{-1} \quad (\text{A.5})$$

where 'd' is the width of the disturbance, 'L' the wavelength, and β the Rossby parameter. For stationary waves, 'c' is zero and the number of waves 'n' around the Earth must be an integral number such that

$$n \approx \left[\frac{2 \Omega R_E \cos^3 \phi}{U} \right]^{1/2} \quad (\text{A.6})$$

At a given latitude, the number of waves is only a function of the zonal wind speed. Table A.1 gives 'L' and 'U' for several 'n'.

If β is zero, i.e. the Coriolis parameter is constant with latitude, the wave train does not appear in the model results. For easterly flows, both the model and a theoretical analysis show waves decreasing in amplitude downstream: no long-wave train is generated. These results agree with the experiments of Frenzen (1955) for flow past an obstacle. The fluid goes into a series of oscillations extending around the globe for westerly flow; an easterly flow does not oscillate and is little disturbed.

Vergeiner & Ogura (1972) investigated the influence of the Andes Mountains using both smoothed and unsmoothed

Table A.1

Wavelength 'L' and zonal wind speed 'U' of Rossby waves at latitude 45° for 'n' waves around the Earth.

n	L (km)	U ($\text{m}\cdot\text{s}^{-1}$)
3	9600	36.5
4	7100	20.5
5	5650	13.1
6	4700	9.1

profiles. The differences in the flow in the lee were surprisingly small: both mountain profiles produced a planetary wave with a jet-like gradient of zonal wind 40° downstream of the mountain. This jet occurs in a barotropic model, one without any thermal contrasts. Thus, the intensification of the jet stream downwind of mountain barriers in the mean charts of Namias & Clapp (1949) is a result of orography. However, for a baroclinic flow, the downstream difference between the two profiles may be greater.

The most sophisticated models simulate the general circulation of the Earth. Manabe & Terpstra (1974) used such a model (with and without mountains) to examine the effect of topography on the circulation in winter. At 1000 mb, the temperature contrast between land and sea is almost entirely responsible for the formation of the mid-latitude lows over the oceans; this type of cyclogenesis is thus not dependent on the presence or absence of mountains. The only significant differences in the mountain model (M-model) are the northward shift and intensification of the Siberian high by the Tibetan Plateau and the poorer corres-

pondence between heat sources and mean centers of low pressure. Döös (1962) shows that the trough of sea-level pressure is located 20° east of the heat source maximum.

In the upper troposphere at mid-latitudes, the M-model is more realistic than the no-mountain model (NM-model) by producing higher-amplitude perturbations: it simulates the well-developed troughs and gives a local jet maximum 30° to 40° downstream of the Tibetan Plateau and the North American Cordillera. In the stratosphere at 30 mb, the M-model reproduces the observed pattern, especially the anticyclone over the Aleutians.

Examining the eddy kinetic energy in the troposphere, though the total energy is unchanged, the mountains increase the kinetic energy of stationary disturbances, i.e. the amplitude of the semi-permanent troughs. This increase is most evident in the stratosphere of the northern hemisphere. Compared to climatology, the NM-model is not realistic in the positioning of the stationary disturbances. Because the model lacks seasonal variation, the amplitude in the M-model is greater than that observed, but the general features agree well. Thus, mountains affect the position of the stationary disturbances, especially in the upper troposphere and in the stratosphere. With a positive correlation between temperature and meridional wind, these disturbances in the M-model transport heat poleward very efficiently. Topography has a large influence in the global circulation of the atmosphere.

The increasing importance of the mountains with height has been noted by Döös (1962) and other authors but not by Sankar-Rao & Saltzmann (1969). One major difference between the models of Manabe & Terpstra (1974) and Sankar-Rao & Saltzmann is the heating profile of the troposphere by the release of latent heat and the flux of surface sensible heat. The model of Sankar-Rao & Saltzmann heats the upper troposphere more than that calculated by the NM-model, decreasing the response of the upper troposphere to topographic influences. Manabe & Terpstra (1974) note that mountains affect the thermal forcing by altering the distribution of precipitation and sensible heat flux. By including mountains in the model, orographic forcing is added, thermal forcing is modified, and the influence of each cannot be separated.

A.3 Synoptic-scale Waves

Surface cyclones and anticyclones and the upper-troposphere "short wave" troughs and ridges occur at wavelengths of 500 to 2000 km. From charts giving frequency of occurrence of cyclogenesis [see Petterssen (1956), Figures 13.6.1 and 13.6.3] maxima occur in the lee of major mountain barriers in all seasons. For the North American Cordillera, these maxima occur in Nevada in the lee of the Sierra Nevada, and in Colorado and Alberta in the lee of the Rocky Mountains. Using one year of surface maps, Chung (1972, Figure 11) gives the frequencies of cyclogenesis in the lee

of the Canadian Rocky Mountains, and shows a correlation between barrier height and lee cyclogenesis --- the largest maximum (12 per 1.5 degree square per year) occurs in southern Alberta downwind of the Selkirk and Rocky Mountains, while lesser maxima of 6 units are found in north-eastern B.C. and near Norman Wells, downwind of the Cassiar-Rocky and the Mackenzie Mountains, respectively. These maxima of cyclogenesis indicate that positive vorticity is being created by the mountain barrier. Using a simplified version of the vorticity equation (Equation A.1) and the equation of continuity in the form

$$D_p = \nabla_p \cdot \vec{V} = - \frac{\partial \omega}{\partial p}$$

one obtains

$$\frac{\partial Q}{\partial t} = - \nabla_3 \cdot (Q \vec{V}) + Q \frac{\partial \omega}{\partial p} . \quad (A.7)$$

The local change of vorticity is the sum of the advection by the wind and production by the gradient of vertical motion. As air flows over a barrier, surface air will be forced to ascend ($\omega < 0$) and then descend ($\omega > 0$). Schram (1974) shows that this orographic vertical motion will decrease to negligible values at some height above the crest, about the 500-mb (5.5-km) level for the Cordillera. Thus, upwind of the crest, the gradient of orographic vertical motion $\partial \omega / \partial p$ will be negative and anticyclonic vorticity will be generated; downwind, $\partial \omega / \partial p$ will be positive and cyclonic vorticity

will be created. Descent on the lee slopes has been reported by Newton (1956) and McClain (1960) and is often quoted to explain the increase of vorticity during cyclogenesis by stretching of the air column. This is in agreement with Schram (1974) who found a mountain barrier, through orographic vertical motion and frictional convergence, induces vorticity production to its lee, and inhibits it on the windward slope.

A mathematical description of cyclogenesis is given by the Petterssen development equation, derived from the simplified vorticity equation at the level of zero divergence (LZD)

$$\frac{dQ}{dt} = \frac{\partial Q}{\partial t} + \vec{V} \cdot \nabla_2 Q + \omega \frac{\partial Q}{\partial p} = -D_p Q = 0$$

the definition of thermal wind \vec{V}_T

$$\vec{V} = \vec{V}_s + \vec{V}_T \quad Q = Q_s + q_T$$

and the thermodynamic equation including latent heat

$$dh = c_p dT - \alpha dp - L dr$$

The change of vorticity at the surface is

$$\frac{\partial Q_s}{\partial t} = \underbrace{-\vec{V} \cdot \nabla_2 Q}_{A_Q} + \frac{R}{f} \ln\left(\frac{P_s}{P_{LZD}}\right) \nabla_2^2 \left[\underbrace{\overline{\vec{V} \cdot \nabla T}}_{A_T} + \underbrace{\overline{\omega(\Gamma - \Gamma_a)}}_S + \underbrace{\overline{\left(\frac{-1}{c_p} \frac{dh}{dt}\right)}}_H \right] \quad (A.8)$$

where the bars indicate means over the atmospheric layer from the surface to the LZD

Γ_d = dry adiabatic lapse rate

$$\Gamma_a = \frac{\alpha}{c_p} - \frac{L}{c_p} \frac{dr}{dp} = \Gamma_d - \frac{L}{c_p} \frac{dr}{dp} = \text{adiabatic lapse rate}$$

$$\Gamma = \frac{dT}{dp} = \text{lapse rate (in pressure coordinates)}.$$

When using the simplified vorticity equation in the derivation of the development equation, the tilting, solenoid, and other forces terms were neglected. During the initiation of a cyclone, these terms may be as large as the A_Q and A_T terms. When studying the circulation increase during cyclogenesis, Newton (1956) found that surface friction contributes significantly during the early stages. Hume (1975) found that frictional effects are at least as important as large-scale orographic lift and subsidence. If $\frac{\partial Q_s}{\partial t} > 0$, there is an increase in cyclonic vorticity at the surface. Any one of the four terms on the RHS of Equation A.8 may contribute to this increase, A_Q and A_T being the most important terms.

For $A_Q > 0$, the wind at the LZD will advect absolute vorticity from high values toward low, i.e., there must be positive vorticity advection (PVA). This is a general situation in advance of an upper trough. The development equation contains three thermal components. Each will contribute to cyclogenesis in the lee of a mountain range: warm air advection (WAA) A_T , stability S by the subsidence of downslope flow, and heating H by solar radiation in the summer.

The Laplacian (∇^2) of the terms A_T , S , and H is

positive when each has a relative minimum in the layer: A_T , when the wind advects air from a maximum to a minimum temperature region, i.e. at a maximum of warm air advection (WAA); S , for a stable atmosphere ($\Gamma_a > \Gamma$), at a maximum of descent ($\omega > 0$); H , at a maximum of heating, but not that due to the release of latent heat of condensation. The production of vorticity is the result of an imbalance between the vorticity advection at LZD (A_Q term) and the Laplacian of the three thermal components in the surface-to-LZD layer: the thermal advection A_T , stability S , and local heating or cooling H .

Using Equation A.8, Petterssen (1955; 1956, Chapter 16, page 377) formulated the working hypothesis:

Cyclone development at sea level occurs where and when an area of appreciable positive vorticity advection in the middle and upper troposphere becomes superimposed on a slowly moving or quasi-stationary frontal zone at sea level.

The most recent formulation of Pettersen's development hypothesis (Petterssen & Smebye, 1971) is:

Cyclone development at low levels commences when and where an area of positive vorticity advection in the upper troposphere (normally on the forward side of an advancing trough) begins to spread over an area of warm air advection (or near-absence of cold air advection) in the lower troposphere.

In both formulations, positive vorticity advection (PVA) is hypothesized as the most important term in Equation A.8 for cyclone development. The last formulation deletes reference to the "frontal zone" and substitutes warm air advection (WAA). Equation A.8 gives no explicit reference to "frontal zones" though a baroclinic zone is implied

in the terms A_Q and A_T .

The development hypothesis has been tested in many studies with excellent results for Type 'A' cyclones but not Type 'B'. 'A' and 'B' refer to Petterssen's classification for the initiation and support of development of extra-tropical cyclones: Type 'A' cyclones are the classical frontal wave, the amplifying baroclinic instability; Type 'B' cyclones are initiated by finite disturbances in the upper troposphere and are not associated with a frontal zone. Type 'B' cyclones were identified in studies of cyclogenesis in the lee of the Rocky Mountains by Schallert (1962).

The terms "initiation" and "development" refer to two separate and distinct processes. A cyclone once initiated may either remain weak and dissipate, or intensify and develop into a major long-lived storm. For summer cold lows over the Cordillera, Hage (1961) noted cyclones may be initiated in Alberta without appreciable positive vorticity advection in the upper troposphere but did not develop until a PVA area crossed the Continental Divide.

Egger (1974) studied lee cyclogenesis using a 3-level numerical model simulating the Rocky Mountains and Greenland by barriers 4000 km and 2400 km in length, 1000 km in width, and 2 km in height. With an initial condition of a cold low west of the barriers, the surface low during the first 24 hours moves eastward, then decelerates, turns northward, and starts filling, similar to the action of

observed surface cyclones. To the lee of the barrier, after 24 hours, surface pressure begins to fall, forming a long narrow lee trough well ahead of the cold front. Further east, a surface high builds, producing a southerly flow to the lee of the barrier.

Pressure falls in the lee can be investigated using a pressure tendency equation in the form

$$\frac{\partial p_s}{\partial t} = -g \int_0^\infty \frac{\partial \rho}{\partial t} dz = \int_0^{p_s} \frac{1}{\rho} \frac{\partial \rho}{\partial t} dp \quad (\text{A.9})$$

The change of density is the result of horizontal advection and internal heating

$$\frac{\partial \rho}{\partial t} = -\nabla_p \cdot (\rho \vec{V}) + \left. \frac{\partial \rho}{\partial t} \right|_{\text{int}} = -\nabla_p \cdot (\rho \vec{V}) - \frac{\rho}{T} \frac{\partial T}{\partial t}$$

Using the thermodynamic equation and the simplified vorticity equation, Equation A.9 becomes

$$\frac{\partial p_s}{\partial t} = \int_0^{p_s} \left[\underbrace{\frac{1}{Q} \frac{\partial Q}{\partial t}}_{(1)} + \underbrace{\frac{\vec{V} \cdot \nabla_p Q}{Q}}_{(2)} + \underbrace{\frac{\omega \partial Q}{Q \partial p}}_{(3)} + \underbrace{\frac{\vec{V} \cdot \nabla_p T}{T}}_{(4)} - \underbrace{\frac{1}{c_p T} \frac{\partial h}{\partial t}}_{(5)} + \underbrace{\frac{\omega}{T} (\Gamma - \Gamma_a)}_{(6)} \right] dp \quad (\text{A.10})$$

where

Term	Pressure Rise	Pressure Fall
(1)	Q increasing	Q decreasing
(2)	NVA	PVA
(3)	ascent	descent
(4)	CAA	WAA
(5)	local cooling	local heating
(6)	ascent	descent
		for stable atmosphere

If the atmosphere is unstable, i.e. $\Gamma > \Gamma_a$, ascent will produce a pressure fall, as is observed in tropical storms and

convective areas at mid-latitudes.

Egger (1974) found that the pressure fall to the lee of the barrier is initiated and maintained by an increase in temperature in the lower and middle levels. Warm air is advected from the warm sector ahead of the trough. Maximum warming occurs above the greatest pressure falls. When ω is positive (subsidence), the stability term $\frac{\omega}{T}(\Gamma - \Gamma_a)$ will cause a decrease in surface pressure while ascent gives the opposite effect. This will produce the observed surface ridge upwind of the barrier and a trough in the lee.

In Egger's model, divergence $\nabla_2 \cdot (\rho \vec{V})$ occurs at mid-levels for 45 hours and in the lower levels for 50 hours. In the lowest level the barrier acts as a block, preventing inflow from the west and allowing divergence long after the start of the pressure fall. At 60 hours, surface-pressure falls end with the penetration of cold air across the barrier. The low moves southeast, a characteristic of most lee cyclones in Alberta. Meanwhile, the upper low decelerates while approaching the barrier and curves southward. In this particular instance, the amplitude of the 500-mb trough was too weak and did not simulate the observed motion of cold lows.

Similar results were obtained with the short barrier. However, after the lee cyclone has formed, PVA strengthens the cyclone. Compared to the simulation with no barrier, no major difference in surface pressure was noticeable. Rather than cyclogenesis, a more apt terminology for

the process of a system crossing a barrier would be the "leap-frog effect".

A.4 Mesoscale Waves

At the mesoscale, mountain barriers create gravity waves, more commonly known by the names mountain or lee waves, with wavelengths of the order of a kilometer to tens of kilometers. The scales of atmospheric flow over an obstacle of width 'w' were given by Queney (1947). Using the upstream velocity 'U', the stability, and the Coriolis parameter 'f', two length parameters may be defined (Queney uses reciprocal length)

$$l_s = \frac{U}{N} \quad l_f = \frac{U}{f}$$

where N = Brunt-Vaisala frequency

$$= \left[\frac{g}{\theta} \frac{\partial \theta}{\partial z} \right]^{1/2} = \left[\frac{g}{T} \left(\frac{\partial T}{\partial z} + \Gamma_d \right) \right]^{1/2}.$$

Queney's results are generalized by Corby (1954):

$$(a) \quad w \ll l_s \quad w < 100 \text{ m}$$

The air flows over the hill as a single symmetrical wave with decreasing amplitude upwards. No train of lee waves is produced.

$$(b) \quad l_s \ll w \ll l_f \quad w \approx \text{few km}$$

There is a single wave above the hill extending to great heights, but no lee-wave train. The wave crest tilts upstream with height, giving a sinusoidal displacement of streamlines above the ridge. The Earth's rotation is not

important on this scale but the stability of the atmosphere is.

$$(c) \quad l_s \ll w \lesssim l_f \quad w \approx 100 \text{ km}$$

In this case, both stability and Coriolis forces are significant. A train of lee waves is produced downstream with vertical and horizontal displacement of the streamlines. As in (b), the wave crests tilts upstream, with height. Vertical wavelengths are approximately $2\pi l_s$; horizontal ones, $2\pi l_f$.

$$(d) \quad w \gg l_f \quad w \approx 1000 \text{ km}$$

Only the variation of the Coriolis parameter is important. A system of stationary lee waves in the horizontal with wavelengths of several thousand kilometers is produced. These waves are of the nature of Rossby waves discussed in Section A.2.

The mountain wave equation, derived using the method of perturbation, is given by Scorer (1949):

$$\left(1 - \frac{f^2}{k^2 U^2}\right) \frac{\partial^2 \psi}{\partial z^2} - \left(\frac{g}{c^2} - \frac{N^2}{g}\right) \frac{\partial \psi}{\partial z} + \left(\frac{N^2}{U^2} - \frac{1}{U} \frac{\partial^2 U}{\partial z^2} - k^2\right) \psi = 0$$

where $U = U(z)$ = upstream wind velocity

ψ = stream function: $\vec{V} = \hat{j} \times \nabla \psi$

C = velocity of sound = $(\gamma p \alpha)^{1/2}$

$k = (k_x^2 + k_z^2)^{1/2}$ = wavenumber of the disturbance

N = Brunt-Vaisala frequency

This equation is usually simplified to

$$\frac{\partial^2 \psi}{\partial z^2} + [k^2(z) - k^2] \psi = 0 \quad (\text{A.10})$$

where $k^2(z) = \frac{N^2}{U^2} - \frac{1}{U} \frac{\partial^2 U}{\partial z^2}$ is the Scorer parameter (often written as ℓ^2), a function of wind speed and potential temperature with height. The simplifications used in obtaining this equation as given by Sawyer (1960) are:

- (a) the flow is steady and non-turbulent;
- (b) viscous forces are negligible;
- (c) the motion is adiabatic --- there is no condensation;
- (d) the motion is two-dimensional, in the x-z plane;
- (e) the disturbance is of small amplitude so nonlinear terms in the perturbation equations may be neglected;
- (f) the horizontal scale is small enough to neglect the Earth's rotation;
- (g) there is no separation of flow or hydraulic jump in the lee of the barrier.

As a lower boundary condition, the mountain is modelled with a smoothed profile of height 'h' and half-width 'b'

$$H(x) = \frac{hb^2}{(x^2 + b^2)} \quad (\text{A.11})$$

Corby & Sawyer (1958), Wallington & Portnall (1958), and

others concluded that the boundary conditions at the top of the atmosphere did not significantly influence the wavelengths of tropospheric waves.

Allowing a variation of both wind speed and stability in the vertical such that $k^2(z)$ is constant in three atmospheric layers, Scorer (1949) obtained a solution for Equation A.10 using the mountain profile Equation A.11. Evaluation of the solution of the equations is easiest done using a digital computer. Subject to several approximations, Scorer derived the streamlines for the flow over the barrier showing, in some cases, a train of waves in the lee. The solution given by Danielsen & Bleck (1970) consists of the product of two terms:

(a) a forcing function $U(0) h b k_x e^{-b k_x}$ which is maximum when the horizontal wavelength $L_x = 2\pi/k_x$ equals $2\pi b$. In the case of large wind shears below the mountain crest, the forcing of the surface wind $U(0)$ will underestimate the actual forcing. This may be corrected by increasing the mountain's slope and height, which is equivalent to replacing $U(0)$ by approximately $3/4 U(h)$. The modified mountain decreases the wavelength which is most strongly amplified.

(b) a resonant function dependent only on $k^2(z)$, the vertical structure of the atmosphere, not on the shape of the mountain. It determines the horizontal wavenumbers k_x (of which there may be several) and their relative amplitude as a function of height.

The product of the forcing and resonant functions is summed over all wavenumbers which are solutions. The streamlines downwind of the mountain are the addition of waves of different wavelengths and amplitudes.

The lee-wave model of Danielsen & Bleck (1970) divides the atmosphere into several layers and fits the observed Scorer parameter $k^2(z)$ with the formula

$$k(z) = k e^{\alpha(z-z_0)} .$$

Figures A.4 and A.5 give the computed streamlines of airflow over a mountain barrier of height $h=1.9$ km and half-width $b=10$ km, using observed upper air data. In Figure A.4, the Scorer parameter near the surface is large, a result of either an inversion, or weak winds at the surface. When this occurs $k^2(z) = k_x^2 + k_z^2 \approx k_z^2$, giving a short wavelength less than twice the height of the mountain. For example, $k^2(z) > 2.5 \text{ km}^{-2}$, $k_z > 1.6 \text{ km}^{-1}$ and $L_z < 4 \text{ km}$. The physical effect is the trapping of the air by the barrier --- a process termed blocking. Mathematically, a nodal plane is introduced below the crest and, since the effect of the barrier is changed, the solution must be recomputed using the uppermost nodal plane as the $z=0$ surface. Vergeiner (1971) shows that, with partial upstream blocking, the very strong lee waves disappear.

Danielsen & Bleck (1970) show that long mountain waves (20 to 100 km) occur primarily in the stratosphere, while shorter waves (5 to 30 km) occur in both the tropo-

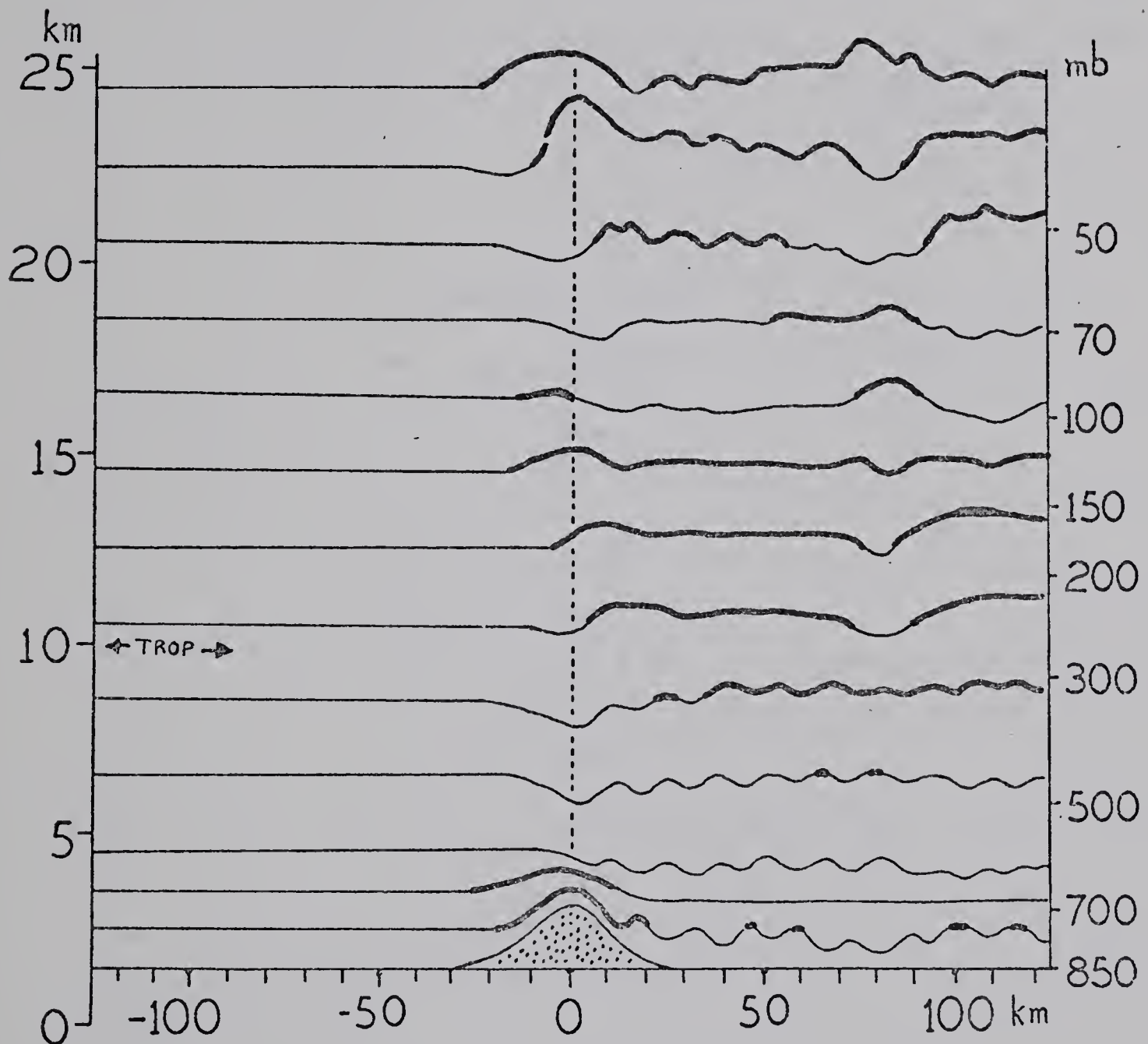


Figure A.4. Total response of all resonance waves on 68-10-10-1200Z using a 6-layer model and a medium-heavy filter on U and Θ . The 14.2-km resonant wave in the troposphere is close to that observed. A nodal surface was introduced at 1.5 km above ground level. The streamlines are evenly spaced upwind of the mountain and include the effects of the 'u' and 'w' perturbations. Thick streamlines represent air above its original level. [from Danielsen & Bleck, 1970, Figure 4c]

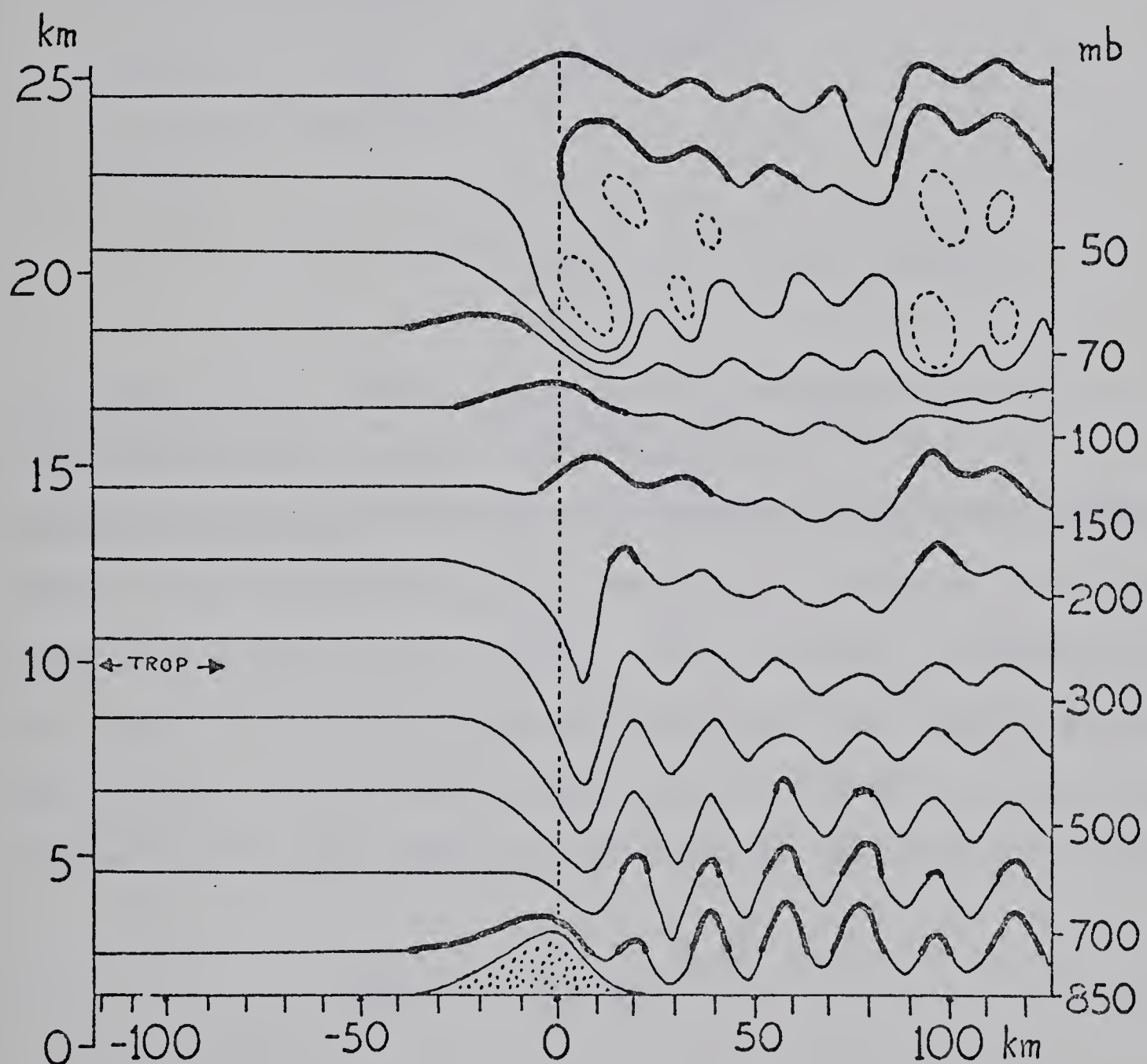


Figure A.5. Total response on 69-01-08-0000Z using a 7-layer model and a medium-heavy filter on U and Θ . Dominant wavelength is 19.4 km. [from Danielsen & Bleck, 1970, Figure 6]

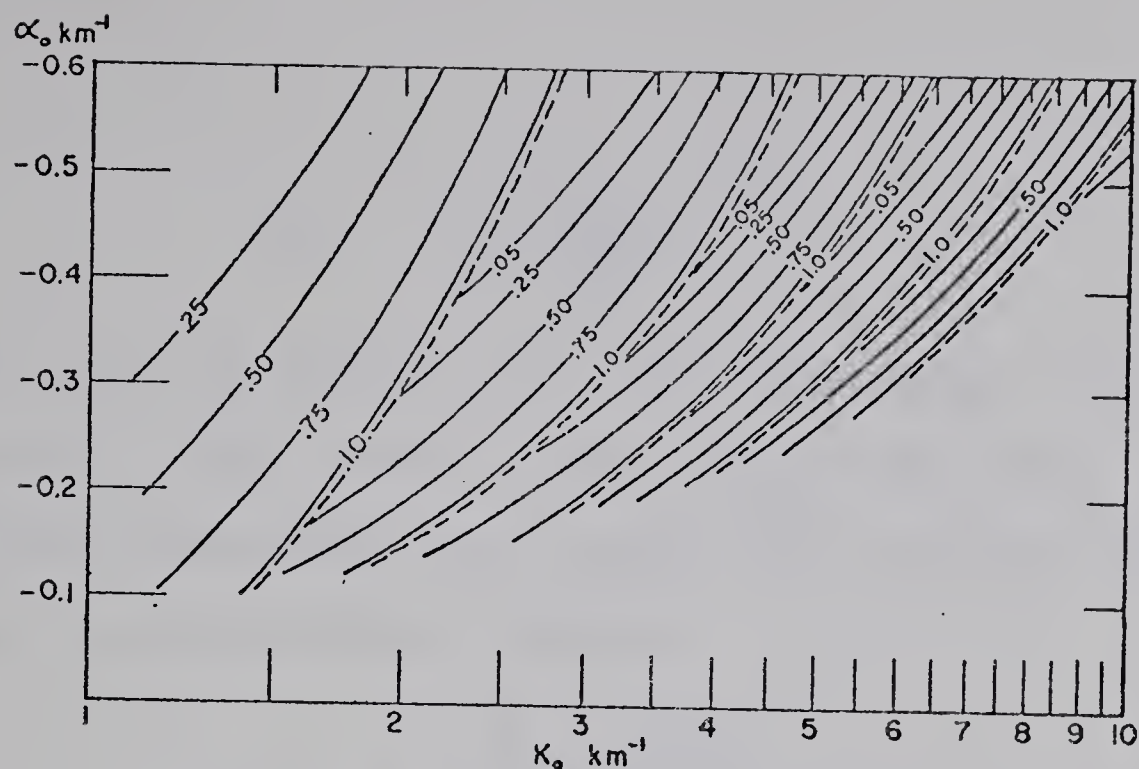


Figure A.6. Dominant horizontal wavenumber in the tropospheric duct as a function of K_0 and α_0 . [from Danielsen & Bleck, 1970, Figure 10]

sphere and the stratosphere. There are typically two short waves and 6 to 9 long waves. The dominant tropospheric wavelength is a very sensitive function of the Scorer parameter $k^2(z)$ in the lower troposphere. Figure A.6 gives the wavelength of this wave as a function of K_0 and α_0 where

$$k(z) = K_0 e^{\alpha_0 z} \quad (\text{A.12})$$

Similar curves were obtained by Palm & Foldvik (1959; see WMO, 1973b, Figure 32a). From observations, Corby (1957) found the wavelength L_x to be linearly related to the mean wind speed in a deep layer in the troposphere. Fritz (1965) uses the equation given in WMO (1960)

$$L_x \approx \frac{2\pi}{\left(\frac{g}{\bar{\theta}} \frac{d\bar{\theta}}{dz}\right)^{1/2}} \bar{U} \quad (\text{A.13})$$

in his study of mountain lee wave clouds seen in satellite pictures. WMO (1973a, page 219) gives the following empirical relationship for L_x and \bar{U} , the mean wind speed in $\text{m}\cdot\text{s}^{-1}$ between 850 and 200 mb:

$$L_x = \frac{\bar{U} - 3.3}{1.6} \quad (\text{A.14})$$

The models of Danielsen & Bleck (1970) and Vergeiner (1971) reproduce a number of features recognized by previous authors in actual flow over mountain barriers. These are summarized by Sawyer (1960):

(a) Lee waves occur downstream of a ridge with waves of different wavelengths being superimposed.

(b) If two or more waves are present, the shortest dominates in the lower troposphere and the longer at higher levels.

(c) Downslope flow on the lee side is more intense than upslope flow on the windward side. This is enhanced by blocking.

(d) The streamline crest over the ridge tilts upstream.

(e) The upward displacement of the streamlines over the ridge reverses with height --- in some cases, at quite low levels.

A mountain barrier produces a spectrum of gravity waves of wavelengths between about one kilometer and up to hundreds of kilometers. These waves will increase the fluctuations in the observed wind speed and direction. Using FPS-16 radar and Jimsphere balloons, Scoggins (1967) determined upper winds over Cape Canaveral to within $0.5 \text{ m}\cdot\text{s}^{-1}$ in speed and 2° in direction (both rms errors) an order more accurate than rawinsonde data. Examining sequential sets of wind profiles [see DeMandel & Scoggins (1967) or Endlich & Singleton (1969)], 3- to 15-hour wind-speed fluctuations of more than $5 \text{ m}\cdot\text{s}^{-1}$ over vertical distances of a few hundred to 2000 meters can be found. Usually even rawinsonde winds must be smoothed to remove the effects of gravity waves if the upper-air wind observations are to be used for synoptic-scale computations. The influence of the longer mountain waves may be impossible to remove. A comparison of two stations, one upwind, one downwind of a barrier, for example Yakutat and Whitehorse, or Grand Junction and Denver, will illustrate this problem.

A.5 Blocking

In the preceding section on lee waves it was noted that blocking of the upstream flow occurs for certain values of $k^2(z)$. For a flow of a homogeneous fluid over an obstacle, Long (1970) uses the Froude number 'F' to describe the upstream flow, where 'F' is defined by the dimensionless ratio

$$F = \frac{U}{(gh_o)^{1/2}} \equiv \frac{U^2}{gh_o} \quad (\text{A.15})$$

where 'U' is the upstream velocity, and h_o the fluid depth. When the fluid has a density gradient, the Froude number is given by (Long, 1955)

$$F = \frac{U}{\left(g \frac{\Delta \rho}{\rho} h_o\right)^{1/2}} \quad (\text{A.16})$$

Expressing $\Delta \rho / \rho$ in terms of a temperature gradient, one obtains

$$- \frac{h_o}{T} \left(\frac{g}{R} + \frac{\partial T}{\partial z} \right)$$

which is very similar to

$$\frac{1}{T} \left(\frac{g}{c_p} + \frac{\partial T}{\partial z} \right) = \frac{1}{\theta} \frac{\partial \theta}{\partial z} = \frac{N^2}{g}$$

where g/R = lapse rate in a homogeneous atmosphere

g/c_p = dry adiabatic lapse rate (Γ_d) = $9.76^\circ\text{C}\cdot\text{km}^{-1}$

The denominator of Equation A.16 becomes

$$g \frac{\Delta \rho}{\rho} h_o = h_o^2 \frac{g}{\theta} \frac{\partial \theta}{\partial z} = h_o^2 N^2$$

Wilson (1974) relates the Froude number to airflow over a mesoscale barrier. Neglecting surface friction, the kinetic energy of the surface wind is equivalent to a vertical displacement of an air parcel by U/N . Replacing the gravitational force by the bouyant force hN^2 ('h' being

the barrier height), the Froude number becomes

$$F = \frac{U^2}{h^2 N^2} \quad (\text{A. 17})$$

When $F=25$, the effect of the barrier becomes detectable, and increases with decreasing 'F'. The flow passes directly over the barrier when $F \gg 1$ while it is forced to detour horizontally across-isobar when $F \lesssim 1$. For air flowing over the barrier with velocity V_c at the crest, the upstream velocity normal to the barrier approximately equals

$$U \approx V_c + (5/3) N h$$

where the factor $(5/3)$ compensates for surface friction. A displacement of $V_g/2f$ towards lower pressure doubles the kinetic energy of the air parcel where V_g is the upbarrier geostrophic wind speed. Letting V_c equal V_g , a displacement

$$Y = \frac{1}{\sqrt{2}} \left(\frac{5/3 N h}{2f} + \frac{V_g}{2f} \right)$$

toward lower pressure is required. Inserting numerical values ($1/N=50$ s, i.e. isothermal atmosphere, $V_g=8$ m·s⁻¹, $h=1000$ m, $1/(2 \times f)=5000$ s) then $F = 0.08$ and $Y = 300$ km.

Long's fluid experiments (1955, 1970) showed that, when the lower layers were blocked by an obstacle, the upper layers descend to the surface. When air is brought from higher levels to lower levels, it is heated at the dry adiabatic lapse rate. In the lee-wave model of Vergeiner

(1971), partial blocking of the upstream flow in two pre-chinook cases changed the very strong lee waves into one wave resembling a hydraulic jump. Scorer & Klieforth (1959) outlined four processes which produce a chinook:

- (a) subsidence and compressional heating at the dry adiabatic lapse rate
- (b) condensation and the release of latent heat over the barrier
- (c) gravity waves on the interface between cold surface air and warmer air aloft
- (d) mixing and advection at the lower levels, especially at night.

Beran (1967) investigated the relationship between blocking and the occurrence of chinooks using Scorer & Klieforth's hypothesis "... Foehn (chinook) winds will occur if an airstream reaches a mountain whose height exceeds $\pi/k(z)$ ". Inserting typical values, the critical lapse rate was found to be nearly isothermal. In the two cases with a strong cross-barrier flow, mountains above $\pi/k(z)$ were found to have an area of large dew-point spread downwind. The observed lag between the upstream profile becoming isothermal and the onset of the chinook is approximately equal to the delay caused by the finite wind speed.

The criterion that $\pi/k(z)$ be less than the mountain height is a necessary but not sufficient condition for chinooks of the subsidence type, i.e. Type (a). Types (b) and (c) are independent of windward blocking.

CHAPTER B

CLOUDS AND VERTICAL MOTION

B.1 Introduction

Clouds are composed of either water droplets or ice crystals, as well as various combinations of the two, along with rain drops, snow flakes, graupel, hail, and other less common hydrometeors. Parameters important in cloud formation are the deficit water-vapor saturation and the upward vertical motion the air is undergoing. Dissipation depends on the liquid water content and downward air motion, as well as on coalescence and growth of the water droplets and ice crystals into precipitable hydrometeors.

B.2 Formation of Clouds

Five processes are important in cloud formation:

(a) Synoptic-scale supersaturation.

By lifting a layer of air, the cooling by adiabatic expansion will decrease the saturation deficit and may in time lead to supersaturation over a large region. In this event, condensation will result in large stratiform shields of cloud such as altostratus, nimbostratus, and cirrostratus. Mid- and high-level cloud associated with mid-latitude baroclinic zones and cyclones originates through

this process.

(b) Cooling of the air by radiation and conduction.

Cooling of a clear atmosphere by infrared radiation at the equator has been calculated by Stephens (1976). The rate of cooling is observed to be approximately 2°C per day for the layer 800 to 300 mb, increasing to 3.5°C per day at 950 mb, and decreasing to 1.5°C per day at the poles. Over land, the surface temperature may drop as much as 30°C in 12 hours. By conduction and radiation, the air near the ground will also be cooled. If water-vapor saturation results, fog will form. Continued cooling at the top of the fog will deepen the layer and form stratus cloud. The result of this process is often observed in mountain valleys, for example, in the San Joaquin Valley of central California (NESC, 1969, Figure 6-B-19). Fog may also be formed by the cooling of a warm, moist air mass which moves over a colder surface. This often occurs over water, especially "cold" ocean currents, for example, over the Grand Banks and off the coast of California.

Above the surface boundary layer, cooling is of lesser importance. A decrease of 2°C is equivalent to lifting the air about 20 mb, a change which would take a fraction of a day in cyclones by process (a).

(c) Convective instability.

If the atmosphere becomes unstable by heating of the air at the surface, by the addition of water vapor, or the cooling of the air at upper levels, convective currents will

arise and the atmosphere will "boil" until stability is restored. Cumulus, towering cumulus, and cumulonimbus result from low-level convection; altocumulus castellanus and cirrocumulus, from mid- and high-level convection. The stability of the atmosphere may be determined using the static energy 'H' and the saturated static energy H^* as defined in Haltiner (1971):

$$H = c_p T + gz + Lr \quad (B.1)$$

$$H^* = c_p T + gz + Lr^* \quad (B.2)$$

where 'r' is the actual mixing ratio, r^* is the saturated mixing ratio, and 'L' is the latent heat of condensation for water vapor. The static energy can be derived in the same manner as the Montgomery potential for adiabatic motion [refer e.g. to Petterssen (1956), Section 1.10]. Replacing the potential temperature θ with the equivalent potential temperature

$$\theta_e = \theta \exp \left[\frac{Lr}{c_p T} \right]$$

the pressure gradient on a constant θ_e surface is given by

$$-\alpha \frac{\partial p}{\partial x} = - \frac{\delta}{\delta x} \left[\overline{\left(c_p - \frac{Lr}{T}\right) T} + gZ + Lr \right] \Big|_{\theta_e}$$

The static energy 'H' is the potential on a constant surface:

$$H = \overline{\left(c_p - \frac{Lr}{T}\right) T} + gZ + Lr \simeq c_p T + gZ + Lr$$

Two layers of the atmosphere will be unstable if

$$H_{\text{lower}} > H_{\text{upper}}^*$$

and conditionally unstable if

$$H_{\text{lower}} > H_{\text{upper}}$$

(d) Evaporation of precipitation.

The increase of water vapor through the evaporation of precipitation may produce a layer of stratus cloud. This often occurs when rain falls through a colder layer of air at the surface, particularly ahead of a warm front.

(e) Turbulence.

Mixing of the air near the ground by turbulence will produce low stratus and stratocumulus if the lifted air parcels become saturated. Combined with an addition of water vapor by evaporation from the Earth's surface or from precipitation, turbulence will cause large areas of low-level cloudiness.

B.3 Precipitation

When air becomes supersaturated, excess water vapor condenses onto condensation nuclei, forming cloud droplets of radius $10\ \mu\text{m}$ or less. If the temperature is well below freezing, water vapor deposits onto ice nuclei, forming ice crystals. Cloud droplets become rain drops (radius of $\sim 1000\ \mu\text{m}$) by the diffusion of water vapor to the drop and by collision and coalescence with other droplets. Ice crystals grow into snowflakes by sublimation and by the accretion of water droplets.

Water droplets may remain liquid at temperatures much below freezing. This super-cooling limit for pure water droplets lies in the range -40°C for $0.5\ \mu\text{m}$ radius droplets to -33°C for $500\ \mu\text{m}$ droplets. Below this temperature, the droplets will freeze by homogeneous nucleation. With the inclusion of foreign particles always present in water droplets, the freezing temperature increases for the larger droplets to -20°C .

At below freezing temperatures, water-vapor saturation pressure over water is greater than that over ice. Air saturated for water droplets will be supersaturated for ice crystals, by 10 percent at -10°C and 20 percent at -20°C . Water vapor will diffuse towards and sublimate onto the ice crystals while the droplets will slowly evaporate. This growth of ice crystals into snow flakes at the expense of water droplet growth (referred to as the Wegener-Bergeron process) plays a major part in the formation of precipita-

tion in subfreezing clouds. In addition, ice crystals will rime by accreting cloud droplets by collision. Because of their greater weight and larger fall velocities, rain droplets and snow flakes will precipitate from the cloud.

B.4 Dissipation of Clouds

Processes resulting in the dissipation of clouds are:

(a) Large-scale subsaturation by subsidence.

When a layer of air subsides, it warms by compressional heating, changing saturated into unsaturated air. Water droplets and ice crystals will evaporate and the cloud will dissipate. Since the water-vapor saturation pressure is greater over water than over ice, water droplets will evaporate first, followed by the ice crystals when the air becomes unsaturated with respect to ice. The time required depends on the rate of subsidence and the initial water content of the cloud.

(b) Precipitation

The loss of water droplets and ice crystals through precipitation reduces the water content of the cloud. This decreases the subsidence required to evaporate the remaining droplets and crystals. If the lost droplets are not replenished, the "thickness" (i.e. brightness) of the cloud as observed from satellites will also decrease. For layer clouds associated with cyclones, the lag for cloud formation in the area of ascent downwind of a trough is greater than

that for dissipation in the descent downwind of the ridge, assuming troughs and ridges represent zero vertical motion axes. For convective clouds, new cells must be added to replace cloud droplets lost by precipitation, otherwise the cloud will disappear in less than one hour, as is observed over the oceans in winter using geostationary satellite images.

(c) Heating of the air.

Since solar radiation is most effective in heating the Earth's surface, especially over land, stratus and fog are most directly affected. Heating of thin layer clouds at higher levels results in the decrease of cloudiness during the mid-morning.

(d) Mixing.

The mixing of cloud air with the surrounding air along cloud boundaries is most effective in dissipating convective clouds such as cumulus and towering cumulus. The drier the ambient air, the more pronounced is the effect.

B.5 Methods of Computing Omega

Four methods may be used to calculate the vertical motion ω defined (in pressure coordinates) by

$$\omega = \frac{dp}{dt} = -p g \frac{dz}{dt} = -p g w \quad (\text{B.3})$$

For upward motion, ω is negative; for downward motion, positive. Each of the four methods has its advantages and

disadvantages.

(a) The Kinematic Method (Panofsky, 1946; Petterssen, 1956, page 295) is the most straight forward in principle, but requires extreme accuracy in wind measurements. Vertical motion is related to divergence by the equation of continuity

$$\frac{\partial \omega}{\partial p} = -D_p = -\nabla_p \cdot \vec{V} \quad (\text{B.4})$$

Integrating between pressure levels p_1 and $p_2 < p_1$

$$\omega_2 = \omega_1 - \int_{p_1}^{p_2} D_p dp = \omega_1 - \int_{p_1}^{p_2} (\nabla_p \cdot \vec{V}) dp \quad (\text{B.5})$$

This method can be used only in areas of dense and accurate wind observations. The observational errors must only be a fraction of $\nabla_p \cdot \vec{V}$. The result must be smoothed to remove the noise introduced by the sub-station distance gravity waves.

(b) The Adiabatic Method (Panofsky, 1946) assumes adiabatic motion, hence the potential temperature θ is a conservative property of the air flow. Thus, for adiabatic motion

$$\frac{d\theta}{dt} = 0$$

Expanding the derivative following the air parcel into a local derivative and advective terms:

$$\frac{d\theta}{dt} = \frac{\partial\theta}{\partial t} + \vec{V} \cdot \nabla_p \theta + \omega \frac{\partial\theta}{\partial p} = 0$$

whence

$$\omega = - \frac{\left(\frac{\partial\theta}{\partial t} + \vec{V} \cdot \nabla_p \theta \right)}{\left(\frac{\partial\theta}{\partial p} \right)} \quad (\text{B. 6})$$

The term $\frac{\partial\theta}{\partial t}$, the local rate of change of potential temperature, may be estimated from two consecutive charts. In most cases, $\frac{\partial\theta}{\partial t}$ is much smaller than $\vec{V} \cdot \nabla_p \theta$ and may be neglected.

If $\frac{\partial\theta}{\partial p}$ is near zero, as is the case for a nearly dry-adiabatic lapse rate, the solution will be very sensitive to small changes in $\frac{\partial\theta}{\partial p}$. In regions of saturated ascent, the adiabatic method no longer applies, since $\frac{d\theta}{dt} \neq 0$. Under such conditions, the upward motion will usually be underestimated.

Graphically, ω may be calculated by plotting winds and pressure for an isentropic surface and using the equation

$$\omega = \left. \frac{dp}{dt} \right|_{\theta} = \left(\vec{V} \cdot \nabla_2 p \right) \Big|_{\theta} \quad (\text{B. 7})$$

(c) The Vorticity Method (Petterssen, 1956, page 297) is derived using the vorticity equation A.2 and the equation of continuity on constant pressure surfaces

$$\frac{\partial Q}{\partial t} + \vec{V} \cdot \nabla_p Q + \omega \frac{\partial Q}{\partial p} = -D_p Q$$

$$D_p = \nabla_p \cdot \vec{V} = -\frac{\partial \omega}{\partial p}$$

to give

$$\frac{\partial Q}{\partial t} + \vec{V} \cdot \nabla_p Q = Q^2 \frac{\partial}{\partial p} \left(\frac{\omega}{Q} \right)$$

Integrating between pressure levels p_1 and $p_2 < p_1$,

$$\frac{\omega_2}{Q_2} = \frac{\omega_1}{Q_1} - \int_{p_1}^{p_2} \frac{1}{Q^2} \left(\frac{\partial Q}{\partial t} + \vec{V} \cdot \nabla_p Q \right) dp \quad (\text{B. 8})$$

The absolute vorticity 'Q' is computed from the observed winds using

$$Q = f + q = f + \hat{k} \cdot (\nabla \times \vec{V}) = f + \left(\frac{\partial v}{\partial x} - \frac{\partial u}{\partial y} \right) \quad (\text{B. 9})$$

Using the geostrophic wind assumption

$$\vec{V} = \vec{V}_g = -\frac{g}{f} (\nabla Z \times \hat{k}) = -\frac{g}{f} \left(\frac{\partial Z}{\partial y} \hat{i} - \frac{\partial Z}{\partial x} \hat{j} \right) \quad (\text{B. 10})$$

the wind components 'u' and 'v' may be replaced by the observed geopotential height 'Z' at that pressure level. Equation B.9 then defines the absolute geostrophic vorticity

$$Q_g = f + \frac{g}{f} \nabla_p^2 Z + \frac{\beta}{f} u_g . \quad (\text{B.11})$$

The last term containing the Rossby parameter β is small compared to the other terms and is usually neglected when computing 'Q'.

The geostrophic assumption implies that the wind is non-divergent (neglecting the term $\frac{\beta}{f} v_g$)

$$D_g = - \frac{\partial \omega}{\partial p} = \nabla_p \cdot V_g = - \frac{\beta}{f} v_g \simeq 0$$

and either a maximum or a minimum in ω occurs with height. Applying the geostrophic assumption throughout the atmosphere and setting ω equal to zero at the Earth's surface, ω will be zero at all heights.

In principle, the most accurate method for calculating relative vorticity 'q' is to use the observed winds. This method has, however, the same disadvantages as the kinematic method. Landers (1956) shows that substantial errors (up to 250 percent) result when using the geostrophic vorticity equation. The problems ensuing from the geostrophic assumption may be circumvented by using the "balance equation" to determine the wind field from the height field (McClain, et al., 1965).

As in the adiabatic method, the local term $\frac{\partial Q}{\partial t}$ must be evaluated. In a ridge where 'Q' becomes small, the integral is very sensitive to errors in 'Q'.

(d) The technique employed in recent diagnostic studies (Schram, 1974) and numerical progs (Hume, 1975) uses the quasi-geostrophic Omega Equation derived by Wiin-Nielsen (1959). Combining the vorticity equation and the adiabatic equation gives

$$\sigma_s \nabla_p^2 \omega + \frac{f_0}{g} \frac{\partial^2 \omega}{\partial p^2} = \frac{f_0}{g} \frac{\partial}{\partial p} [\vec{V} \cdot \nabla_p Q] + \frac{R}{fg} \nabla_p^2 [\vec{V} \cdot \nabla_p T] - \nabla_p^2 H \quad (\text{B.12})$$

(1)
(2)
(3)

where f_0 = mean value of the Coriolis parameter

σ_s = stability parameter, a function of pressure only

$$= \frac{1}{\theta} \frac{\partial \theta}{\partial p} \frac{\partial z}{\partial p} = -\frac{\alpha}{g\theta} \frac{\partial \theta}{\partial p}$$

and $H = \frac{R}{c_p g p} \frac{dh}{dt}$, the local diabatic heating term.

In a center of upward motion ($\omega < 0$), $\nabla_p^2 \omega > 0$ and the forcing function on the RHS must be positive:

-in term (1), the vorticity advection must increase with increasing height, i.e. decreasing pressure.

-in terms (2) and (3), the temperature advection and the diabatic heating must be a maximum.

The omega equation is solved for ω on a multi-level finite-difference grid. As with the vorticity method, the absolute vorticity 'Q' must be calculated. Using a mean value for σ_s at a pressure level will underestimate (or overestimate) the vertical motion if the local σ_s is less (or greater). One advantage is that the relative magnitude of the individual terms [(1), (2), and (3)] in the forcing

function can be determined and the relative importance of each term (vertically and horizontally) in the development of a storm may be evaluated. However, Barr, et al. (1966)

warn:

"As Phillips [1963] has shown, the geostrophic theory upon which [Equation B.12] is based is most appropriate for synoptic-scale circulations, of hemispheric wave numbers of four to eight. The small mesh length used in these computations permits vertical motion patterns more than an order of magnitude smaller in scale. Identifiable cloud elements in TIROS [or ESSA 8 or NOAA 2 or 3] photographs are at least two orders of magnitude smaller."

B.6 Boundary Conditions

The lower boundary of the atmosphere is the Earth's surface. At the surface, ω equals approximately the change of surface pressure, i.e.

$$\omega_s \approx \frac{\partial p_s}{\partial t} \quad \bullet$$

Using the 1000-mb pressure surface, the surface vertical motion ω_s is given approximately by

$$\omega_s \approx p_{1000} \left(\frac{\partial z}{\partial t} \right)_{1000}$$

and is only a fraction of the vertical velocities at mid-levels in the atmosphere. Thus, ω_s may be neglected. The upper boundary is taken at the top of the atmosphere, where the pressure and vertical motion are assumed to vanish.

Above the surface, frictional convergence and orographic ascent contribute to vertical motion at the top of

the shallow planetary boundary layer. This value is used as the lower boundary condition. The orographic vertical motion ω_t is given by

$$\omega_t = -\rho_s g \vec{V}_s \cdot \nabla h_s \approx \vec{V}_s \cdot \nabla p_s \quad (\text{B.13})$$

where p_s is calculated from terrain heights h_s using the U.S. Standard Atmosphere. Upward motion occurs where the surface wind \vec{V}_s blows toward higher terrain. The friction term ω_f is given by Haltiner (1971) as

$$\omega_f = \frac{g}{f} \left[\frac{\partial}{\partial y} (\rho_s C_D u_s V_s) - \frac{\partial}{\partial x} (\rho_s C_D v_s V_s) \right] \quad (\text{B.14})$$

$$\approx \frac{g}{f} \left[C_D \left(\frac{\partial u_s V_s}{\partial y} - \frac{\partial v_s V_s}{\partial x} \right) + \left(u_s V_s \frac{\partial C_D}{\partial y} - v_s V_s \frac{\partial C_D}{\partial x} \right) \right] \quad (\text{B.15})$$

where V_s is the wind speed measured at 10 m, which Hume (1975) estimated from the geostrophic wind at the 850-mb pressure level, using a proportionality factor and a turning angle. Both are functions of the surface drag (C_D) and the stability (σ_s).

u_s, v_s are the components of V_s .

C_D is the drag coefficient for winds at 10 m, a dimensionless parameter calculated from the terrain roughness.

The term ω_f is sometimes set equal to gKq_s where 'K' is

a constant and q_s is the relative vorticity of the surface winds which may be approximated by the 1000-mb or the 850-mb relative vorticity.

The first term in Equation B.15 produces convergence into a low, divergence from a high; the second term, convergence and divergence around areas of varying drag. An excellent example of the latter is given in WMO (1966, Figure 97). With moist southerly flow over the Ozark Mountains, the eastern portion is clear while cumulonimbus clouds form over the western portion.

CHAPTER C

OBSERVED CLOUD PATTERNS

C.1 Planetary Waves

Characteristic cloud patterns associated with various scales of atmospheric flow are best observed from satellites. Examining monthly mean satellite-derived cloud cover (actually pseudo-albedo) for the years 1967-70 (Miller & Feddes, 1971) no planetary wavelength cloud features were found in the positions of the upper-air semi-permanent troughs. Instead, "cloud amounts" are dominated by land-ocean contrasts, rather than by the influence of mountain barriers. A closer examination reveals that the two dominant factors are the fluxes of water vapor and sensible heat from the surface. In winter, these fluxes produce a band of cloud along the eastern coasts of Asia and North America, extending east-northeast across the ocean. Heating of the colder continental air by the ocean (one term in the Omega equation) contributes to upward motion. In addition, convective clouds will form as the air mass is heated from below and becomes unstable. The evaporation from the ocean provides a source of water vapor for continuing cloud formation.

C.2 Synoptic-scale Waves

The evolution of cloud patterns during the life cycle of an extratropical cyclone is given by Widger (1964). More recent descriptions are given by Conover, et al. (1969) and Barrett (1974). Numerous authors have investigated the role of horizontal and vertical motion in the development of cloud patterns during the life cycle of cyclones --- cyclogenesis with frontal waves or shortwave troughs, intensification through to occlusion and maturity, and, finally, dissipation. Timchalk & Hubert (1961) and Lesse (1962a, 1962b) recognized the role of horizontal advection of dry air in the creation of a nearly cloud-free "dry" slot behind the cold front. At the mature stage, this produces a characteristic vortex spiral. Barr, et al. (1966), Nagle (1966), Rogers & Sherr (1966, 1967), Broderick & McClain (1969), and others, by calculating vertical velocities using the Omega equation, or by assuming adiabatic motion, show that cloud configuration at a particular instant is a function of both horizontal and vertical motion, and the initial relative humidity. Thus prior history of the air near cloud-top level must be considered when viewing satellite pictures. Large-scale vertical motion cannot be directly inferred from cloud patterns in satellite pictures without reference to horizontal advection, the only exceptions being clouds produced by convection.

Rogers & Sherr (1967) relate the sequence of cloud patterns to the low-level cyclonic development defined by

the height, intensity, and size of the closed wind circulation, and the vertical motion due to vorticity advection ω_v and thermal advection ω_T . Their basic hypothesis on the nature of cloud patterns is the following:

"The observed cloud patterns result principally from characteristic patterns of vertical motions during the earlier stages of storm development. In later stages, horizontal advection of the previously formed cloud masses becomes progressively more important in shaping the cloud field, especially as closed circulations develop at higher levels."

Ignoring thermal and monsoon lows, lee cyclones, and cold lows, cyclones may be initiated by either a frontal wave or a mid-tropospheric vorticity maximum associated with a trough. The frontal wave is the more common and usually recognized by a bulging of the frontal cloud band. A vorticity maximum produces a comma or crescent-shaped cloud pattern. In both situations vertical motion is produced primarily by ω_v ascent occurring ahead of the trough. The crescent pattern is the result of the initially drier air present in the southern end of the trough.

As the cyclone develops during the pre-occlusion stage, subsidence occurs to the southwest of the center at low levels, as a result of cold air advection (ω_T term) while initially very dry air undergoes ascent (ω_v term) at mid-levels. As the air is advected eastward, a "clear" slot is produced behind the cold front. North and east of the clear slot, both ω_v and ω_T contribute to produce thick layer clouds. ω_T provides the major contribution to the east at low levels. Cloud to the northwest of the slot is

advected by the northerly winds as the closed circulation reaches mid-levels.

During the occlusion stage, the cyclone reaches maximum intensity. The clear slot has expanded into a relatively large clear area (which may contain low-level bands of cloud) by the movement of the eastern and northern cloud edges away from the low center. The cloud spiral southwest of the low center results from the advection of pre-existing cloud from the northwest. At this stage, vertical motions are generally weak and subsiding over the spiral. The cloud edge to the south and west has been determined to lie along the axis of maximum wind at the 5000-foot (approximately 850-mb) level: to the south, anticyclonic shear increases subsidence; to the north, cyclonic shear gives weak ascent. At the mature stage, the clear slot circles the vortex center one to three times. Frontal layer cloud to the north and northeast is due to upward ω_v and ω_T , becoming primarily ω_v at the mature stage.

After reaching the mature stage, the cyclone slowly dissipates. Vertical motions become weak, and existing middle and high-level cloud is shaped by advection and the resulting deformation. The vortex degenerates into a number of bands of convective cloud, and the frontal cloud band is advected away from the cyclone center.

Rogers & Sherr (1967) relate these cloud patterns to the synoptic conditions during cyclone development:

- (a) developing low (usually frontal wave) stage:
 - (1) slow fall of surface pressure,
 - (2) little change in 500-mb vorticity;
- (b) pre-occlusion and occlusion stages:
 - (1) surface pressure falls most rapidly,
 - (2) 500-mb absolute vorticity increases most rapidly,
 - (3) closed circulation extends to mid-tropospheric levels;
- (c) mature and dissipating stages:
 - (1) surface pressure stops falling,
 - (2) 500-mb vorticity stops increasing,
 - (3) closed circulation extends through the troposphere.

Not all developing cyclones generate the cloud sequence described above. In most cases, the cloud spiral is poorly developed or does not occur at all. Cyclones with spirals occur most often over the oceans, and less frequently over non-mountainous continental areas. However, they are never observed over extensive mountainous terrain such as the Cordillera.

Mountain barriers influence cloud patterns by altering the normal sequence of the horizontal flow regime and vertical motion pattern. Since the change in horizontal and vertical flow is greatest at the surface and decreases

with height, the effect of the barrier is most pronounced on low-level cloud, but of diminishing importance for mid- and high-level cloud.

C.3 Mesoscale Waves

Conover's (1964) classification of satellite-observed orographically-induced clouds is given in Figure C.1.

(a) Lee-wave clouds are the result of mountain-induced gravity waves discussed in Section A.4. They are observed whenever water vapor condenses in the wave crests, and cloud droplets evaporate in the troughs. The simple relation of Equation A.14 may be used to determine mean tropospheric wind speed from the wavelength. The minimum wavelength observable in satellite images is about twice the sensor resolution, or about 10 km for APT images. Figure III.2.3 a&b in WMO (1973a) provides an excellent example, showing the increase in satellite-observed wave clouds when sensor resolution is increased. At a resolution of 1 km, parallel cloud bands are observed everywhere, over oceans as well as over mountains.

(b) Crest waves are the result of orographic ascent. If the upstream air mass is stable, a cap cloud forms over the ridge, evaporating in the subsiding lee flow to give a foehn wall cloud when observed from downwind. This type of crest wave frequently occurs over the Selkirk and Rocky Mountains in winter. Enhanced snowfall in the Rogers Pass results from the cap cloud. For a conditionally unstable air mass,


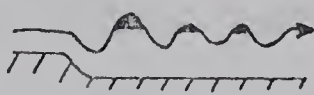
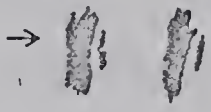



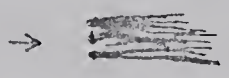



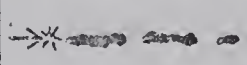

CLASSIFICATION		LEVEL	SCHEMATIC	
			PLAN VIEW	SIDE VIEW
WAVE -- LIKE PATTERN	LEE WAVES	LOW		
	CREST (PART THERMAL)	LOW		
ISOLATED LENTICULAR		MIDDLE OR HIGH		
FIBROUS PLUMES		MIDDLE OR HIGH		
LARGE SINGLE LINE	ARCS	LOW		
	STRAIGHT (MOSTLY THERMAL)	LOW		

Figure C.1. Classification of orographic clouds.
[from Conover, 1964]

convective cloud will form on the upstream slope, a frequent occurrence along a first line of barriers such as the mountain ranges (Coast, Cascade, Sierra Nevada) along the Pacific Coast. Crest clouds will also form when the surface air is heated by solar radiation. South-facing slopes will be cloudy while north-facing slopes and valleys will be clear.

(c) Isolated lenticular clouds are the product of a single large-amplitude wave (or hydraulic jump) in the downstream flow at mid-levels. For a long barrier, a parallel band of lenticular cloud may form. When viewed from ground-level, the leading edge may assume the form of a chinook arch (Lester, 1976).

(d) Fibrous plumes occur when the air temperature is approximately -40°C or less. Ascending wave motion causes the condensation of water vapor into water droplets. As discussed in Section B.3, these nucleate and grow into ice crystals. When the flow subsides to its downstream level, the air may be supersaturated with respect to ice, and the crystals continue to grow; if not, the ice cloud slowly evaporates. The plume has a sharply-defined windward edge and a long tail of ice cloud. This orographic cirrus usually takes the form of a band extending downstream from the mountain crest (see e.g. Figure II.3.96 in WMO, 1973a). It may also be produced by isolated hills or mountain peaks, as over Wrangel Island in the Arctic or the Cotswolds in England (Ludlam, 1952). Occasionally, a large cirrus cloud shield covering $4 \cdot 10^5 \text{ km}^2$ (i.e. an area as large as Montana) may form downstream from a long barrier.

(e) Long, single-line arcs (von Karman vortices) are only observed on higher resolution images downwind of small oceanic islands, such as the Canary Islands and Guadalupe.

(f) Long, single straight lines parallel to the wind occur over and downstream of a barrier. As with lee wave clouds, the sensor resolution is important in identifying these lines. If the air mass is conditionally unstable, the cloud elements will grow into a detectable line of heavy cumulus downstream of the source. Passes in a barrier may also generate a parallel cloud band by the funnel effect of the air.

The subsiding flow in a lee wave also clears cloud along the downwind slope of a barrier. For a long barrier such as the Rocky Mountains, clearing of cirrus and higher mid-level cloud occurs over the crest, and of low-level cloud along the lee slopes.

C.4 Boundary Conditions

As discussed in Section B.6, the vertical motion induced at the surface is the sum of friction and terrain terms. The friction term provides convergence and cloud around cyclones --- particularly noticeable in dissipating cyclones where mid-level vertical motions are weak --- and divergence and a decrease in cloud around anticyclones. The magnitude of the friction term over the Cordillera is about six times larger than over the ocean or over level terrain. Schram (1974, Figure 5) gives drag coefficients C_D equaling $1.296 \cdot 10^{-3}$ over the Pacific Ocean, exceeding $8 \cdot 10^{-3}$ over the western United States, and $6 \cdot 10^{-3}$ over central B.C. The effect on clouds of the friction term is impossible to separate from the terrain term and mountain-generated gravity waves.

Hobbs, et al. (1973, 1974) and Lamb, et al. (1974, 1976) investigated the orographic influence of a mountain barrier on synoptic-scale storms. In both studies, precipitation was found to be enhanced by a factor of two on the windward slopes, the maximum occurring 35 to 75 km upstream of the crest. Over the Sierra Nevada, Lamb, et al. (1974,

1976) observed that this maximum was produced by strong convection in the potentially-unstable upstream air mass. With the passage of a cold front over the Cascade Range, Hobbs, et al. observed post-frontal orographic cloud and precipitation continuing for over 10 hours, with the rear edge of the frontal cloud band becoming indistinguishable from the orographic cloud. To the lee, Lamb, et al. observed only glaciated cirrus clouds at high levels, and a crest cloud at low levels which dissipated in the subsiding mountain wave and the low-level downslope flow. Precipitation from the frontal band ceased abruptly 30 km downwind from the crest.

In the global circulation model of Manabe & Terpstra (1974), precipitation at mid-latitudes became much less zonal when mountains are introduced. This is particularly noticeable in the northern hemisphere. A band of greater precipitation lies along the western slope of the Cordillera while the interior of the continent becomes much drier. Average cloud cover (Miller & Feddes, 1971) decreases markedly east of the Cordillera, especially during the summer months. Without a major mountain barrier across the prevailing flow, as in the case of Europe, the mid-latitude precipitation and cloud band extends well into the interior. In the rain shadow to the lee of the Cordillera, Reinelt (1970) showed that precipitation decreases away from the Continental Divide. The eastern slopes of the Rockies provide orographic lift for air masses with northeasterly circulation components. Precipitation in the foothills peaks

during May and June with the deep easterly flow of cold lows.

As noted in Section C.1, fluxes of water vapor and sensible heat are important in the formation of clouds. When the Earth's surface is a source of water vapor, evaporation and the upward flux is dependent on the moisture content of the surface, the vertical gradient of water vapor, the difference between ground and surface air temperature, and the turbulent mixing by the wind. In the present context, the major difference between a water surface and a land surface is the availability of moisture: the former is always 100 percent water whereas the latter may range from zero percent of complete dryness to 100 percent of complete saturation. Other variables being the same, evaporation from a water surface will greatly exceed that over land. This flux of water vapor into the lower troposphere is apparent in the greater mean cloud amounts over the oceans (Miller & Feddes, 1971).

The upward flux of sensible heat from the surface causes the troposphere to be convectively unstable. Clouds form during the day over oceanic islands (e.g., the British Isles have a greater afternoon cloud amount than the surrounding seas), over large continental regions such as the Amazon basin, and over the oceans and larger lakes whenever the water temperature is appreciably higher than the air temperature --- as happens, for example, in winter over the Great Lakes and along the eastern coast of North America.

C.5 Convection

As noted in the previous section, convective clouds (cumulus, towering cumulus, and cumulonimbus) occur when the surface layer of the troposphere is heated either by solar radiation or by the advection of cold air over a warmer surface. None of the methods used to calculate ω (described in Section B.5) explicitly includes the mesoscale vertical motions due to convection. Several authors have investigated convection within synoptic-scale systems by using precipitation signatures.

Elliott & Hovind (1964) observed that bands of convective showers are a component of precipitation within Pacific-coast storms. To explain showers, the mesoscale vertical motion pattern must be much more complex than that calculated by using only synoptic-scale data. Using radar data, Austin & Houze (1972) found four scales of precipitation:

(a) Synoptic areas ($>10^4$ km²) which are large enough to be delineated by synoptic weather reports and have lifetimes of several days;

(b) large mesoscale areas, LMSAs, (10^3 to 10^4 km²).

These grow and dissipate within synoptic areas, each lasting several hours. In all cases observed by Austin & Houze, LMSAs tend to organize into elongated areas and band-shaped structures;

(c) small mesoscale areas, SMSAs, (50 to 1000 km²).

Several of these are found within every synoptic precipitation or frontal band LMSA. Each SMSA lasts about an hour and, except for air mass thunderstorms, are rarely observed outside LMSAs;

(d) Convective elements or cells (10 km²).

At least one cell or convective element is found in each SMSA. Such cells are almost always located within SMSAs. Lifetimes range from a few minutes to about one-half hour.

If the synoptic precipitation intensity is denoted by R_s , then LMSAs give 2 to 4 R_s , SMSAs 4 to 8 R_s , and cells 8 to 80 R_s .

Even though the upward synoptic-scale vertical motion and resulting precipitation are concentrated into convection cells, precipitation forecasts using synoptic-scale ω agree quite well with observations. Forecasting air mass convective cloud is a problem that is best resolved by using an air mass stability parameter such as the static energy defined in Section B.2.c. Static energy is used in the GISS model of the global atmosphere (Somerville, et al., 1974) to define low, middle, and penetrating convection.

C.6 Summary

Mountain barriers influence the mean positions of the semi-permanent (Rossby) long-wave troughs and ridges. Average cloud amounts do not reflect the long-wave features but do show the land-ocean difference in heat capacity of

the surface and the potential for evaporation of water vapor. However, the long-wave pattern determines the track of the moderate to intense synoptic (cyclone) waves as well as the location of their development --- in general, downstream of the long-wave trough position. The response of the cyclone to a mountain barrier is a function of the state of development of the system: a developing cyclone may either recurve northward or may "leap-frog" across the mountains; the mature cyclone will weaken upwind and cyclogenesis occurs to the lee of the barrier. In both cases, an extended period of southerly winds often occur to the lee of the mountains ahead of the synoptic wave.

Meso-scale changes in the flow pattern caused by frictional vergences, by terrain roughness, and by blocking, produces comparatively large ageostrophic winds which slowly alters the synoptic-scale ω_y and ω_T fields and acts, on the synoptic-scale, as a smoothing operator. The change of upper cold lows into troughs and the weakening of short-wave troughs over the Cordillera illustrates this smoothing. The cloud pattern sequence associated with the cyclone (refer to Conover, et al., 1969) is rapidly terminated. Meso-scale sub-synoptic terrain-induced vertical motion and gravity (mountain) waves are more important in restructuring the cloud. Orographic ascent produces a cap cloud and enhanced precipitation over the barrier. If the lower levels of the troposphere are conditionally unstable, the instability may be released by the forced ascent, producing thick cumulo-

nimbus or nimbostratus cloud. With orographic vertical velocities decreasing with height, low-level divergence (using Equation B.4) will occur upwind of the crest and convergence downwind. With convective ascent at mid-levels, $\partial\omega/\partial p$ will become more positive and the upwind air column will be less divergent (or more convergent). If $\partial\omega/\partial p$ becomes positive, convergence will occur along the upwind slope. The air mass is changed: stabilized if initially unstable, heated through the addition of latent heat, and dried out from the loss of precipitated water vapor. Low-level descent to the lee, and at higher levels in mountain waves, produces clearing and a rain shadow in the lee of the barrier. Since orographic vertical motions decrease with height, only lower-level cloud is affected. Thus a coastal barrier prevents the penetration of moist, cloudy marine surface air into the interior of the continent.

Mountain waves produce low-level wave clouds, mid-level lenticular clouds, and high-level cirrus plumes. The response of the air flow over the barrier depends on the Scorer parameter, a function of wind speed 'U' and temperature θ with height. Blocking of the upwind flow, i.e. the Scorer parameter becomes large, changes the flow over the barrier significantly. Blocking is also an important influence in the flow of cold air southward to the east of the Cordillera. The barriers reduce the westward flow of air to the ocean as well as trap pools of cold air in interior mountain valleys and basins.

During the summer season, convective clouds form over and along mountain barriers, especially to the lee. Convection is enhanced if the air mass is cold, deep, and contains low-level moisture.

The formation, advection, and dissipation of clouds, and the precipitation from clouds can be forecast using numerical techniques. On the synoptic-scale, atmospheric water vapor, temperature, and horizontal geostrophic winds are required, the vertical motion field being computed using the Omega or the adiabatic equation. The initial cloud pattern would be determined using data from all possible sources: upper air soundings, surface observations, aviation pilot reports, and satellite images. Ascending motion would saturate the air, forming the cloud layer or adding to the liquid water content of existing cloud, while descent would evaporate existing clouds. Horizontal winds advect cloud (and liquid water content) and atmospheric water vapor. Use of cloud physics would be required to predict precipitation from the clouds. Without considering surface influences, these parameters would forecast mid- and high-level stratiform cloud with considerable skill, except possibly over mountainous areas.

The meso-scale influence of the surface would be required to predict low-level and convective clouds and the modification of mid- and high-level cloud. Surface terrain heights, roughness (i.e. drag), moisture, heat capacity and conductivity, and temperature are required. From the sur-

face boundary, the following may be calculated:

- (a) vertical motion from topography;
- (b) ageostrophic winds (and convergence and divergence) from friction and the cross-isobar flow over the barrier;
- (c) mountain waves, especially the longer wavelengths in the upper troposphere. This calculation requires accurate vertical profiles of 'U' and Θ ;
- (d) surface evaporation of water and the fluxes of sensible and latent heat into the troposphere;
- (e) diurnal surface heating and cooling;
- (f) convective instability of the surface air or of air forced to ascend over a barrier. This is important in tropospheric dynamics, although the number, size, and locations of the convective cells would be very difficult to forecast.

Winds, temperatures, and water vapor may be represented on a three-dimensional grid. However, since cloudiness is not a continuous property, the grid representation is not suitable, especially for partly-cloudy areas and the edges of cloud layers.

CHAPTER D

CASE STUDIES DATA

D.1 Case Selection

The following criteria were used in the selection of the cases:

(a) A distinct, meridional frontal cloud band was observed on satellite images near ocean station (Ship) PAPA (50N145W).

(b) This band moved eastward to the West Coast with no significant change in the satellite-observed cloud pattern.

(c) To illustrate summer to winter contrast, one case was chosen from the period May to August and one from October to March.

Table D.1 contains a summary of the observed frontal cloud bands for the year 1972 using weekday images only. No images were available on weekends or on holidays. Three-quarters of the well-defined bands were zonal in character or became stationary along the coast. Of the 12 meridional, moving bands, 4 occurred during the warm season (May to August) and 7 during the cold months (October to March). The summer band of 19-22MAY72 was chosen on the basis of the cloud crossing the mountains as a readily identifiable

feature which could be tracked over several days. The bands in the other 3 cases disappeared after crossing the Coast Mountains.

Two winter cases were selected: 07-10NOV72, illustrating blocking along the Coast Mountains, and 19-20NOV73, the opposite --- the cloud band moved rapidly across the mountains.

D.2 Storm Tracks

With each case, the tracks and 1200Z position of 500-mb lows and major troughs and surface lows are plotted. On the 500-mb chart, the symbol \bigcirc indicates a low with at least one closed height contour while \otimes indicates a major trough with the symbol positioned approximately at the vorticity maximum. On the surface chart, the intensity of the low, given by the symbols \otimes \bullet \odot for weak, moderate, and strong, is estimated. Very weak lows (e.g. those with one closed contour) and lows with a short life are not plotted. Schallert (1962) classified lows according to trajectory and intensity into 4 types given in Table D.2.

The intensity \mathcal{J} of a pressure system is given by

$$\mathcal{J} = \nabla_2^2 p$$

(see Petterssen, 1956, page 52, equation 3.6.4) which is invariant in regard to orientation of coordinate axis. When the calculation is done using finite differences, large errors may affect the result. Assume for example a circular

Table D.1

Observed frontal cloud bands for 1972.

Month	Total Cases	Zonal	Meridional	
			Stationary	Moving
Jan	1	1	0	0
Feb	4	2	1	1
Mar	5	1	2	2
Apr	4	2	2	0
May	3	0	2	1
Jun	5	1	2	2
Jul	3	0	3	0
Aug	4	1	2	1
Sep	2	2	0	0
Oct	4	3	0	1
Nov	7	1	3	3
Total	42	14	16	12

Meridional Moving Cases:

Total winter (Oct to Mar) = 7

Total summer (Mar to Sep) = 4

pressure distribution of the form

$$p(r) = \sum_{i=0}^{\infty} a_i r^i = a_0 + a_1 r + a_2 r^2 + \dots$$

where 'r' is the distance from the center. Expressing the Laplacian ∇_2^2 in polar coordinates leads to the expression

$$\Delta = \nabla_2^2 p = \frac{1}{r} \frac{\partial}{\partial r} \left(r \frac{\partial}{\partial r} \sum a_i r^i \right) = \sum_{i=1}^{\infty} i^2 a_i r^{i-1} = \frac{a_1}{r} + 4a_2 + 9a_3 r + \dots$$

Thus intensity is independent of 'r' only if

$$p(r) = a_0 + a_2 r^2$$

However, from observations, the pressure varies approximately linearly with distance from the center of a low so that isobars are spaced uniformly; in that case

Table D.2

Schallert's (1962) classification of surface lows
by trajectory and intensity

	Moderate to Strong		Weak
Long Trajectory	A1	A2	C
No or Short Trajectory	B		D

where A1 have a single maximum of intensity
A2 have a double maximum.

$$p(r) = a_0 + a_1 r .$$

Using finite differences, the intensity depends thus on the
grid length 'r' used: $g = \frac{a_1}{r} .$

D.3 Satellite Data

The automatic picture transmission (APT) satellite images used in this study were received and imaged onto 35-mm film by the University of Alberta satellite receiving station. The "weather" satellites transmitting the real-time APT data received by the University are owned and operated by the National Oceanic and Atmospheric Administration (NOAA), formerly the Environmental Science Services Administration (ESSA), of the United States Department of Commerce. The images used in this study are from two series of satellites:

- (a) the Television and Infra-red Observing Satellite (TIROS) Operational Satellite (TOS) series, and
- (b) the Improved TOS (ITOS) series.

The last operational APT TOS satellite, ESSA 8, used a vidicon (TV) camera to produce images of the Earth in the visible spectrum (NESC, 1969a). In the ITOS series (NOAA 2 and later spacecraft) the vidicon camera is replaced by a scanning radiometer which detects radiation from the Earth in the far infra-red (10.5 to $12.5 \mu\text{m}$) as well as in the visible (0.5 to $0.7 \mu\text{m}$) range of the spectrum (Schwalb, 1972). The additional IR image permits a new dimension to interpretation --- the height of cloud tops observed by reflected solar radiation (visible image) may be estimated using the IR image. Since infra-red radiation is emitted from the Earth's surface and clouds, the IR image is independent of solar illumination. Thus an image is possible at night and at high latitudes during the winter season. Case 3 uses images from NOAA 2 and 3 of the ITOS series.

The TOS and ITOS series of weather satellites that transmit APT data are placed into morning descending sun-synchronous near-polar orbits. For a morning descending orbit, the satellite crosses the equator southbound during the morning, approximately at 0830 to 0900 local time. If the satellite orbital plane with respect to the stars rotates 360 degrees per year, and in the same direction as the Earth revolves around the sun, the orbit is said to be sun-synchronous, and the local equator crossing time will

remain constant. The selection of the orbit for weather satellites (given by Widger, 1966) is constrained by the following parameters:

- (a) sun-synchronous orbit,
- (b) overlap of images at the equator on successive orbits,
- (c) orbital decay --- the minimum satellite height is about 150 nmi (280 km),
- (d) ground resolution.

Table D.3 gives the orbital parameters for the weather satellites used in this study.

Gridding

To facilitate interpretation of the images, especially those without any identifiable landmarks, they must be "gridded", i.e. latitude and longitude lines, coastlines, political boundaries, etc. must be marked on the image. For TOS ESSA 8, the latitude/longitude of the satellite subpoint, indicated by the fiducial mark (+) in the center of each TV frame, may be determined if the picture time is known (refer to NESR, 1969a). The imaging system at the University recorded the time of the start of each frame onto film. Using formulae given by Bonner (1965, 1969), latitude/longitude intersections may be calculated for the complete frame. For ITOS imagery, time marks are manually inserted into the image, and the time written into a notebook. Each mark appears as a dark line across the image. Using formulae given by Reinelt, et al. (1975, part III)

Table D.3

Orbital Parameters for Weather Satellites

Parameter	ESSA 8	NOAA 2	NOAA 3
Period (minutes)	114.7	115.0	116.2
Height (km)	1450	1460	1510
Inclination (degrees)	101.6	101.7	102.0
Longitude/Orbit	28.67	28.75	29.04
Local Time Descending	0955	0850	0830
	(May72)	(Nov73)	(Nov73)

The ascending node (i.e. the northbound equator crossing) of the next orbit occurs 'Longitude/Orbit' degrees to the west.

based on work by Madden & Parsons (1973), similar gridding may be done for scanning radiometer images.

In all gridding calculations, spacecraft attitude errors (i.e. in roll, pitch, and yaw) are assumed to be zero. Actual attitude errors may be $\pm 0.5^\circ$. A pitch or roll error equal to 0.5° results in a gridding error of about

$$1470 \text{ km} \times 0.5^\circ \times \frac{\pi}{180^\circ} \simeq 13 \text{ km}$$

at the subpoint. As a first approximation, the Earth is assumed to be a sphere rather than an oblate spheroid, and the satellite orbit circular rather than elliptical. The gridding of ESSA 8 images includes the small corrections due to spheroidal Earth and elliptical orbit. If surface landmarks are visible, the grid may be adjusted to correct for the above assumptions.

Srinivasan (1970) analyzed 216 ESSA 8 TV frames to determine gridding errors due to

(a) lens and electronic distortion, and

(b) spacecraft attitude errors.

Latitude and longitude errors were within 0.2° (12 nmi, 22 km) in 60 percent of the frames for (a) and 75 percent for (b), and within 0.5° (30 nmi, 56 km) in 95 percent for (a) and almost 100 percent for (b). The extreme error is 100 to 200 km: 70 to 140 km attitude error plus a 50 to 70 km distortion error.

Resolution

The resolution of the satellite sensor determines the pixel size: the smallest observable cloud or ground feature on the images. Increasing the resolution decreases the pixel size and vice versa. For the TOS series (ESSA 8), the resolution (NESC, 1969a, page 7) is

(a) 2.8 km (1.5 nmi) at the subpoint indicated by the center fiducial mark (+), and

(b) 9.0 km (4.8 nmi) at the edge of the frame.

For the ITOS series (NOAA 2 and NOAA 3), the resolution (Schwalb, 1972, page 12) is

(a) at the subpoint, 7.5 km (4 nmi) for the IR image and 4 km (2 nmi) for the VISible image. Since the satellite travels 7.5 km per scan, a gap of 3.5 km occurs between successive 4 km wide VISible scans;

(b) at a distance of 1670 km (900 nmi, 15° arclength) from the subpoint, 15 by 22 km (8 by 12 nmi) for the IR image and 7.5 by 15 km (4 by 8 nmi) for the VISible image.

The processes of signal transmission, reception, and

imaging onto film, followed by reproduction onto photographic paper decreases the resolution --- the pixel size increases. Each of the processes introduces noise and signal degradation. The effective resolution of the ESSA 8 prints is probably 3 times less than that given above and for NOAA prints, 1.5 times less. At the subpoint, on ESSA 8 mosaics, the resolution is about 8 km; on NOAA mosaics, about 12 km (IR), 6 km (VIS).

Resolution is important in determining the lower limit for wavelengths of lee-wave clouds which may be observed on the images. A wavelength of 2 pixels (one cloudy, one clear) would be the minimum giving a lower limit of about 14 km on the visible mosaics. This wavelength would only be detected if a large area of lee-wave clouds formed and the contrast (brightness difference) between cloud and no cloud was large. A more realistic estimate of minimum observable wavelength would be 3 pixels, about 21 km on visible mosaics.

As noted in Section A.4 (Mesoscale Waves) typical tropospheric wavelengths are 5 to 30 km. Assuming a constant frequency distribution, only 40 percent of the mountain waves would be observed on the mosaics used for the case studies. However, the frequency distribution peaks between wavelengths of 5 to 10 km, so a more realistic estimate would be 10 percent or less. Using higher resolution VHRR imagery (1 km resolution), all 15 areas of waves over B.C. and Washington State on two dates had wavelengths of

10 km or less.

Interpretation

Analysis of the cases assumes the reader is familiar with interpretation of cloud and surface features on the images. The following publications give examples for the analysis of weather satellite images:

- (a) NESC, 1969a: ESSA Direct Transmission System Users Guide,
- (b) NESC, 1969b: Application of meteorological satellite data in analysis and forecasting,
- (c) WMO, 1966 and WMO, 1973a: The use of satellite pictures in weather analysis and forecasting,
- (d) Barrett, 1974: Climatology from Satellites.

Caution should be exercised when estimating cloud cover. Young (1967) shows that the standard deviation of the estimates of 10 people analyzing satellite photographs is a maximum of about 2/8 when the estimated cloud cover is 4/8. The standard deviation decreases towards clear (0/8) and cloudy (8/8) conditions. Using a paper-cloud test, a tendency exists to overestimate cloud coverage by 1/8, with the greatest error occurring for cloud cover in the range 3/8 to 5/8. Particularly important is the overestimate of 2/8 for convective-type patterns.

Shenk & Solomonson (1972) in considering sensor sensitivity and spatial resolution, come to the same general result: cloud cover is overestimated. When using a cloud/no

cloud brightness threshold, the estimate of cloud cover may be corrected if 'R', given by

$$R = (\text{cloud size}) / (\text{areal resolution of sensor})$$

is known. If 'R' is 200, the estimate will be high by less than 10 percent. Using a clear/partly-cloudy/cloudy weighted criterion, a cloud/no-cloud, and a partly-cloudy/cloudy brightness thresholds are required. The former value is particularly difficult to obtain over land masses, especially mountainous and snow or ice-covered regions. Using the double threshold, for 'R' greater than about 20, the cloud estimate is very close to the true percentage. As 'R' decreases, the estimate approaches 50 percent for all cloud amounts.

A complicating factor is the dependence of reflection of solar radiation on four parameters: cloud thickness, solar zenith angle (i.e. solar illumination), and the two satellite viewing angles. Park, et al. (1974) and Kaveney, et al. (1977) show that cloud brightness (i.e. reflectance) is related to cloud thickness by the following relation:

$$\text{Brightness} = A \cdot (\text{thickness})^B$$

where 'A' and 'B' are constants for a particular cloud type, i.e. tropical, mid-latitude frontal, etc. Ruff, et al. (1968) give figures of reflection versus solar zenith angle and the two satellite viewing angles.


D.4 Conventional Maps

Combining several ESSA 8 frames or NOAA images produces a cloud mosaic covering western North America and the adjacent Pacific Ocean. For ease of comparison, the data on the following maps normally used at weather offices was replotted onto the projection of the Earth as seen by the satellite:

(1) Surface Map --- The 1800Z analysis from the Edmonton Weather Office and Arctic Weather Center was selected as it is the six-hourly surface synoptic map near the time of the satellite data (1700 to 2000Z). The following information was transferred:

- (a) reduced-to-sea-level station pressure isobars at 4-mb intervals,
- (b) analyzed surface frontal positions,
- (c) total cloud cover and cloud types at selected stations, and
- (d) precipitation areas.

(2) 700-mb Map --- To represent the contribution of warm or cold air advection to the vertical motion field in the lower atmosphere, the 1200Z 700-mb CMC chart was used. Station data --- wind direction and speed (knots), temperature ($^{\circ}\text{C}$), and dew-point depression ($^{\circ}\text{C}$) --- were plotted before the geopotential height contours (decameters) and isotherms ($^{\circ}\text{C}$) were transferred. Canadian upper-air station observations were checked using the Summary of Canadian Upper Air

Stations. Stations missing on the CMC analysis are marked with a circle around the station dot (). Note, however, that any discrepancy between the analysis and the station data has not been corrected.

(3) 500-mb Map --- When the 500-mb chart is contoured with isopleths of height and absolute vorticity, it may be used as a mid-level indicator of the contribution by vorticity advection to the vertical motion field. Normally the CMC 1200Z (early) 500-mb analysis (height + vorticity fields) would be used: this chart is not archived, thus not readily available. The analysis of the data-sparse North Pacific is often suspect --- especially when Ship PAPA data is missing.

To produce a 500-mb chart, an objective analysis of the 500-mb station data was done using a computer program adapted from that used by Hume (1975) and originally developed by Glahn & Hollenbaugh (1969). "Bogus" stations were added in data-sparse regions: two in the Northwest Territories, the height, and wind direction and speed estimated using the 500-mb chart analysed by the Edmonton Weather Office; 12 over the Pacific Ocean, based on a hand analysis using as guides the cloud pattern on the satellite mosaics, the 500-mb map in the Daily Weather Maps issued by NOAA (United States Department of Commerce), and Ship PAPA and coastal station data. Hayden (1968) and Nagle & Hayden (1971) have investigated the application of satellite images in correcting the 500-mb height field.

Absolute vorticity may be calculated approximately using Equation B.11, the absolute geostrophic vorticity equation:

$$\begin{aligned} Q_g &= f + \frac{g}{f} \nabla_p^2 Z \\ &= f + \frac{gm^2}{fd^2} \nabla^2 Z \end{aligned} \quad (\text{D.1})$$

where m = map factor for a polar stereographic projection true at 60°N

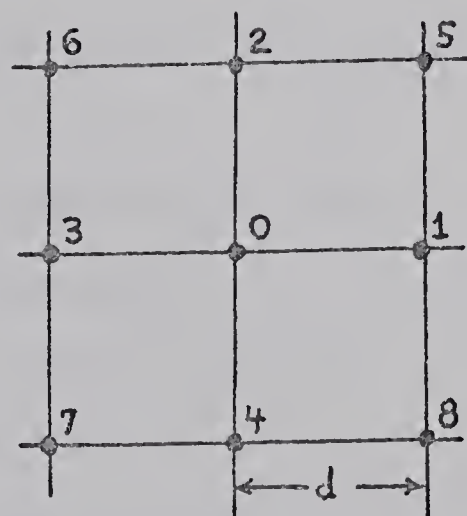
$$= \frac{1 + \sin 60}{1 + \sin \phi} = \frac{1.86603}{1 + \sin \phi}$$

$d = 200 \text{ km} = \text{grid spacing}$

$f = \text{Coriolis parameter} = 2\Omega \sin \phi = 1.4584 \times 10^{-5} \sin \phi$

$$\nabla^2 Z = \frac{(Z_5 + Z_6 + Z_7 + Z_8) + 4(Z_1 + Z_2 + Z_3 + Z_4) - 20Z_0}{6}$$

is the nine-point finite difference formulation of the Laplacian operating on the height field, the numbering system given by the sketch on the right. Compared with the five-point formulation, the nine-



point Laplacian reduces truncation errors (order Z^4 compared to order Z^2) and produces a smoother field.

Only the Laplacian of the height field $\nabla^2 Z$ was computed and plotted on the 500-mb chart as dashed lines at 15-meter intervals with the zero line in heavy dashes and

labelled '0'.

Use of the geostrophic approximation in calculating vorticity is only valid if the divergence of the real wind is zero or negligibly small. Moreover, the value calculated is numerically correct only if the height contours have parabolic shapes.

D.5 Vertical Time-sections

The sequence of weather at a station is easier to follow when parameters such as temperature, humidity, cloud, and winds are displayed on a pressure-time plot. This gives the sequence of air motion at a fixed station. Vertical time-sections were prepared for the following four areas. In each area, the station name, state/province, letter identifier, and latitude/longitude are listed.

(a) far pre-mountain:

Ocean Station (Canadian Weather Ship) PAPA, 50N145W

(b) pre-mountain:

Annette Island, Alaska, ANN, 55.03N 131.57W

Port Hardy, B.C., ZT, 50.68N 127.37W

Quillayute, Washington, UIL, 47.95N 124.55W

(c) intermountain basin:

Prince George, B.C., XS, 53.88N 122.67W

Vernon, B.C., WVK, 50.23N 119.28W

(d) post-mountain:

Fort Nelson, B.C., YE, 58.83N 122.58W

Edmonton (Stony Plain), Alberta,

***, 53.55N 114.10W

The time section for each station covers the period from 12 hours before the first satellite mosaic to 12 hours after the last, and a vertical section between the surface and 300 mb. The variable used to represent air-mass properties is the equivalent potential temperature θ_e , drawn at two-degree intervals in the troposphere, calculated from the equation

$$\theta_e = T \left(\frac{1000}{P} \right)^K e^{\left(\frac{Lr}{c_p T} \right)} \quad (D.2)$$

where θ_e and T are in degrees K and 'r' is the mixing ratio in gm water/gm dry air. A thick solid line denotes the tropopause.


The equivalent potential temperature θ_e is a conservative property for the atmospheric processes of dry and moist adiabatic motions and loss of condensed water vapor by precipitation but not for

(a) turbulent mixing and convection (θ_e becomes constant in the mixed layer)

(b) addition of water vapor from falling precipitation (θ_e increases),


(c) surface-boundary-layer effects of evaporation and heating (θ_e increases) or condensation as dew or frost and

cooling (θ_e decreases).

Observed winds at 850, 700, 500, and 300 mb are plotted. The letter 'M' indicates only the wind direction and speed are missing. Dotted lines are 10°C dew-point depression contours. Stippled areas () are cloudy layers determined using the following criteria given in Rogers & Sherr (1966, Appendix A) for saturated (cloudy) conditions versus dew-point depression as a function of pressure:

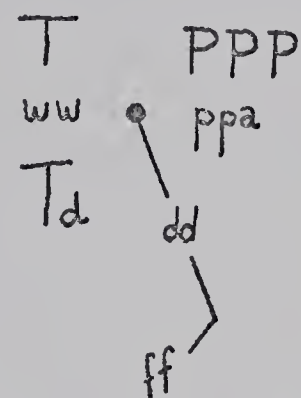
Pressure Level (mb)	<800	700	600	500	400	300
Dew-point Depression ($^\circ\text{C}$)	2	3	4	5	6	7

At any level, a depression larger than that given indicates unsaturated air, hence a cloud-free layer. Moisture content of the air is not reported when the temperature becomes less than -40°C ; the stippled areas in the upper troposphere end with a question mark (?).

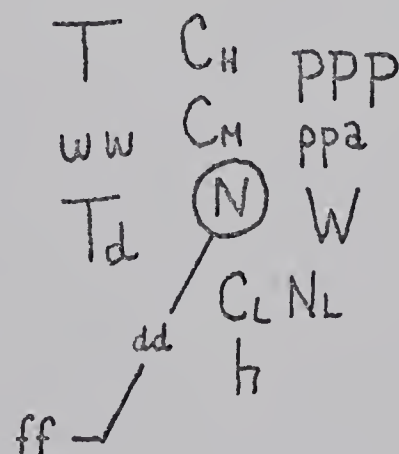
Reports of surface weather are plotted above the vertical time-section. For Case 1, a cloud time-section for the upper-air station or a selected nearby station gives hourly cloud opacity (in tenths summed from the surface, ten-tenths denoted by the symbol ), cloud base (in thousands of feet [kft] above ground level), and cloud type. Clouds above 18 kft are entered at 18 kft. Since cloud opacity is summed from below, that for upper cloud layers may be overestimated. This is particularly true for cirrus clouds. Cloud observations were extracted from the hourly

surface aviation weather reports which do not distinguish between the thickness of altocumulus clouds: thick AC ($\overline{\omega}$), thin AC (ω), patchy AC ($\overline{\cup}$), or banded AC ($\overline{\omega}$).

Underneath the cloud time-section, station air temperature 'T' ($^{\circ}\text{C}$), dew-point temperature 'T_d' ($^{\circ}\text{C}$), wind direction 'dd' and speed 'ff', present weather 'ww', barometric pressure 'PPP' (tenths of millibars with leading 9 or 10 omitted), and pressure tendency 'ppa' (tenths of millibars in last 3 hours and pressure characteristic) [see station model at right] are plotted at 6-hour intervals.



For Cases 2 and 3 (and UIL, Ship PAPA in Case 1), only the 6-hourly station weather is plotted above the vertical time-section. Total cloud amount 'N', observed low 'C_L', middle 'C_M', and high 'C_H' clouds, opacity 'N_L' and coded height 'h' of the lowest cloud layer, and past weather 'W' [see station model at right] are added to the model. In all 3 cases, the water temperature ($^{\circ}\text{C}$) at Ship PAPA is given in parenthesis below the dew-point temperature.



Because of the difficulty in determining cloud

amounts at night, especially cloud above 8 kft, cloud time-sections were not drawn for Cases 2 and 3 (14 hours darkness, 10 hours light). The reliability of lower-cloud amount estimates is increased at stations near or in large cities (e.g. Edmonton, Vancouver) as the clouds are illuminated by the diffuse light from the city, mainly from street lighting. Cloud time-sections are given for Edmonton City (XD) for Cases 2 and 3.

CHAPTER E

CASE HISTORIES

CASE 1: 19-22MAY72

E.1 Synoptic Situation

At 500 mb (refer to Figure E.1) the long-wave ridge position is over central Canada (along 100W) with troughs at 60W (east coast of Canada) and 140W (Gulf of Alaska). During the two-week period, two lows crossed the northern United States at a speed of 10 kts, along the northern limit of the mT air mass near the surface. On MAY 19 and 20, the major feature at 500 mb is the simultaneous development of cut-off lows along the west and east coasts of the United States near 35N. Weak surface lows and areas of precipitation reflect the presence of these upper systems.

At the surface (refer to Figure E.2) 75 percent of the lows on the map are Type C or D, reflecting the weak baroclinity of the atmosphere during the summer season. This may also be seen in the vertical time-sections of summer Case 1 versus winter Cases 2 and 3 --- cold frontal zones in Case 1 have weaker temperature gradients and do not extend to the tropopause. Lows of Type C form in the lee of the Rocky Mountains from 45N to 65N and move eastward (with one exception) into the upper ridge position. The short-

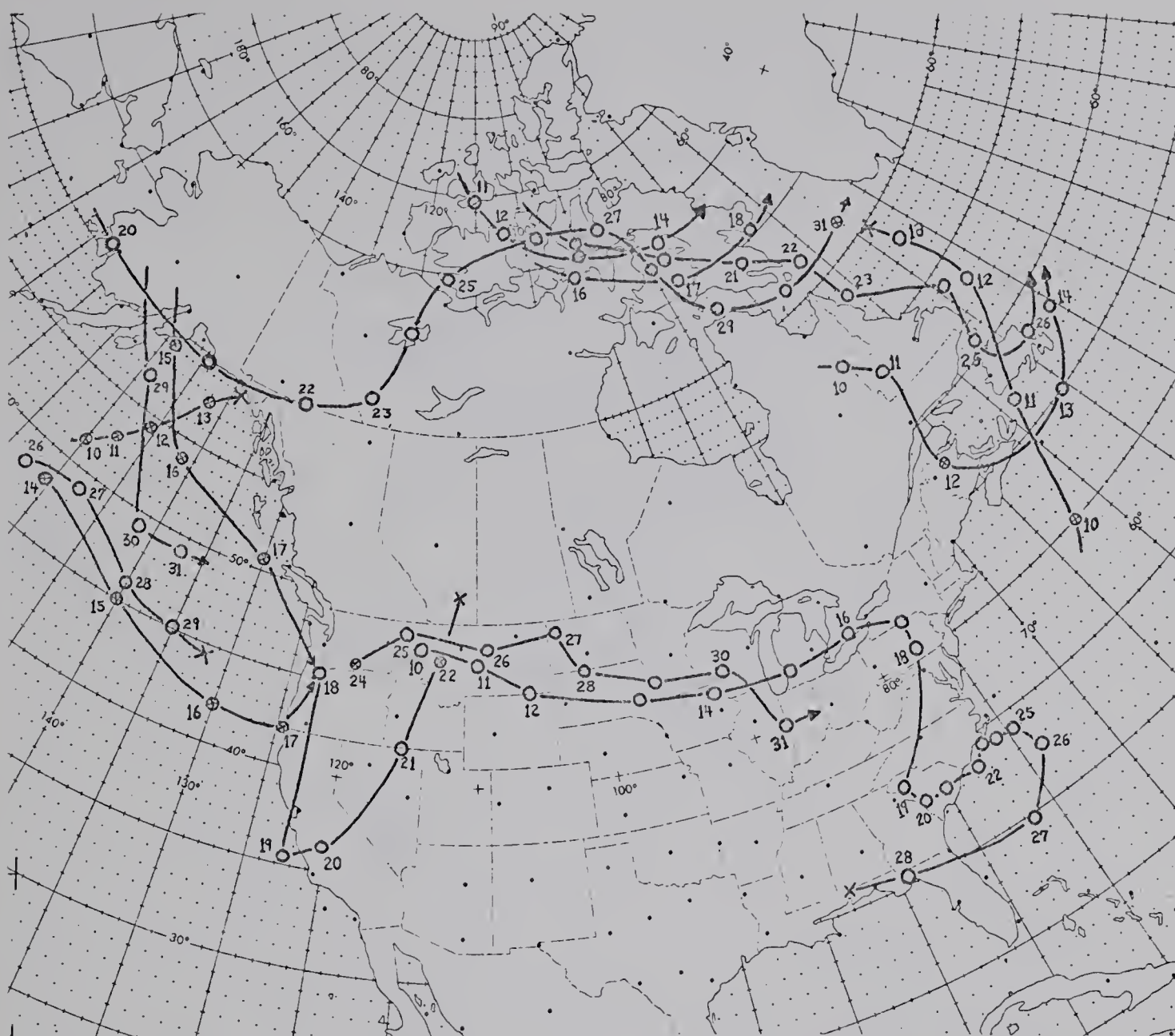


Figure E.1. Track and 1200Z position of 500-mb troughs and lows for the period 10-31 MAY 72.

wave troughs at upper levels associated with these lows are weak and are not plotted on the 500-mb chart (Figure E.1). Lows which form to the lee of the Mackenzie Mountains (65N) and move southeast define the southern limit of the Arctic air mass. Those that cross the southern Prairies and the northern United States are associated with waves on the Polar and maritime Arctic fronts.

At the start of the period (19MAY) a cut-off cold

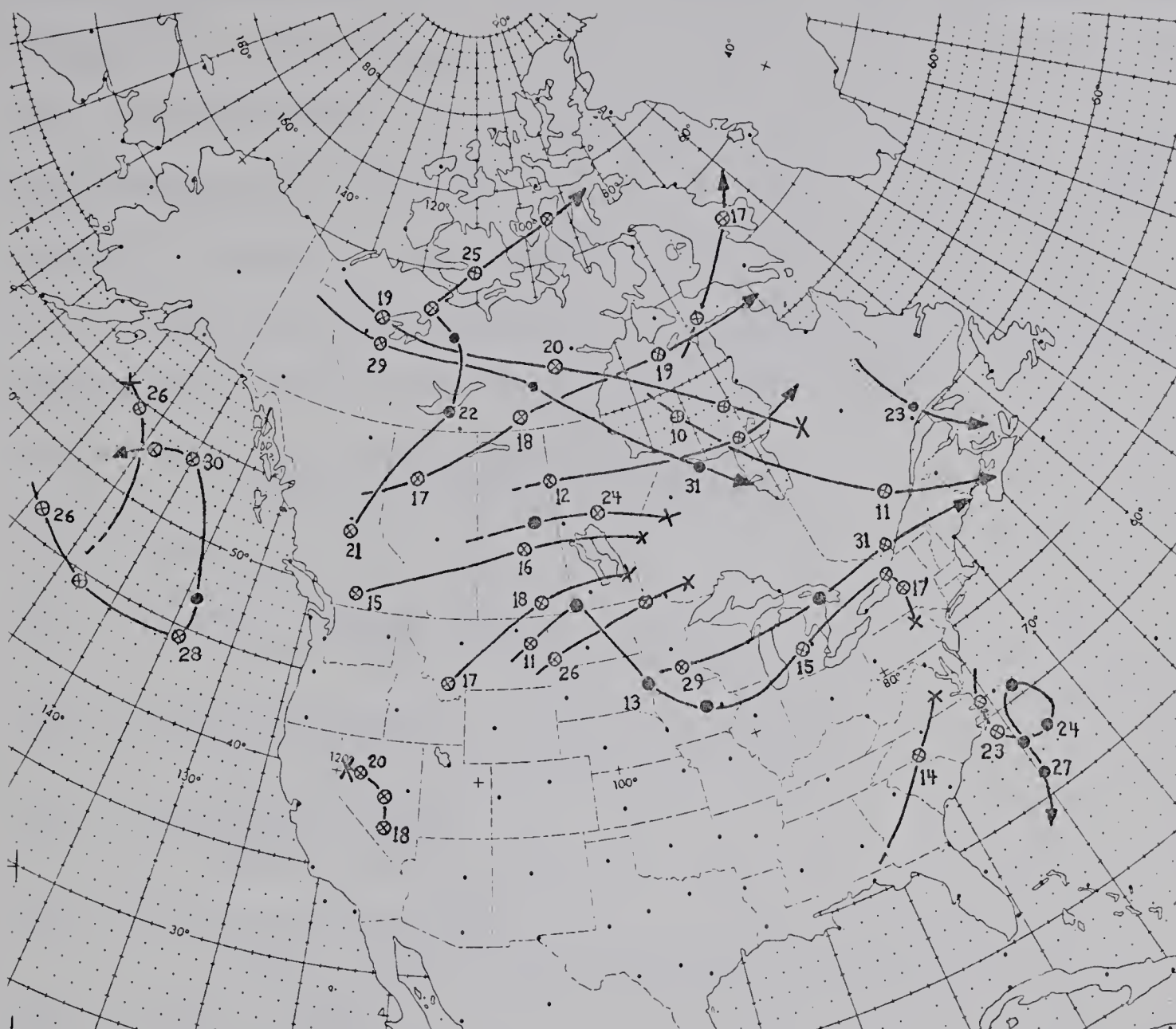


Figure E.2. Track, intensity, and 1200Z position of surface lows for the period 10-31 MAY 72.

low lies along the California coast with an upper ridge over the eastern Pacific and western Canada. With the approach of an upper-level low on 20 MAY along 60N, the upper ridge collapsed, shifting eastward to lie along 100W. At the surface, the high over western Canada is replaced by a thermal low over central B.C. The frontal cloud in the Gulf of Alaska along the western side of the upper ridge on 19-20 MAY moves southeastward to the B.C. coast. By 22 MAY, the cold

low over California has moved northward and rejoined the Westerlies. The frontal zone crosses the Cordillera and lies southward from a moderate-intensity surface low which has developed as a thermal low to the lee of the Rocky Mountains, in advance of the frontal zone and the upper low.

The following vertical time-sections and cloud time-sections are used in the analysis of this case:

Figure Vertical Time-section Station
Cloud Time-section Station(s)

- E.3 Ocean station (Ship) PAPA
- E.4 Annette Island (ANN)
Prince Rupert (PR), Sandspit (ZP)
- E.5 Port Hardy (ZT)
Port Hardy (ZT), Vancouver (VR)
- E.6 Quillayute (UIL)
Estevan Point (EP)
- E.7 Prince George (XS)
Prince George (XS), Williams Lake (WL)
- E.8 Vernon (WVK)
Penticton (YF)
- E.9 Fort Nelson (YE)
Fort Nelson (YE), Fort St. John (XJ)
- E.10 Edmonton (Stony Plain)
Edmonton International (EG), Calgary (YC)
- E.2 19MAY72: Notes, Comments, and Observations
Refer to Plate 1 and Overlays 1a (SURFACE),
1b (700 mb), and 1c (500 mb).

Ocean station PAPA is missing on the 700-mb analysis: analyzed height and temperature fields are 4 dam and 2°C too high. Since the initial guess of the computer anal-

ysis is its 12-hour prognostic, the "prog" is slow in moving the upper trough onto the coast.

The frontal cloud band lies along the analyzed position of the surface front --- from the Pacific to the Alaska Panhandle, thence over the mountains into the southern Northwest Territories. The southern portion 35N158W - PAPA - 53N142W is bright (thick) OVC multilevel cloud. No PVA occurs on the 500-mb chart to produce ascent; the cloud is probably due to convergence along the front and to convection. According to Ship PAPA vertical time-section, the air mass ahead of the front (at 19/1200Z) is potentially unstable below 850 mb. The bright cloud band associated with the frontal passage at PAPA just before 19/1800Z (near the time of mosaic) is missed completely by the upper-air soundings.

To the east of the frontal band, OVC/BKN ST/SC occurs below the inversion at 850 mb; above the inversion, the air mass is very dry. Note that the ocean surface stabilizes the air mass --- the water temperature (6°C) is lower than air temperature (8°C).

Immediately behind the front, a BKN band of less bright SC/CU (with possible embedded TCU/CB) and AC lies through 49N150W. The ship at 50N149W reports OVC SF; Ship PAPA reports OVC SF for the entire period of frontal passage --- all very helpful in ascertaining amount, type, and height of middle and high clouds. After the frontal passage, Ship PAPA vertical time-section at 20/0000Z indicates

cloud below 700 mb. This band gives the thunderstorm reported in past weather at PAPA at 20/0600Z and is associated with the deepening of the cold air mass: an upper cold front. Both the surface cold front (before 19/1800Z) and the upper cold front (before 20/0600Z) produce pressure rises and windshifts. The veering of the wind is much more dramatic for the upper front, from SW to NW, compared to the shift from S to SW for the surface front.

To the west, subsidence due to cold air advection (CAA) produces a band of clearing: only SCT CU is present. This clear slot is followed by SCT CU/SC+TCU and showers (45N160W) caused by convective instability of cold surface air over warmer water: Ship PAPA air temperature decreases to 5°C, the water temperature is 7°C.

Between 53N142W and the coast (57N135W) the frontal band is less bright OVC low and middle cloud, which abruptly terminates in a band of cloud over the snow-covered Coast Mountains. Orographic ascent in the southwesterly flow gives an area of precipitation along the coast. Along the southern edge of the cloud band, the ANN vertical time-section shows only low and high clouds; the 700- to 400-mb layer is very dry. Further north, Yakutat (59.5N140W) and Whitehorse (61N135W) have small dew-point depressions at 700 mb, indicating middle cloud. Over the Cordillera, the band becomes a large area of mid-level lee-wave clouds with OVC orographic clouds over the higher terrain of the Selwyn (62N129W) and Pelly (61.5N132W) Mountains. Approximate

wavelengths of the lee waves are 22 and 25 km.

Low-level cloud OVC ST/SC over the ocean is blocked by the Coast Mountains: only SCT SC is reported to the lee. Anticyclonic bands of CI can be seen at 62N135W; the CI probably extends as far south as 56N.

To the lee of the Mackenzie and Rocky Mountains (along 120W) the skies are CLR/SCT CU+AC; the clearing is due to subsidence from downslope flow, and NVA at upper levels, downstream of the ridge line along 128W.

Strong cross-barrier flow (50 kts at 700 mb) over the Coast and Mackenzie Mountains produces on the surface chart a ridge upstream of the barriers and a trough downstream. The trough to the lee of the Mackenzie Mountains forms a moderate-intensity Type B surface low. The low pressure is the result of heating from orographic subsidence at low levels, subsidence at upper levels (though the pressure decrease due to heating is partly compensated by a rise from NVA) and WAA at mid-levels (700 mb). The subsidence is so complete that the southern front does not have a cloud band. A band of BKN AC reforms northeast of the surface warm front 62N105W - 65N115W. Bands of BKN CC+AC can be seen faintly extending southward from 60N110W. In this clear area, surface landmarks are visible: the ice covered Lake Athabasca (59N110W) Great Slave Lake (62N115W) Lac la Martre (63.5N118W) and Great Bear Lake (66N120W) and the snow-covered Horn Mountains (62.5N119W).

The cut-off cold low at 38N124W (500-mb position)

with the surface low at 41N120W lies to the south of the west-to-east upper ridge and surface high through the eastern Pacific and western Canada. In the north and northeast quadrant of the low (45N110-120W) in the easterly low-level flow, a bright multilevel OVC cloud band covers the mountainous terrain of eastern Oregon and northern Idaho, the northern edge lying along a weak 500-mb ridge line. The band extends eastward from the Rocky Mountains (47N107W-53N95W) as bright BKN/OVC low and middle cloud with embedded TCU/CB in the low-level (surface to 700 mb) easterly flow south of the surface high over the Prairies. This section of the band marks a weak stationary front which has not been analyzed on the surface chart. Orographic ascent over the plains intensifies along the east slope of the Rocky Mountains, broadening the cloud band and giving an area of precipitation over the barrier. CI plumes (49N109W) extend eastward in the westerly flow at high levels. Again a surface ridge and trough occur across the barrier but, because of the easterly flow, the locations are reversed from that expected, i.e. the ridge occurs on the eastern slopes. The westward advection of moisture at 700 mb has extended the band over the mountains as far west as Oregon.

Around the center of the surface low over the interior plateau, the cloud consists of SCT/BKN TCU/CU plus SCT AC, the convective cloud being caused by instability in the cold air mass produced by solar heating at the surface. The western edge of the upper cold low is defined by a

cyclonically curved band of CS (?) at 37N126W which lies over BKN SC.

The clear area from over the ocean 40N130W to over land 60N110W (surface stations report only 1/10 CU/AC) is due to subsidence in the upper ridge, combined with low-level divergence from the surface high. Dew-point depressions throughout the troposphere at Edmonton, XS, WVK, UIL, and ZT at 20/0000Z are greater than 10°C. The white patches in the clear area are the dendritic patterns of snow-covered mountain ridges, the Coast Mountains (51N124W) and the two parallel NW-SE ranges of the Rocky Mountains (52N118W). Low-level off-shore flow of warm, dry continental air (air and dew-point temperatures at UIL are 24°C & 2°C; at EP, 16°C & 11°C) produces the clear area over the ocean.

BKN SC/CU at 55N102-111W lies downwind of a north-to-south 500-mb trough line through 112W. From the Edmonton vertical time-section, the trough corresponds to the maximum depth of the cold air mass or, alternatively, the leading edge of the warm front at upper levels of the troposphere. The cloud in the cold air mass is formed by convective instability from solar heating of the moist air at the surface and by PVA ahead of the trough.

E.3 20MAY72: Notes, Comments, and Observations

Refer to Plate 2 and Overlays 2a (SURFACE), 2b (700 mb), and 2c (500 mb).

Again ocean station PAPA (50N145W) is missing on the

700-mb chart: height contours and isotherms are in error by 4 dam and 6°C respectively. The computer prog is continuing to retard the eastward motion of the approaching trough and the subsequent breakdown of the ridge that stretches into western Canada.

The frontal cloud band has moved southeastward 5.5 degrees in 24 hours at 45N (giving a speed of 14 kts) and now lies along 40N145W - 45N140W - 57N133W (on coast). The brightness of the cloud has decreased significantly from that on 19MAY. This change in brightness, i.e. thickness, reflects the change in surface pressure pattern over the 24-hour period: the high-pressure center and surface ridge are now behind the front rather than ahead. The surface flow ahead of the front is now northwesterly rather than south to southwesterly: the flow of potentially unstable air from the south has ceased. The position of the surface front was not analyzed over the Pacific Ocean but has been added on the basis of the cloud pattern on the satellite mosaic.

The brightest cloud along the band of OVC SC/ST BKN/OVC AS/AC (with possible CI) occurs at 50N140W. There appears to be a weak circulation center (low ?) at 47N142W with an occluded wave ahead of a short-wave trough approximately NW-SE through 40N145W. To the south, the cold frontal cloud band is very narrow and thin, probably consisting only of BKN/OVC ST/SC. To the west behind the cold front, BKN SC and a comma-shaped cloud of BKN SC+AC

(45N146W) east of an upper-level trough along 148W. The trough corresponds to the maximum depth of cold air (to 450 mb) which passes Ship PAPA (50N145W) before 21/0000Z.

Between the wave and the coast, OVC ST/SC BKN middle cloud, probably some CI as well. Note: PVA at 500 mb is nonexistent over the entire length of the band, except to the northeast of the wave where cloud brightness decreases. This is the result of poor bogus data; the trough line was to be farther southwest.

Ahead of the front, the BKN/OVC SC band (along 40-50N137W) is similar to that of 19MAY. In the cold air mass behind the front (50N150W), SCT SC/CU with no clouds occurring in the very dry air above 850 mb (refer to PAPA vertical time-section). Ships report BKN/OVC SC. Much of the cloud must be thin and will not appear on the images. Only the thicker, more reflective (i.e. brighter) cloud is obvious on the background of thin cloud over the dark ocean surface.

Along the coast, the cloud band appears much brighter because of the snow-covered Coast Mountains (58N133W) and the orographic clouds produced in the ascending southwesterly flow. Precipitation occurs north of the front (58N135W) as well as deep in the cold air mass along the Alaskan coast at 60N145-155W in the southerly orographic flow at 700 mb.

To the lee of the Coast Mountains, there is again OVC orographic cloud over the Pelly and Selwyn Mountains,

with BKN cloud in the inter-mountain valleys. To the south of the surface front, there is BKN/SCT AC; to the north, BKN SC in the cold air mass along with BKN AC at higher levels.

The large area of lee-wave clouds no longer exists: lee waves of 15-km wavelength are faintly visible at 59N128W. The cloud associated with the TROWAL on the surface chart at 60-63N130W can not be discerned among the orographic clouds over the Cordillera.

To the lee of the Rocky Mountains, the low pressure center has remained stationary and has decreased in intensity. The 500-mb ridge has flattened, so the NVA area no longer exists and the 700-mb flow has weakened from 50 kts to 25 kts --- thus heating due to subsidence will be less. The upwind ridge and lee trough no longer appear on the surface chart.

Cloud again reforms to the northeast of the low center and the warm front: an OVC/BKN AC band lies along 65N120W - 62N110W. To the west, low-level subsidence to the lee of the Mackenzie Mountains again clears or prevents cloud forming along the southern cold front. Farther north at 65N123W, BKN AC reforms immediately beyond the lee clearing.

The cut-off cold low over California has remained almost stationary, while the surface low has moved northward with an intensified trough extending northwest along the B.C. coast. The easterly flow of 20 kts at 700 mb is too

weak to cause a large pressure decrease to the lee of the Coast Range. The cloud in the northeast sector has been advected west & northwestward in the easterly flow, and now has invaded the CLR zone of 19MAY. BKN/OVC multilevel cloud --- SC, AC, and CS --- with embedded TCU now covers Washington and Oregon in a band NE-SW through 45N120W, and extends offshore to the west of the center of the upper low (40N125W). Using a 700-mb wind speed of 15 to 20 kts, the cloud edge would advance 6 to 8 degrees (360 to 480 nmi) per day, approximately the observed motion. Since both thermal advection at 700 mb and vorticity advection at 500 mb are very weak, the vertical motion field is also very weak. More important is the cloud formation from convective instability: BKN TCU is reported at YF (Penticton, see cloud time-section) as the edge advances northwestward through southern B.C. Off the edge of the mosaic, at 44N115W near the upper low center, surface stations again report SCT TCU/CB --- the cold air mass becomes convectively unstable when the surface is heated by solar radiation.

The easterly upslope flow to the east of the Rocky Mountains maintains the band of SCT CU/TCU BKN/OVC AC and rain.

The dendritic pattern of the Coast, Rocky, and Cassiar (57N127W) Mountains is again observable in the CLR area underneath the upper ridge. The ridge has intensified over the Prairies and weakened over the Pacific Ocean. The intensification caused by the advection of a warm and dry mT

air mass to the north of the ridge across northern B.C. (shown on the ANN and YE vertical time-sections) and then southward (shown on the XS and Edmonton vertical time-sections) so that at 500 mb, ZT, XS, WVK, Spokane, and Edmonton are in the mT air mass. Upper-air stations in the CLR area report very dry air from the surface to 300 mb, dew-point depressions averaging 15°C at 700 and 500 mb. The bright spot at 53N121W along the western slopes of the Cariboo Mountains is sunglint from Lake Quesnel.

E.4 21MAY72: Notes, Comments, and Observations

Refer to Plate 3 and Overlays 3a (SURFACE), 3b (700 mb), 3c (500 mb), and 3d (ω_{600}). Overlay 3d (from Schram, 1974, top half of Figure 23) gives the vertical motion ω at 600 mb in units of $\mu\text{b}\cdot\text{s}^{-1}$ using full surface boundary conditions (orographic ascent and frictional convergence are calculated using observed surface winds). Ascending motion is negative in the p-coordinate system. In the z-coordinate system, at 600 mb the vertical velocity 'w' ($\text{cm}\cdot\text{s}^{-1}$) is given by

$$W \approx -1.27 \omega .$$

Longitude lines on the mosaic along the coast are displaced about 2° eastward. Using the grid, latitude 50N longitude 125W is at 50N127W. Smaller gridding errors occur at 50N115W (displaced 1° east), 60N110W (displaced 0.5° north), and 60N95W (displaced 1° east). The lack of iden-

tifiable landmarks, especially over the Pacific Ocean, makes the detection of grid errors difficult. Longitude references along the coast will give the grid longitude with the correction as a superscript, e.g. 50N125W will be given as 50N127⁻²W.

A major change has occurred in the surface pressure pattern. A low which was initiated in central B.C. has moved northeastward to northeastern B.C. (58N120W) to the lee of the Rocky Mountains. Pressure falls of approximately 14 mb are caused by local (solar) heating below 700 mb (maximum temperature at YE on the 20MAY was 30°C) and by PVA ahead of the trough line along 54N115-125W. XS and YE vertical time-sections show tongues of warm air extending upward from the surface. Note: the low is not associated with a frontal (baroclinic) zone or with a pressure fall caused by cross-barrier flow --- the weak southerly winds almost parallel the Rocky Mountains. Nor is the low associated with a maximum of vertical motion: Overlay 3d shows weak ascent of $-1 \mu\text{b}\cdot\text{s}^{-1}$ over the center of the low; the strongest ascent is located to the northwest along the cloud band.

At upper levels, the ridge over B.C. has vanished, being replaced by a trough. A surface pressure fall of 14 mb corresponds approximately to a height fall of 12 dam. Actual height falls at 700 mb and 500 mb are

13 dam and 17 dam at XS and

7 dam and 7 dam at YE.

In the lower levels of the troposphere, XS has cooled during the 24-hour period, which increases height falls, while YE has warmed.

Over the ocean, the frontal band of BKN/OVC closed-cell CU/SC lies along 36N160W - 41N145W - 49N127-2W (on coast), at which point there is a break in the band. This break occurs at the 500-mb trough line which lies offshore and parallel to the Coast Mountains. Motion of the front (17 kts) is greatest at 50N, decreasing to 10 kts at 55N, and to zero to the southwest. Motion of the trough from about 148W on 20MAY is approximately 35 kts.

Because of subsidence caused by NVA, the air mass along the front at the coast is dry. The ZT vertical time-section indicates cloud below 850 mb and between 650 & 500 mb, in sharp contrast to the thick AS cloud along the front as it passes ANN. Orographic cloud covers both Coast Mountains and Vancouver Island mountains (49N127-2W). However, because of the upper-level trough, the thickness of the orographic cloud over the Coast Mountains has decreased: the dendritic pattern of the snow-covered mountains can be faintly seen through the cloud. Note: since the XT vertical time-section shows the frontal passage before 21/1200Z, the analyzed surface front position along the coast is incorrect. No ready reason can be given for the presence of the CLR area at 52N131-2W.

Subsidence in the westerly flow at 700 mb dissipates the cloud in the lee of the Coast Mountains (53N125-2W).

The frontal band reforms at 54N128-2W and continues northward in the southwesterly upper flow over the Cassiar Mountains, 57N128-2W. The band OVC AS/AC with ACC/CB along the eastern (leading) edge, produces an area of rain. The vertical motion field (see Overlay 3d) shows ascent of $2 \mu\text{b}\cdot\text{s}^{-1}$, produced in part by orographic ascent, but mostly by PVA downwind of the trough (refer to Schram, 1974).

The brightness of the cloud band increases along the east-to-west line through 60.5N127-134W, ahead of a weak trough at 500 mb and over the Pelly, Selwyn, and Mackenzie Mountains. The OVC thick NS cloud forms downwind of an ascent maximum ($-4 \mu\text{b}\cdot\text{s}^{-1}$). The broadening of the frontal band has the signature of a developing cyclone. If this is the same wave as that over the Pacific Ocean on 20MAY, the motion of the wave and the short-wave trough is about 35 kts. The cloud shield occurs in an area devoid of reporting stations; nearby stations report BKN AC/ACC.

To the east, the NS cloud deck extents to 125W, narrowing to a band of OVC/BKN bright (i.e. thick) AS/AC+CI downstream of the upper ridge. No subsidence clearing occurs to the lee of the Mackenzie Mountains because 700-mb wind speeds are weak --- less than 10 kts --- and the easterly surface flow gives orographic clouds; however, reported surface winds in the Mackenzie valley at Fort Simpson (62N121W) are northerly. The line 63N110W - 60N95W (on coast of Hudson Bay) defines the tree line: snow in the coniferous forest to the south appears darker than the snow-

covered tundra to the north.

Behind the cold front, SCT/BKN open-cell SC/CU/TCU is observed over the Pacific Ocean 40N160W - 55N132-2W (at coast), continuing northward over the Cordillera. This "clear" zone is associated with CAA at and below 700 mb. The vertical motion field shows maximum descent of $4 \mu\text{b}\cdot\text{s}^{-1}$ at 52N140W near the center of maximum CAA. The convective cells are smallest at this location. Farther into the cold air, behind the zone of CAA, BKN/OVC closed-cell CU/SC with SCT AC has formed giving showers. From Ship PAPA vertical time-section, though the cold air begins to shallow, the layer below 700 mb continues to cool. The near-surface layer (5°C) is colder than the ocean (7°C) and thus subject to becoming convectively unstable. The cyclonic, comma-shaped cloud at 57N141-2W is associated with the 500-mb trough southwest from the low center, while BKN SC+AC over the mountains at 61N143-2W is located at the center.

Cloud associated with the frontal passage at PR (Prince Rupert) and ZP (Sandspit, Queen Charlotte Islands, see cloud time-sections) is similar: increasing CI, SCT AC ahead of the front, then suddenly OVC in low SC at the frontal passage, and clearing to SCT SC. The ANN vertical time-section indicates frontal cloud extending throughout the troposphere. Differences at PR are due to orographic ascent on the Coast Mountains: rain occurs for 6 hours and post-frontal clearing is BKN SC rather than SCT/CLR. The frontal-passage cloud at ZT and EP (Estevan Point) is

similar to PR. Because of the upper-level trough, the cloud does not extend throughout the troposphere, and only drizzle falls from the low cloud.

Cloud associated with the cold low over the northwestern United States has continued to be advected north & northwestward and now merges with the frontal cloud band. An extensive area, from 40N120-125W to southern B.C. (51N117-1W - 49N123-1W), is covered with OVC AS/AC, with low level ST/SF in the band of precipitation. To the southeast (43N115W), BKN/OVC TCU/CB with OVC/BKN AC, the convective cloud is again caused by surface heating of the cold air mass by solar radiation. The cloud pattern is completely independent of the mountain ranges. The vertical motion field shows weak ascent of $-2 \mu\text{b}\cdot\text{s}^{-1}$ or less over the entire area; cloud formed by convective instability will persist as the air nears saturation.

The WVK (Vernon) vertical time-section and the YF (Penticton) cloud time-section show the northward advection of cloud and moisture. As noted on 20MAY (Section E.3), the leading edge of the cloud consists of TCU from daytime convection which becomes a layer of AC. Though cloud tops at WVK are below 500 mb (18 kft), the dew-point depressions on the 500-mb chart indicate cloud tops extending above 500 mb in the northwestern United States.

To the north over the interior plateau of B.C. (50-54N123-1W), SCT/BKN cellular AC/ACC occurs ahead of the front, the moisture and cloud being advected northward from

the cold-low cloud. XS and WL (Williams Lake, see cloud time-sections) report no cloud below approximately 4 kft during the frontal passage. The only exception is the formation of low cloud in areas of precipitation. This is in contrast to the coast stations --- the Coast Mountains block the low-level cloud and act as a sink for moisture flowing over the barrier. Orographic ascent saturates the air, forming clouds which precipitate over the barrier --- thus reducing the moisture content of the air, as well as increasing its temperature by the release of latent heat. Descent to the lee unsaturates the air, evaporating the low-level clouds. An initially saturated cloudy layer on the windward slopes becomes cloud-free to the lee.

Again in contrast to the coastal stations, showers occur along this band, with embedded CB from solar heating; the XS vertical time-section at 22/0000Z shows a potentially unstable air mass between the surface and 500 mb.

The frontal passage at UIL and VR (Vancouver) is slow because the frontal cloud band and frontal zone lies almost parallel to the 700-mb flow. VR shows a typical cold frontal cloud sequence in spite of the orographic effect of the mountains: amounts of CI increasing to OVC CS, lower BKN AC then low level ST SC appear, and a period of rain falls from cloud which extends throughout the troposphere. Though the 700-mb winds are west-southwesterly and the surface gradient is northwesterly, the blocking by the mountains produces southerly winds; the surface air converges at

the front which lies midway between ZT and VR.

To the east of the Rocky Mountains, a very bright area of BKN CB/TCU has developed at 50N105W with thunderstorms along the southern edge and AC plus anvil CI plumes downwind to the north. This area has formed from the band of moisture and cloud that lay in the easterly upslope flow on 19 and 20MAY. Paralleling the mountains at 50N115-1W are the remains of convective cloud from the previous day; BKN AC/ACC is shown on the YC (Calgary) cloud time-section. The southerly flow at 850 and 700 mb along the Rocky Mountains produces orographic descent and frictional divergence in the clear area to the east of the crest.

The thin band of SCT AC/CI through 57N120W lies in the area of PVA ahead of the west-to-east trough along 55N. Although the 700- and 500-mb flow almost parallels the mountains, the lee wave produces cloud in a band of mid-level moisture. The thicker AC band at 58N125W occurs downwind of the upper trough (PVA) as well as over the Rocky Mountains (orographic ascent).

E.5 22MAY72: Notes, Comments, and Observations

Refer to Plate 4 and Overlay 4a (SURFACE), 4b (700 mb), and 4c (500 mb).

The low in the lee of the Cordillera has moved northeastward to 62N115W and intensified, even though the pressure at the center has risen slightly. Since the areas of maximum PVA at 500 mb and WAA at 700 mb are located to

the north & northeast of the low center, the low should not develop further; during the next 12 hours the intensity ($\partial p / \partial r$) does decrease, from 16 mb/300 nmi to 13 mb/300 nmi.

The cold front extends southward from the low center and is marked by two cloud lines: a thin line of CU/TCU 52-57N111W from convergence along the surface front, followed by a wider brighter BKN line of TCU/CB+AC, giving rain- and thundershowers 52-63N112W where the cold air deepens and lifts the conditionally unstable air ahead of the front. The Edmonton vertical time-section at 22/1200Z shows the air mass to be unstable between about 800 and 300 mb; frontal lift produces BKN CB and OVC AC. A third cloud line 55N115W - 63N118W (just to the west of the north-to-south surface trough through the low center) is much wider, consisting of SC+NS/AS with embedded CB along the eastern edge, giving rain south of the Arctic front and snow the the north. From the passage of this band on the YE vertical time-section, cloud tops are below 450 mb (20 kft). This cloud band corresponds to a secondary cold front analyzed on the surface chart.

The second and third cloud lines extend into a bright cloud shield 63N110-120W - 67N110-122W to the north & northeast of the low center, consisting of OVC multilevel SC+AS/NS+CS with embedded TCU/CB along the southern edges. The shield is located in an area of ascent from WAA and PVA, and downstream of the cloud bands to the south. The cold front and the cloud lines parallel the flow at 500 mb. The

cloud shield becomes less bright east of 110W, "ahead" of the second cloud line, indicating thinner OVC SC/AC cloud.

The break at the southern margins of the three bands 52N112W - 54N116W occurs along the 500-mb trough line. The frontal cloud band resumes over the Rocky Mountains (49N115W) extending to the Cascade Range, then along the BKN/OVC closed-cell CU/SC SCT AC band over the Pacific Ocean to 40N135W, thence into a small cyclonic circulation center at 38N137W. Inland from the coast, two north-to-south lines of orographic SC+AC cloud at 43-50N123W correspond to the Coast Mountains and the Cascade Range. The VR cloud time-section illustrates the orographic cloud on the Coast Range: no clearing occurs after the passage of the frontal band. Subsidence clearing to the lee of the mountains is greatest in the Columbia Basin near 47N120W. At 44N120W, BKN/OVC AC (frontal) cloud reforms over the mountains in Oregon and extends eastward to 45-50N115W where thicker OVC AC covers the Salmon River (45N114W) and the Rocky Mountains. Only showers occur along the band, except at the Rocky Mountains where the higher barrier produces an area of rain. To the south & southeast of the front (43N112W), BKN TCU+AC is all that remains of cloud that was associated with the cold low. The cold low itself has moved northeastward and become a trough in the Westerlies. The AS cloud shield over the northwest United States on 21MAY vanishes. Advection at 15 kts would move the cloud area north- and eastward 6 degrees (360 nmi) during the 24-hour period: to the lee of

the Rocky Mountains at 55N (into the CLR area) and over the mountains at 45N115W.

To the lee of the Rocky Mountains, a narrow, clear zone caused by subsidence in the west & northwesterly flow at 700 mb, and frictional divergence in the northwesterly flow near the surface, is followed by a band of SCT/BKN AC/ACC+CI with streamers of AC downwind. The northern end of the band terminates in a small area of TCU/ACC cells and rain showers. The YC cloud time-section shows that the cloud to the lee of the mountains persists, whether the 700-mb flow is southerly as on 21MAY or westerly as on 22MAY. To the east, thin SCT/BKN CU+AC occurs in the "clear" area.

In the warm sector, ahead of the cold front, a broad line of BKN AC/AS with CI plumes 45N98W - 50N104W - 58N105W parallels the southerly flow at 700 and 500 mb. The northern portion of the band through Saskatchewan is entirely due to the advection of convective clouds at 50N105W on 21MAY. Assuming a southerly wind velocity of 30 kts, the predicted location would be 12° (720 nmi) further north --- the observed location is 8°, giving a velocity of 20 kts. Cloud cells are added to the southern end along the Polar cold front (not analyzed on the surface chart) extending the band southward to 45N. The southwestern edge of the band lies downstream of the 500-mb trough through 45N106W. Comment: how should the band of cloud through Saskatchewan be portrayed on the surface chart? The band is neither a

TROWAL nor a squall line. It is not marked by a line of surface convergence although convergence does occur along the Polar cold front in the northern United States.

Behind the cold front, subsidence by CAA at and below 700 mb produces a "clear" slot along 45N140W - 50N126W - 60N123W. Over land, the 1/8 (SCT) CU reported by the surface stations cannot be detected on the mosaic --- cloud elements are much smaller than the resolution and are thin --- and the area appears CLR. To the lee of the mountains, BKN SC forms along a NW-SE line through 56N120W, corresponding to a band of low-level moisture in the cold air mass; dew-point depression at 22/1800Z is 16°C at YE in the CLR area to the north and 6°C at XJ near the edge of the SC band. Even though the air at YE is potentially unstable between the surface and 600 mb during the afternoon, the air mass is too dry for extensive convective cloud to form --- only SCT CU is reported. Over the Pacific Ocean, SCT open-cell SC/CU with SCT AC ends along the Coast Mountains, again showing the blocking effect of a mountain range.

To the north & northwest of the clear slot (60N130W), BKN/OVC SC+AC/AS with cloud tops below 500 mb gives showers to the south and snow to the north of the Arctic front. The cloud is associated with the 500-mb closed center (60N131W) and the advection of cloud around the northern part of the 700-mb closed low (61N125W). The easterly upslope flow at and below 700 mb against the Mackenzie Mountains (63N120W) does not produce any increase in

cloud brightness, i.e. thickness, remembering to consider the effect of snow covering the mountains. The upstream ridge and lee trough again appear on the surface chart. Over the ocean (50-55N 130-140W), BKN/OVC CU/SC with patches of BKN AC/AS is giving showers (refer to PR and ZP cloud time-sections) in the convectively unstable cold air (5°C) over the warmer ocean (8°C). The ANN vertical time-section indicates that the cloud tops are below 700 mb; the air is very dry above. In the layer surface-to-850 mb, the equivalent potential temperature θ_e is constant, indicating a well-mixed layer.

The cloud time-sections for YE, XJ, EG, and YC show similar frontal cloud features:

(a) SCT CU/TCU due to daytime solar heating occurs during the previous day (21MAY). As a result of the very dry surface air (dew-point depressions are 15 to 30°C) the cloud bases are high (5 kft). Overnight, the convective cloud becomes SCT AC/ACC with cloud bases rising to 8 kft. Some CI is present, though the amount is difficult to determine;

(b) A layer of SCT increasing to BKN AC/ACC at 14 kft appears above the CU/TCU;

(c) Ahead of the cold front, cloud increases to BKN/OVC AC, with the two cloud layers merging into one layer at 10 kft;

(d) At the front, low-level BKN/OVC CB/TCU/SC gives showers and thundershowers, the cloud base (at approximately 4 kft) depending on the moisture content of the air. The position and orientation of the upper trough determines the amount of frontal cloud and the existence of a post-frontal rain band;

(e) Cloud clears to 5 kft-based SCT/BKN CU/TCU in daytime heating, and SCT AC at 10-15 kft. Surface dew-point depressions again become 15 to 20°C.

Individual stations will show differences as a result of:

(a) The time of frontal passage: The passage at YE during the early afternoon halts the development of convective cloud;

(b) Nearness to the upper trough: YE and XJ, distant from the trough, exhibit a post-frontal rain band; YC and stations to the east along the trough line are missing the line of CB/TCU.

(c) Moisture content of the air mass: The surface air at XS and WL is too dry for convective cloud to form. Advection of moisture from the cold low affects YF and VR. Coastal stations have a marine stratum of moist air caused by evaporation from the ocean surface;

(d) Effects of the mountains: Calgary (YC) lies in the region of frictional convergence beyond the lee clearing.

Comparison with coastal stations

At the coastal stations, no middle cloud is observed ahead of the frontal passage. At the front, OVC/BKN SC occurs with low cloud bases of less than 3 kft, more typically, less than 1 kft, showing the influence of the ocean as a moisture source. No convective cloud (TCU, CB, or ACC) occurs. Because of the low cloud, the amount and type of middle and high clouds is difficult to determine. In the clearing after the frontal band, only low-level SC is present.

Table E.1 gives dew-point depressions at the stations used for the time-sections. Depressions for the coastal stations are less than 10°C, compared to 15 to 30°C over the land, except on days with off-shore flow of dry continental air. Table E.2 gives the period of southerly winds ahead of the cold front. Note the increase in duration to the lee of each mountain barrier.

Table E.1

Afternoon (0000Z) dew-point depressions (°C)
Frontal Passage is denoted by an "X"

Station	19	20	21	22	23
PAPA	2	X 0	3	5	5
PR	5	9	3 X	4	4
ZP	5	12	4 X	10	7
ZT	11	12	9 X	7	8
VR	5	24	2	5 X	9
UIL	12	22	2	1 X	9
EP	2	5	4 X	2	5
XS	21	22	26	X 12	22
WL	17	19	24	X 8	19
YF	8	17	14	7 X	14
YE	17	20	22	X 9	20
XJ	25	23	31	23 X	19
EG	1	16	21	17	X 18
YC	7	17	21	23	X? 9

Table E.2

Hours of southerly winds ahead of the cold front

Station	Pressure Level				Average
	Surface	850 mb	700 mb	500 mb	
PAPA	>24	>36	>36	>36	>36
ANN	0	0	<12	<12	
ZT	0	0	0	0	
UIL	<24	0	0	0	0
XS	6	12	0	<12	
WVK	12	<12	<24	<12	<12
YE	<6	<12	24	24	
Edmonton	54	48	36	24	30

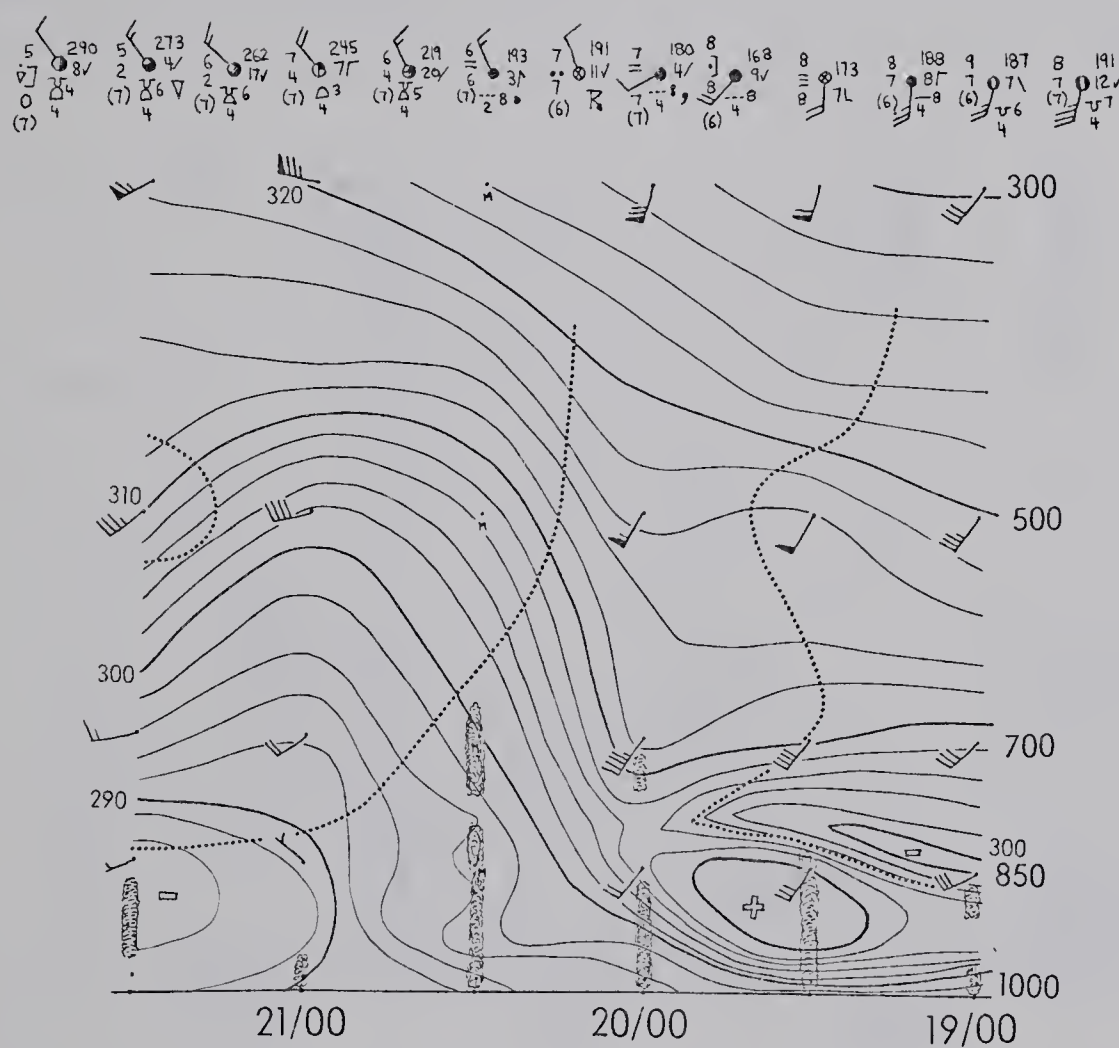


Figure E.3. Vertical time-section plus 6-hourly station weather for Ocean Station (Ship) PAPA.

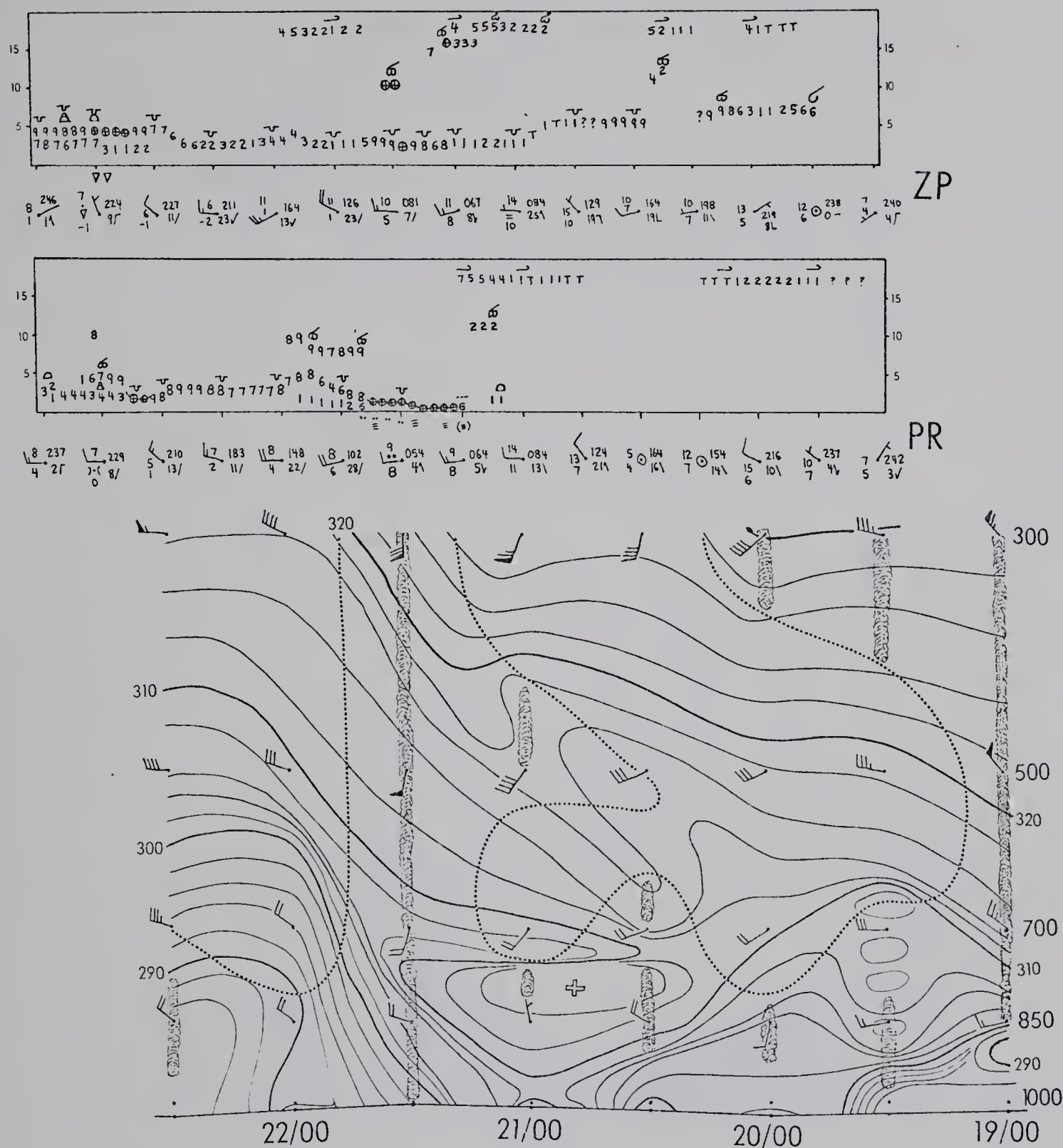


Figure E.4. Vertical time-section for Annette Island (ANN) and cloud time-sections plus 6-hourly station weather for Prince Rupert (PR) and Sandspit (ZP).

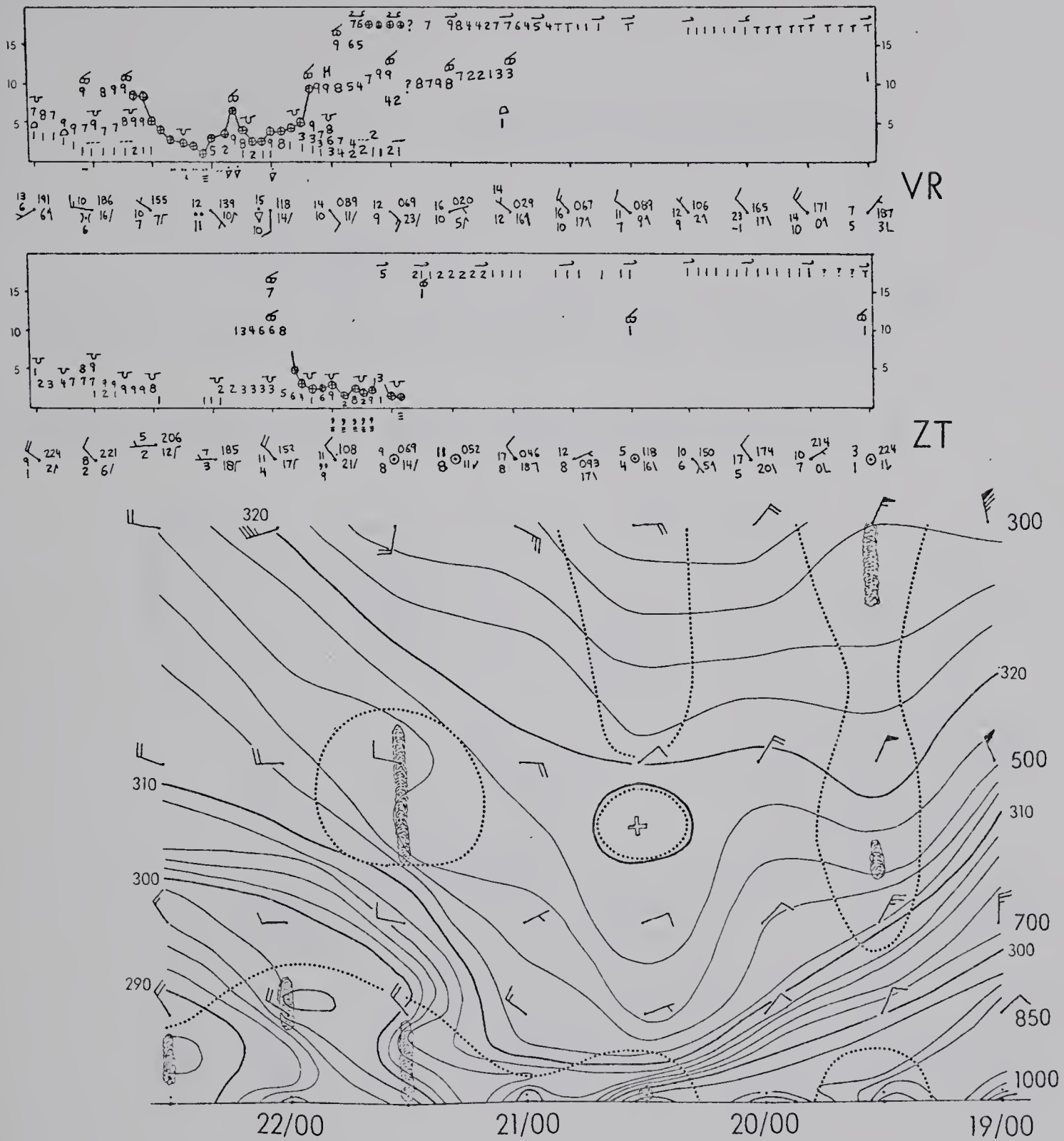


Figure E.5. Vertical time-section for Port Hardy (ZT) and cloud time-sections plus 6-hourly station weather for Port Hardy (ZT) and Vancouver (VR).

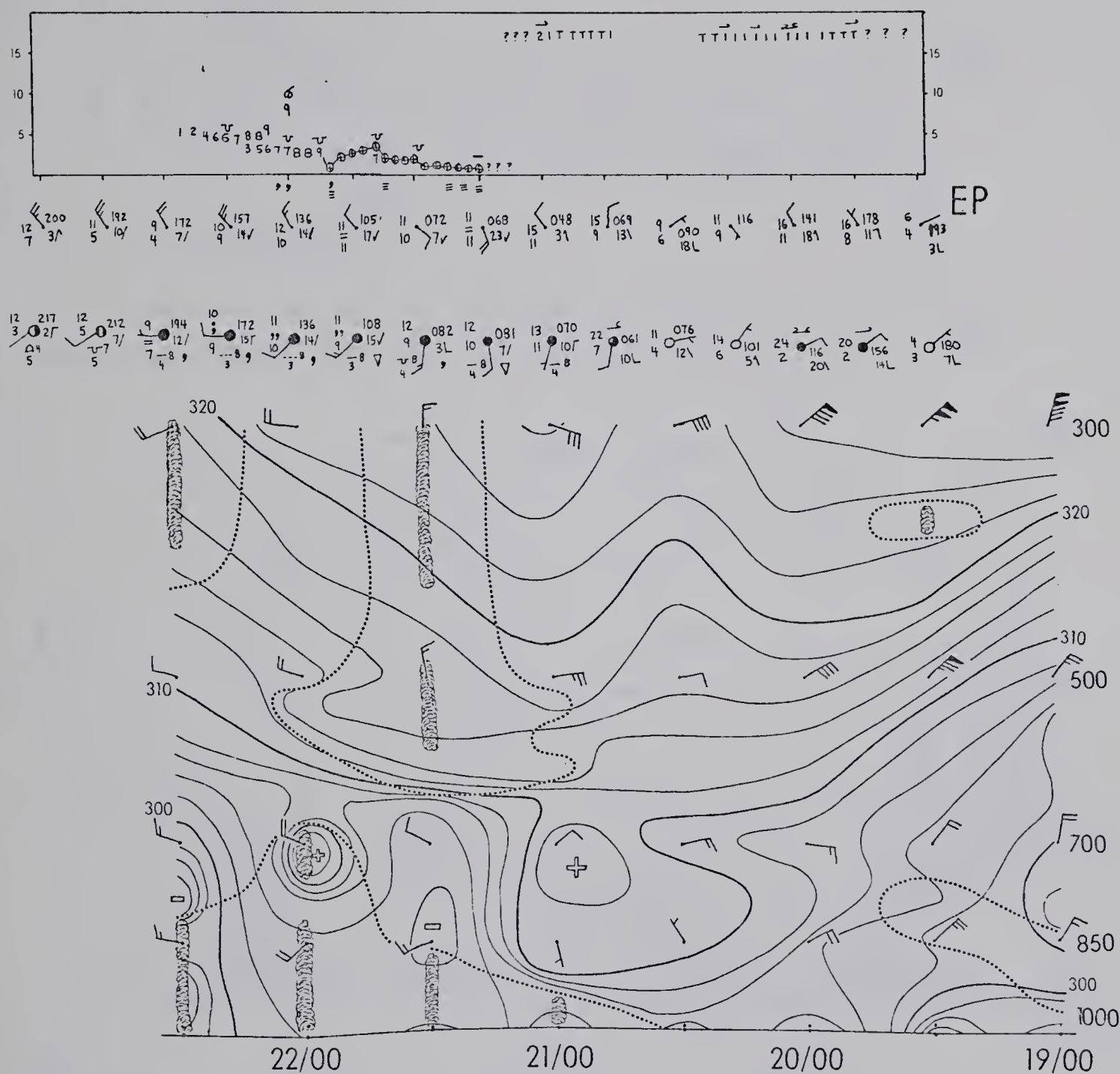


Figure E.6. Vertical time-section plus 6-hourly station weather for Quillayute (UIL) and cloud time-section plus 6-hourly station weather for Estevan Point (EP).

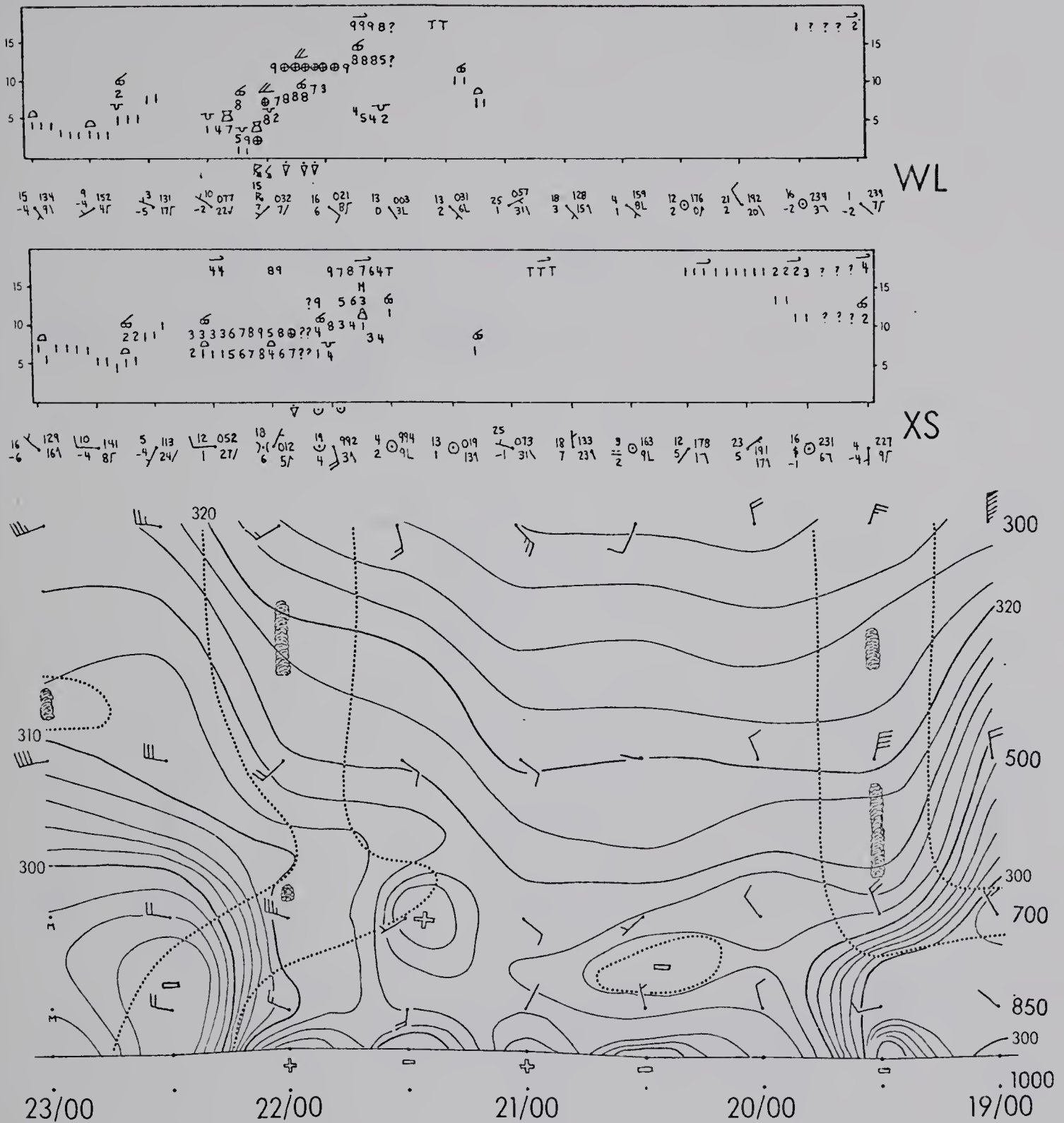


Figure E.7. Vertical time-section for Prince George (XS) and cloud time-sections plus 6-hourly station weather for Prince George (XS) and Williams Lake (WL).

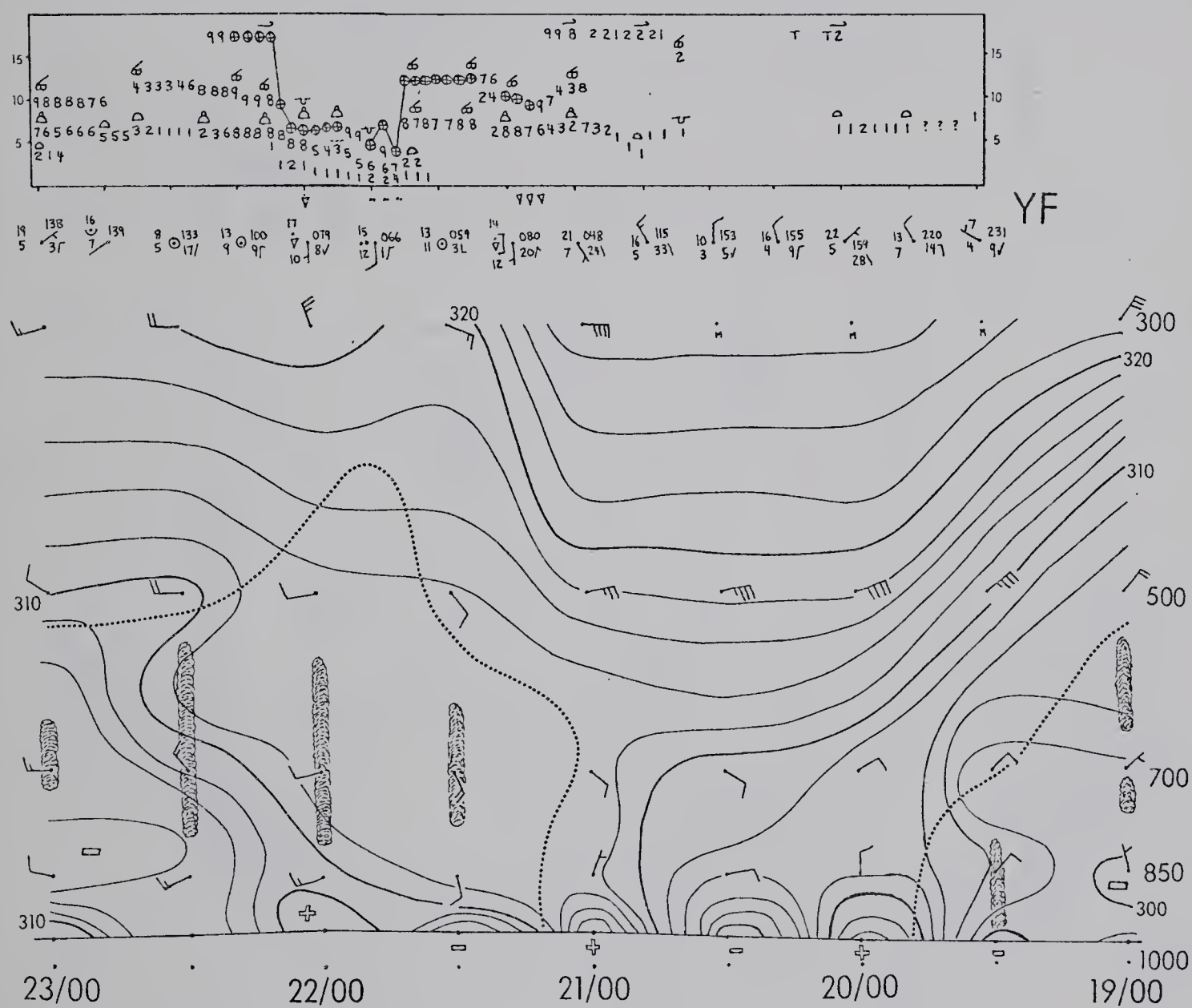


Figure E.8. Vertical time-section for Vernon (WVK) and cloud time-sections plus 6-hourly station weather for Penticton (YF).

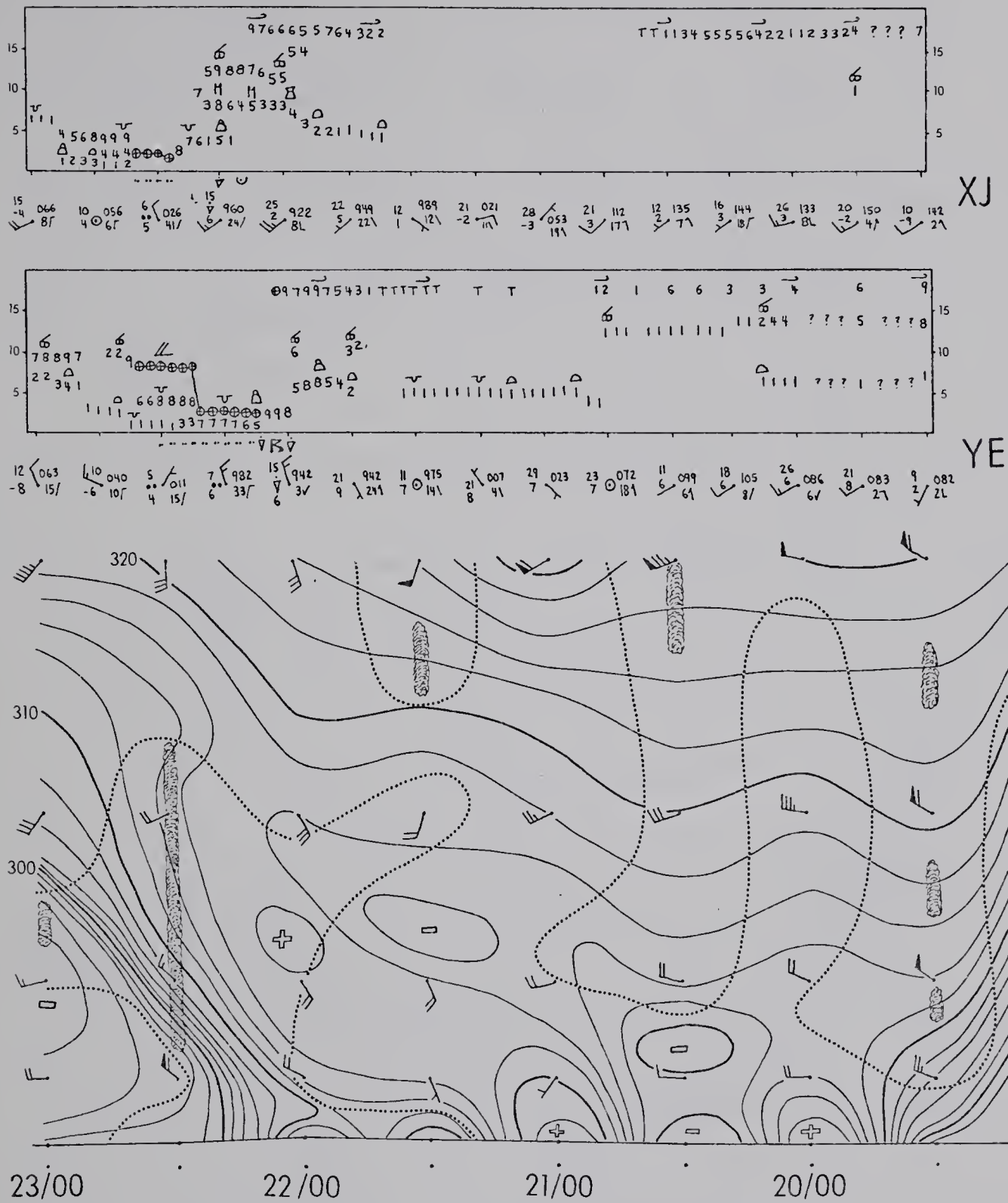
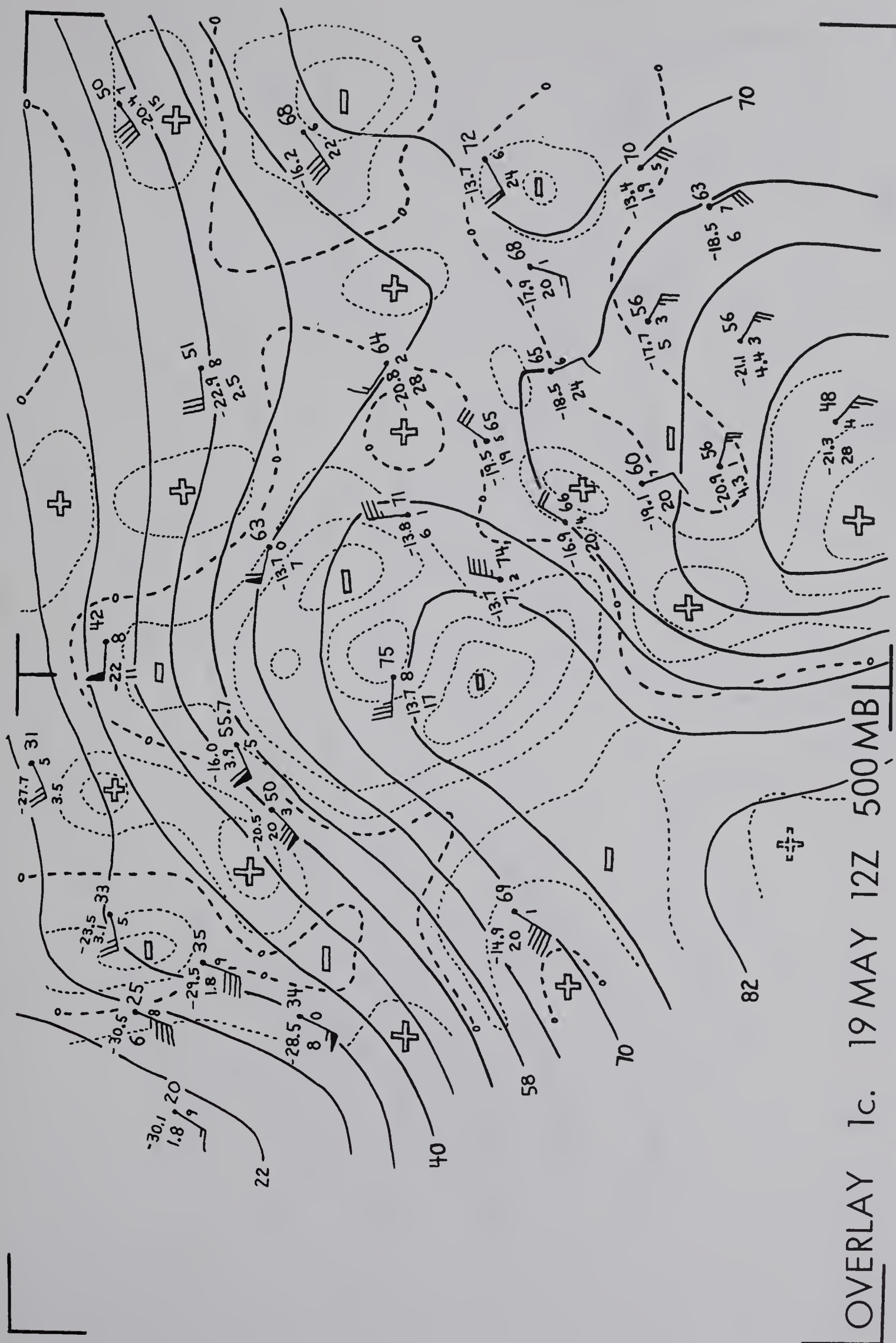
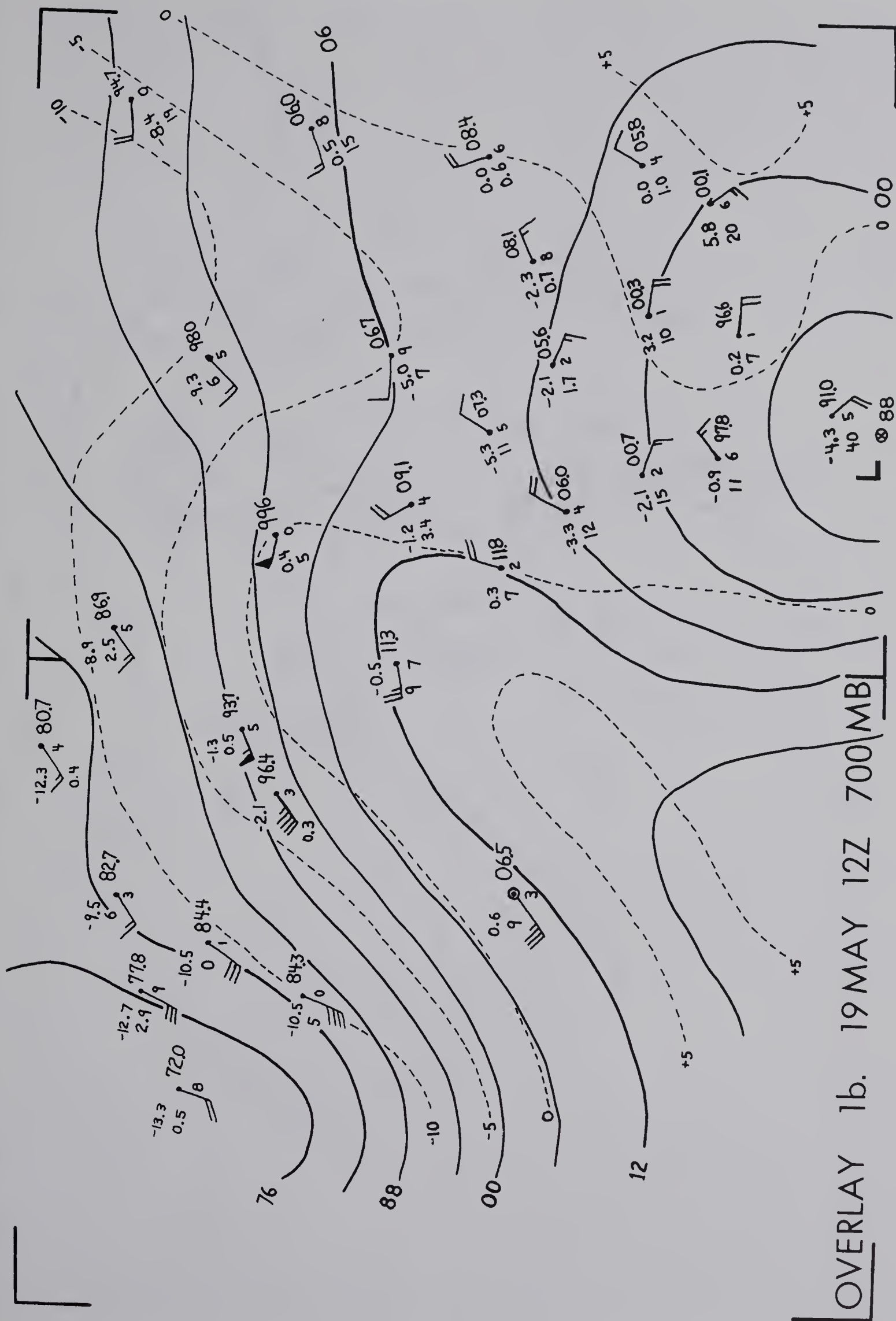
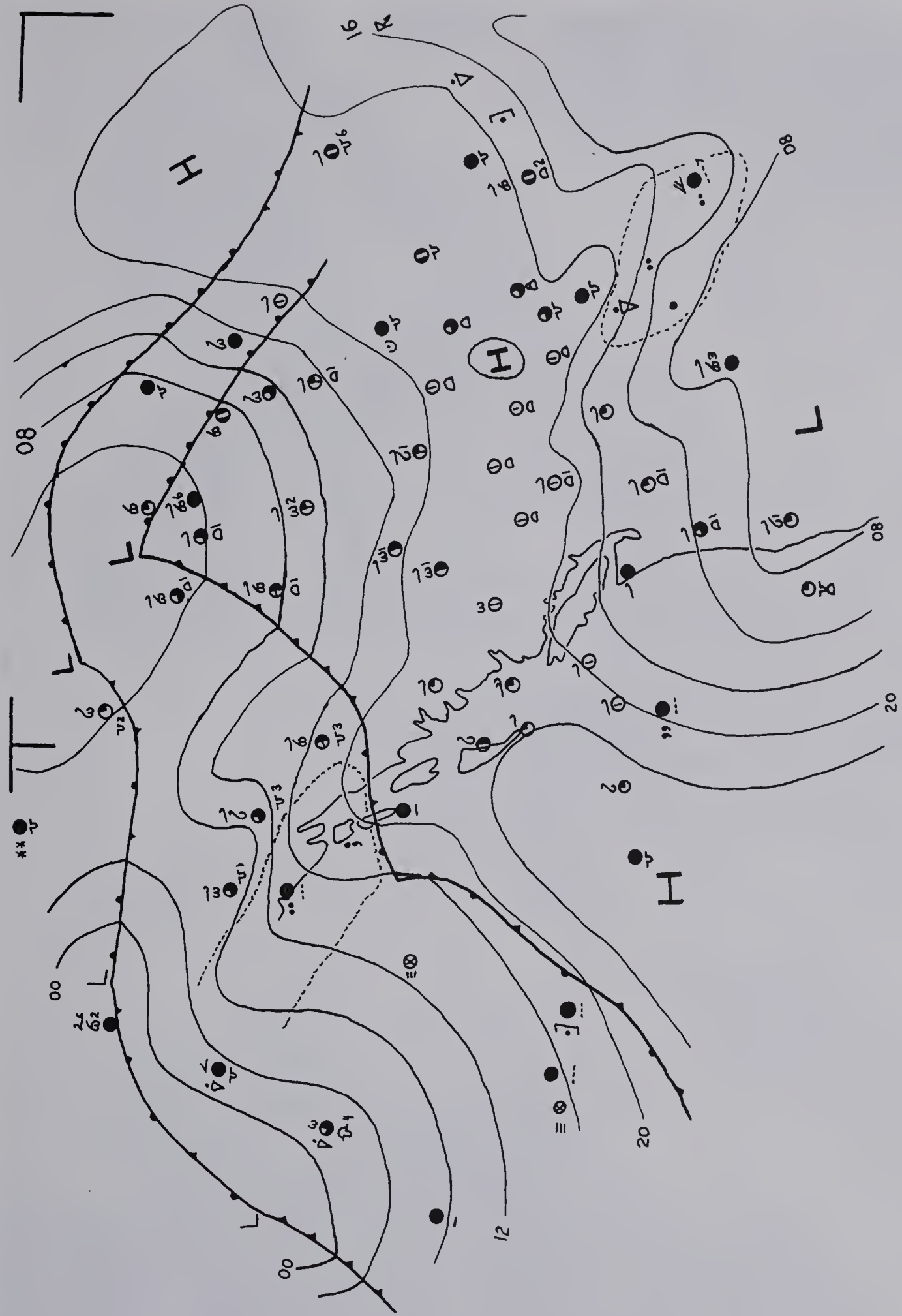


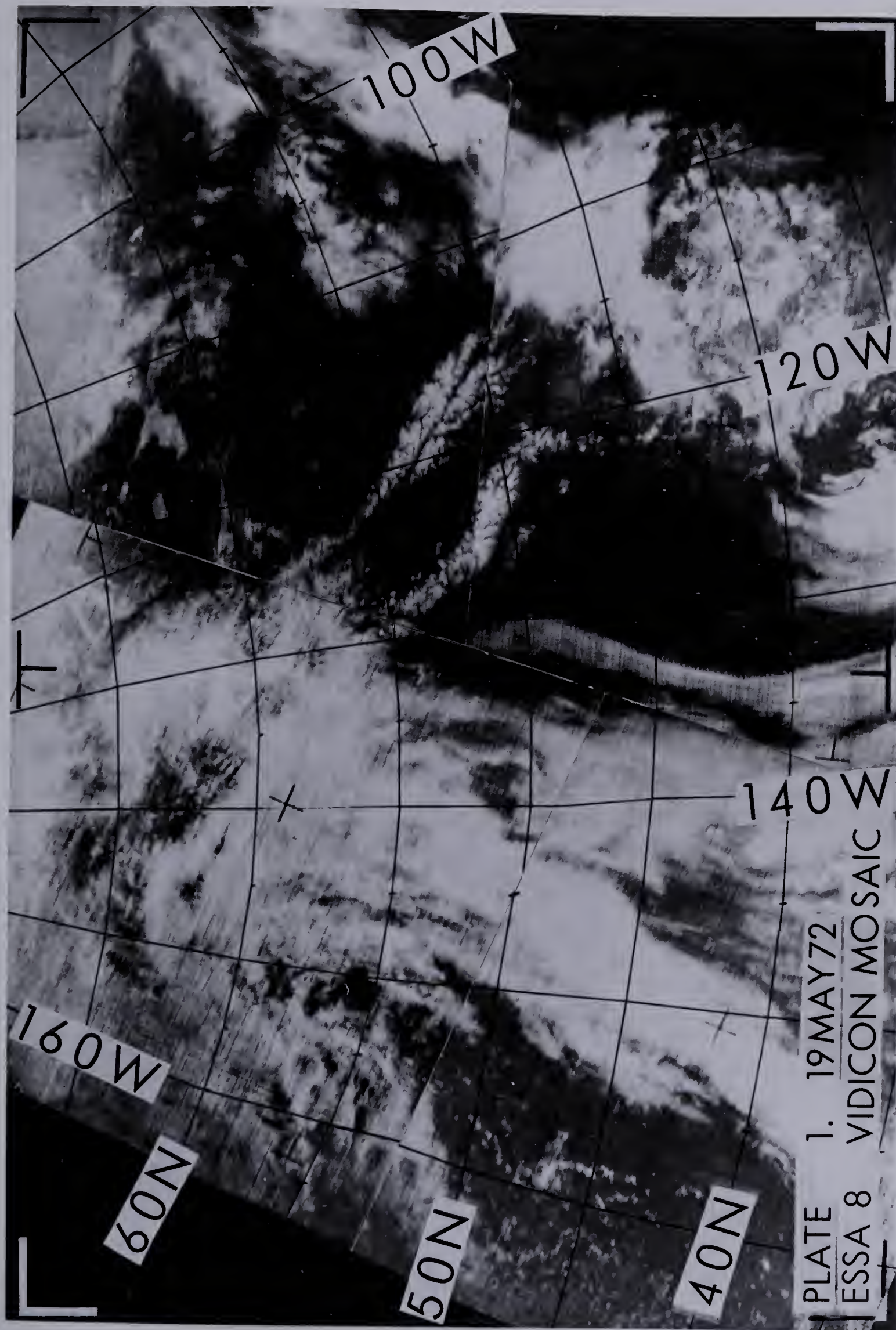
Figure E.9. Vertical time-section for Fort Nelson (YE) and cloud time-sections plus 6-hourly station weather for Fort Nelson (YE) and Fort St. John (XJ).

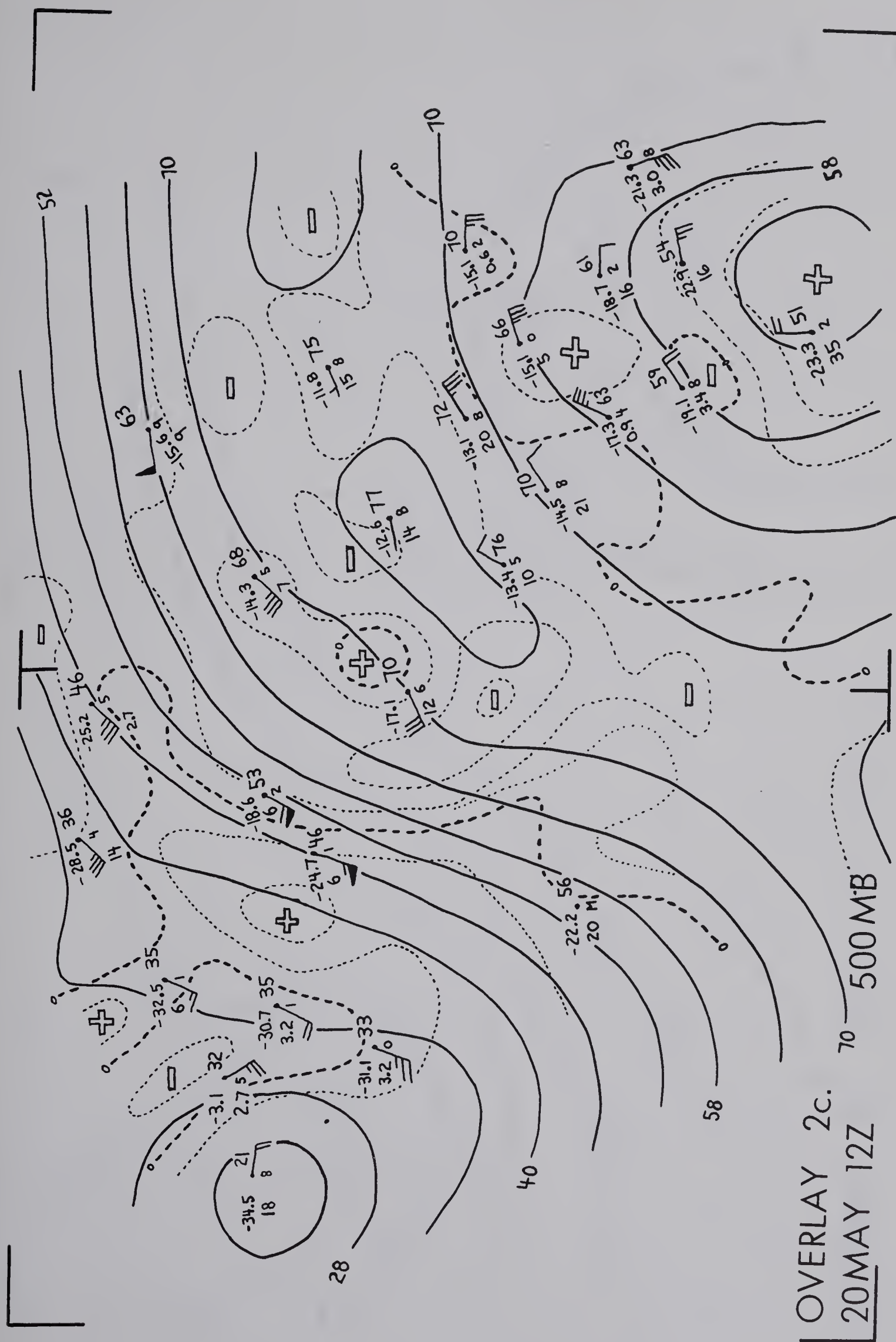


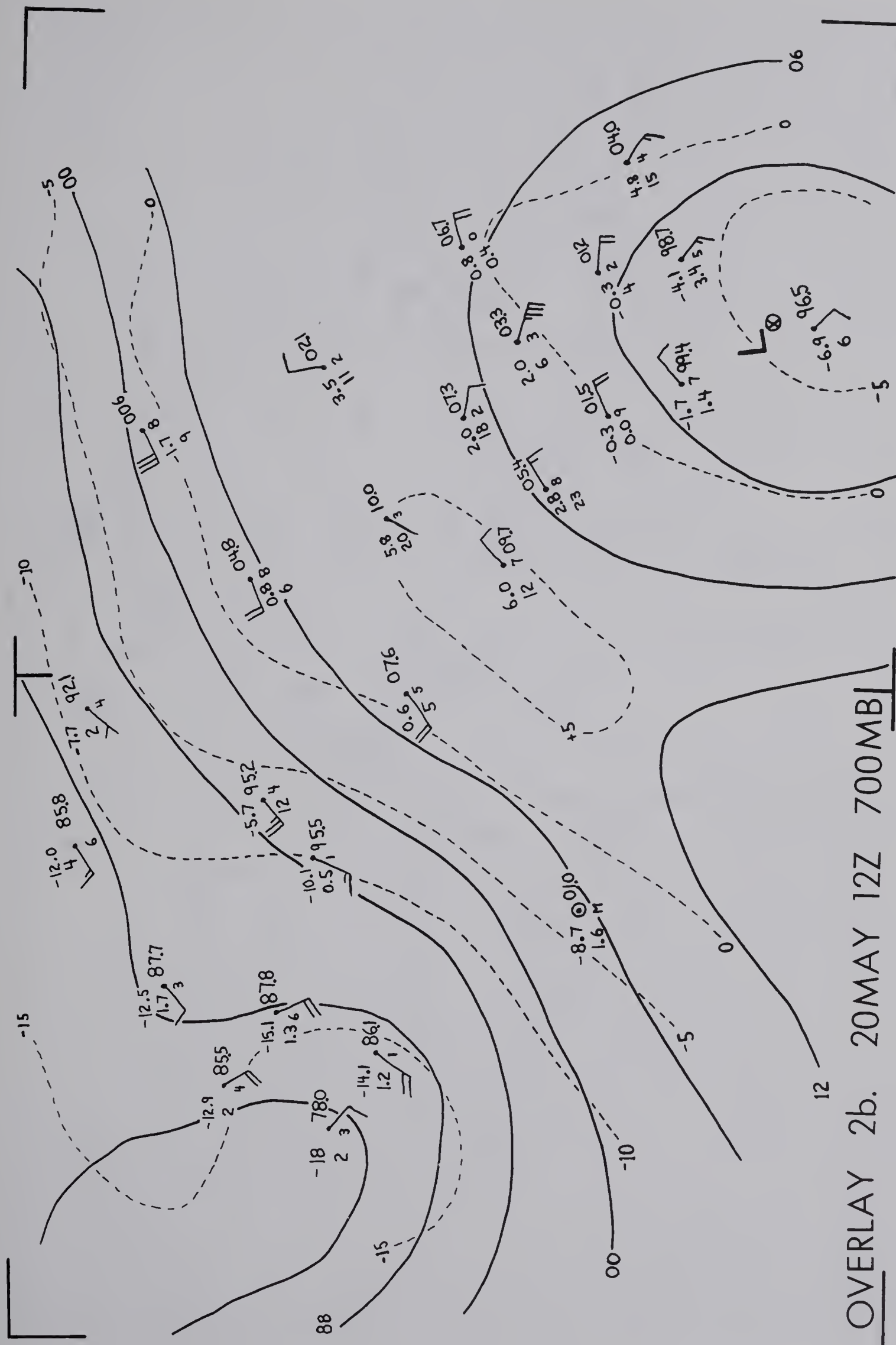


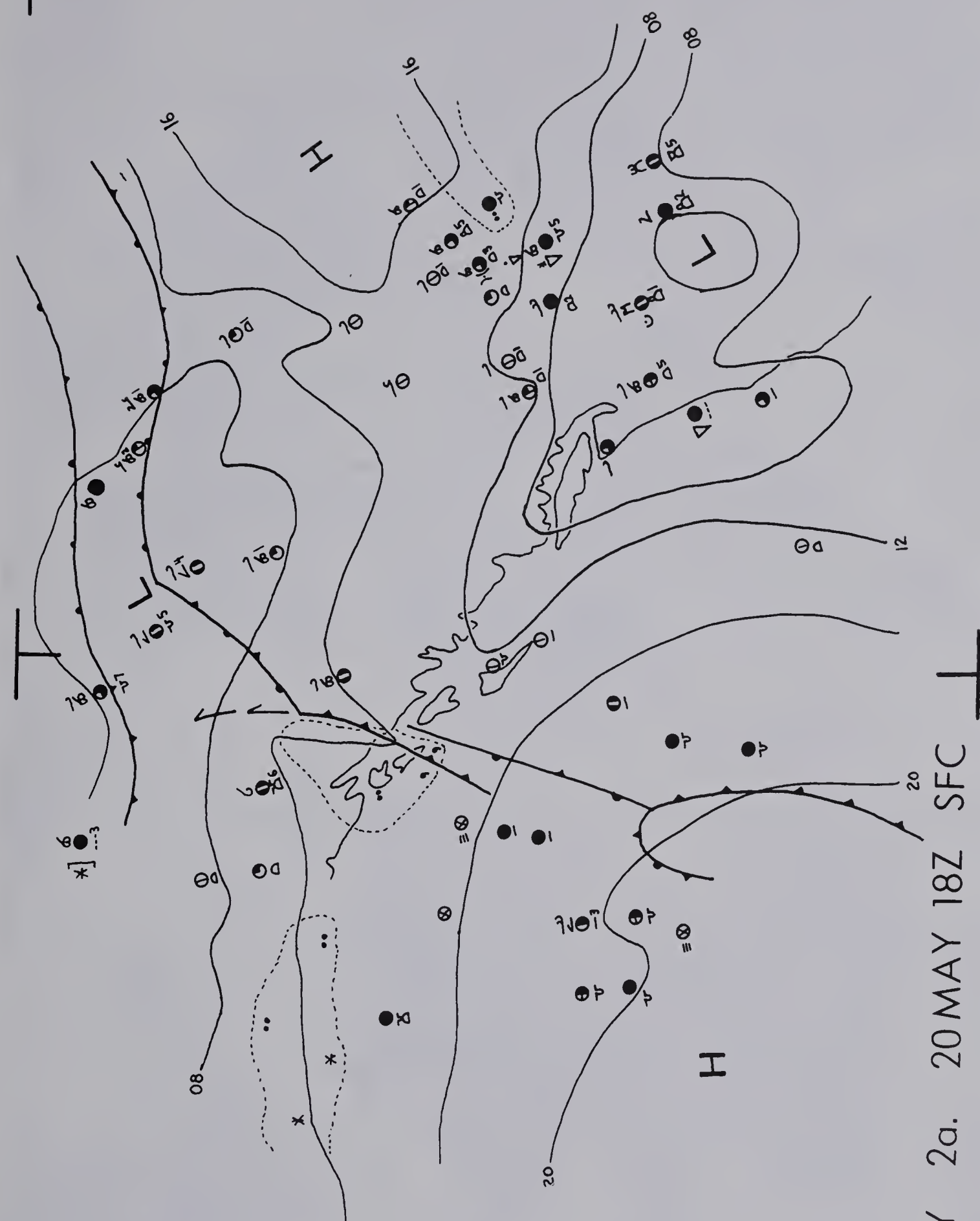


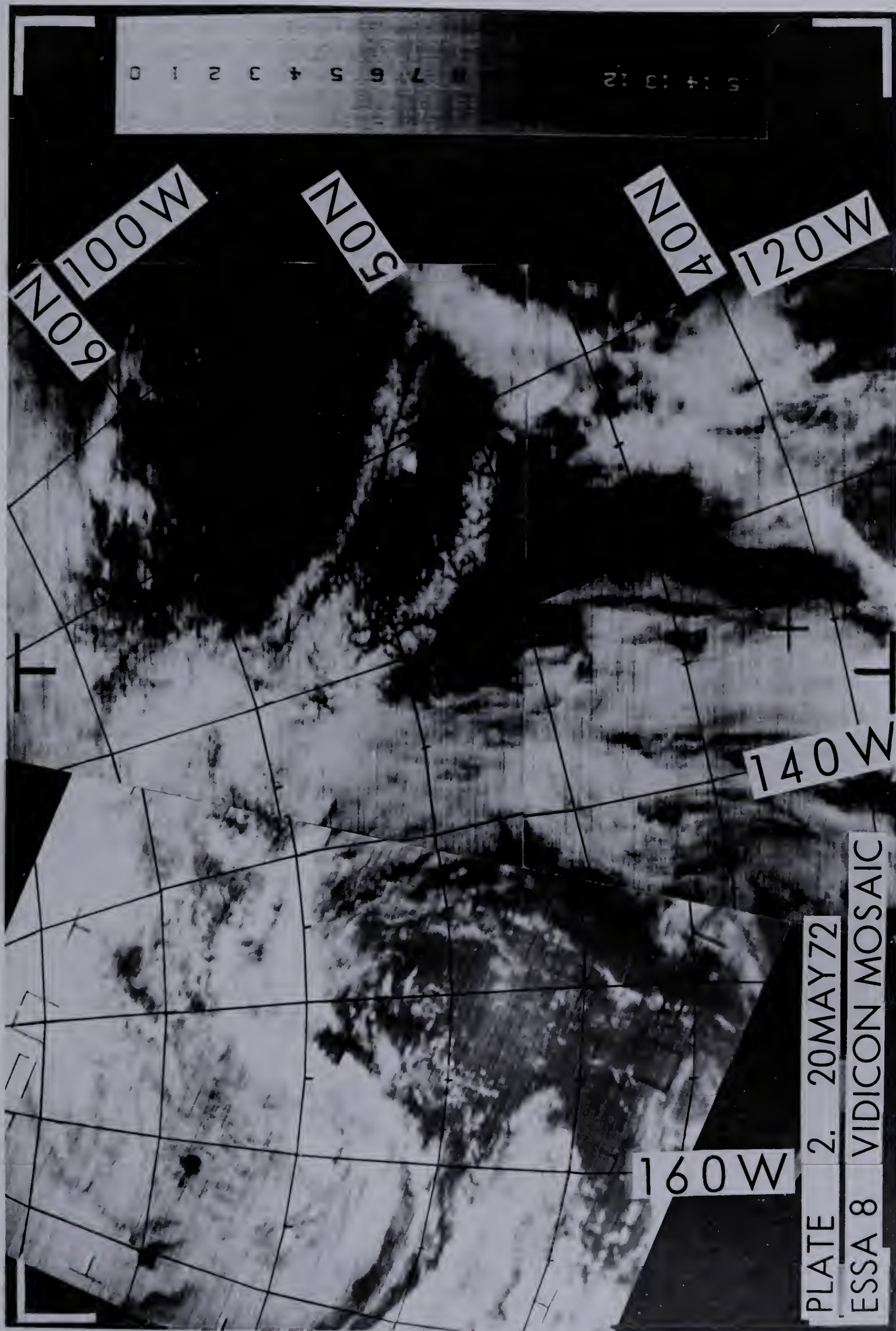
OVERLAY 1a. 19 MAY 18Z SFC

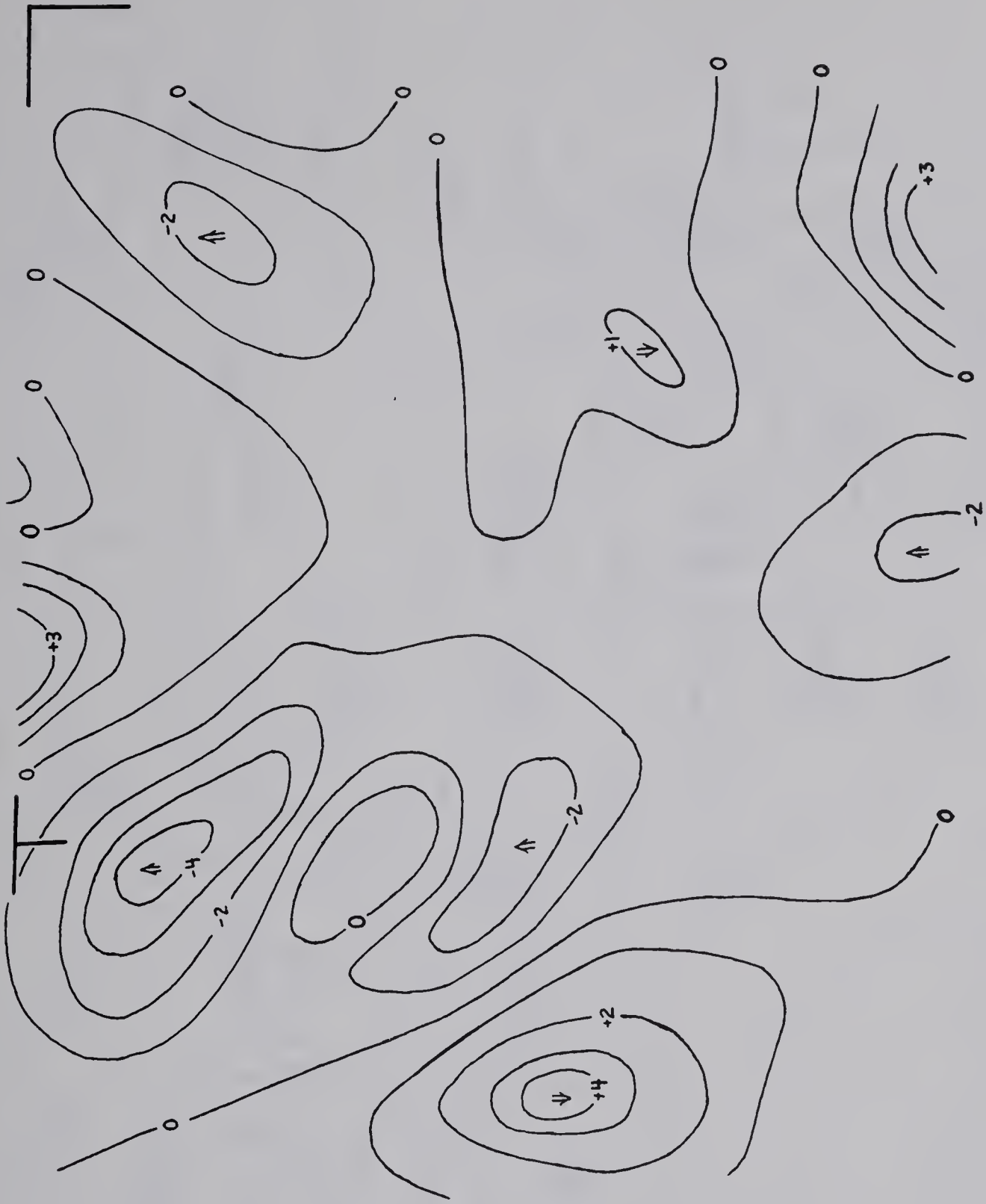




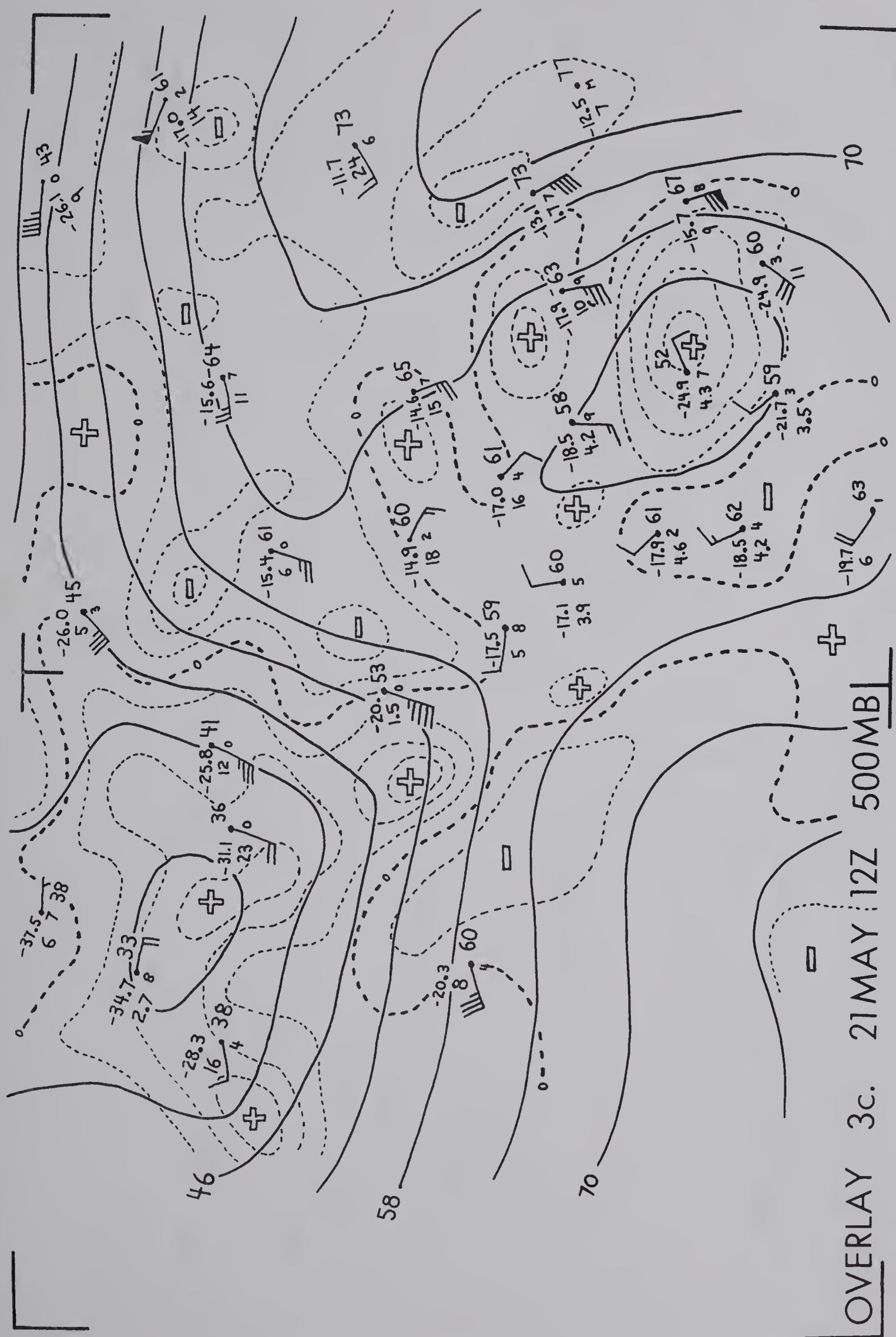


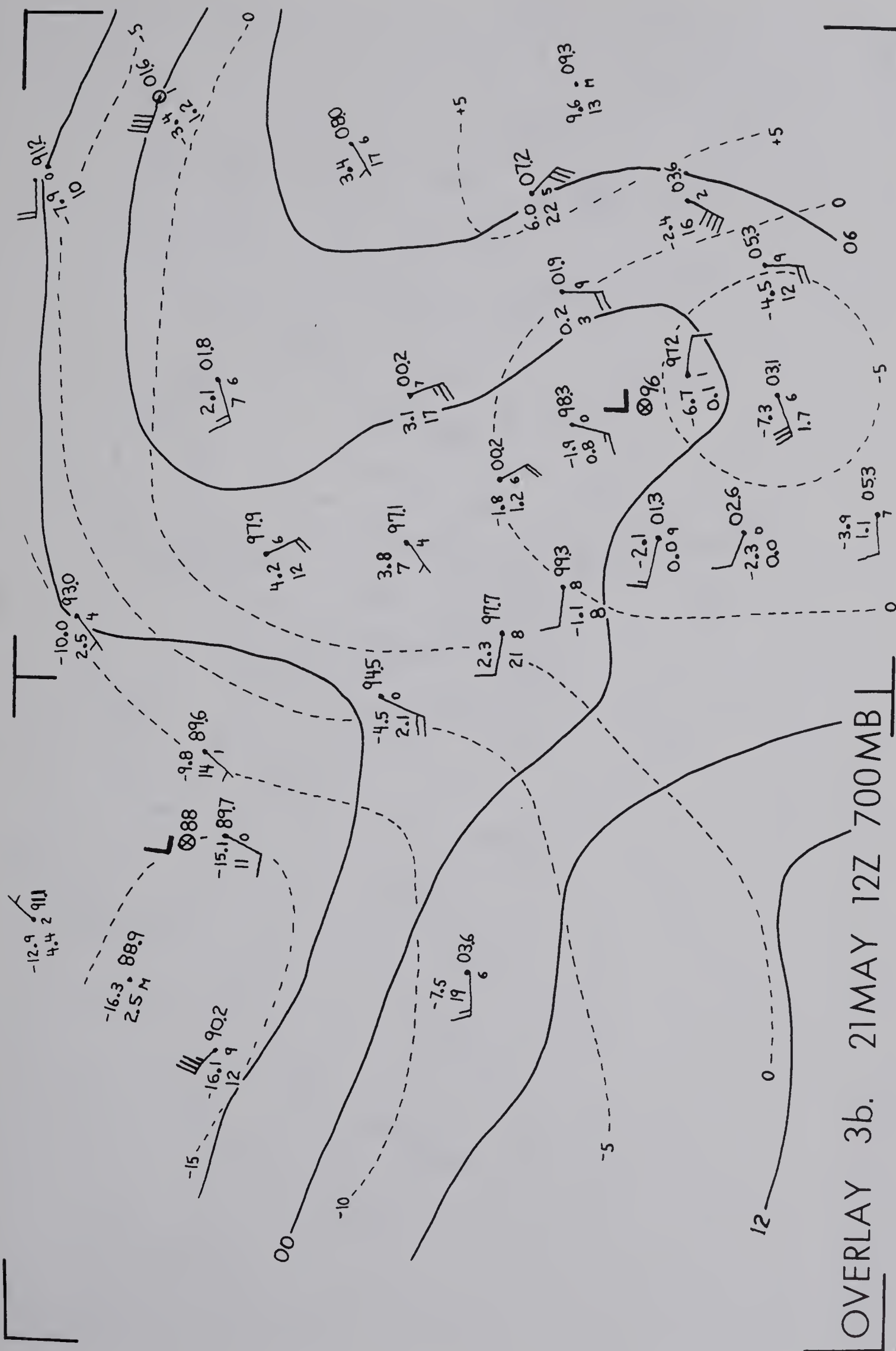


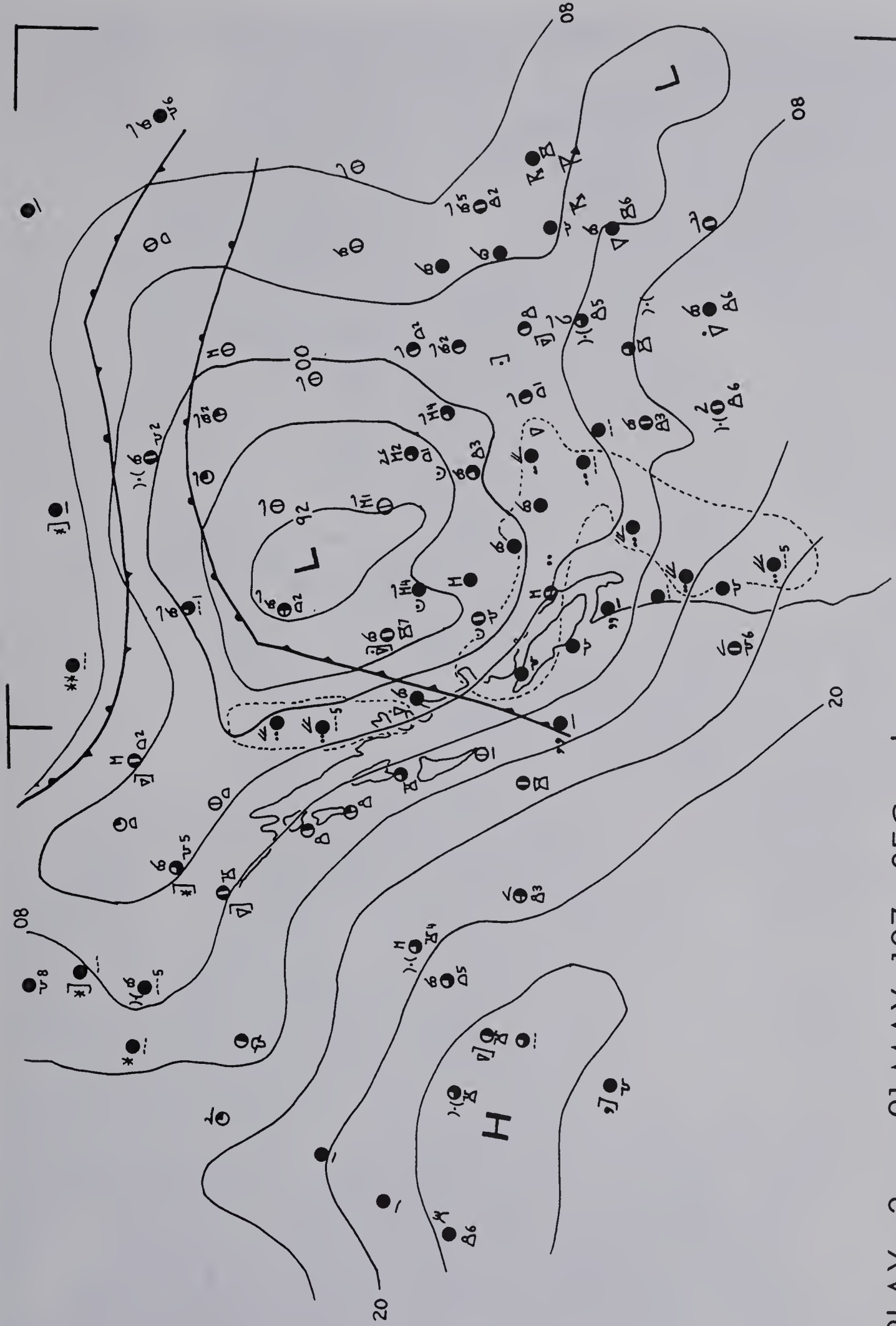




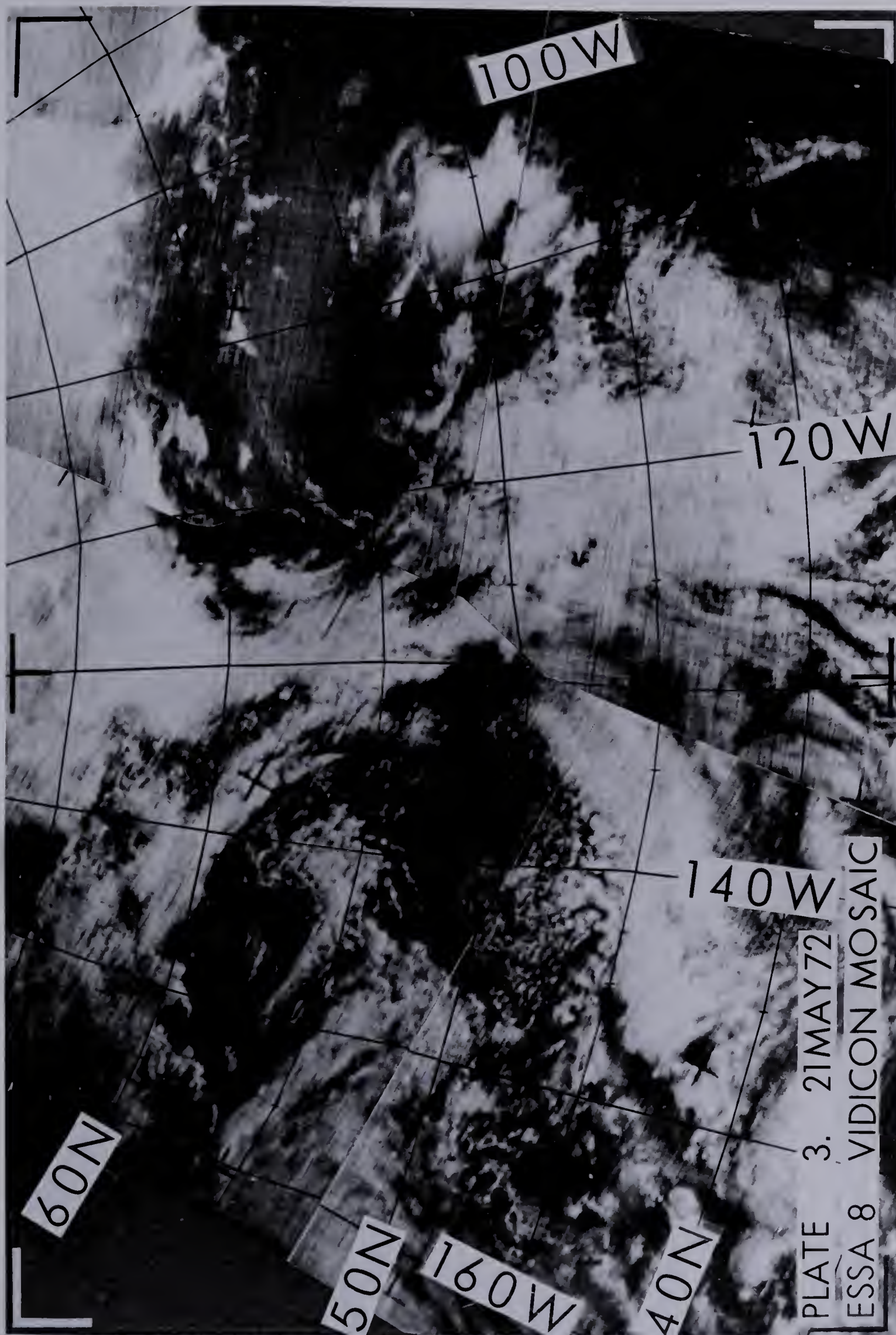
OVERLAY 3d. 21 MAY 12Z ω 600MB

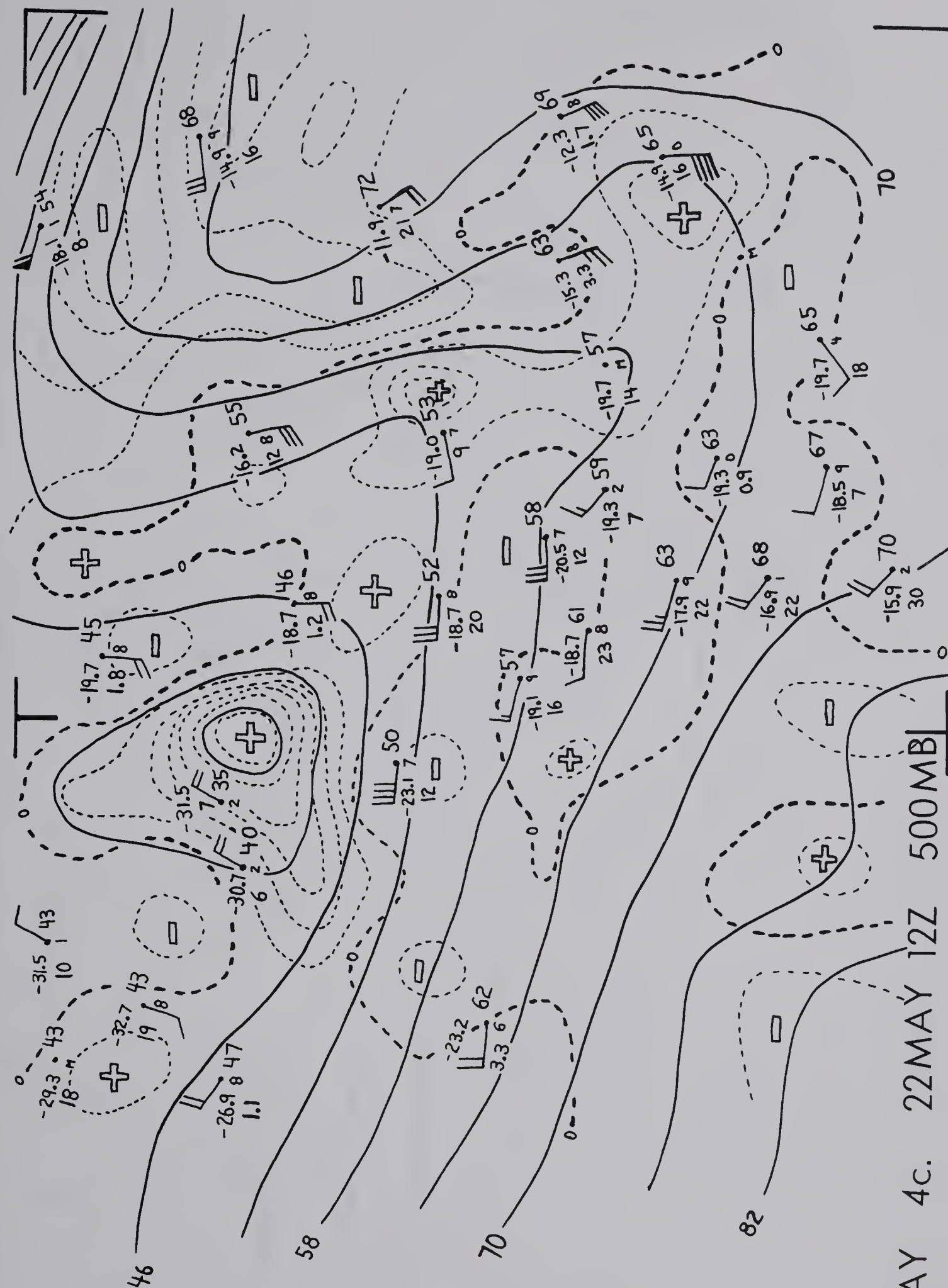


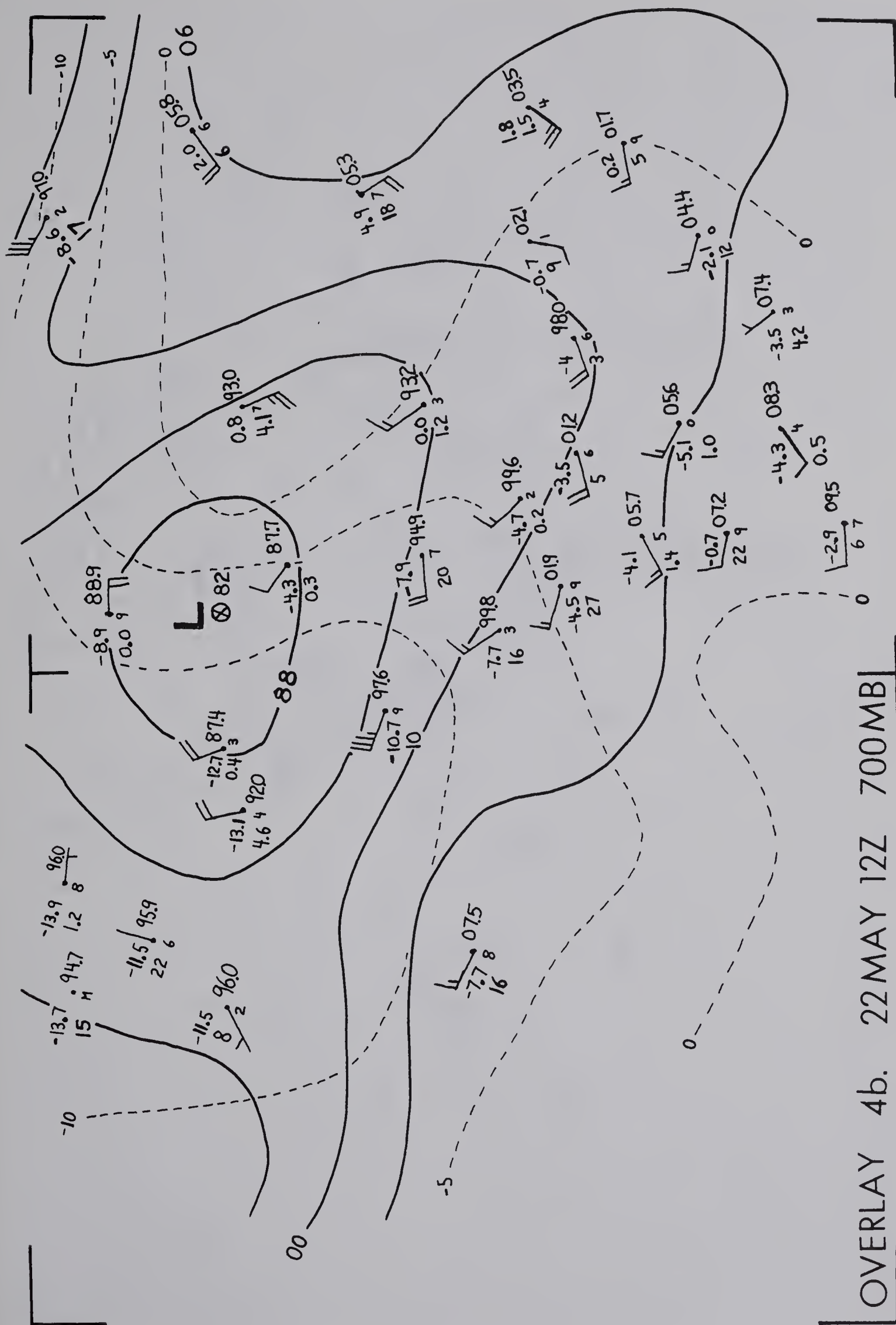


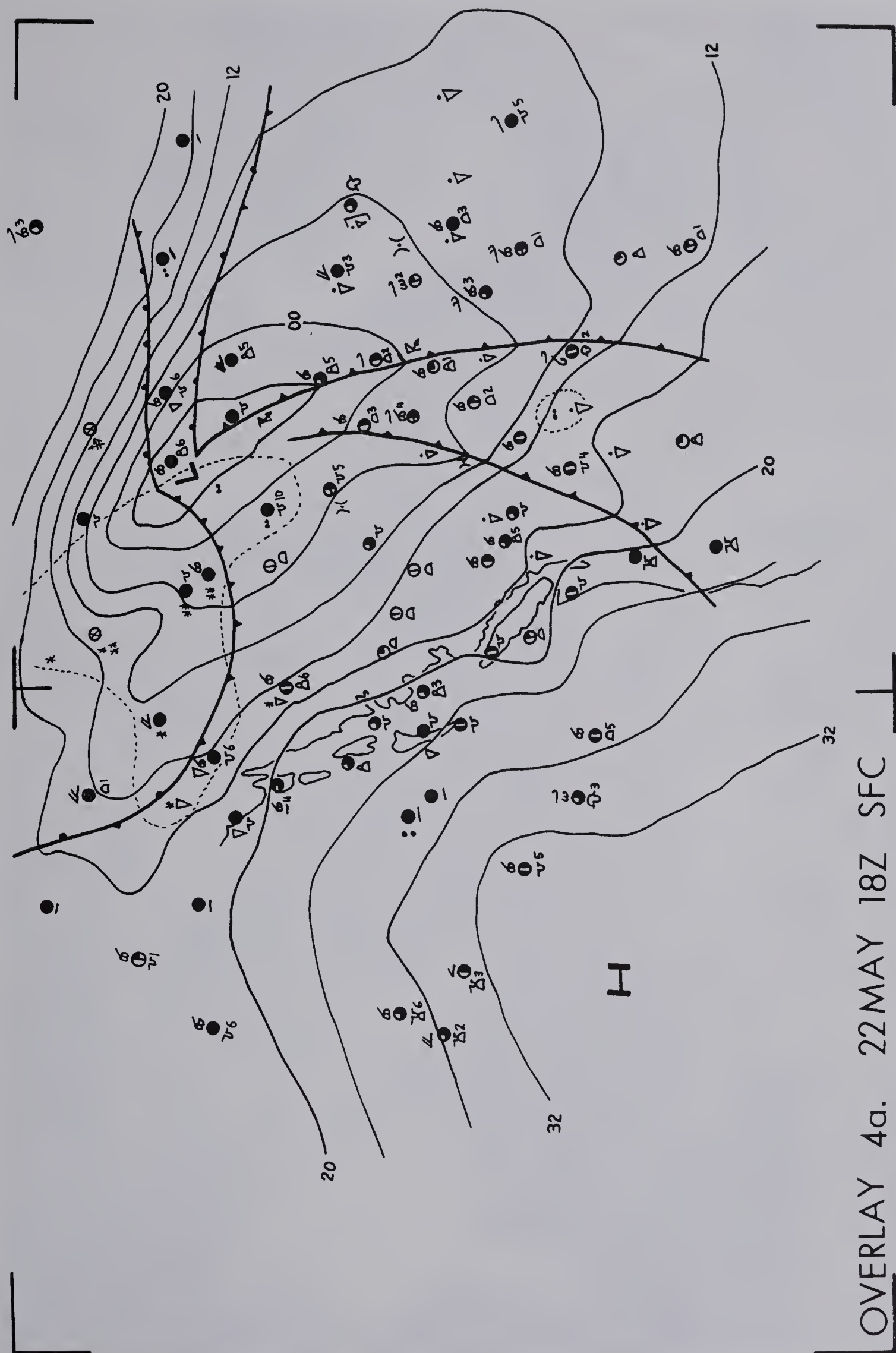


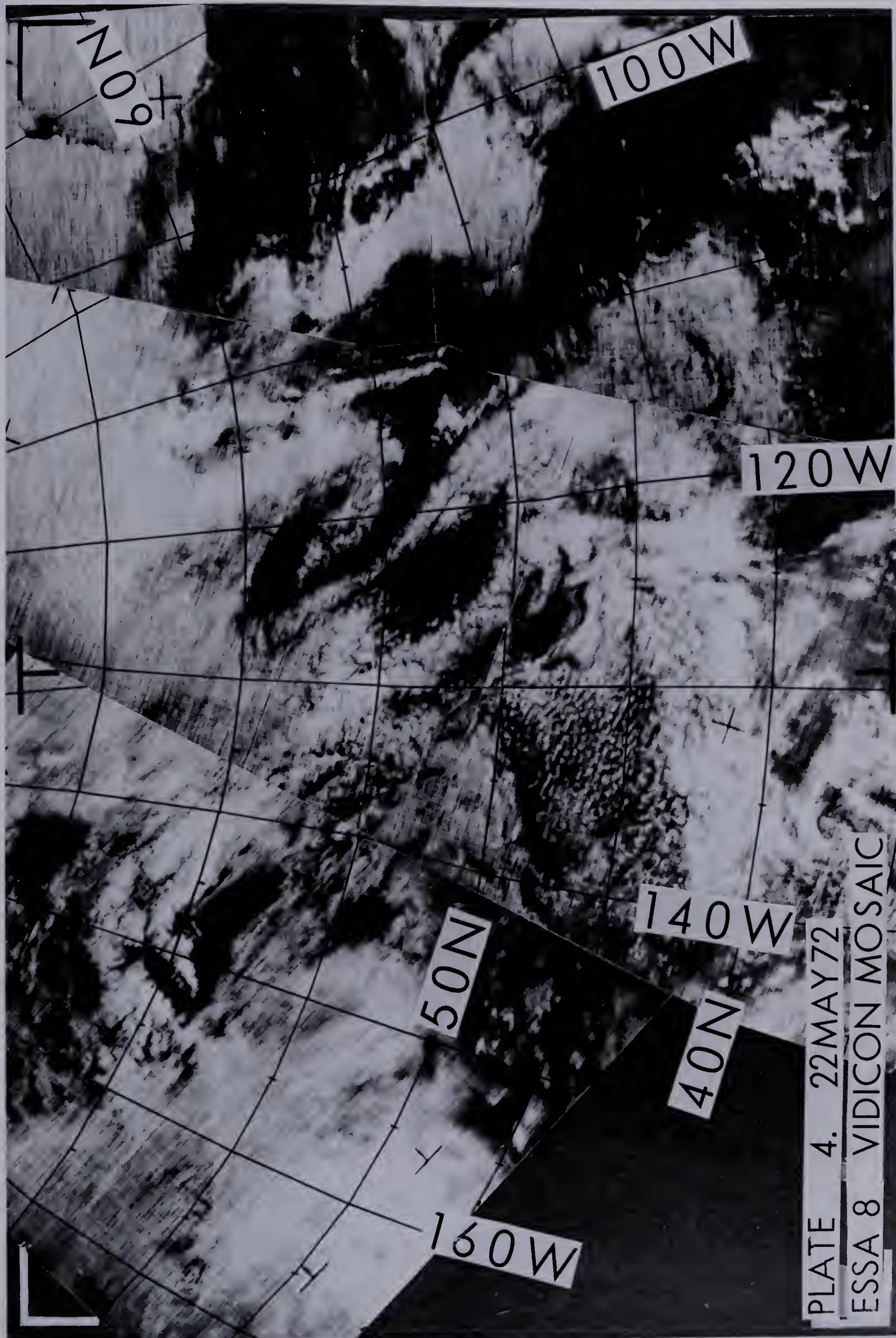
OVERLAY 3a. 21 MAY 18Z SFC











CHAPTER F

CASE HISTORIES

CASE 2: 07-10NOV72

F.1 Synoptic Situation

During the period 01-19NOV72, the large-amplitude long-wave trough position remained stationary over western North America along 110W (refer to Figure F.1). Short-wave troughs and ridges progressed eastward at intervals of about four days. With the troughs separated by about 30 to 35 degrees longitude, they move at speeds of about 20 kts. Intensification of the short-wave troughs occurred at latitude 35N along the long-wave trough position, i.e. in the southwestern United States. Open troughs usually developed closed centers as the short wave moved eastward.

The mainstream of the Westerlies lies through the Gulf of Alaska - southwestern United States - northeastern United States. The tracks of the short-wave troughs are not symmetric about 110W but are depressed southward along the Atlantic coast by the polar vortices over the eastern Canadian Arctic. The track of the short-wave troughs is not the same as the trajectory of a one-fluid layer over a barrier given in Figure A.3 (30°-upstream ridge position): the tracks do not recurve northward downwind of the barrier,

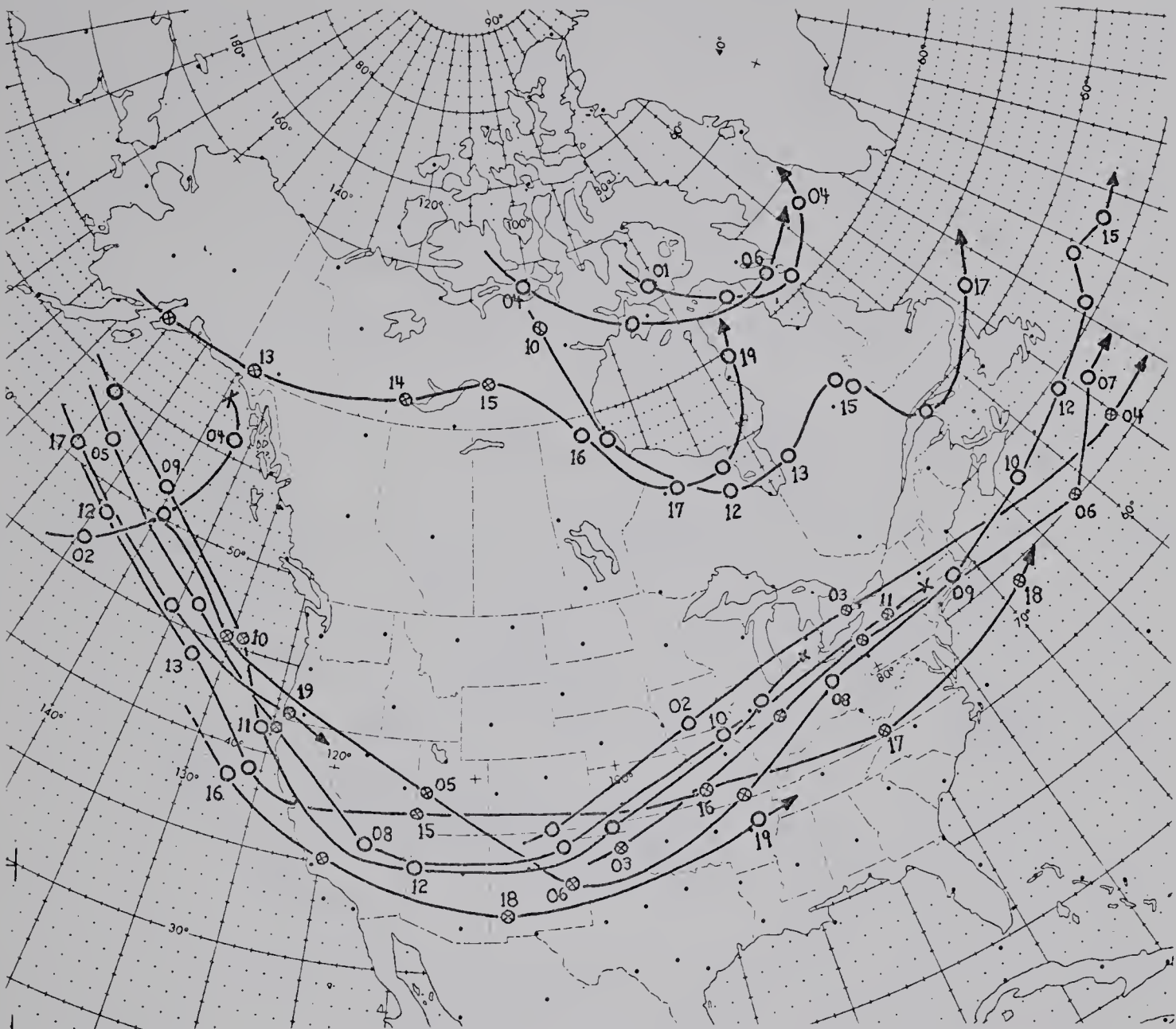


Figure F.1. Track and 1200Z position of 500-mb troughs and lows for the period 01-19NOV72.

although the flow is similar to the 50°-upstream ridge location.

On the 07NOV, Day 1 of the case study, short-wave troughs lie over the Aleutians (about 160W), along the Pacific coast (125W), and over the mid-continent (93W). These troughs reach the coast (130W), 93W, and 63W, respectively, four days later.

The surface positions of highs and lows in the West-

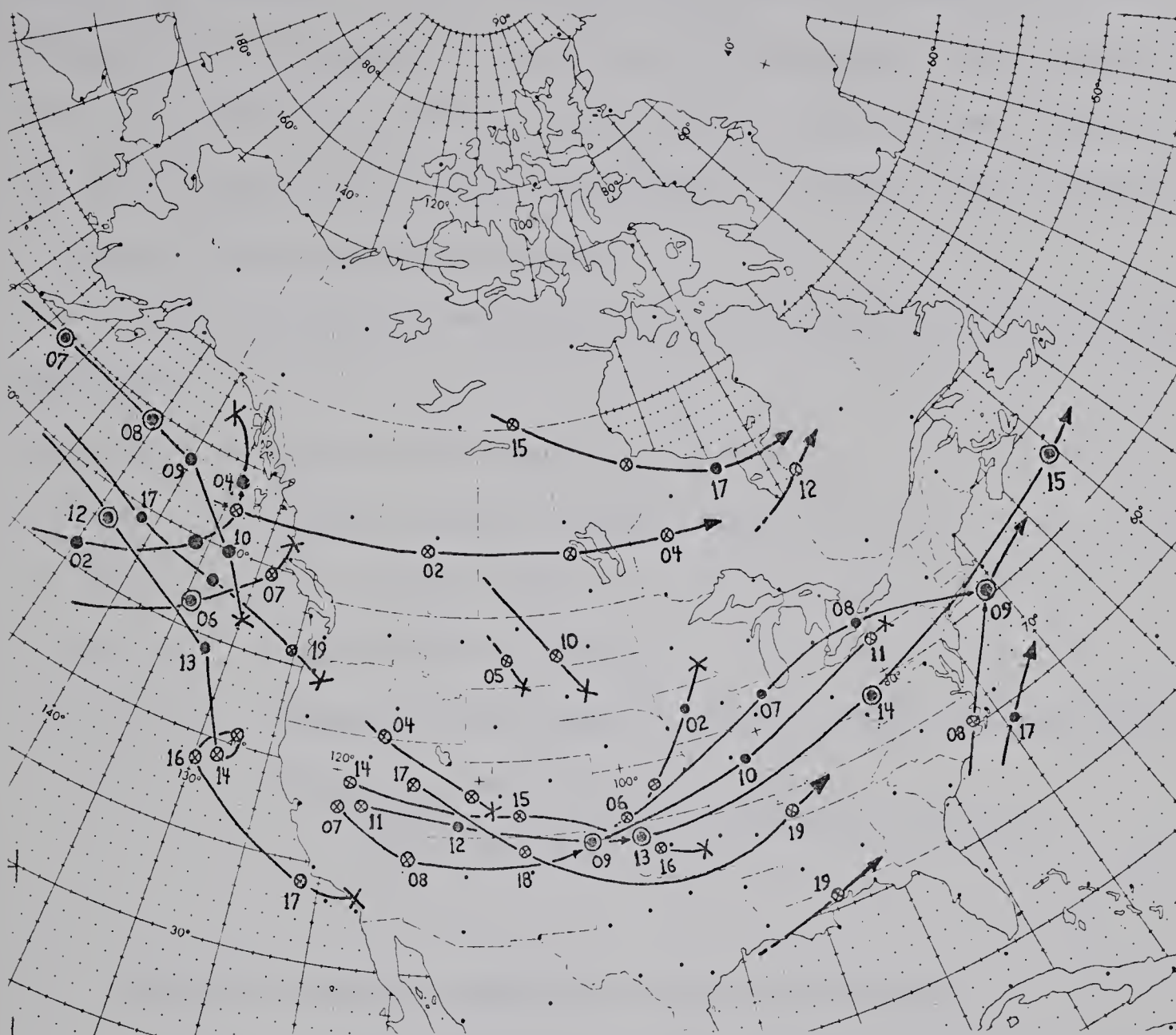


Figure F.2. Track, intensity, and 1200Z position of surface lows for the period 01-19NOV72.

erlies (Figure F.2) reflect the position of ridges and troughs at 500 mb --- the surface systems are located about 5° longitude downstream of the upper system. Cyclones moving across the eastern Pacific Ocean weaken, suffer cyclo-lysis along the coast, redevelop in the southwestern United States, and intensify as they move east of the Cordillera. Over the mountains, 9 low centers in this sample period are weak, 1 is moderate, and none is intense. Over the Plains

(east of 105W), 5 low centers are weak, 4 moderate, and 3 intense --- the number of moderate and intense lows increasing significantly. To the north of the Westerlies, only a few weak lows occur, while mid-Canada is under the influence of Arctic high-pressure centers.

The following vertical time-sections are used in the analysis:

Figure Vertical Time-section station

- F.4 Ocean station (Ship) PAPA
- F.5 Port Hardy (ZT)
- F.6 Prince George (XS)
- F.7 Vernon (WVK) with Penticton (YF) station data
- F.8 Edmonton (Stony Plain) with
 Edmonton City (XD) station data and
 cloud time-section

F.2 07NOV72: Notes, Comments, and Observations

Refer to Plate 5 and Overlays 5a (SURFACE), 5b (700 mb), and 5c (500 mb).

In the eastern Pacific Ocean, the frontal cloud band is associated with an intense surface low at 55N158W, and an upper-level low farther west over the Aleutians (off the edge of mosaic):

A cold front with BKN/OVC ST/SC OVC AS/AC embedded TCU/CB (and a band of CS), giving rain showers, lies along 40N155W - 45N147W to wave at 52N144W. Note the eastward displacement of CS band (42N150W - 45N147W - 50N144W) from the trailing edge of middle and low cloud.

A warm front with OVC low cloud (SC/ST) SCT/BKN AC, giving rain and drizzle, extends from the wave southeast to 40N137W. The Ship PAPA time-section indicates cloud below 850 mb; the air above is very dry.

An occluded front, with OVC low cloud, OVC AS/NS BKN/OVC CI/CS and embedded CB, extends from the wave around to the north of the surface-low center. Considering the 8-hour difference between the 500-mb chart and the satellite mosaic, the leading edge of the warm and occluded frontal cloud corresponds approximately with the north-to-south axis of NVA downstream of the upper ridge. Neglecting the occlusion (which is not shown on the surface map) the position of the surface front is very good.

The warm sector (45N142W) clouds consist of closed-cell BKN/OVC SC with SCT CI occurring ahead of the cold front.

The clouds in the cold air mass (50N155W, along the western edge of the mosaic) show considerable development. Behind an initial band of clearing, open-cell BKN/SCT TCU/CB SCT/BKN SC/CU are giving rain and snow showers, with some middle cloud forming from the convective cloud. The cold air mass is convectively unstable over the warmer ocean.

The cold front passes Ship PAPA (50N145W) between 07/1800Z and 08/0000Z; wind direction changes from SSW to SW, the pressure continues to fall (but less rapidly), and the dew-point temperature drops. The time-section indicates a thick layer of AS cloud from 700 mb to above 400 mb. Behind the front, the cold air mass deepens very quickly,

reaching the tropopause within 12 hours and producing a very strong baroclinic zone; the 300-mb winds are 105 kts. The cold air mass is convectively unstable from the surface to the tropopause at 380 mb --- the 4/8 to 5/8 CB/TCU and showers are produced by surface heating of the cold air (surface temperature 8°C) over the warmer ocean (temperature 10°C) and by the addition of water vapor by evaporation, enhanced by the moderate winds (20 kts) and by the large ocean-to-dew point temperature spread (7°C).

In the PVA area to the east of the 500-mb trough along the coast, the clouds over the Cordillera are disorganized. No definite cloud pattern exists, except for the comma cloud at 41N122W in the southwestern United States. The head of the comma contains OVC NS/AS+CS, producing a band of rain and snow; the tail extends northeast to 42N118W as OVC AS+CI, thence south & southwest through 36N120W and over the ocean (off the mosaic) as a narrow band of cloud. The tail cloud is broken and the dry slot (SW-NE through 38.5N120W) filled with cloud by orographic motions caused by the Sierra Nevada Mountains, which lie NNW-SSE through 38N119W, normal to the southwesterly flow in the troposphere. Orographic ascent and frictional convergence at the Coast Mountains (37N121W) contributes BKN AC in the clear slot. OVC AS and banded (parallel to the flow) AC/CI orographic cloud covers the crest of the Sierra Nevada, clears to the lee because of subsidence, and then reforms over the mountains in Nevada (40N117W). Downwind of the comma cloud

(43N115W - 50N105W) the air mass at 700 and 500 mb is very dry and only patches of cloud occur over the Rocky Mountains (40N110W). The OVC band of AS+CS through 40N112W lies along the Polar jet stream and downwind of the 500-mb trough along the coast, the northwestern edge of the cloud defining the core of the jet. Mountain wave cloud formed over southern California (off the mosaic) adds to the cloud band.

Northward along the coast, transverse (to the 700-mb flow) bands of orographic BKN SC SCT TCU and showers occur over the Coast Mountains (124W) and the Cascade Range (121W) with a zone of clearing to the lee of each range. Downwind, over the Columbia Basin (46N120W), parallel bands of thin BKN AS form. Farther north, along the Coast Mountains in B.C. (50N122W), OVC SC OVC/BKN AS/NS with rain forms downwind of the area of stronger PVA at 500 mb, though the cloud is undoubtedly enhanced by orographic effects. The ZT time-section indicates that the cloud extends from the surface to the tropopause. The band of cloud extends northward along the Coast Mountains (downwind of the 500-mb trough) and over the Cassiar Mountains (57N127W). Showers occur south of the Arctic front and snow to the north. To the lee of the Coast Mountains (53N125W) subsidence clearing ends at the Cassiar Mountains. As the trough passes ZT (between 07/1200Z and 08/0000Z) the depth of the cold air increases about 100 mb, the upper-level winds shift from southerly to weak westerly, and rain falls during the subsequent 18-hour period.

Between the trough along the coast and the frontal cloud to the west, the cloudiness in the northwesterly flow can be divided into three sections:

(a) south of 40N: SCT CU/SC. The warm frontal cloud also ends at 40°N latitude. This dividing line is the signature of a surface ridge position.

(b) 40-47N: open-cell SCT TCU/CB ahead of a weak short-wave trough.

(c) north of 47N: BKN/OVC patches SC/ST with SCT AC.

Upslope flow at 700 and 500 mb causes OVC SC+AS over the Rocky Mountains (NW-SE line through 51N116W). Cloud bands from the Columbia Basin and southern B.C. (52N121W) terminate along the barrier. To the lee, subsidence clearing (50N114W - 58N123W) is followed by a broad band of BKN AS/AC cloud, with low-level OVC ST/SC and higher bands of CI (the Edmonton vertical time-section indicates low, middle, and high cloud) which reforms immediately at 52N114W and extends northeast, parallel to the 700-mb flow into a weak wave at 56N109W, north of the weak surface low at 50N110W. Snow falls in the cold air mass behind the Arctic front east of 55N110W. Ascent is produced by frictional convergence and orographic (upslope) flow in the low-level southeasterly flow, and by WAA at 700 mb. The WAA is caused by the flow of air over the dome of Arctic air associated with the high pressure center to the east.

A surface ridge is located upstream and a surface

trough in the lee of the Rocky Mountains. The lee trough contains a weak surface low (Type D) which lies underneath the 500-mb ridge. South of the cloud band, thin patches of SCT AC+CI are visible near 50N110W; to the north, SCT bands of AC, OVC ST are observed, although higher ground (e.g. Swan Hills, 54.5N115W) appears above the low-level ST.

The Edmonton vertical time-section shows the passage of a weak, upper cold front after 07/1200Z, ahead of the weak short-wave trough located at 54N119W. Cloud tops decrease from above 400 mb to 600 mb after the trough passes. The cloud time-section is of no help at this time since low-level ST forms in the shallow layer of moist Arctic air at the surface and blocks viewing of clouds at higher levels.

F.3 08NOV72: Notes, Comments, and Observations

Refer to Plate 6 and Overlays 6a (SURFACE), 6b (700 mb), and 6c (500 mb).

The frontal cloud band has moved eastward and now lies near the coast. The intense 980-mb surface low centered at 55N145W has moved eastward at a speed of 18 kts. Since the central pressure has not changed, the low has reached the mature stage and should start weakening. The 500-mb closed center (53N150W) lies southwest of the surface low.

The cold front has advanced southeastward at 22 kts to a position along 35N160-140W thence northeastward to

40N135W and into a wave near 50N130W. A short section of warm front extends southward from the wave to 40N128W; the occluded front stretches northward from the wave (55N135W - 58N140W - 59N150W) and spirals into the vortex center at 56N150W. The cloud vortex center does not coincide with the position of the surface low. The cloud spiral is formed by advection of middle cloud and the 700-mb center lags behind the surface center. The surface frontal analysis is in agreement with the mosaic although the TROWAL (occlusion ?) should be longer.

Cloud associated with the fronts is unchanged from 07NOV. On the cold front, a line of bright (i.e. thick) embedded CB and CS anvil cloud begins at 40.5N134W and broadens to 47N131W. The entire length of the occlusion cloud is in the mosaic --- OVC low-level cloud, OVC NS/AS with bands of CS to the north of 52N.

No crossing point of the jet stream can be found along the frontal cloud band, although the approximate latitude is about 48N. The signature of the jet stream is a sharp edge of CS cloud along the jet axis with lower middle cloud to the north. Since the discontinuity does not exist, cloud tops in the occlusion must be at CI level.

Wind direction at 700 and 500 mb becomes almost parallel to the cloud band beyond 50N: to the south, the cold front and the cold air mass are still advancing eastward; to the north, the occlusion has become almost stationary. The occlusion cloud becomes deformed by stretching: the meso-

scale convection pattern will be elongated into bands, giving the banded structure observed by radar and seen on the mosaic.

In the cold air mass to the west of the cold front and the occlusion, a narrow zone of clearing is followed by a circular area of convective clouds. Even though Ship PAPA time-section shows a sudden change in air mass (700-mb temperature decreases by 12°C), the 700-mb charts for 07NOV and 08NOV show no areas of CAA, strongly suggesting that the CMC objective analysis of the temperature field over the ocean is very poor.

The convective cloud area can be divided in half along a north-to-south line through 145°W , which probably defines an upper-level short-wave trough. The 500-mb vorticity analysis does not indicate a trough, even though one was introduced by the use of bogus stations.

To the east of the line, SCT disorganized, large closed-cell CB is embedded in BKN AC; the convective elements are aligned parallel to the cyclonically-curved frontal cloud band. To the west, SCT open-cell convective polygons of small-cell CB/TCU plus BKN CU are found with a band of jet-stream CS NW-SE through $45^{\circ}\text{N}150^{\circ}\text{W}$. On the northwest side of the convective area ($53^{\circ}\text{N}158^{\circ}\text{W}$) BKN CU/SC cloud streets form as the cold air flows southward from the Aleutian Islands over the warmer ocean. The cloud streets grow to become lines of TCU/CB. The western side ($45^{\circ}\text{N}160^{\circ}\text{W}$) borders the OVC AS+CS of the next frontal system

while along the southwestern side, BKN closed-cell SC forms in the shallowing cold air.

A well-defined comma cloud (51N148W) which terminates the northern end of the line along 145W is associated with a vorticity maximum and short-wave trough WSW-ENE through 52N150W. A vorticity maximum is analyzed at 52N154W on the 500-mb chart. The trough line cuts the tail of the comma (51N152W) where SC/CU/TCU cloud streets develop into lines of TCU/CB and isolated CB cells. The clear slot contains only some low cloud.

From the passage at Ship PAPA (50N145W, see time-section) the cloud consists of OVC AS/NS, with SCT/BKN TCU/CB embedded in the trailing edge, giving rain and rain-showers. From the time-section, the cloud is found to be associated with an upper warm front ahead of a TROWAL, rather than the trough assumed above. The depth of the cold air decreases from the tropopause (380 mb) to about 700 mb, with only a small wind shift.

Ahead of the comma, the cold air mass is convectively unstable from the surface to the tropopause, giving deep convection; behind, the air mass is only unstable to about 600 mb, giving low-level convection. In both areas, instability is created by the addition of heat and water vapor from the ocean surface.

Thus the line along 145W divides areas of low-level convection on the west from deep convection on the east, and corresponds to an upper warm front.

Downwind of the 500-mb ridge line along the coast, subsidence from NVA produces clearing. The air mass (see ZT time-section) is very dry. Correcting 2 degrees (120 nmi) for the time difference between 500-mb chart and mosaic, the edge of the bright (i.e. thick) cloud again occurs just downstream of the ridge line, the only exception being the thick band of AS+CS at 56N128W. The NVA is strong at 45N126W along the edge of the warm frontal cloud. Downwind, the air is very dry at 700 and 500 mb. Along with the weak winds at and below 700 mb, no orographic cloud forms along the coast south of 45N. To the north, the air below 700 mb is moister and SCT/BKN SC+AC forms along the mountain ranges, with orographic clearing to the lee (45N120W - 50N120W - 54N125W).

The trough along the coast on 07NOV has moved southeast at 20 kts to lie along 35-48N121W. BKN/OVC SC+AS/AC+CI cloud occurs downwind of the trough in the area of strong PVA, the cloud being transformed into an unorganized, random cellular pattern by the orography of the Rockies and interior basin mountains.

Orographic SCT/BKN AC and a band of precipitation (WVK time-section shows cloud tops below 600 mb) covers the Rocky Mountains NW-SE through 52N118W. To the lee, after a narrow line of subsidence clearing, the AC cloud reforms. With the weak flow at and below 700 mb (less than 10 kts), the surface lee trough no longer exists. South of 48N, bands of thin lee-wave AC+CI extend downwind to the north-

east (51N109W - 55N100W) producing shadows on the underlying SC cloud. Freezing drizzle and snow are reported at the surface in the Arctic air mass.

The cold air immediately behind the dissipating Arctic front is very shallow in southern Alberta and in Montana. The low-level SC cloud clears. Above the cold air, a weak westerly flow of very dry air is present in the layer at 850 mb (see Edmonton vertical time-section). Using wind speeds of 10 kts, the air parcels 24 hours previously would be 4 degrees (240 nmi) to the west, somewhere along the windward slopes of the Rocky Mountains. Since both WVK and XS time-sections (07/0000Z - 08/0000Z) indicate cloud in the lower levels, the dry air is not advected. The only other possibility is the loss of moisture by precipitation from clouds produced by orographic ascent over the Rocky Mountains. Since a BKN AC cloud layer between 700 and 600 mb (10 to 13 kft) prevails downwind of the mountains, this loss only occurs below 700 mb, approximately the height of the barrier. θ_e values (296 to 298 K) are the same at Edmonton and XS, indicating the air mass is the same. The barrier removes water vapor by orographic-induced precipitation and produces a drier warmer air mass to the lee.

East of 108W, the cold air deepens sufficiently for OVC ST to form. Overlying AC can be distinguished from the ST by the shadows along the northern edges and the bright lines on the southern sun-facing edges. The AC cloud in northern Alberta downwind of the 500-mb trough at 59N124W

has no obvious pattern or organization.

F.4 09NOV72: Notes, Comments, and Observations

Refer to Plate 7 and Overlays 7a (SURFACE), 7b (700 mb), and 7c (500 mb).

The frontal cloud band has moved eastward at a speed of 17 kts at 40-45N and 7 kts at 50-55N, and now lies along 35N132W - 40N124W (on coast) thence northward and inland parallel to the coast. The surface low has weakened --- its central pressure has risen from 980 to 994 mb --- and moved slightly east to 55N142W, underneath the 500-mb center. A secondary low center has formed to the southeast, at 48N133W, near the area of enhanced CB. 500-mb height rises of 8 dam over central B.C. combined with falls of 20 dam off the coast (45N130W) intensify the upper ridge over the Cordillera, producing southerly flow along the coast.

Only a small fragment of warm frontal cloud remains (38N124W). The conjunction of the warm and cold fronts (41N123W) is also the crossing location of the jet stream (40N126W - 42N120W): to the southwest, OVC bright (i.e. thick) NS+CS; to the north, OVC/BKN thinner AC/AS along 120W and BKN AC+CB, giving rain showers over the mountains along 123-124W.

Orographic ascent in the south-southwesterly flow along the Coast Mountains and the Cascade Range produces cloud lines along 42-48N124W and 44-47N122W, respectively, with clearing to the lee of each barrier, for example,

northeast of the Olympic Mountains (48N124W). Even though the flow almost parallels the barriers, the ascent releases potential instability in the cold air mass, producing CB cloud and convective showers. The cyclonically-curved frontal band of 07 and 08NOV has ceased to exist; only a faint band remains, extending along 41N123W - 45N120W - 50N123W, and ending at the comma cloud at 50N127W.

On the ZT, XS, and WVK time-sections, the air mass near the surface ahead and behind the passage of the cold front remains unchanged --- the occlusion has now become a TROWAL, or perhaps more appropriately, an upper cold front. The comma cloud of bright (i.e. thick) OVC SC+AS/NS+CS with embedded convective cloud, and giving an area of rain, is associated with a short-wave trough in the southerly flow. A wave is produced along the upper cold front. The cloud is enhanced downwind of the trough, forming the comma cloud, but suppressed upwind, giving darker (i.e. thinner) cloud to the south (48N). On the surface chart, the cold front is shown as a TROWAL. However, how is a wave to be drawn along this line?

At 19/1200Z, the wave was upstream (south) of UIL (48N124W) --- temperatures and heights on the 700- and 500-mb charts are high compared to surrounding stations. The six-hour motion gives a speed of about 30 kts. Because the wave length is short, the smoothing inherent in the objective analysis program removes the trough. Only a small area of PVA is present, while NVA is absent.

Since the comma cloud lies over the Coast Mountains (51N125W) and the mountains of Vancouver Island (50N126W), orographic ascent in the southerly flow would contribute to the ascent produced by the upper-level trough and that caused by convection. Although the time-section indicates no change in cloud thickness, the mosaic does show thick cloud in the wave and thinner cloud behind. Clearing to the lee of the Coast Mountains (52N123W) is probably due more to the stabilization of the atmosphere by convection and subsidence around the comma cloud, than to orographic subsidence.

The wave (comma cloud) is almost impossible to detect using surface observations. The time-section for ZT shows only the large-scale passage of the upper cold front. No significant change in cloud occurs after the passage of the leading edge of the warm frontal cloud before 09/0000Z (18 hours previously). The 6-hourly surface weather shows only a decrease in wind speed and a 0.7 mb/3 hrs check (✓) pressure tendency after 09/1800Z.

The cloud pattern behind the frontal band is similar to that on 08NOV. To the east of the NW-SE line, 52N138W - 42N126W, a very bright, area of BKN, closed-cell CB with CI plumes downwind, terminates at the southern end in a comma cloud, the signature of a vorticity maximum and short-wave trough. A break again occurs between the deep-convection area and the frontal band. A second north-to-south line, 48N138W - 40N131W, thence southward off the mosaic, sepa-

rates SCT closed-cell CB to the east from the SCT open-cell CB/CU/TCU to the west. Motion of the line from the previous day (08NOV) is 25 kts at 40N, and 15 kts at 50N. Where this line cuts the frontal band (35N130W, off the mosaic) the SCT/BKN SC becomes OVC SC+AS+CS downwind --- the signature of an upper trough (i.e. maximum of vorticity) crossing a frontal zone.

Using bogus data at 500 mb, the trough line was placed upstream of the CB area. However, the analysis is still poor. Using the Laplacian, the trough at 50N135W appears too far east. Part of the problem is the use of grid data to calculate point values. Since the contour lines are not parabolic in shape, the trough axis is displaced eastward. The 'trough' at 40-45N133W curves anti-cyclonically (rather than cyclonically) pushing the vorticity maximum to the north. This error illustrates the problem of providing bogus data for objective analysis.

The comma cloud northwest of Ship PAPA on 08NOV has moved east-southeast at 17 kts to 50N140W, though the cloud spiral no longer exists. The PAPA time-section shows the passage of a TROWAL at approximately the time of the mosaic. Table F.1 gives the wind velocity, thermal-wind velocity and advection speeds over Ship PAPA, ahead (09/1200Z) and behind (10/0000Z) the TROWAL: WAA occurs ahead of the TROWAL above 700 mb, CAA behind. Ascent by WAA produces cloud up to 500 mb; descent by CAA gives dry air above 700 mb. Since the wind shift is small, the trough and the vorticity max-

imum must be weak. The wind direction change at 300 mb is anticyclonic, indicating a ridge rather than a trough at that level.

Ship PAPA time-section shows strong "convergence" ahead and "divergence" behind the TROWAL. However, time-sections may be used to indicate vergences if

(a) streamlines through the station on consecutive isobaric charts coincide;

(b) errors in wind velocity are a fraction of the largest vergence; and

(c) the speed of the system is constant. Vergences are calculated using winds relative to the moving system.

For Ship PAPA, condition (a) is not satisfied.

At the surface, the passage of the TROWAL by Ship PAPA is indicated by a wind shift from west to northwest, a pressure trough on the surface chart extending southwest from the low, and a change of cloud from AS to CB.

The comma-shaped cloud area OVC AS at 43N145W has moved eastward at 35 kts from the wave on the occluded front at 47N165W on 08NOV. The cloud band along 60N158W - 50N150W (and thence to the comma-shaped cloud area) is the remains of the occluded frontal band located previously along 170W. This cloud has invaded the western half of the convective area observed on 08NOV.

The cloud along the occlusion on 08NOV now extends from mountainous northern B.C. (55N127W) into Alaska (64N145W). The bright line along 58N135W - 60N138W -

Table F.1

Winds at Ship PAPA ahead (09/1200Z) and behind (10/0000Z) passage of TROWAL.

Date	Pressure (mb)	Wind Velocity (deg/kts)	Thermal Wind Velocity (deg/kts)	Advection Speed (kts/type)
09/1200Z	850	293/31		
			259/07	18/cold
	700	287/37		
			318/32	19/warm
	500	302/69		
			335/27	37/warm
10/0000Z	300	311/92		
	850	318/25		
			228/07	13/cold
	700	312/31		
			279/24	17/cold
	500	298/53		
			280/26	16/cold
	300	292/78		

62.5N142W - 62N147W is snow-covered ground and orographic cloud over the St. Elias, Wrangell, and Alaska Ranges, not the edge of the occlusion cloud. The spiral into the vortex center no longer exists. Three causes can be given for its demise:

- (a) Stretching of the cloud band;
- (b) Subsidence ahead of the approaching occlusion to the west and behind the comma cloud;
- (c) Removal of moisture through orographically-induced precipitation as the cloud passes over the Cordillera.

A cloud shield of OVC AS/AC with higher AC or CI extends the entire width of the Cordillera at 57N, produced by orographic ascent in the southerly flow over the Coast, Cassiar (56N128W), and Rocky Mountains of northern B.C.

Subsidence clearing occurs downwind of the Cassiar Mountains, with lee waves developing over the Yukon north of the St. Elias Mountains (60N135W).

Over the Rocky Mountains (53N118W) BKN SC OVC AS/AC occurs ahead of the upper cold front. The WVK time-section indicates cloud throughout the troposphere except in a layer at 700 mb. The southerly winds should advect this cloud to XS in about 12 hours --- no such cloud thickness on the XS time-section occurs, although the air is moist. One may conclude that the cloud over the Rocky Mountains is partly due to orographic ascent. On the mosaic, XS lies in a clear zone located over the interior basin. This may be due in part to the weak divergent flow at 500 and 700 mb between WVK and XS.

The time-sections for ZT, XS, and WVK show similar features (although, as noted above, cloud thickness and amount at XS is less):

(a) The upper warm front moves through from the west; the air along the frontal zone is very dry and forms a dry tongue.

(b) High-level CI moves in, thickening to AS/AC as the warm frontal surface lowers. Low-level SC is present in the cold air mass near the surface.

(c) Ahead of the upper cold front, the cloud becomes thick, extending from the surface to above 400 mb as the dry tongue ends. Winds back from westerly to southerly.

(d) Thick cloud continues after the passage of the upper

cold front. Winds remain southerly.

The leading edge of the occlusion cloud, in general, lies just downwind of the 500-mb ridge axis. The NVA and the ridge are particularly strong over the Mackenzie Mountains (64N128W) where the dendritic pattern of snow on mountain ridges can be faintly seen in the low-angle sunlight. The exception occurs over the Rocky Mountains in southern B.C. where the ridge flattens and splits into two.

Over the Prairies, frontal-wave cloud OVC AS/AC+CI is observed at 55N106W, with the cold-front cloud curving westward to 54N115W, and the warm-front cloud extending southeast. The surface analysis shows a very weak low center with an upper Arctic front. Weak lows lie along the surface front position. At 500 mb, the weak short-wave trough lying northwest of (behind) the wave has moved southeast at 20 kts from northeastern B.C. on 08NOV, and from along the coast on 07NOV. Behind the upper cold front, OVC ST/SC (e.g. at 55N112W) occurs in the deepening Arctic air mass; the northwestern edge of the low cloud lies in the Peace River valley of northern Alberta (58.5N117W, 56N119W) with the surrounding higher ground cloud free, including the Caribou Mountains (59.5N115W), Clear (58N120W), Buffalo Head (57N116W), and Swan (54.5N115W) Hills.

Ahead of the upper cold front and below 700 mb is the dry air mass discussed in connection with 08NOV analysis; behind the front, the Arctic air deepens to 750 mb while the air above becomes very dry. The upper trough is

associated with a very weak TROWAL whose warm- and cold-frontal surfaces are at and above 500 mb.

Along the eastern slopes of the Rocky Mountains, a narrow band of AC (57N124W - 53N116W) forms in the south-to-southeasterly flow at 850 and 700 mb, the eastern edge of the cloud corresponding approximately with the ridge axis at 700 mb.

To the south (49N112W), SCT AC+CI occurs downwind of the clearing to the lee of the Rocky Mountains. Low wind speeds (less than 20 kts) at and below 500 mb would generate weak mountain waves. A narrow band of AS lies over the barrier at 48N113W; this is not lee-wave cloud but cloud enhanced by the release of potential instability when the air is forced to ascend over the highest barrier. In the airstream immediately to the south, this occurs over the Bitterroot Range (47N114W).

The upper trough over southwestern United States on 08NOV has moved southeastward and now lies off the mosaic. Only patches of cloud remain over the Rocky Mountains (43N110W).

F.5 10NOV72: Notes, Comments, and Observations

Refer to Plate 8 and Overlays 8a (SURFACE), 8b (700 mb), and 8c (500 mb).

Outstanding features on the mosaic are the two bright comma clouds at 40-45N128W (the WEST comma) and 35-40N121W (the EAST comma), both areas OVC NS with embedded

CB. AS+CS is advected downwind to the east --- especially true of the EAST comma (e.g. the rain area at 43N120W) where the clouds are enhanced by orographic ascent over the Cordillera. The EAST comma corresponds to the enhanced CB area on 09NOV --- the 20 kt motion between 08 (47N142W) and 09 (45N130W) would place the cloud at 41N120W on 10NOV; the WEST comma corresponds to the cloud at 43N145W on 09NOV --- 35 kt motion extrapolated between 08 (47N165W) and 09NOV, including a northward curvature, places the cloud at 40N127W.

The EAST comma lies over the Coast and Sierra Nevada Mountains. Although no obvious bands of cloud or clearing can be found, orographic ascent would enhance the cloud shield by releasing conditional instability in the cold air mass, as discussed by Lamb (1974, 1976).

The WEST comma lies downwind of the trough line bogused along 132W; for the EAST comma, the trough would be along the edge of the 500-mb objective analysis chart, and would not appear in the vorticity pattern. Between the comma clouds, only SCT TCU BKN thin SC occurs while to the west of the WEST comma, SCT TCU is present north of 40N, becoming BKN closed-cell SC with a band of jet-stream CS (36N133W) to the south. Both comma clouds have long narrow tails of SC/TCU which extend westward off the mosaic, the signature of low-level convergence along a shear line which lies through the subtropical high.

The frontal band has vanished completely --- the

only possible remnant being the OVC AS and banded CI at 36N116W. The surface lows in the Pacific have continued to weaken and have moved southeastward at 12 kts. Because the upper flow is northwesterly (rather than west or southwesterly) the northward curvature along of the coast of the approaching low is not observed. The 500-mb center in the Gulf of Alaska has remained almost stationary, while the 500-mb trough line along 130W on 09NOV has rotated about the center and now lies NW-SE through 47N120W. The trough ends approximately along the downstream line from the northern tip of the EAST comma cloud. Thus the trough has split into two parts --- that part with the comma cloud has separated from the 500-mb circulation and headed southeastward towards the California coast. The split has probably been aided by the orographic effects of the Cordillera: since vertical motions and frictional vergences are proportional to terrain height, a decrease in the width and height of the barrier would also decrease orographic effects. Such a change in the coastal barrier occurs in central Oregon north of 43N.

From the WVK and ZT time-sections, the trough corresponds to a sharp maximum in the depth of the cold air (which also shows on the 700-mb chart). As the trough passes from the south, the cold air quickly shallows above 500 mb (upper warm front) and the 500-mb wind shifts from SSE to SW. Ahead of the trough, PVA opposes CAA; PVA is the greater contributor, because the troposphere is cloudy, indicating ascent. Behind the trough, NVA opposes WAA, and

NVA is greater, because the upper troposphere has become cloud-free, indicating descent. Referring to the time-sections, the cold air mass is convectively unstable in the lower layers at ZT and neutral-to-stable above. The air over XS and WVK is near neutral, since θ_e increases only very slowly with height. The neutral to near-neutral stability indicates the air mass has been mixed by convection.

As noted on the previous day (09NOV), the upper cold front invades southern B.C. from the south. On the mosaic, neither the cold front nor the trough line can be found. No frontal cloud band exists along 58N; no difference in cloud amount or brightness can be observed across the trough line.

Along the coastal mountains of Washington and Oregon, orographic cloud at 45N121-124W is very scant, a result of the southerly surface flow paralleling the mountains, and the dry air at and below 700 mb, downwind of the WEST comma cloud. The southern extent of the dry air lies along 43N, to the south, two bands of orographic cloud form over the Coast Mountains and Cascade Range north of the EAST comma cloud. The eastern band extends northward in a less bright (i.e. thinner) band of lee-wave AC+CI along and downwind of the Cascade Range. The clear area (47N117W) corresponds to the Columbia Basin with orographic cloud occurring over the mountains from east through north. The main cloud mass, OVC NS giving rain is found over the highest barrier --- the Selkirk Mountains (50N118W). Cellular, disorganized BKN/OVC AC forms to the south-to-southwest over the moun-

tains of southern B.C., while subsidence clearing and frictional divergence occurs over the Rockies (52N116W). Along the Coast Mountains orographic convective cloud and showers are observed with clearing to the lee in central B.C. (52N124W). Between the coast of B.C. and the WEST comma cloud, SCT TCU/CB in weakly organized bands spirals towards the surface low at 53N135W, the remains of the northern portion of the deep convection line of 09NOV.

Over the Prairies, an Arctic high pressure area has built southward behind the upper trough which is now at 52N104W. The cold air has deepened to about 700 mb at Edmonton. An area of OVC AS/AS+CI cloud (53N100W) giving snow lies ahead of the trough. Behind the Arctic front, OVC ST/SC ends at higher ground, i.e. along the foothills, the Caribou (59.5N115W) and Birch (58N113W) Mountains, and the Swan (55N116W) and Cyprus (50N110W) Hills. Clearing occurs to the lee (i.e. to the northwest for the southeasterly surface wind) of the Swan Hills. To the northeast of 60N110W - 55N106W, the ST thins, so the underlying darker forest becomes visible through the cloud. The discontinuity along 63N110W - 60N99W marks the tree line: snow to the north, darker coniferous forest and snow to the south.

The cloud band east of the Rocky Mountains on the previous day (09NOV) is now a NW-SE band extending from 50N110W to 57N122W. According to the Edmonton vertical time-section (11/0000Z), the band is composed of a thick cloud layer below 500 mb (18 kft) in the south-southeasterly

flow at lower levels to the west of the ridge line. Due to the low-level OVC ST, the XD cloud time-section is of little help in this case.

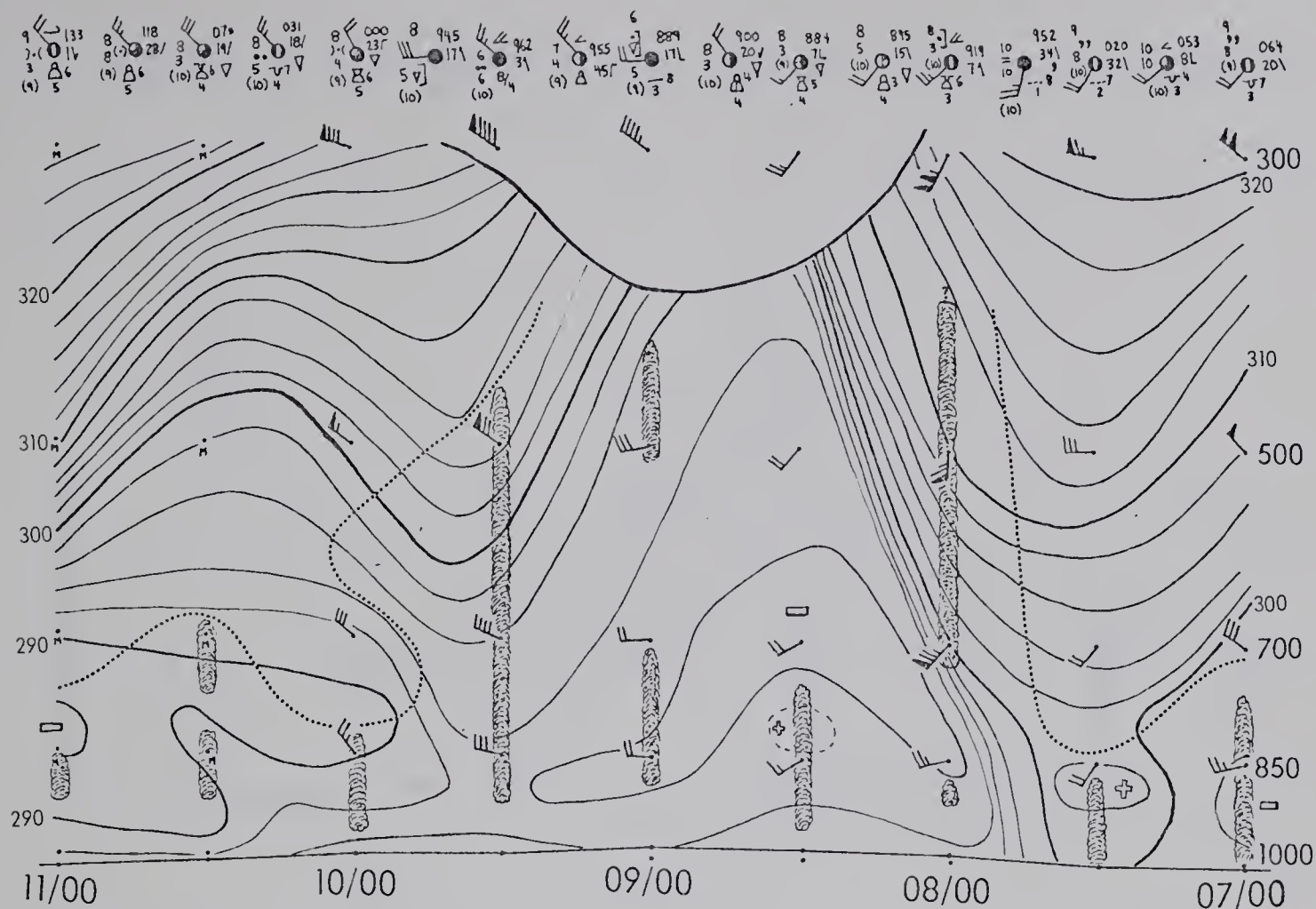


Figure F.3. Vertical time-section plus 6-hourly station weather for Ocean Station (Ship) PAPA.

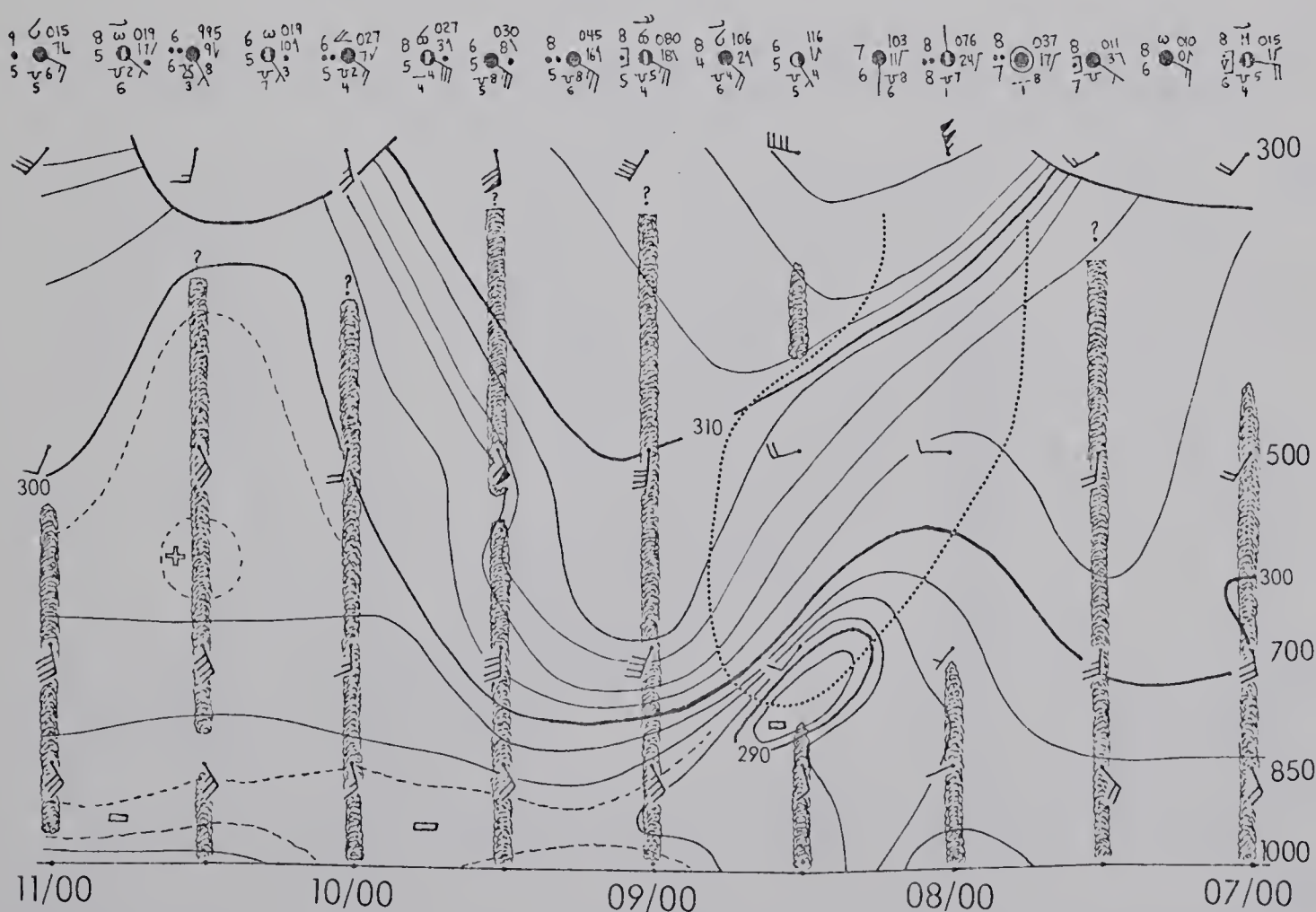


Figure F.4. Vertical time-section plus 6-hourly station weather for Port Hardy (ZT).

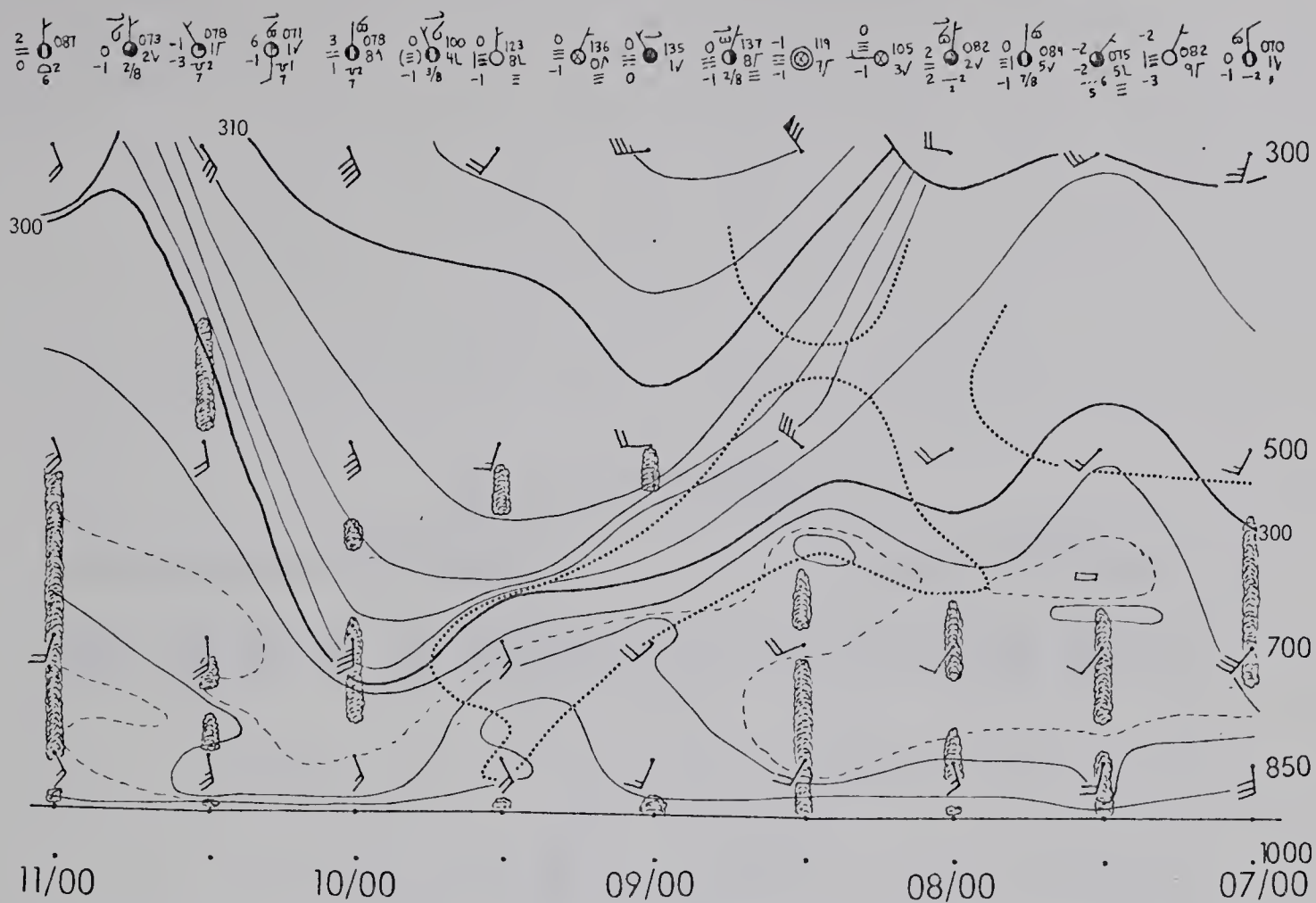


Figure F.5. Vertical time-section plus 6-hourly station weather for Prince George (XS).

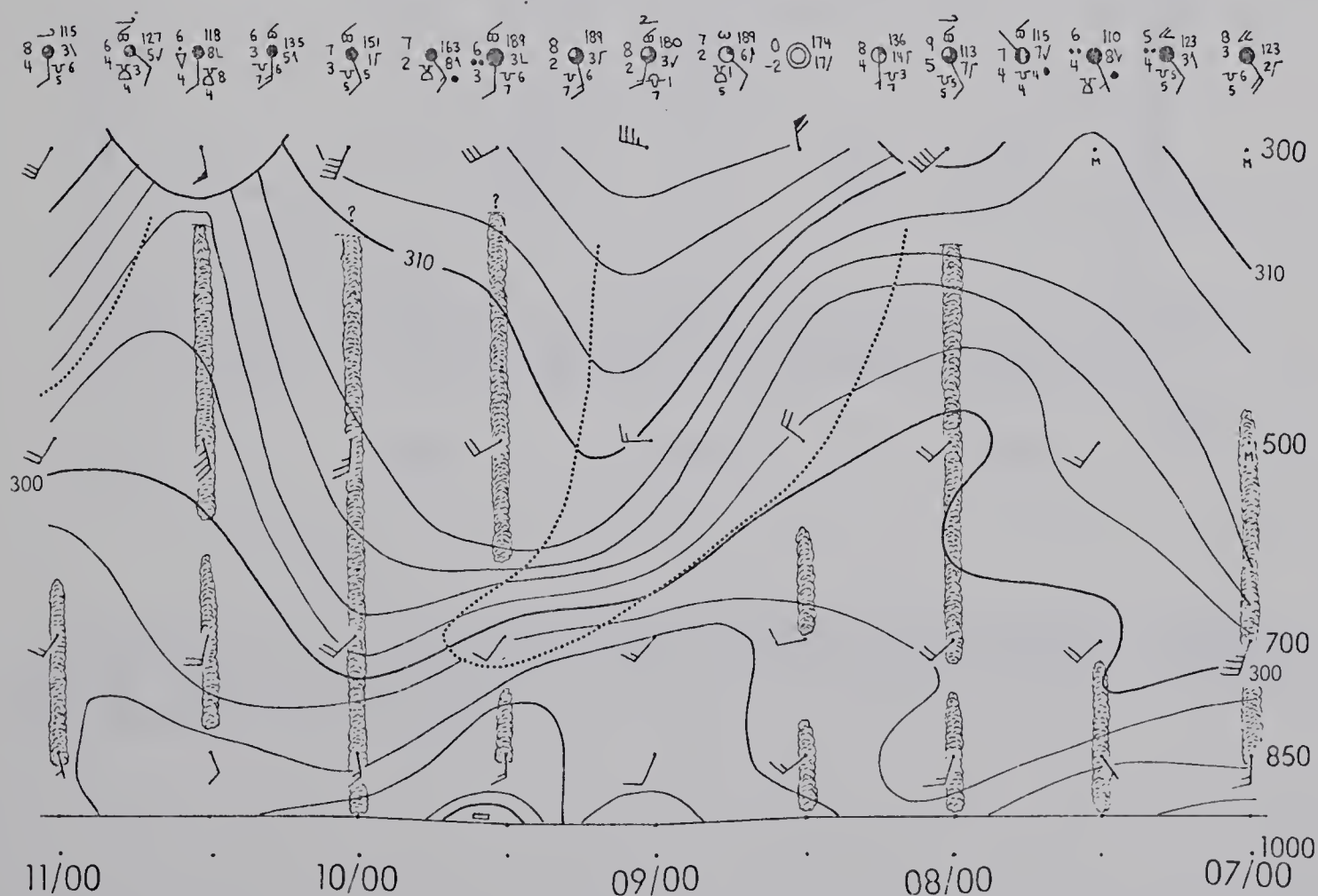


Figure F.6. Vertical time-section for Vernon (WVK) plus 6-hourly station weather for Penticton (YF).

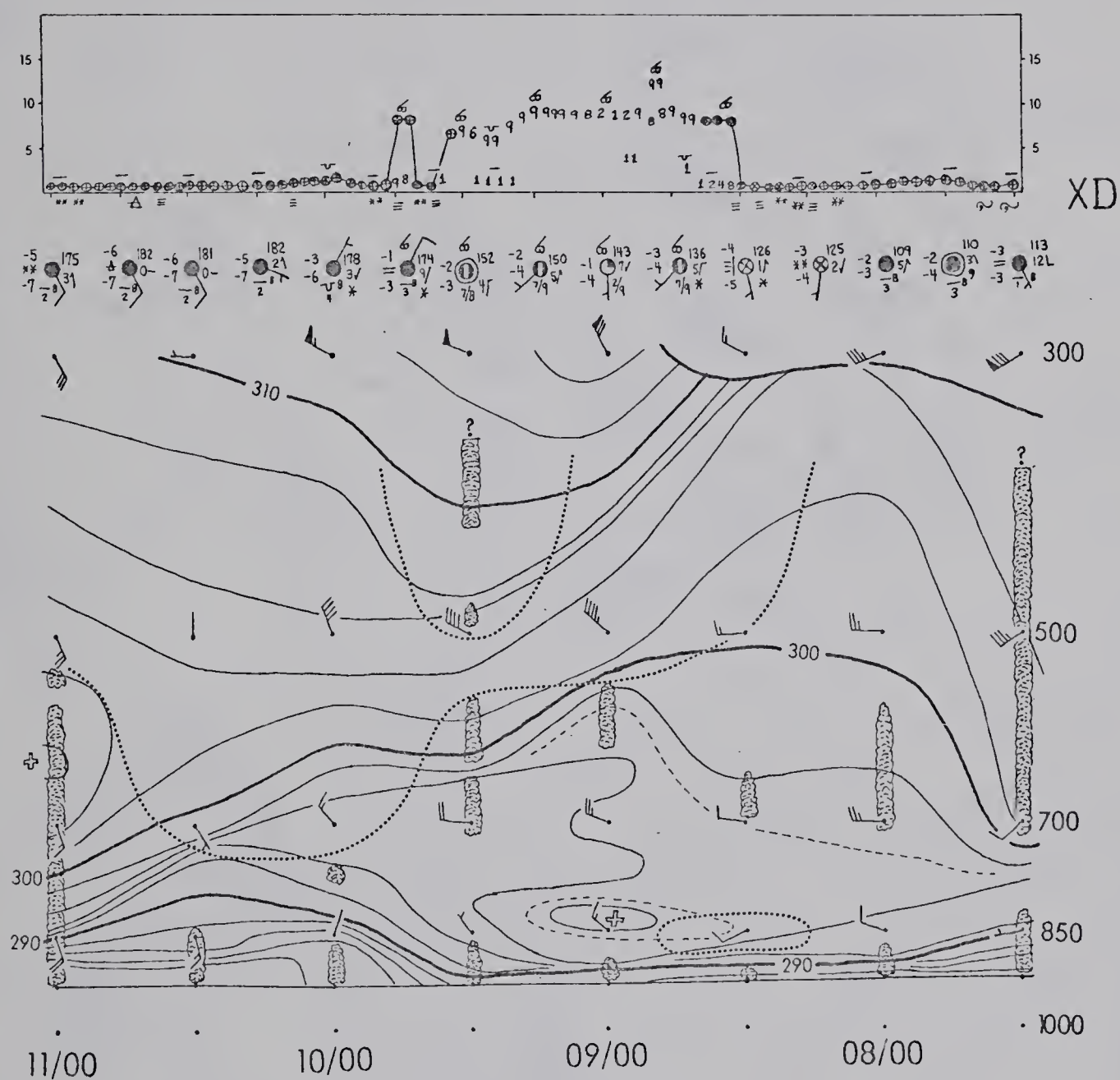
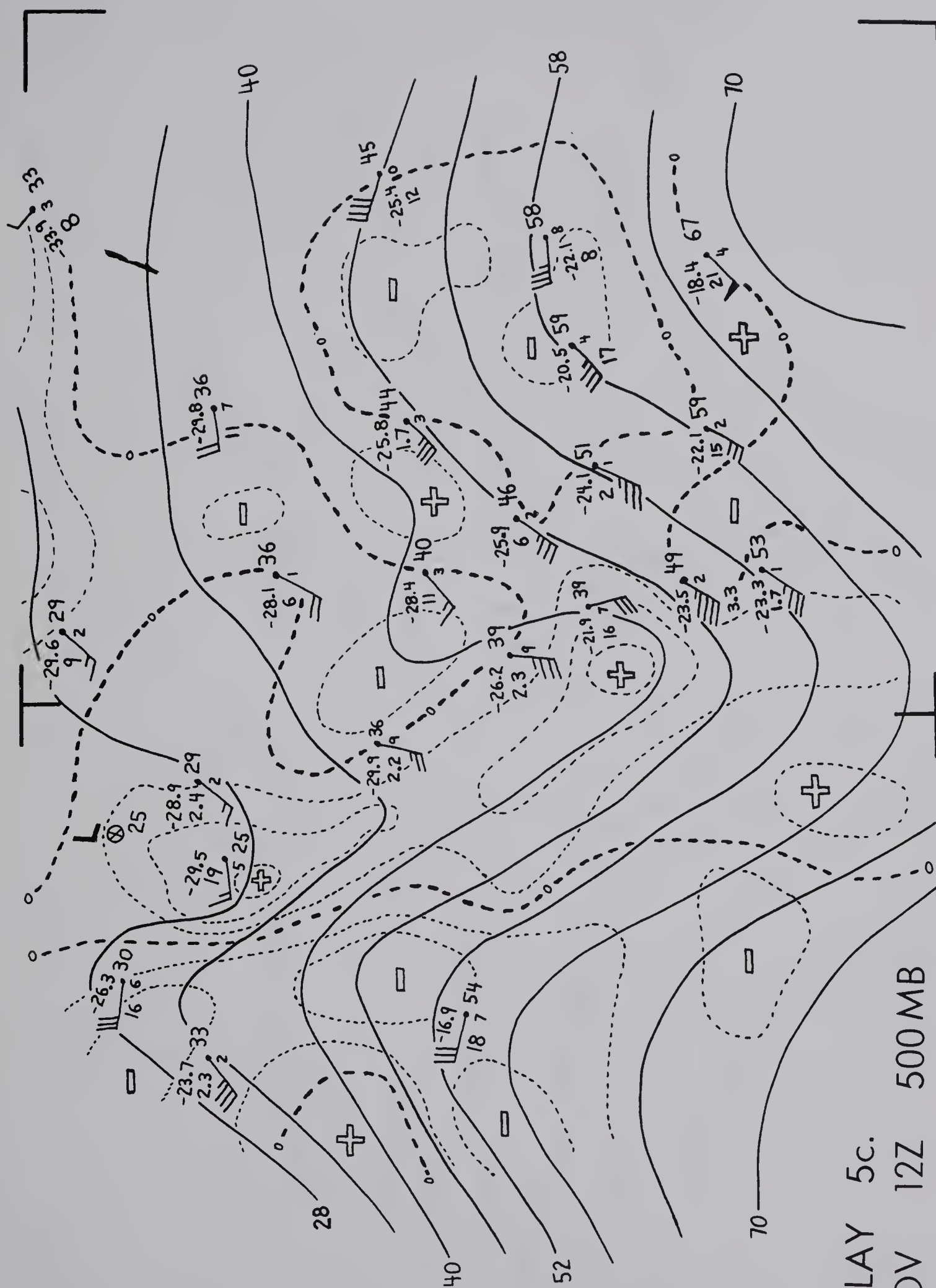
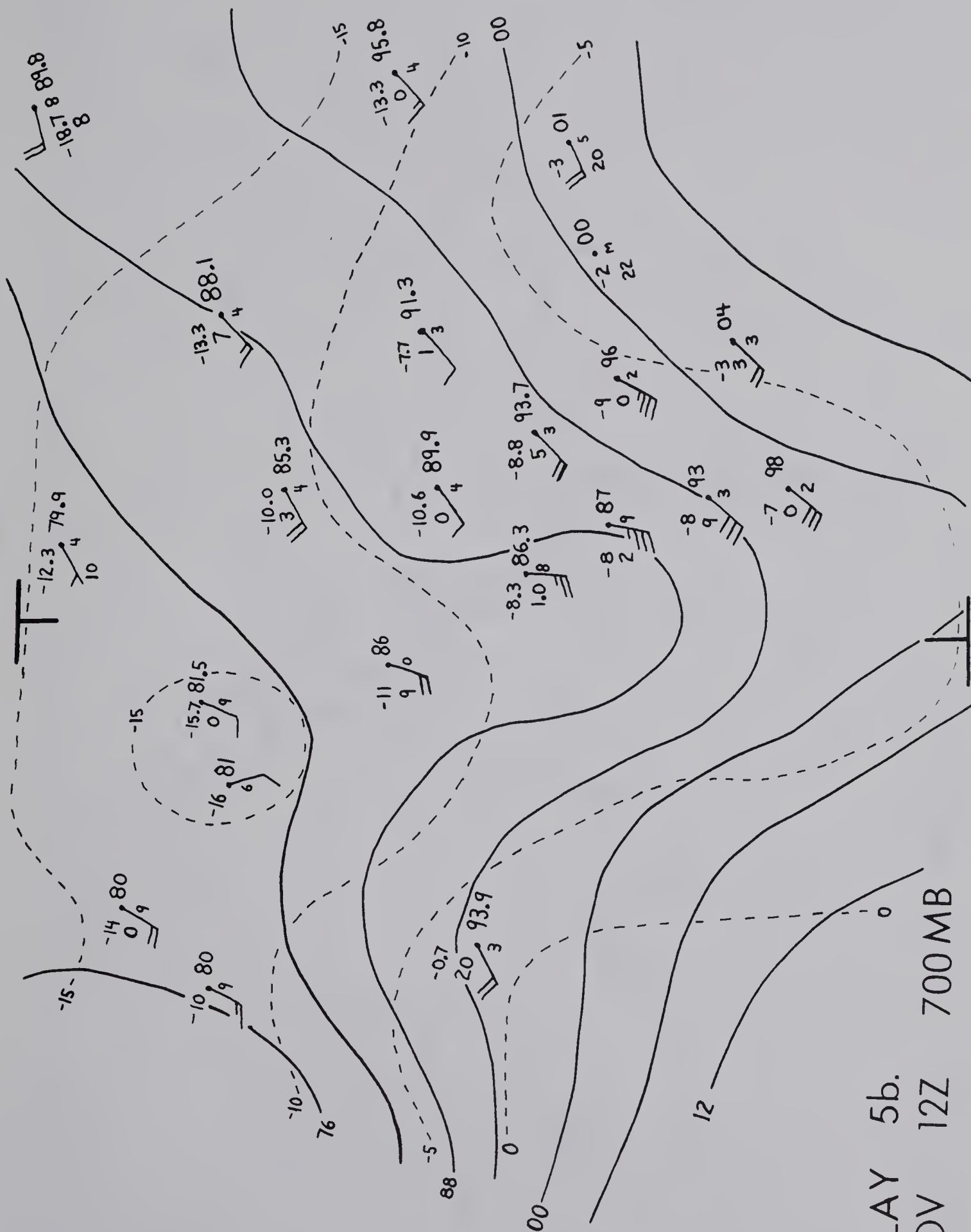
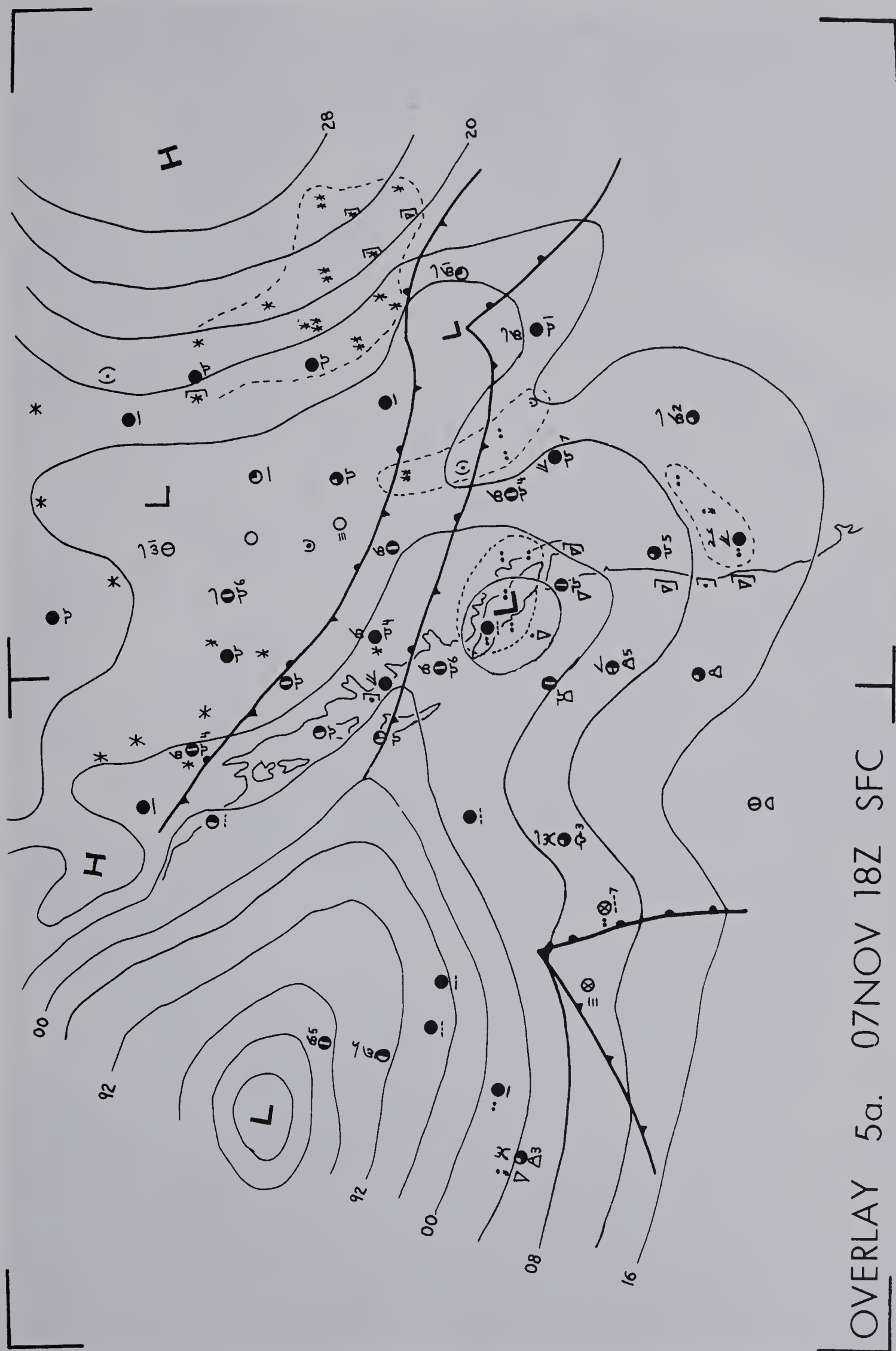
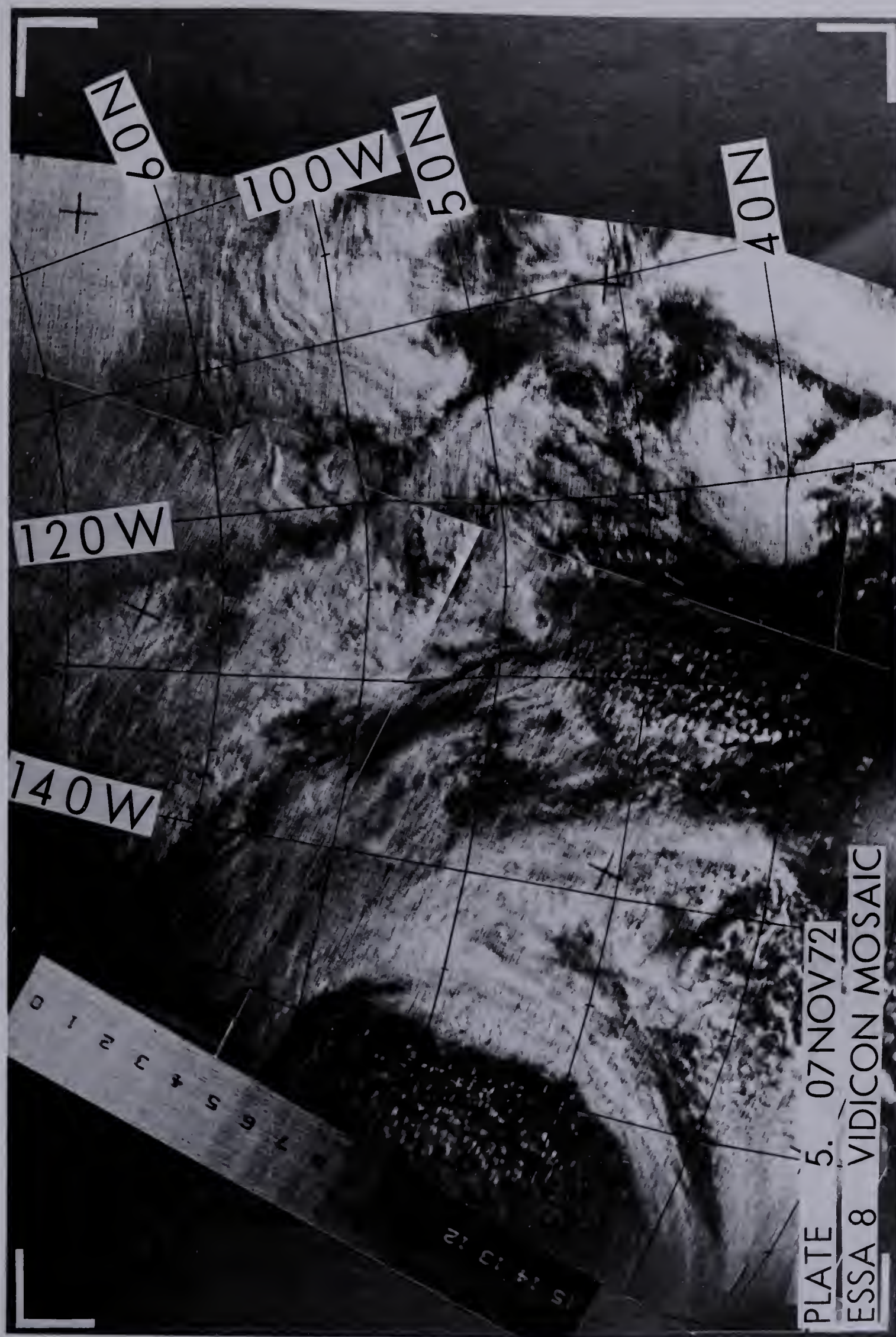


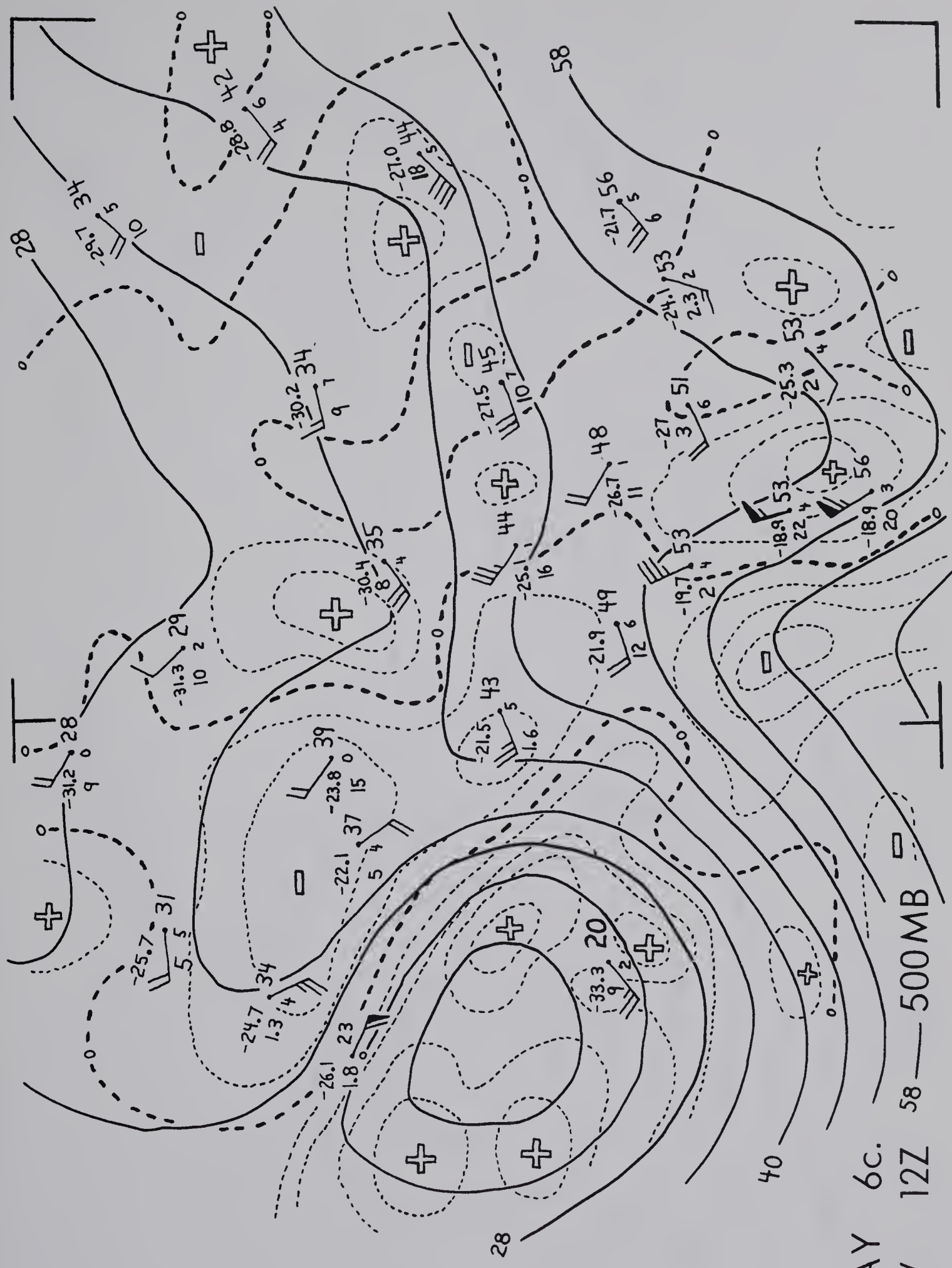
Figure F.7. Vertical time-section for Edmonton (Stony Plain) and cloud time-section plus 6-hourly station weather for Edmonton City (XD).



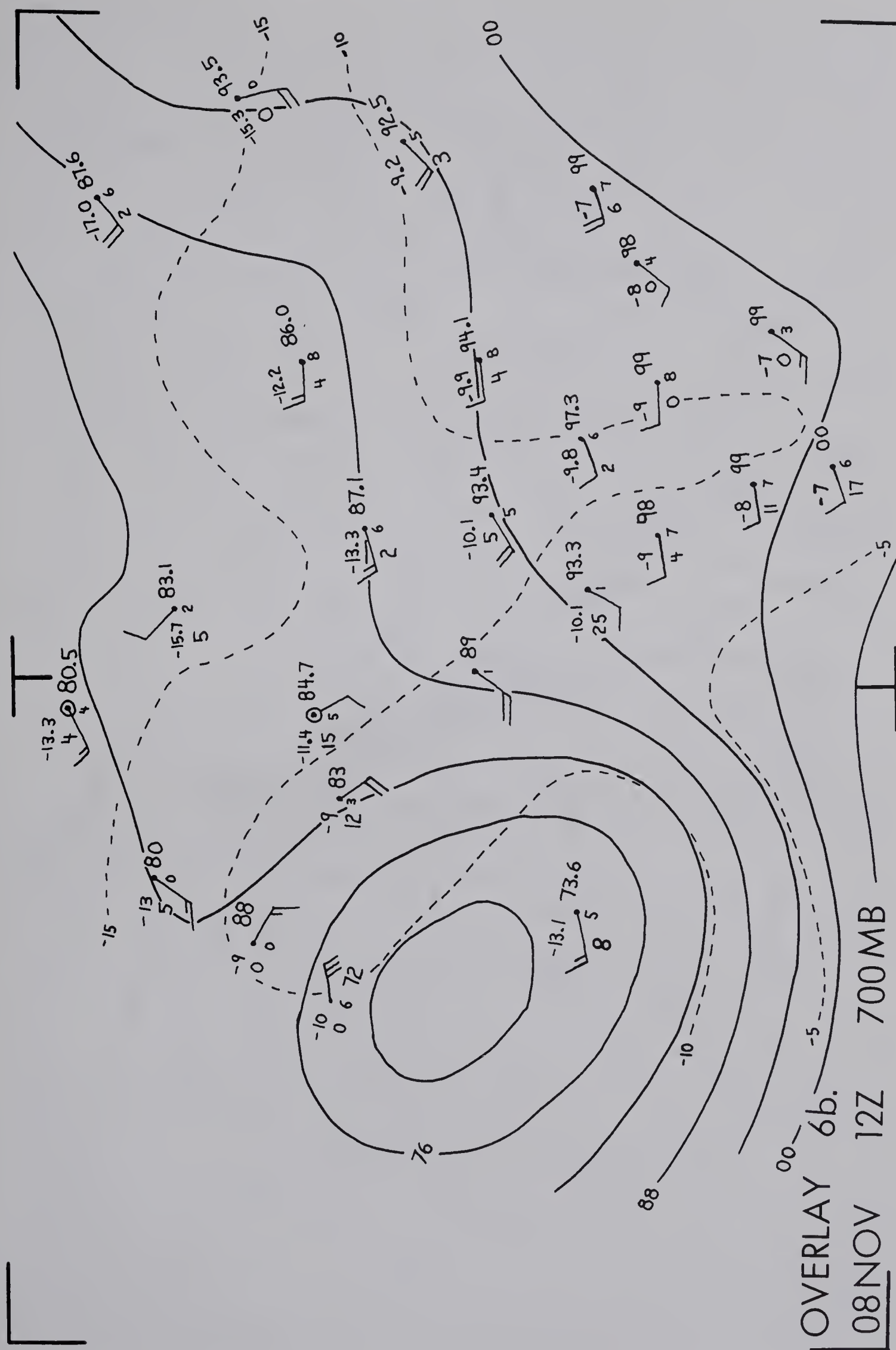


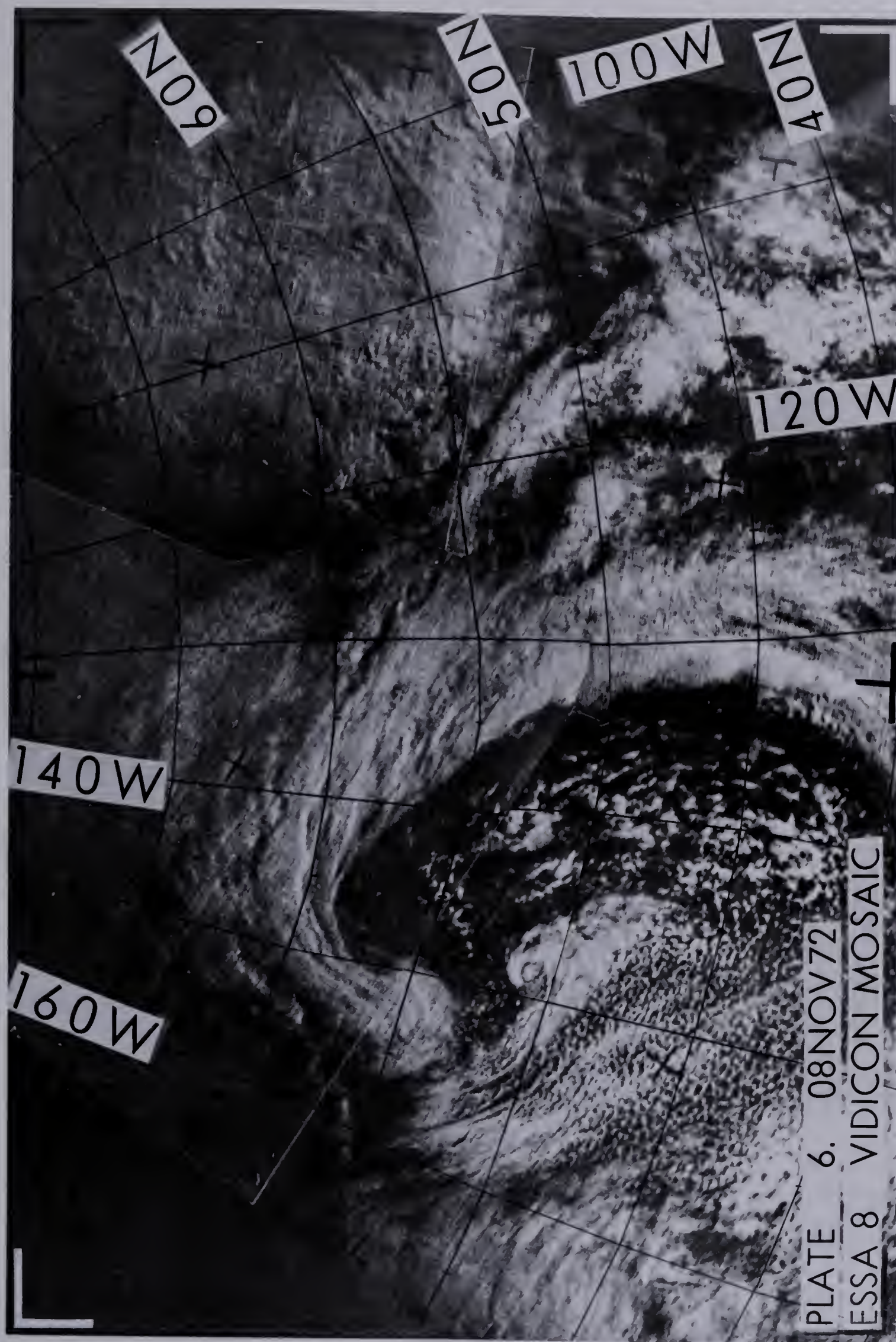


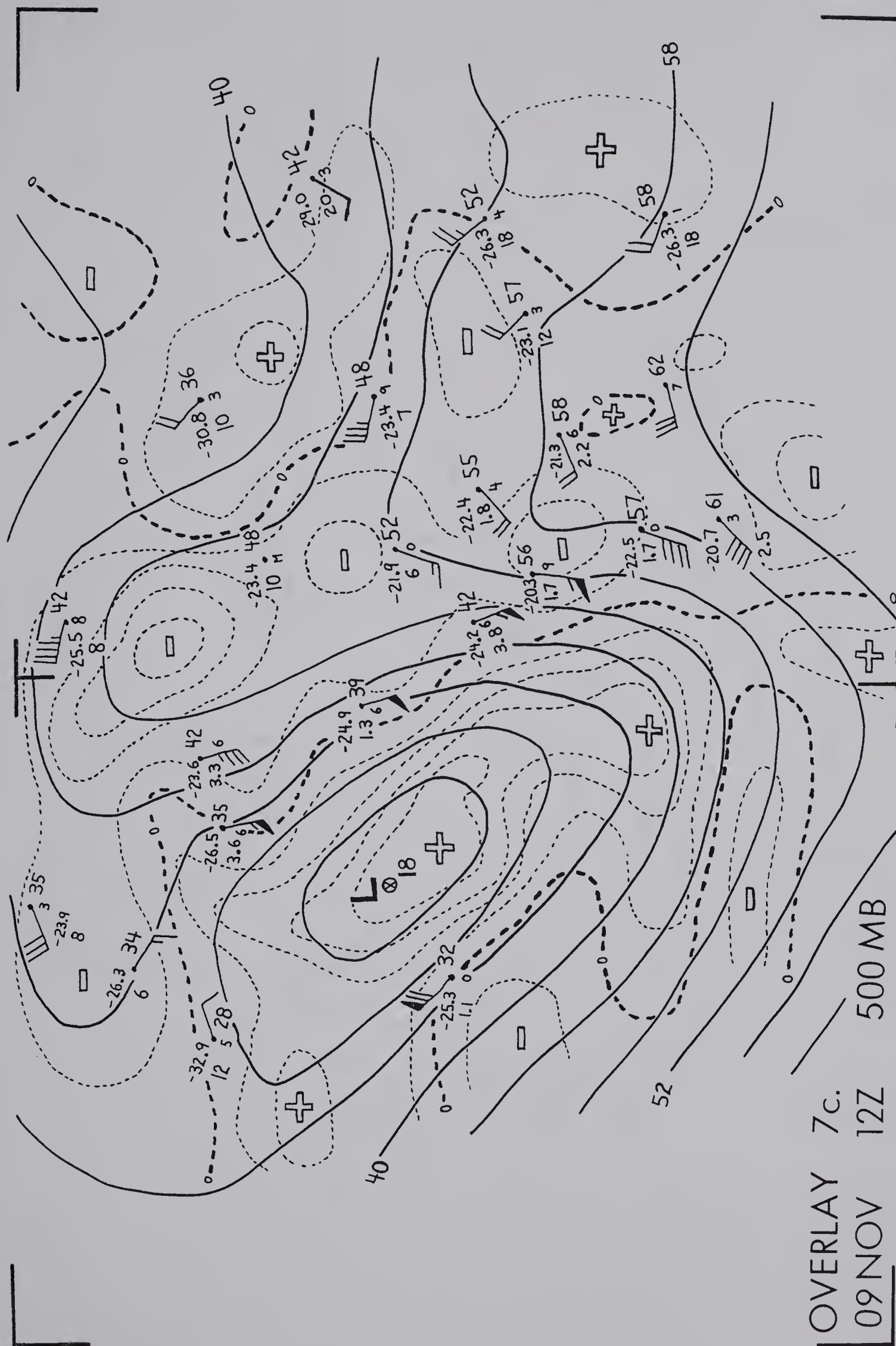


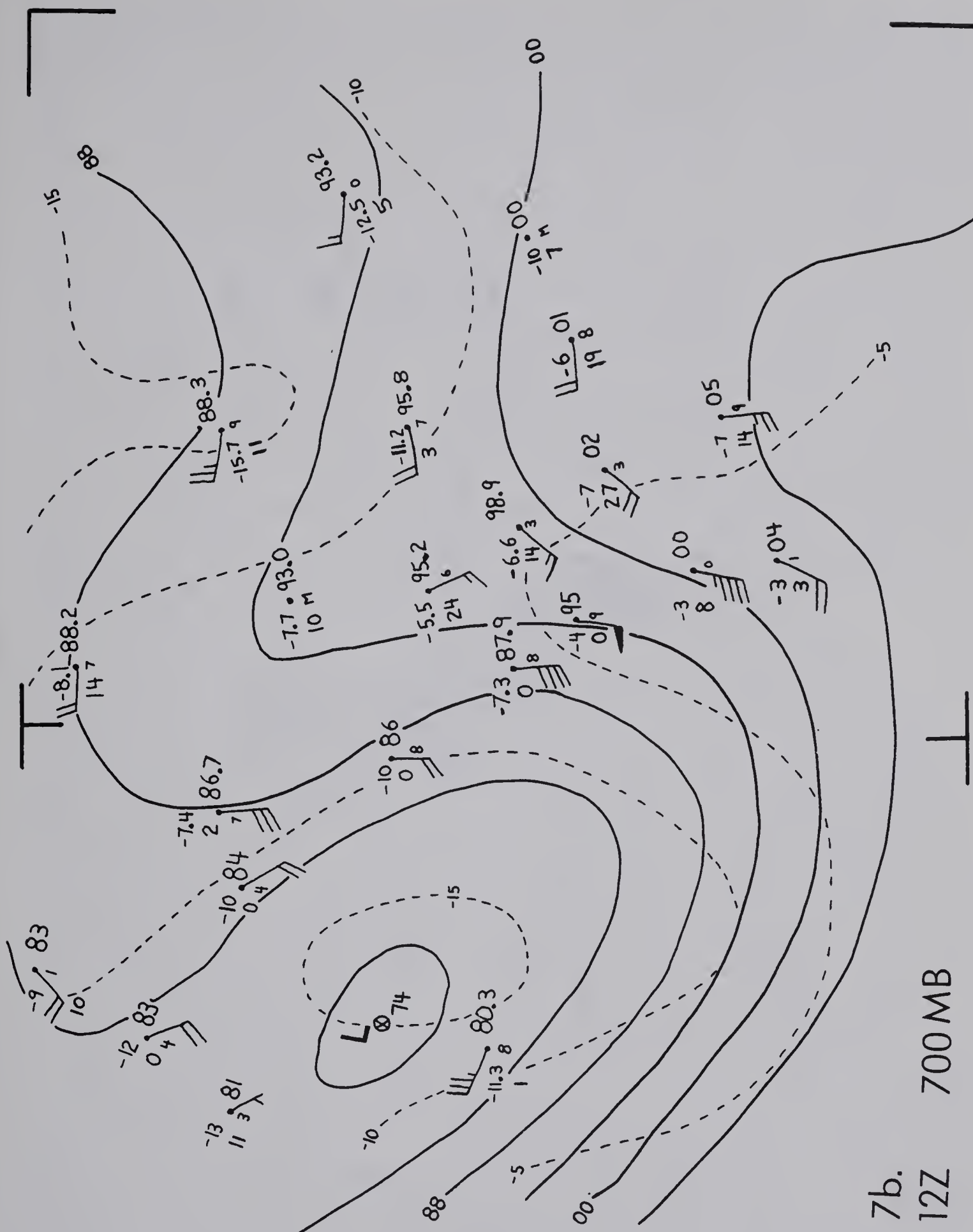


OVERLAY 6C.
08 NOV 12Z 58 — 500MB





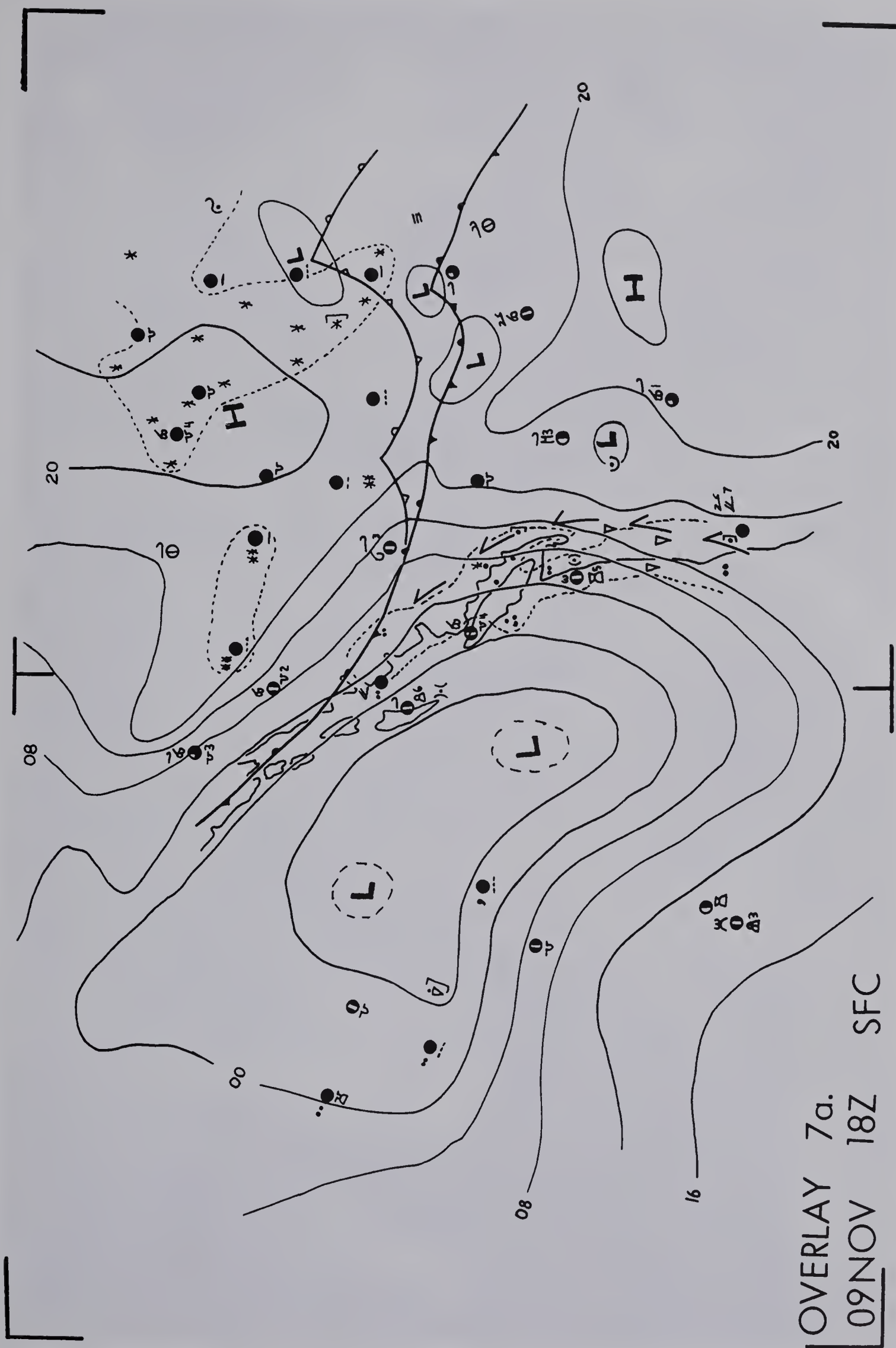


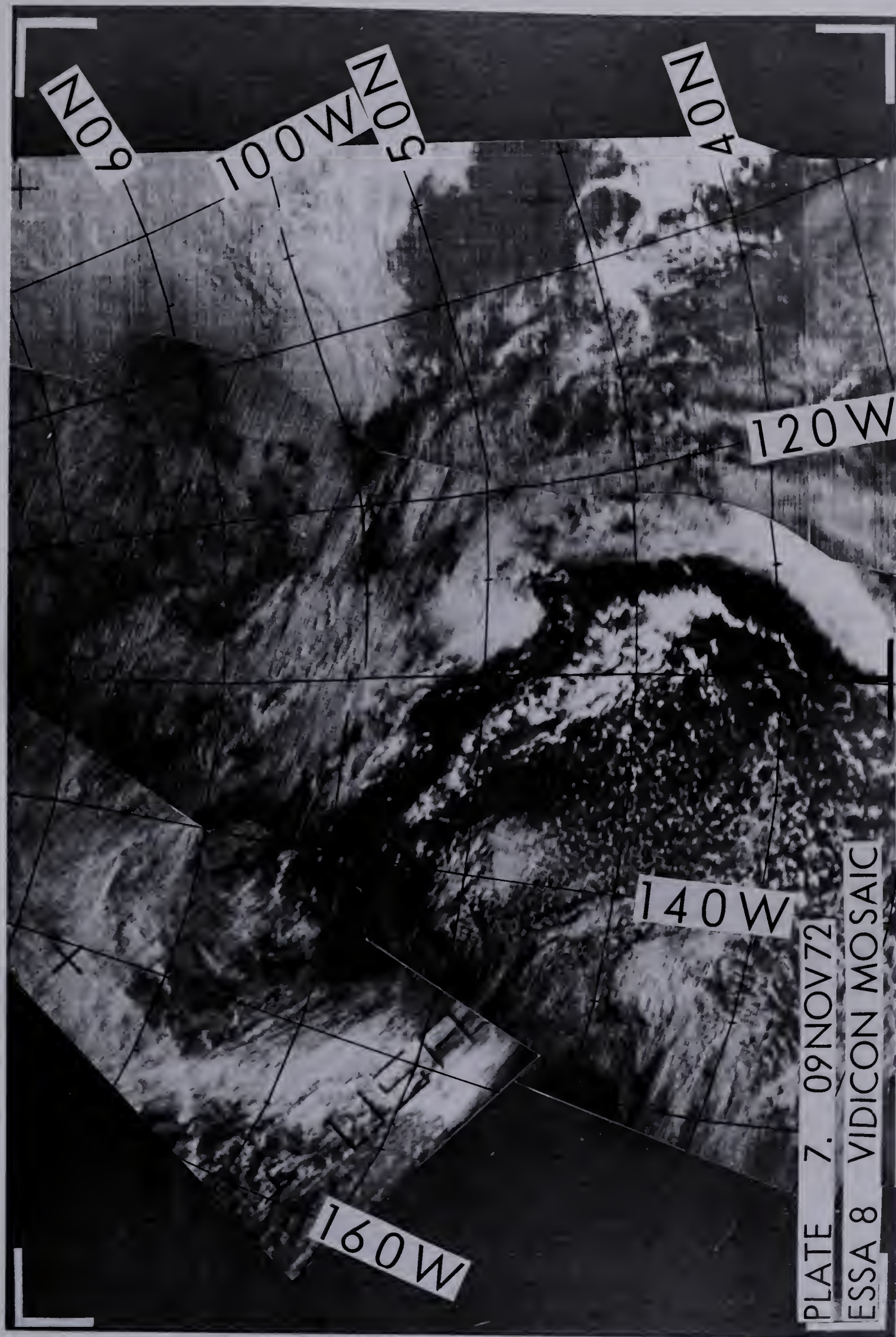


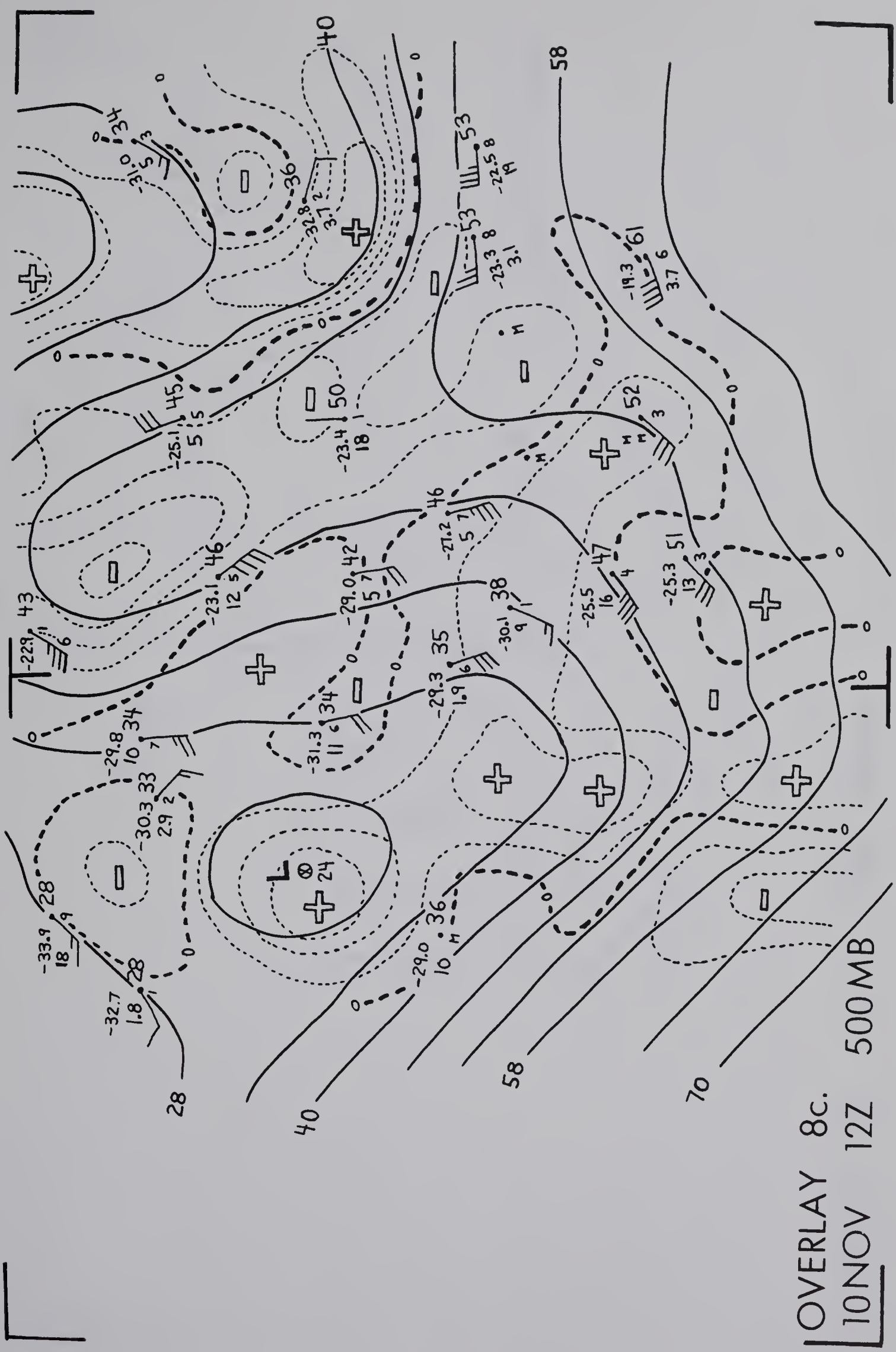
OVERLAY 7b.

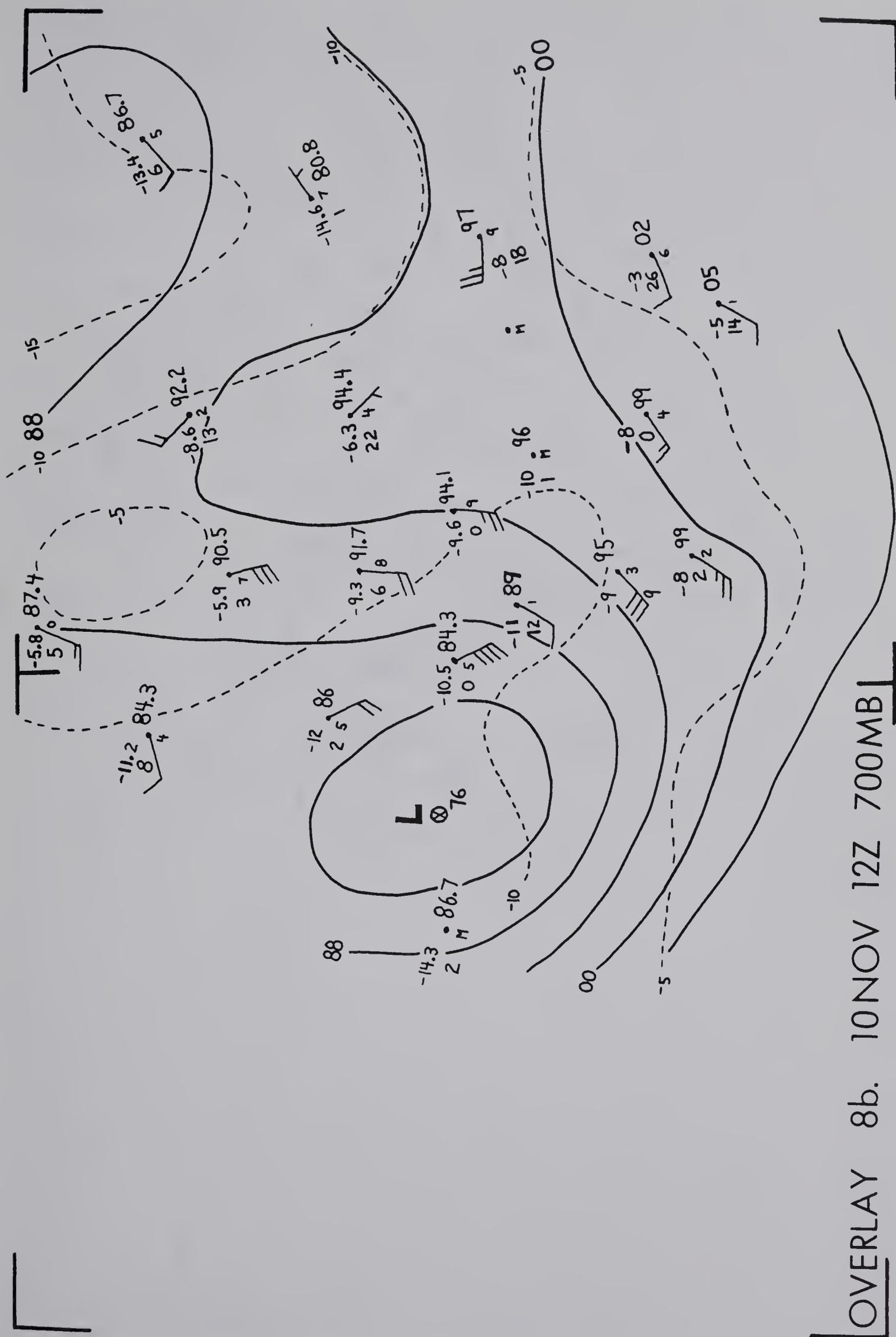
09 NOV 12Z

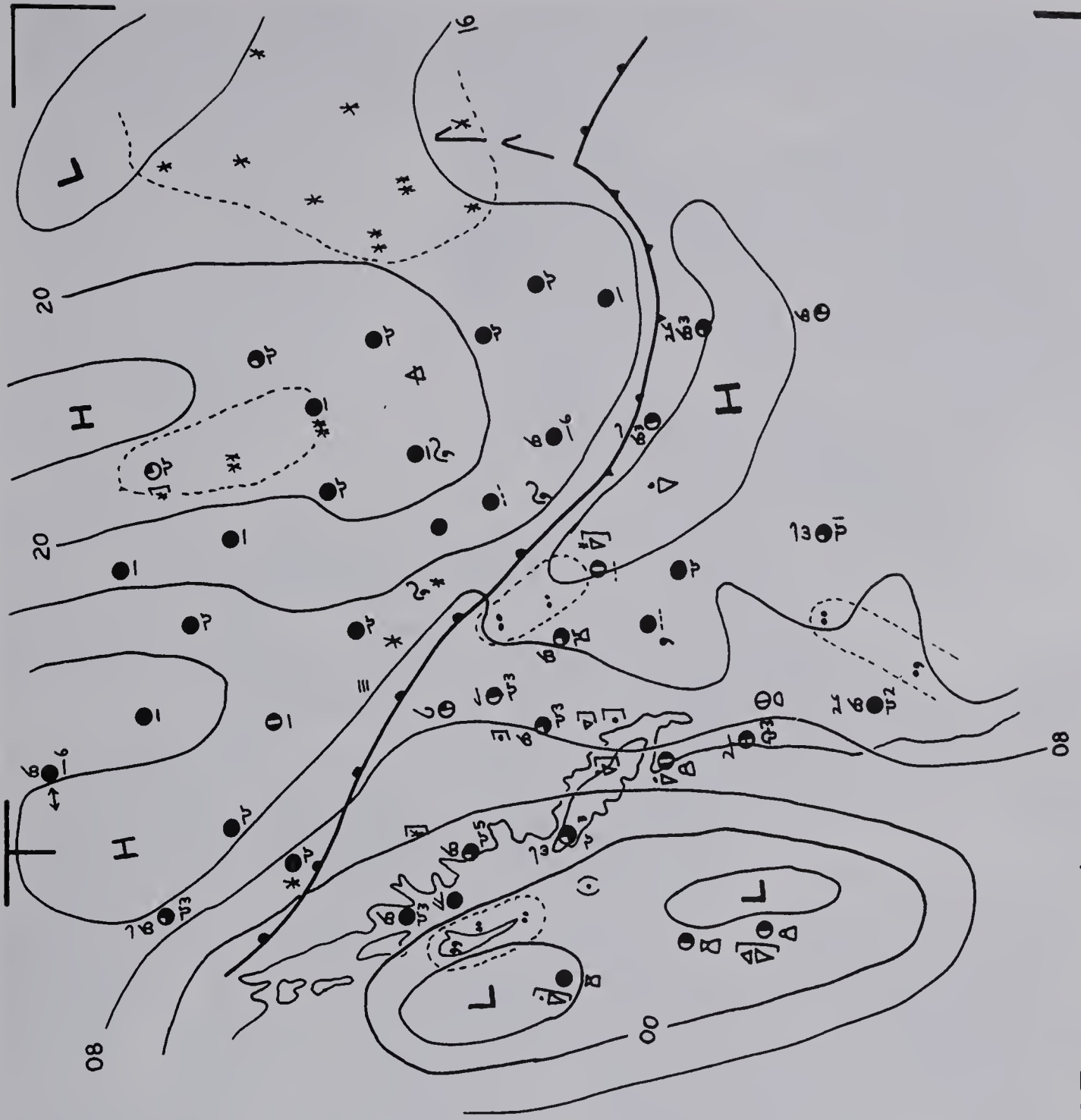
700 MB



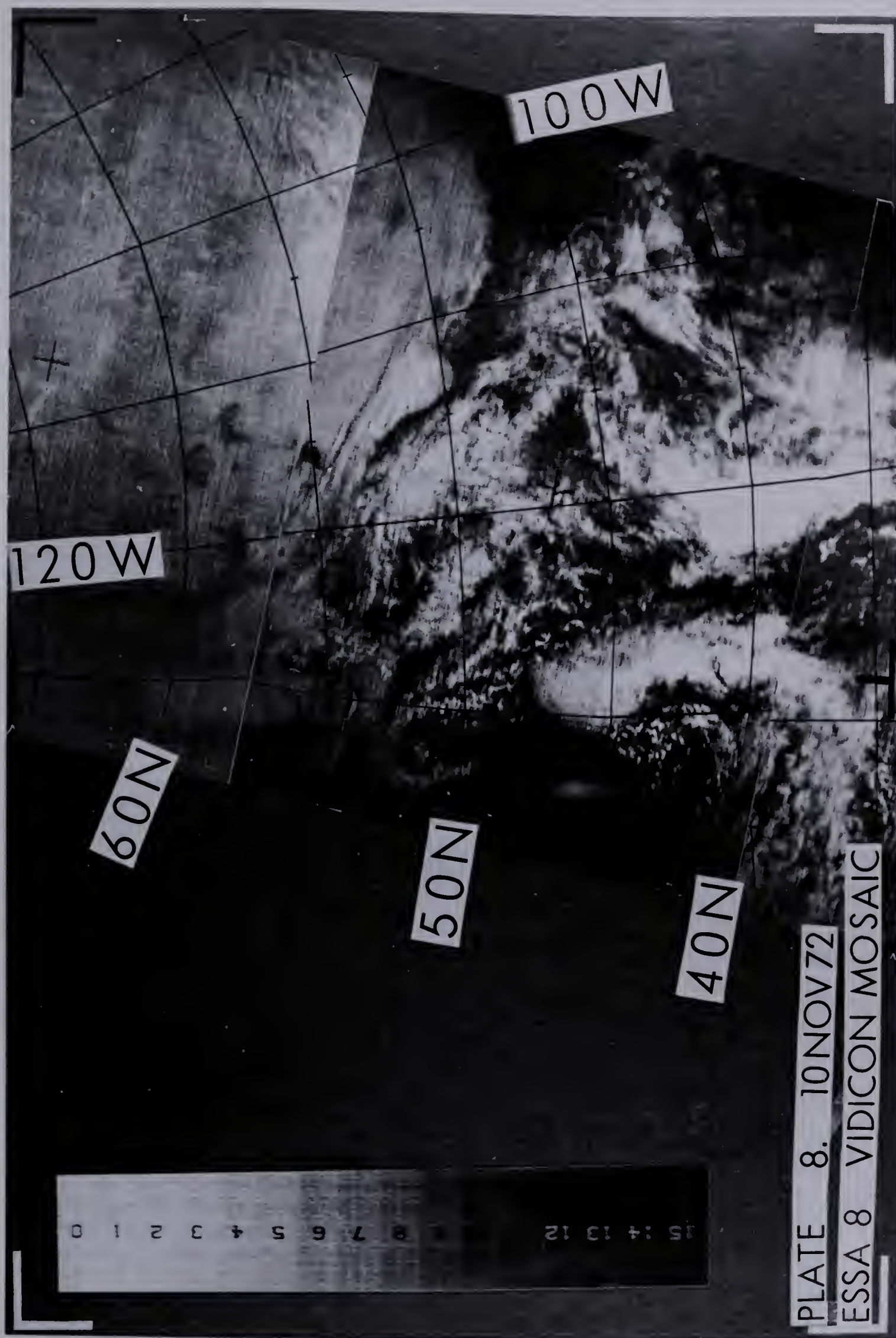








OVERLAY 8a. 10NOV 18Z SFC



CHAPTER G

CASE HISTORIES

CASE 3: 19-20NOV73

G.1 Synoptic Situation

As shown on Figure G.1, 500-mb troughs and lows follow two tracks: one across central Canada from the Pacific Ocean to eastern Canada, and the other southwest from the Pacific through southwestern United States. The longwave pattern is of small amplitude. Tracks along the latter path do not occur before 18NOV, suggesting a shift in the longwave ridge and trough positions. Except for the days 21-24NOV, a closed low is located over eastern North America --- in the position of the long-wave trough. During the period 21-24NOV, the first trough through the southwestern United States is intensifying; a strong cyclone develops at the surface which produces a closed circulation at 500 mb. The cyclone initially moves eastward but recurves northward over the plains. Closed lows continue to track across central Canada after 18NOV, indicating a split in energy of the approaching systems. This is in contrast to Case 2 where the energy follows the very-pronounced large-amplitude longwave pattern.

At the surface (Figure G.2), a series of moderate to

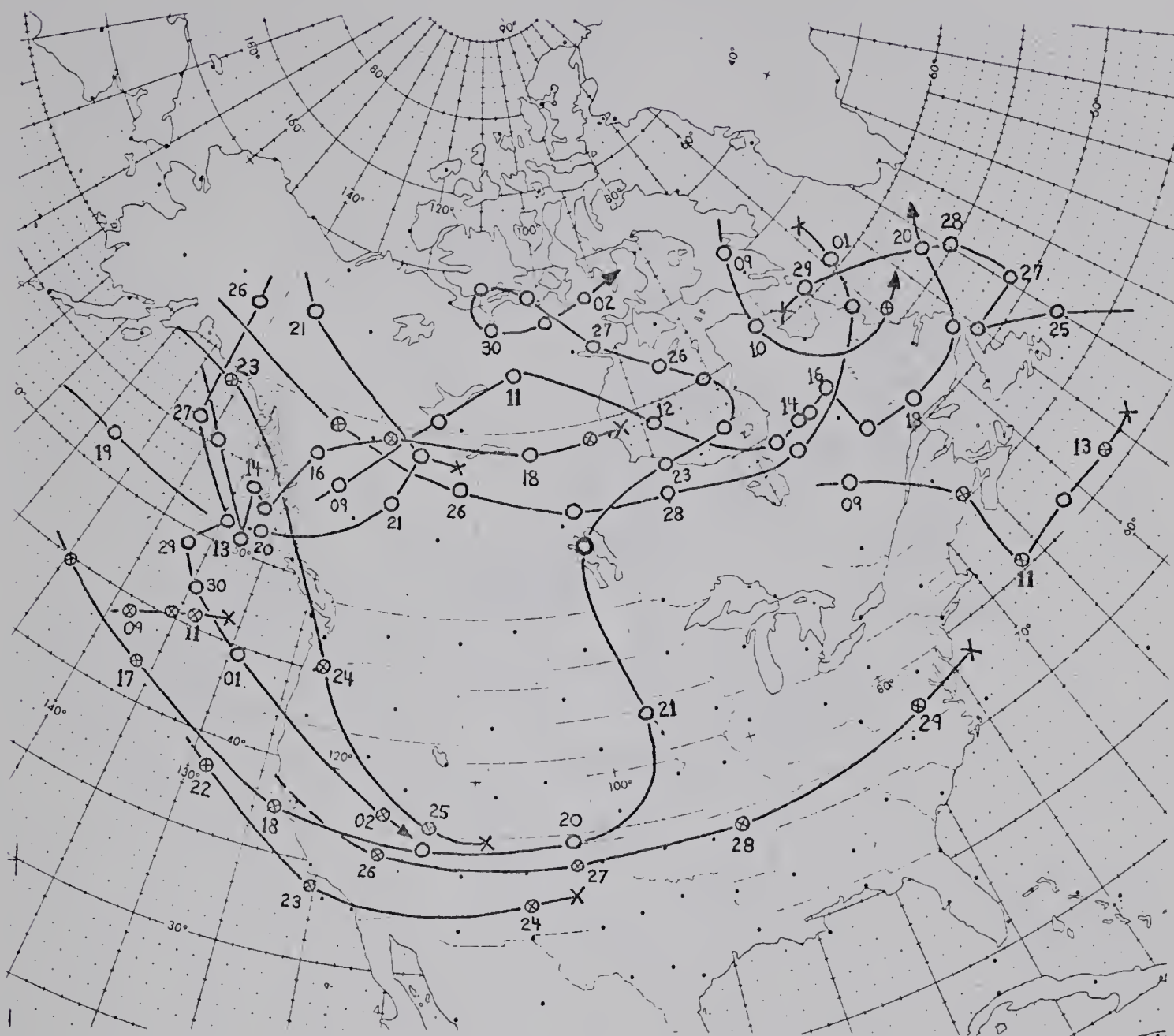


Figure G.1. Track and 1200Z position of 500-mb troughs and lows for the period 09NOV-02DEC73

strong lows (Type A) move towards the Pacific coast, weaken, and disappear. The most intense lows move across the north Pacific into the Gulf of Alaska. To the lee of the Cordillera, weak surface lows (Type D, two Type C's) form primarily in southern Alberta. With the change in upper-level flow, weak-to-moderate-intensity lows (Types A and C) track from the southern United States towards eastern Canada.

The frontal cloud band examined in this case study,

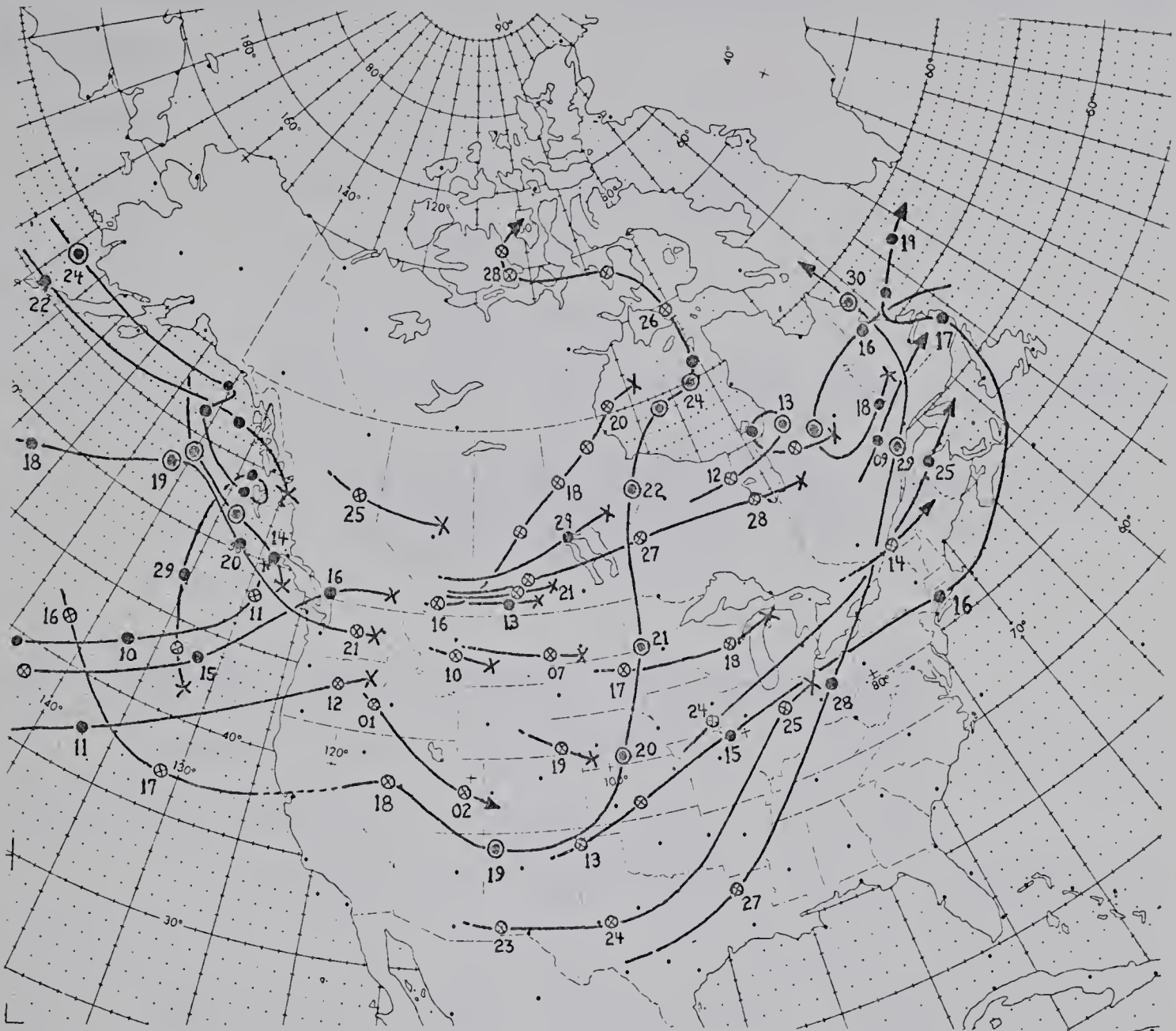


Figure G.2. Track, intensity, and 1200Z position of surface lows for the period 09NOV-02DEC73.

and the very intense surface cyclone move onto the Pacific coast, while the cyclone in the southwestern and mid-western United States is developing.

The following vertical time-sections are used in the analysis:

Figure Vertical Time-section Station

- G.4 Ocean station (Ship) PAPA
- G.5 Port Hardy (ZT)
- G.6 Prince George (XS)
- G.7 Vernon (WKV) with Penticton (YF) station data
- G.8 Edmonton (Stony Plain) with
 Edmonton International (EG) station data
 and cloud time-sections for EG and
 Edmonton City (XD)

G.2 19NOV73: Notes, Comments, and Observations

Refer to Plates 9a (SRIR) and 9b (SRVIS) and Overlays 9a (SURFACE), 9b (700 mb), and 9c (500 mb).

A very intense (968 mb) mature cyclone is located at 54N142W, with a 500-mb center to the southwest at 52.5N147W, and a well-formed cloud spiral into a vortex center at 53N141W. The cold front is marked by a cloud band 42N150W - 45N140W - 50N133W (at wave) with the occlusion extending north-northeastward and spiraling into the vortex center, and the warm front cloud extending southeastward. Using the computer-produced hemispheric images in Environmental Satellite Imagery (NOAA, U.S. Dept. of Commerce), the cold front west of 42N150W (off the mosaics) widens into a weak wave-cloud at 40N150W, ahead of a north-to-south cloud band along 15-40N160W associated with a cut-off (cold) low at 30N170W. The cloud band along 50-60N170W is associated with the upstream trough and surface cyclone; it extends southwestward

and then westward off the mosaics, but does not join the cloud band along the southern edge of the mosaics.

Along the cold front, at 45N140W, a weak trough line produces a decrease in the amount of higher cloud: only bands of BKN AC/AS and SCT CI are observed. The 500-mb chart shows no trough line, again the result of a poor analysis caused by difficulty in providing bogus data. To the east & northeast, the amount of middle and high cloud increases and the cloud band broadens, especially downwind of a north-to-south line in the warm sector at 45N135W. At the wave (50N133W), OVC NS is topped with a large shield of uniform, thick CS, becoming OVC AS+CS along the warm front (50N133W - 45N128W) and ending with SCT/BKN AC, BKN CI southeast of 45N. From Ship PAPA and ZT time-sections, the leading edge of the CS shield thickens to AS/AC, then NS, as the lowering middle-cloud base merges with the low cloud. Along the warm frontal zone, dry air lies underneath the middle cloud and above the low cloud.

The occlusion lies along the cloud edge 50N133W - 52N132W - 55N134W, ending approximately at 57N140W, although the cloud continues by advection into the vortex center. The OVC NS+CS with embedded CB (note thunderstorm along Alaska Panhandle) of the frontal band thins downwind to BKN/OVC AC/AS OVC CS in the weak (<30 kts at 500 mb) diffluent flow through the upper ridge. Two anticyclonic edges can be observed on the shield:

-the first, along 53N134W - 56N130W - 55N123W thence south-southeastward, lying approximately along the 540-dam 500-mb contour line and the northern edge of WAA at 700 mb. To the south, the CS shield is slightly colder (i.e. whiter on the SRIR image, hence higher) than to the north. This edge possibly marks the crossing point of the jet stream. At XS and WVK, the edge lies approximately along the warm-frontal zone at 300 mb, in the area of weak NVA just downstream of the upper ridge.

-the second, along 58N140W - 61N135W - 60N130W thence southeastward, corresponding to the change at 500 mb from open to closed height contours.

Precipitation (rain and snow) occurs along the cold and occluded fronts. Snow has fallen at XS since 18/0000Z (42 hours previously) produced by SC cloud in the Arctic air mass (below 800 mb), and by occasional contributions by mid-level cloud. The Coast Mountains block the Arctic air mass; the front lies along the eastern slopes of the barrier and then through southern B.C.

The surface-frontal analysis can be improved using the satellite mosaics. Positioning the cold front (43N140W) along the leading edge of the cloud band is correct if the frontal zone is weak and shallow. The double band of cloud suggests two frontal zones 2.5 degrees (150 nmi) apart. The occlusion (analyzed as a TROWAL) is drawn too far west, a systematic error in most analyses of data-sparse regions. The worst error is a TROWAL drawn directly from the wave


into the center of an intense mature low, completely ignoring the effects of horizontal advection.

The leading edge of the warm-frontal and occlusion cloud lies over the mountains. No obvious orographic effects are noticeable north of 52N, for the following reasons:

- (a) Winds at and below 700 mb are weak
- (b) Southerly winds at and below 850 mb parallel the mountains. Surface winds blow offshore (e.g. see ZT time-section).
- (c) The lower troposphere is stabilized by the warm-frontal zone and by the underlying modified Arctic air at the surface. Ascent will not produce convective clouds.
- (d) The troposphere is very moist.

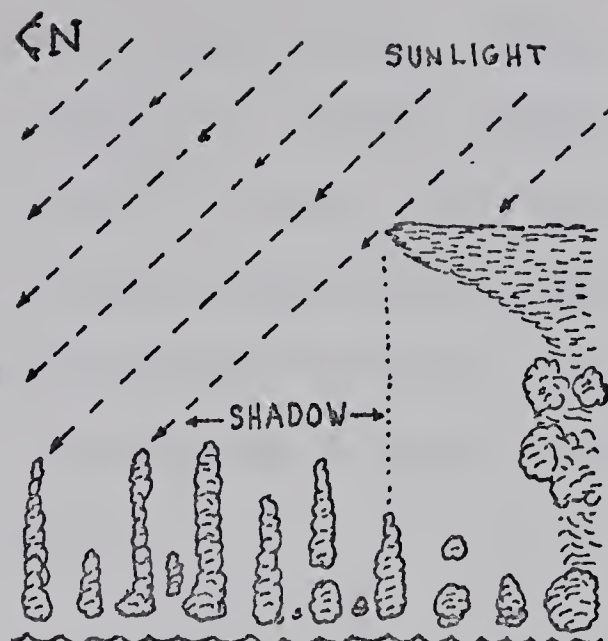
Orographic vertical motions will not perceptibly modify the thick NS cloud, but will only increase or decrease (for ascent and descent, respectively) precipitation.

In the weak westerly flow over Washington and Oregon, orographic AC/AS cloud bands form over the Coast Mountains (124W) and the Cascade Range (121.5W) between 45 and 50N, with subsidence-clearing to the lee of each barrier. The dry air at 700 mb and 500 mb present over the mountains at 19/1200Z has been advected eastward. The break in the middle and high cloud between the Coast and Cascade ranges extends northward across the Coast Mountains of southwestern

B.C. (50.5N122.5W) ending to the lee of the barrier --- on the SRVIS mosaic, the dendritic pattern of snow on mountain ridges can be seen. On closer examination, cloud bands and breaks of 120-nmi wavelength also appear in the upstream flow on the SRIR mosaic as slightly darker (i.e. warmer) north-to-south areas between 45N135W and 52N121W. These bands in the warm-frontal zone approximately parallel the 700-mb isotherms, hence to the thickness lines at mid-levels, similar to the orientation of convection bands observed by Elliot & Hovind (1964). The thin CI streamers (43N123W) over the Coast Mountains are the leading edge of the BKN CI at 43N128W along the southern end of the warm front, not orographic CI. Differential advection to the south of the jet stream causes the cloud lines to become arcs, e.g. .

In the cold air mass behind the frontal band, convective cloud forms in the very pronounced dry slot which spirals into the vortex center. A weak upper-trough line extends south from the vortex cloud along 144W (bogused on the 500-mb analysis) cutting the cold front at the break, 45N143W. BKN SC/TCU to the west of the trough has lower (i.e. warmer, hence darker on the SRIR mosaic) cloud tops than that to the east. The trough on the 500-mb chart through 51N150W does not exist as there is no discontinuity in the cloud, again a problem with the bogus data.

No break occurs in the low cloud immediately behind the frontal band; the CS shield overhangs the middle cloud (see sketch at right). With the low sun angle, the shadow from the high CS cloud produces a dark band, an apparent break, on the SRVIS mosaic.



Even though the surface air is colder than the ocean, it is convectively unstable only to 550 mb (16 kft) and only shallow convection results. Behind the trough, the cold air shallows quickly (see Ship PAPA time-section); this is indicated by the difference in cloud organization along the NW-SE line through 50N153W which approximately parallels the surface isobars. In the deeper cold air to the northeast, SC in cloud streets develop in the cold air advected from Alaska; to the southwest, there is an area of lower cloud-top (i.e. warmer on the SRIR mosaic) BKN open-cell SC. On the SRVIS mosaic, the area of brighter (i.e. thicker) and on the SRIR mosaic colder (i.e. higher) convective cloud at 46N145W is produced by surface convergence: SC cloud-lines converge from the northwest (parallel to the line) and from the west, parallel to the front to the south.

The vortex cloud, OVC low-level (probably below 700 mb) AS/AC BKN/OVC SC, is passing Ship PAPA (50N145W) at the time of the mosaic (near 19/1900Z). The time-section indicates cloud below 750 mb (2.5 kft) with dry air above

600 mb. However, the rawinsonde ascents (1200Z and 0000Z) were taken before and after the passage of the vortex spiral. The very strong winds about the low center at and below 700 mb (greater than 50 kts at 700 mb, decreasing only to 40 kts at the surface) produce very strong advection: the 20-degree (1200 nmi) spiral would be formed from the occluded frontal cloud in about 24 hours.

Comparison with Case 2

(a) No area of enhanced, deep-convection CB is present in the dry slot downwind of the trough line, because of the shallowness of the cold air and to the low height of the tropopause (450 mb, 20 kft).

(b) Wind speeds at Ship PAPA (60 kts) are equal ahead and behind the upper warm front.

(c) The frontal cloud band is more compact. The distance from the vortex center to the edge of the frontal band is less than half that in Case 2 (6 degrees, 360 nmi, versus 15 degrees). The 500-mb wind speed at Ship PAPA near the center of the upper low is more than double (50 kts versus 20 kts). In both cases, the product of wind speed and distance from vortex center to frontal-band edge equals about 300 kts•degrees.

The upper trough over the Prairies along 115W is the northward extension of the digging trough in the southwestern United States and corresponds to a maximum depth of cold

air. The cloud accompanying the passage of the trough (refer to EG cloud time-section) is similar to that of the Pacific cyclone: SCT CI, becoming OVC AC/AS+CI at the trough line. Weak, low-level convergence produces BKN SC in the Arctic air mass. Snow falls from the thick cloud layers (see Edmonton vertical time-section). Cloud amounts at XD (see cloud time-section) 25 km to the north are much less. The cloud terminates abruptly at the trough line, rather than downwind, as in the Pacific cyclone.


On the SRIR mosaic, AC/AS+CI/CS produces snow at 55-60N108W, downwind of the vorticity maximum at 60N116W. To the southwest, lower cloud tops at a temperature nearly equal to that of the surface (i.e. -20°C) create problems in distinguishing cloud from ground on the SRIR mosaic. Cloud identification is not helped by the decreased resolution towards the horizon. However, cloud shadows on the SRVIS mosaic can be used to separate the clouds from the snow-covered ground. A band of BKN AC extends from 55N108W southwest over the mountains to 45N120W, with only a narrow break to the lee of the Rocky Mountains (48N113W). An area of snow occurs downstream of the vorticity maximum at 50N114W and in the easterly upslope surface flow.

Comment on IR Surface Temperatures

Snow on the open prairie (52N114W) appears colder (i.e. whiter) than that in coniferous forests to the west (53N116W) along the foothills of the Rocky Mountains.

Because of the surface inversion, the tree tops radiate at a higher temperature than the surface, thus the areal average of thermal radiation is higher from forest than from the nearby open prairie. Similar differences occur in the farming area of the Peace River district (55.5N119W). The Caribou Mountains (59N115W), the Birch Mountains, and Buffalo Head Hills (to the south) are ringed with coniferous forest, while the relatively flat tops and surrounding lowlands contain lakes, muskeg, and sparse forest: thus, a ring of higher temperatures is found along the slopes.

In mountainous terrain under a dome of Arctic air (e.g. Mackenzie Mountains 60-65N130W), the mountain ridges are warmer than the river valleys. With light surface winds, the cold air drains into the river valleys, producing an inversion. Higher terrain and slopes are warmer.

The dark (i.e. warm) patches on the SRIR mosaic near 65N120W and 60N110W are the open Great Bear and Great Slave lakes and Lake Athabasca. Evaporation from the lakes produces SC cloud and snow. Light land-breeze winds (<10 kts) converge into the lakes, the air-to-water temperature difference being about 20°C. With the gradient wind from the west to northwest, a warmer (i.e. darker on the SRIR mosaic because of the surface inversion) SC plume should exist downwind of the lakes. With Great Slave Lake, this cannot be confirmed because of the higher cloud associated with the upper trough. However, a darker area (of SC cloud ?) exists to the west of Great Slave Lake, forming a -shape around

the Horn Mountains (62N119W) and ending along the Cameron Hills (60N118W) on the south. The slopes of the mountains are forest-covered and appear as a darker ring. Cold-air drainage from the higher ground would clear any low-level cloud at the base of the mountains; indeed, a white ring corresponding to the colder surface does occur outside the dark ring.

G.3 20NOV73: Notes, Comments, and Observations

Refer to Plates 10a (SRIR) and 10b (SRVIS) and Overlays 10a (SURFACE), 10b (700 mb), and 10c (500 mb). Note that the 700-mb CMC chart is a HAND ANALYSIS.

The surface low in the Pacific has filled 24 mb and moved east-southeast at 25 kts to a position along Vancouver Island (50N128W) while the 500-mb low has opened into a trough. A strong southwesterly flow over the mountains has pushed the Arctic air mass northeastward so that it now lies in the lee trough and low (52N113W) along the eastern slopes of the Alberta Rockies.

The frontal-cloud band has advanced eastward across the Cordillera and no longer resembles the cloud band associated with the mature cyclone of the previous day (19NOV). The cold front extends from the wave at 44N123W southwestward across the Sierra Nevada Mountains (NNW-SSE through 39N121W), thence over the Pacific Ocean (34N130-140W, off the mosaics) and into the cloud band east of the cut-off low at 29N170W, on the horizon (i.e. near edge) of the SRIR

mosaic. Over the ocean (off the mosaics), BKN AS/AC frontal clouds start along the trough line at 142W; SCT CI/CS begins at 138W, the cirrus lying along the northern edge of the frontal band. Motion of the trough from the wave of the previous day is 20 to 25 kts.

The frontal band crosses the Coast (37N123W) and the Sierra Nevada Mountains at right angles. At the coast, the cirrus cloud makes a sharp southward shift: to the lee of the mountains, the northern half of the frontal band is devoid of high cloud (CI/CS) except for one thin streamer --- the cirrus-level air parcels exit from the mountain wave at lower heights where the air remains unsaturated (see Figure G.3, west-east cross-section). The lower AS/AC cloud is not affected. A CI/CS band forms along the southern half --- the air parcels exit at greater heights where the air becomes saturated, the water vapor condenses and freezes to form a CI plume (again see Figure G.3). The mountain barrier has produced a separation of middle and high cloud edges (see Figure G.3, north-south cross-section). The difference in the high-level character of the mountain wave is probably caused by the stabilizing effect and the blocking of the surface cold air mass north of the front.

Orographic ascent on the Coast Range produces a BKN/OVC AC cloud shield downwind (northeast) of 40N124W and behind the cold front, widening the frontal cloud band. Ascent on the windward slopes of the Sierra Nevada gives a band of mid-level cloud, while subsidence to the lee clears

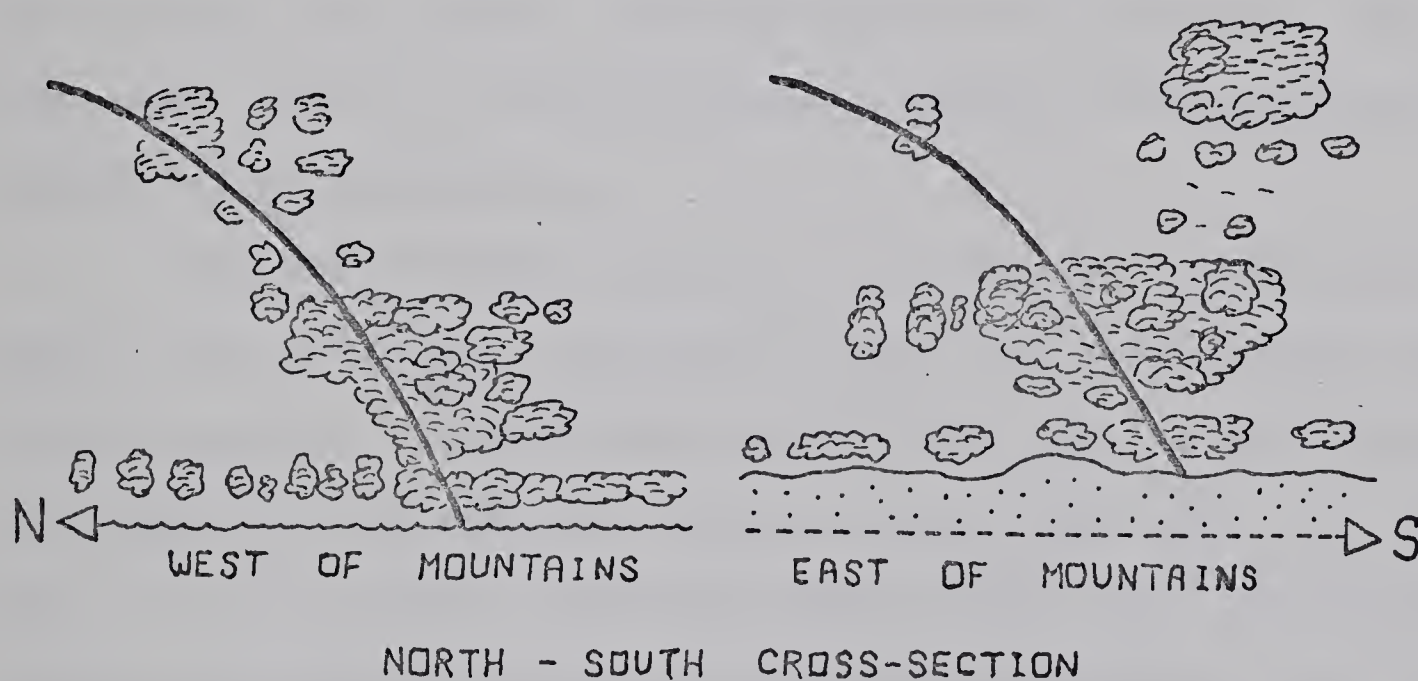
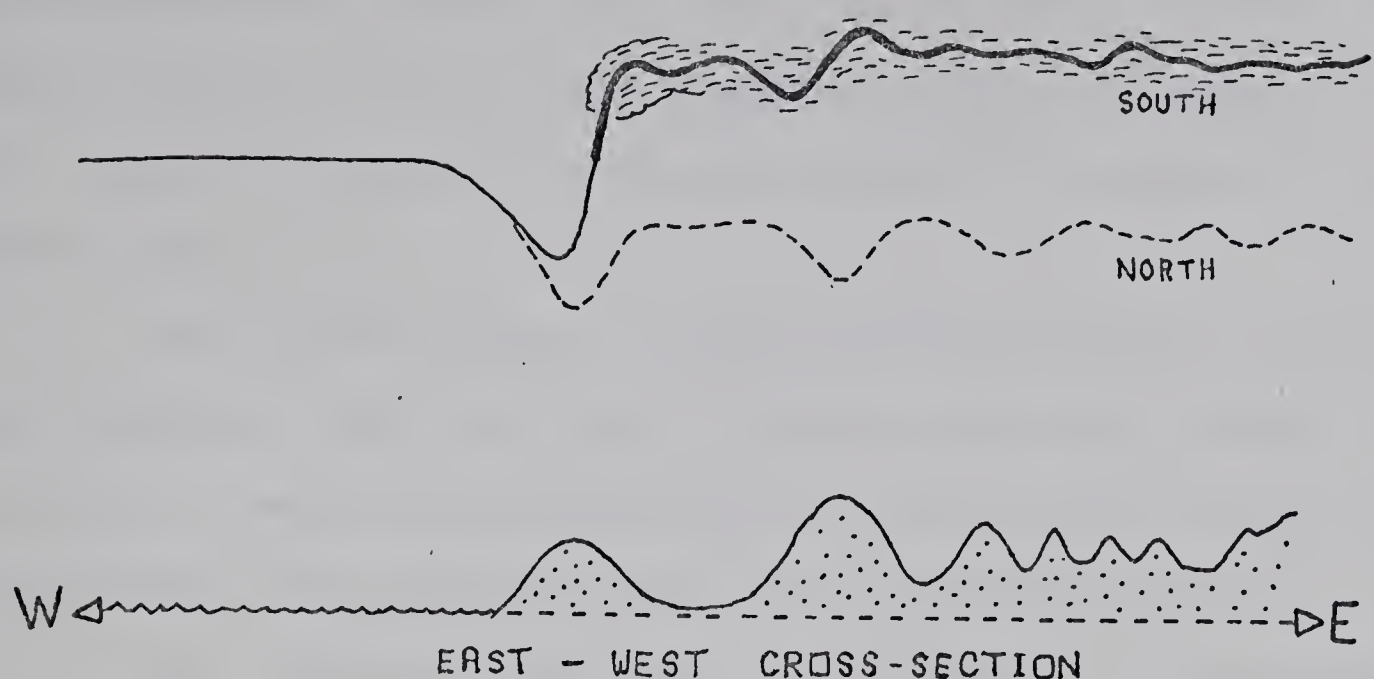


Figure G.3. Diagrams showing air flow and cloud over Coast Mountains of California.

low- and mid-level cloud (NNW-SSE through 37N120W) but produces no break in the CS band. The hole at 40N120W occurs over a basin in western Nevada in the lee of the Sierra Nevada. Only a thin banner of mountain-wave CI forms at and to the south of 36N118W. Further downwind (40N118W), mid-

level BKN/OVC AS reforms over the mountainous terrain of central Nevada. The CS band broadens in the diffluent flow, the mountains having no obvious effect on either AS or CS cloud bands.

The surface front is analyzed along the OVC AS cloud band 40N121W - 45N119W, about 2 degrees (120 nmi) behind the CS band. A band of precipitation lies along the front (no station data was available along the California coast).

The warm-frontal cloud is represented by the OVC AS and BKN CI 38-48N112W, the downstream edge again occurring at the 500-mb ridge line, adjusting for the 6-hour difference between the 500-mb observations and satellite data. Note the lack of precipitation, despite the orographic effects of the mountains.

The CS-AS cloud separation continues northeastward along the occlusion (TROWAL ?) until the band crosses the Rocky Mountains, NNW-SSE through 50N115W. The AS cloud band broadens in the orographic ascent upwind, and ends to the lee of the Selkirk Mountains (51.5N118W) with thinner AC visible over the Rockies, and subsidence clearing to the lee along the foothills in Alberta. The lee clearing extends southeastward into western Montana (48N113W); the middle cloud has cleared completely while the CS band only becomes thinner. The wave amplitude at the CS level is insufficient to cause evaporation of the ice crystals. The CS band at the lee clearing appears warmer since it is semi-transparent to the radiation from the warmer surface below. Northeast

of the break, a narrow band of standing wave cloud (Chinook arch) forms: very high (cold) CS+AS extends from 53N115.5W to 48N113W, merging with the AS+CS cloud shield to the northeast. A precipitation area extends along the occlusion, ending in a band of orographically-induced snow along the Rocky Mountains from 47N (under the CS band) to 55N125W.

In Alberta (55N115W), snow falls along the TROWAL in the cold air mass behind the Arctic front. Note that no precipitation falls from the cloud shield to the south, indicating that ascent is weak and the cloud exists only through advection of previously formed cloud.

The NS/AS+CS cloud shield and spiral vortex associated with the occlusion on the previous day (19NOV) is hardly recognizable. Its approximate position is 50N118W - 57N118W - 57N130W - 50N131W - 46N130W, along the western edge of the area of enhanced CBs. The CS/AS shield at 52N110W again lies south of the 500-mb 540-dam contour line. The tongue of warm air ahead of the occlusion has been missed on the 700-mb hand analysis: temperatures at Great Falls and Edmonton are -2°C and -7.9°C, respectively. Upon re-analysis, a maximum of WAA at 54N109W is located approximately at the center of the cloud shield. The eastern edge, like the warm-frontal cloud, ends downwind of the ridge line. When a strong jet occurs downstream of the ridge, this clearing of mid- and high-level cloud may not occur, subsidence from NVA being offset by ascent by WAA.

Note the diffluent 500-mb contour pattern, but con-

vergent flow between the trough along the coast and the ridge over the Prairies: wind speeds decrease from 75 kts at the trough line to 50 kts over the Cordillera (Spokane and Vernon) and then to 40 kts at Edmonton. The streamlines cross the 500-mb contours toward increasing heights.

To the north of the shield, a break in the high cloud revealing OVC SC+AC (56N114W) occurs in the occlusion band where PVA behind a flattened 500-mb ridge becomes negligible and the 700-mb flow becomes diffluent (and divergent ?). A fragment of occlusion cloud (AS+CS) at 59N118W is present in the PVA area behind the 500-mb ridge line, NW-SE through 60N117W, and the weak WAA in the southerly 700-mb flow. The remainder of the spiral consists of OVC SC and bands of SCT AC. To the west, at 50-58N138W, BKN AC and banded CI are the remains of the frontal cloud band located along 170W on the previous day (19NOV). This gives a speed of 37 kts, which is less than the 700- and 500-mb winds of 45 and 60 kts, respectively.

The spiral vortex is the result of steady-state flow. With weak descent and no external disrupting forces, the cloud spiral will slowly disappear, becoming (over the ocean) bands of convective cloud. The influence of the Cordillera changes the upper-level flow pattern and accelerates the breakup of the cloud spiral. The closed lows shown on the 700- and 500-mb charts have become large-amplitude troughs and the closed circulation required to form the spiral no longer exists.

Behind the frontal cloud, an area of enhanced deep-convection BKN CB has formed at the center of the vortex (48N127W) and the surface low (50N127W) downwind of the 500-mb trough line bogused along 130W. On the ZT time-section, the cold air mass now shows a maximum depth to 400 mb versus 600 mb at Ship PAPA. The strong PVA at 500 mb ahead of the trough only extends southward to about 43N, along the cut-off of the enhanced CB. This latitude denotes also (approximately) the line along which the 700-mb winds are maximum. The trough does not extend southward to the front along 130W, as there is no break in the frontal clouds along this longitude.

Where the enhanced CB cells encounter the coastal barriers (45-55N), a band of NS cloud and showers occurs which ends to the lee of the Cascades (45-50N) and the Coast Mountains (50-55N) in lee subsidence of the cold air mass stabilized by forced convection.

To the south of the enhanced CB area (43N123W), orographic ascent over the Coast Mountains and the Cascade Ranges gives two north-to-south bands of AC cloud in the clear slot. The clear slot appears to extend northward in the lee of the coastal mountains.

To the west of the trough (38-50N 130-138W), an area of SCT open-cell SC/TCU is present although surface stations report BKN/OVC SF, northwesterly winds of 40 to 50 kts, and an air-to-ocean temperature difference of 1 to 2°C. The gale-force winds result in strong turbulent mixing (even

over the relatively smooth ocean surface) and increased evaporation, thus forming a SF cloud layer. The thin SF would produce a uniform dark background on both the SRIR and SRVIS mosaics and only the thicker (i.e. brighter on SRVIS) higher (i.e. colder on SRIR) SC/TCU would be observed. Since the SF is very widespread, the slightly darker ocean (on both mosaics) is not visible. West of 138W, the cloud changes to OVC SC/ST (ships report SF as well) which merges into the middle and high cloud of the next frontal band.

To the northeast of the TROWAL, the southeasterly gradient gives easterly surface winds over Great Slave Lake (62N114W), advecting to the northwest the SC cloud and snow formed by evaporation from the lake into the -20°C Arctic air. Polygons of convective cloud can be seen over the south & eastern part of the lake. To the southeast, Lakes Athabasca (59.5N109W) and Wollaston (58N103W) appear in an area of OVC/BKN SC on the SRIR mosaic. A cloud-free (colder) ring surrounds Wollaston Lake. Heat added by the lake causes a convective loop: ascent over the lake, a land breeze, and subsidence around the lake which clears a hole in the OVC SC cloud. Evaporation from the lake is insufficient to produce observable cloud.

The frontal cloud is very similar to that in Case 2:

- (a) Increasing amount and thickness of CI, becoming OVC CS.
- (b) As the dry upper-warm front descends, the cloud base lowers and becomes AS.

(c) At Edmonton, surface convergence in the moderate southeasterly winds forms low-level SC.

(d) At the occlusion (or TROWAL), the low and middle cloud merges, giving thick NS cloud and precipitation.

(e) After the passage of the occlusion, Edmonton (see XD and EG cloud time-sections) clears to BKN/SCT AC. The other stations (ZT, XS, and WVK) report BKN SC and varying amounts of middle cloud.

Because of the low-level easterly flow of modified Arctic air at the surface along the Pacific coast (see ZT time-section), the frontal structure is that of a warm occlusion. To the north of the Arctic front at Edmonton, no change occurs in the surface air mass, and the occlusion has become a very active TROWAL. In general, an occlusion over the eastern Pacific Ocean becomes a TROWAL (or upper cold front) as it crosses the Cordillera. The mountains block the low-level flow, trapping cold air at the surface in the interior basins, especially in winter. As well, barriers alter the cold air mass by removing moisture and adding latent heat through orographic precipitation and by stabilizing the atmosphere through forced ascent of conditionally unstable air.

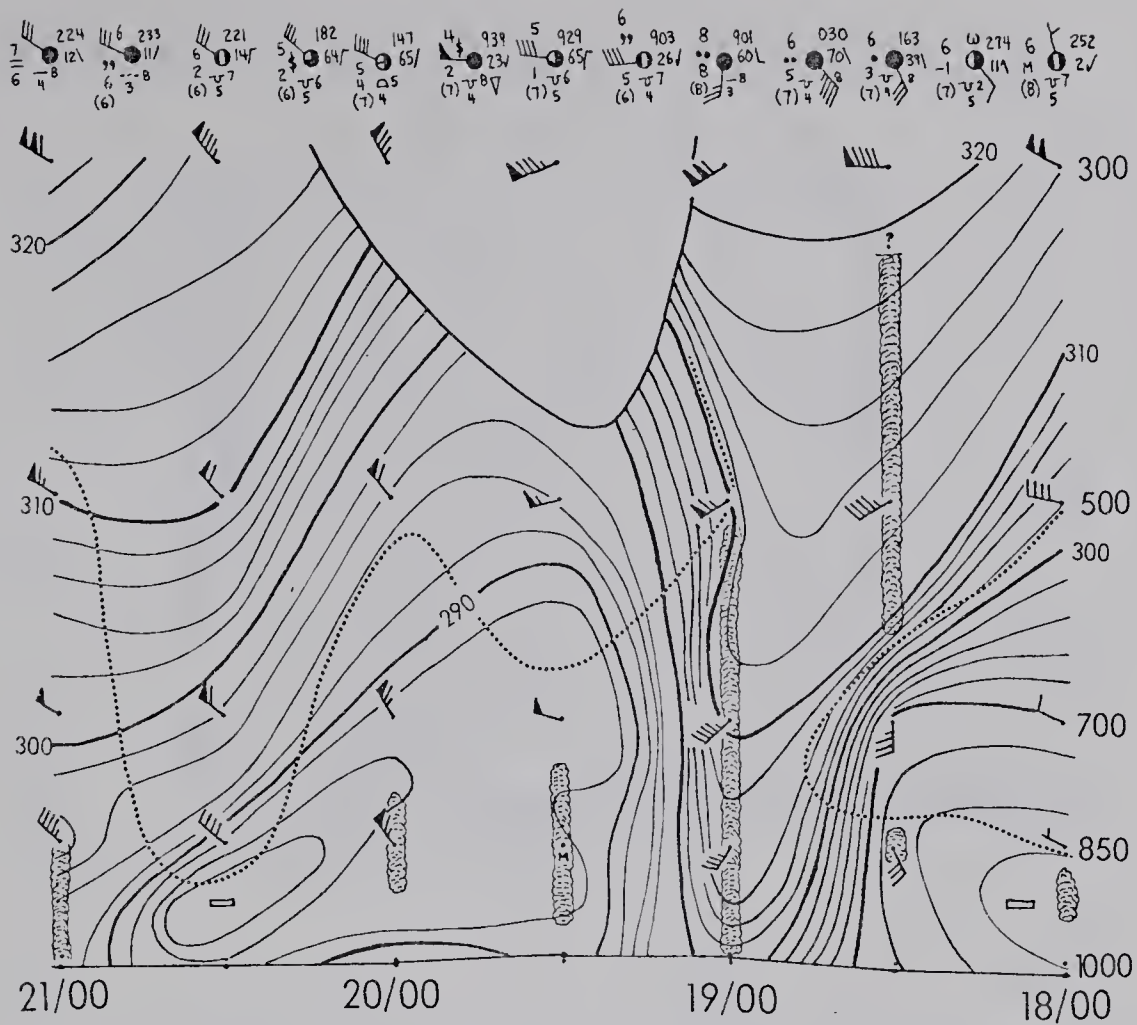


Figure G.4. Vertical time-section plus 6-hourly station weather for Ocean Station (Ship) PAPA.

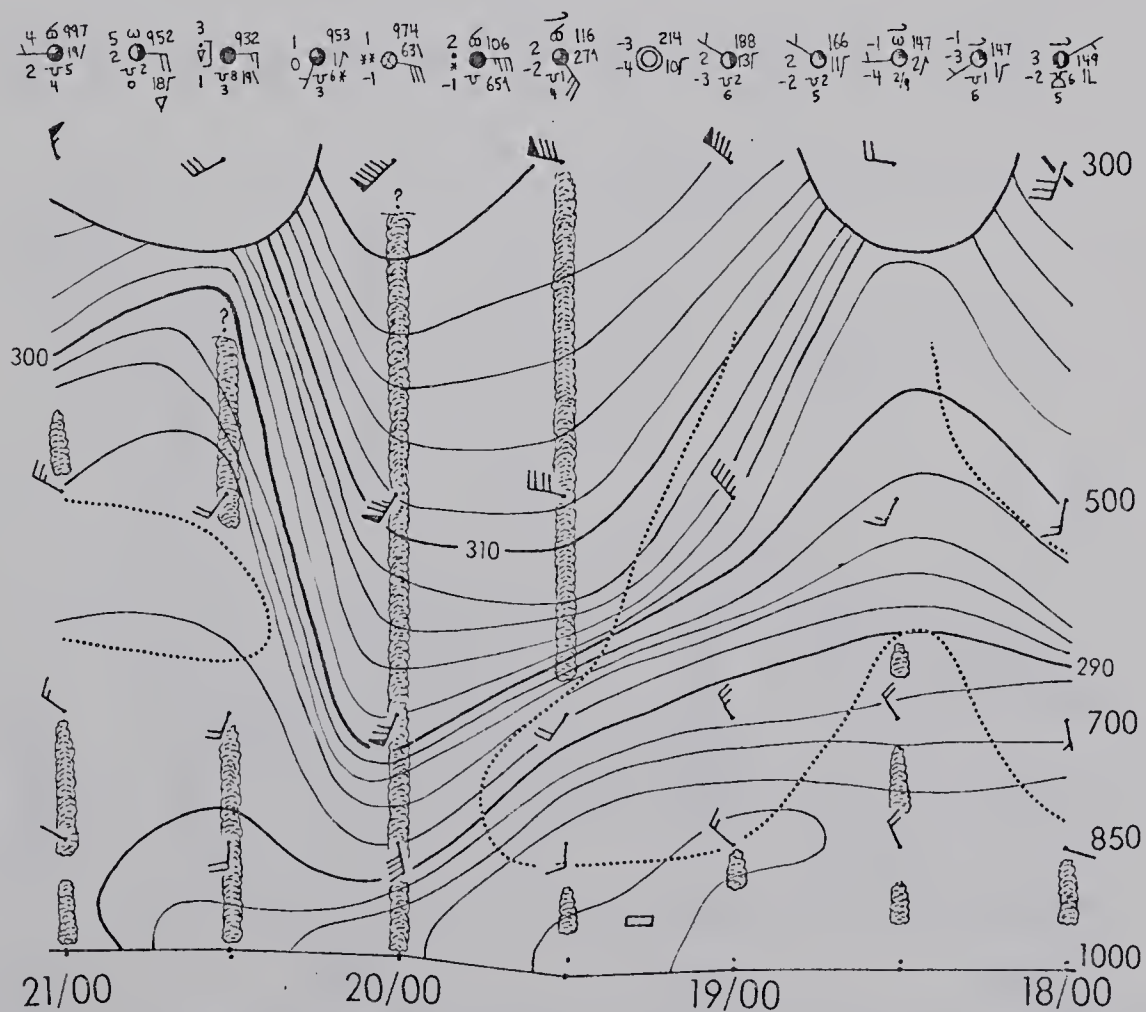


Figure G.5. Vertical time-section plus 6-hourly station weather for Port Hardy (ZT).

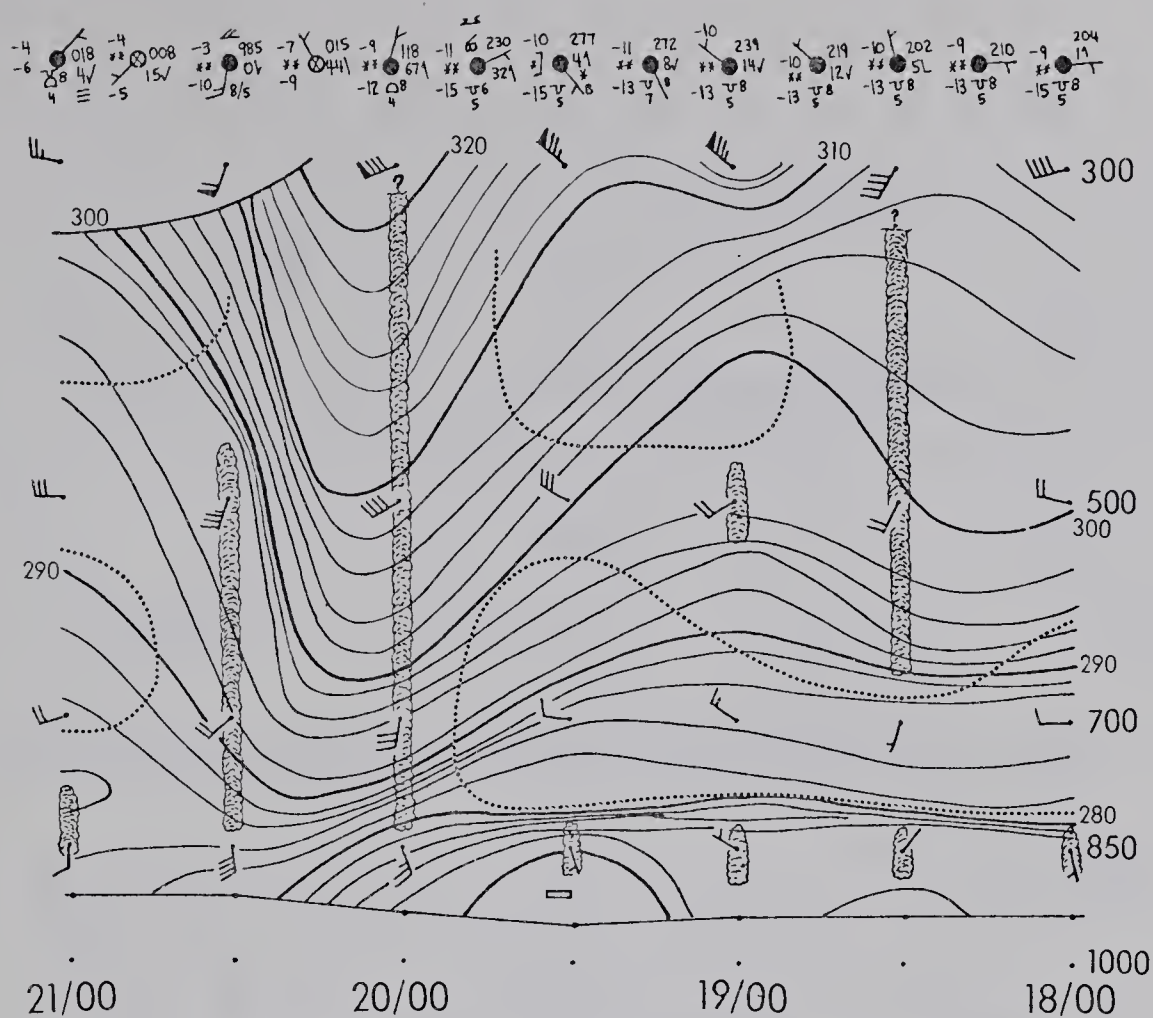


Figure G.6. Vertical time-section plus 6-hourly station weather for Prince George (XS).

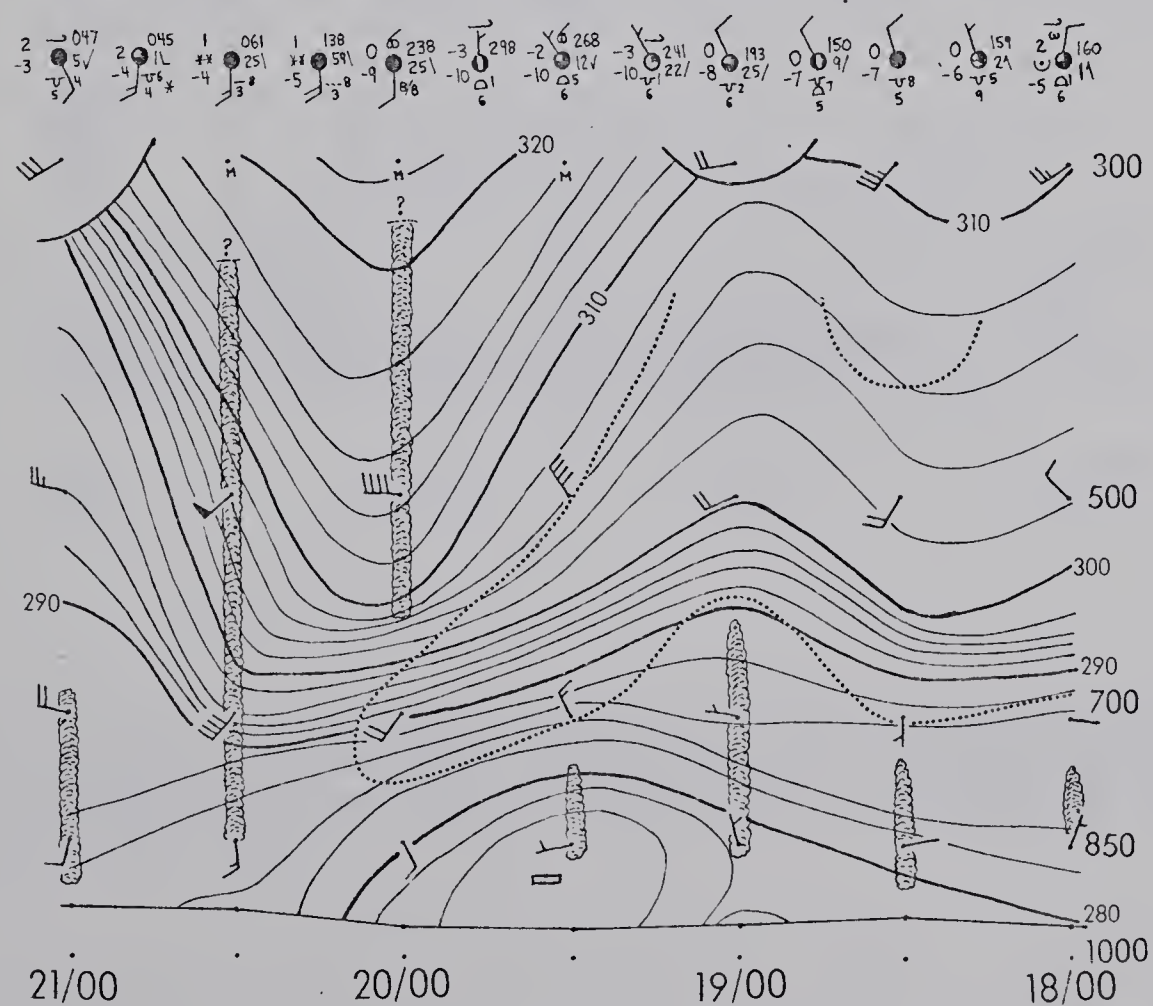


Figure G.7. Vertical time-section for Vernon (WVK) plus 6-hourly station weather for Penticton (YF).

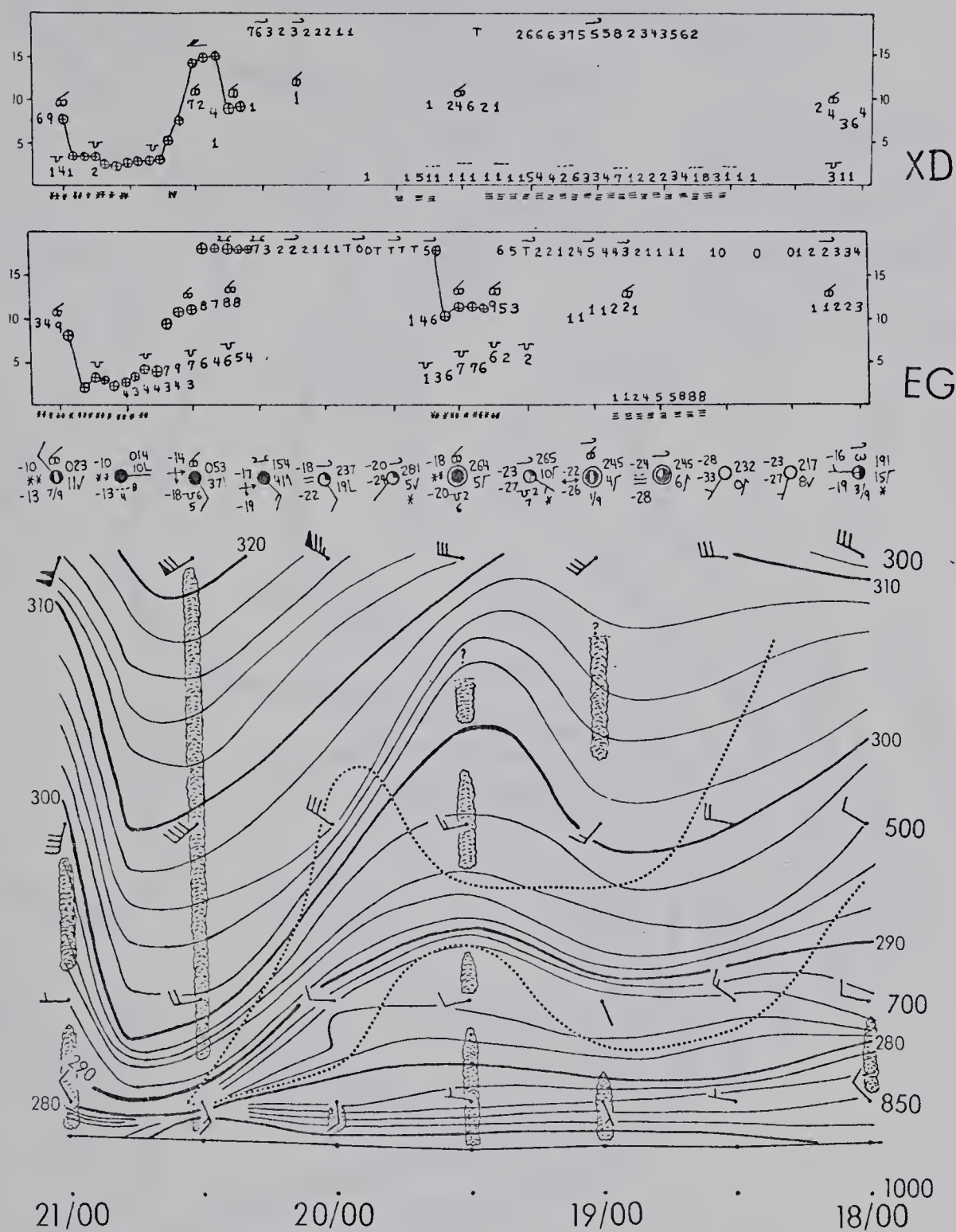
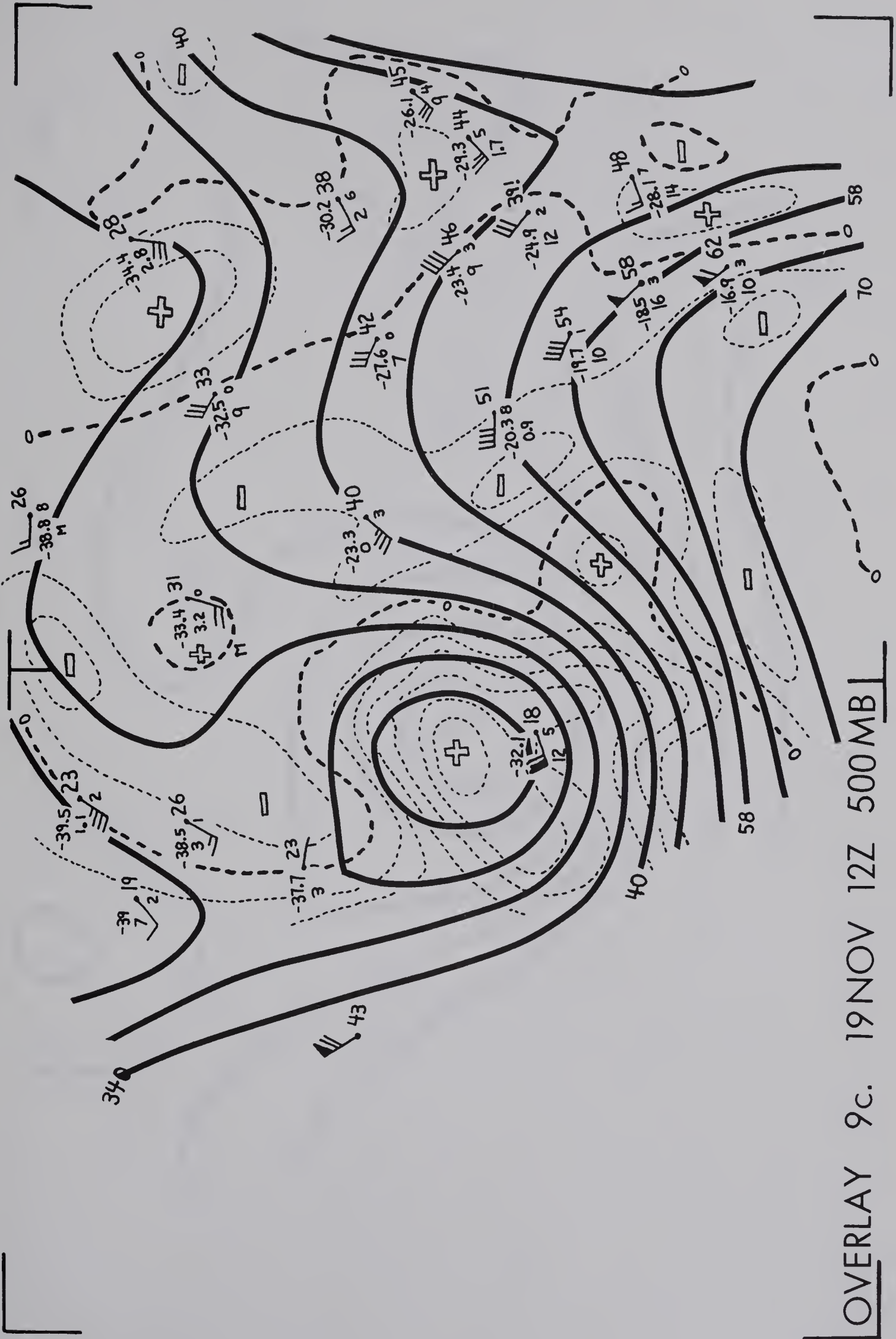
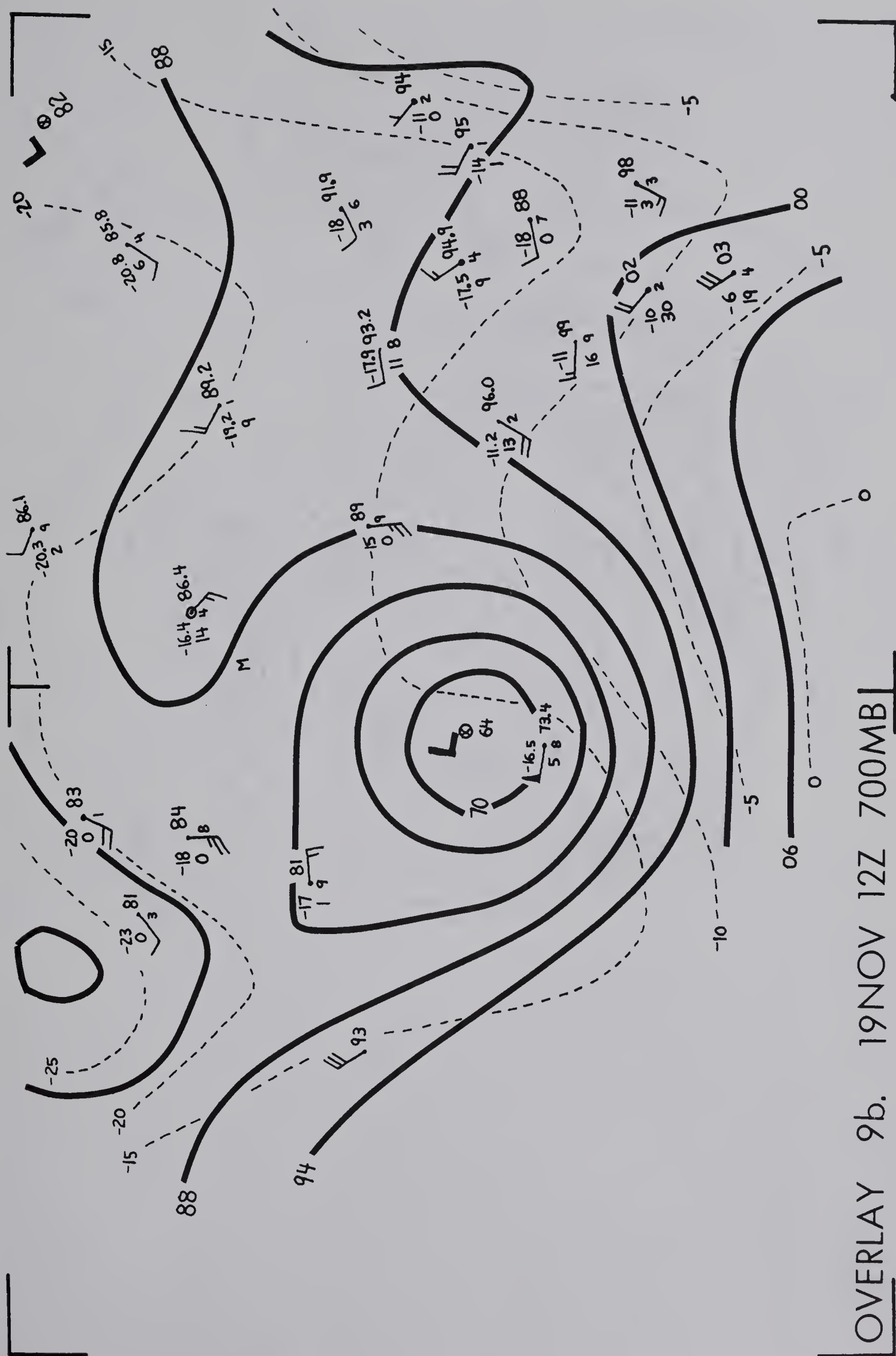
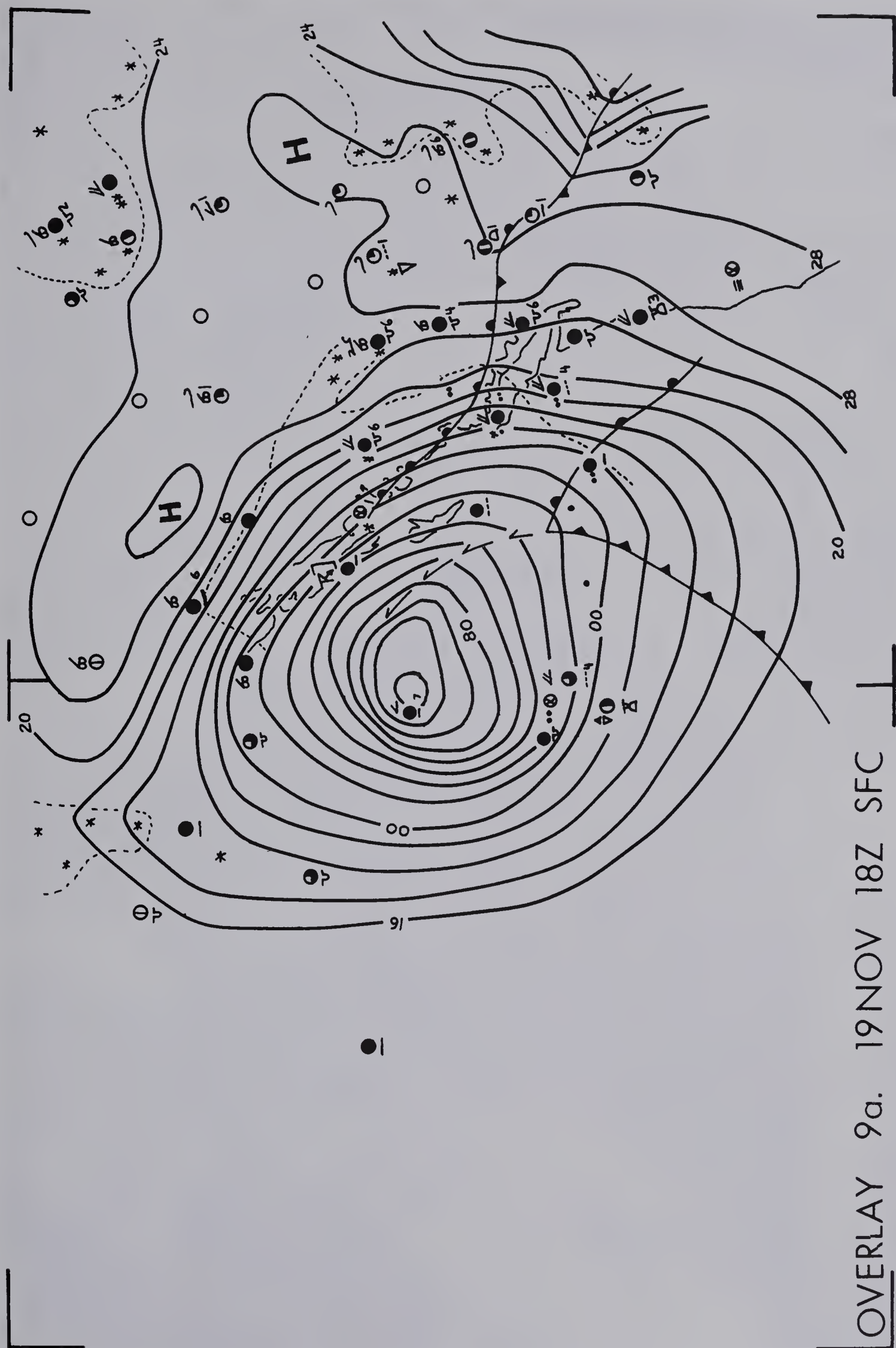
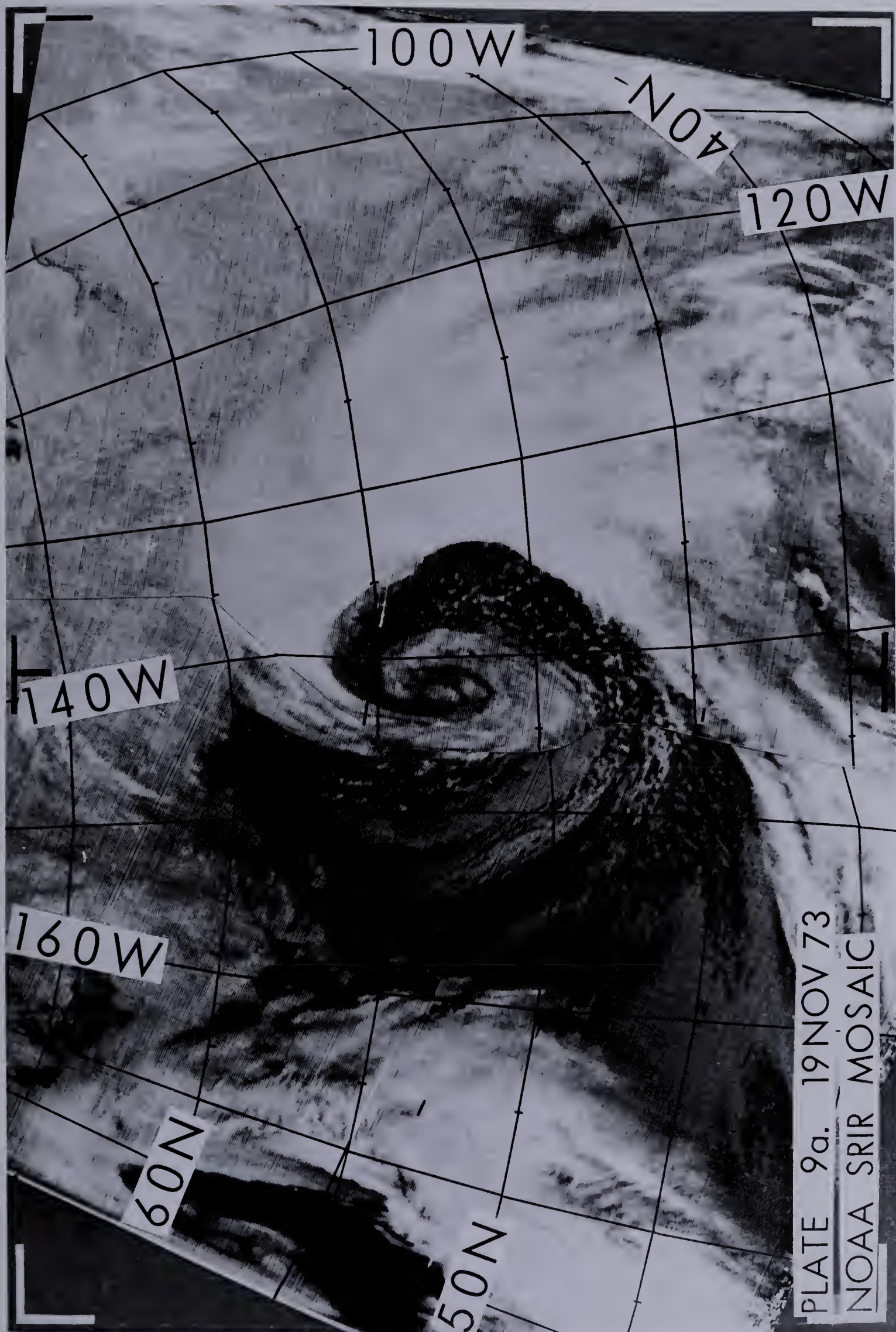


Figure G.8. Vertical time-section for Edmonton (Stony Plain), cloud time-section plus 6-hourly station weather for Edmonton International (EG), and cloud time-section for Edmonton City (XD).









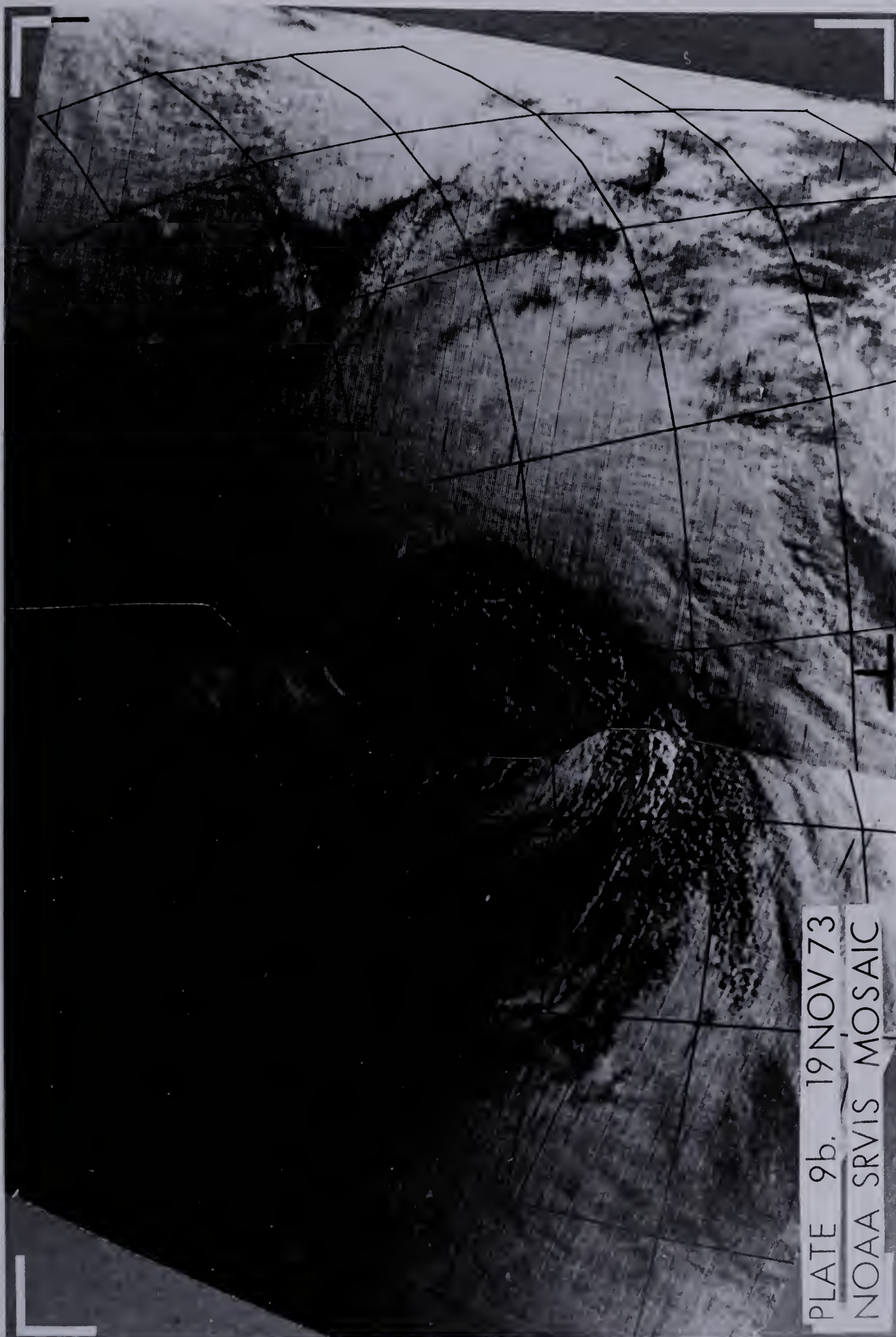
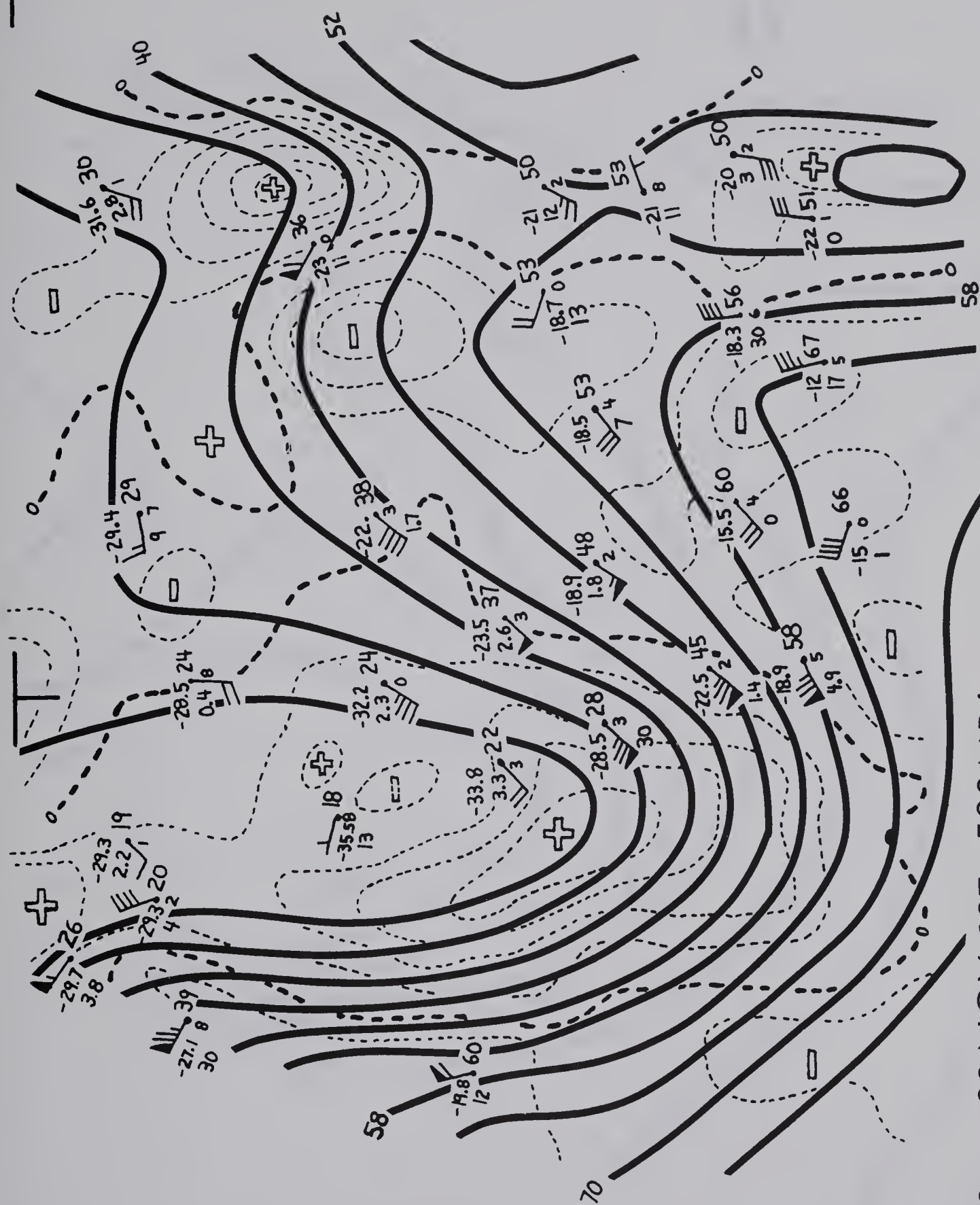
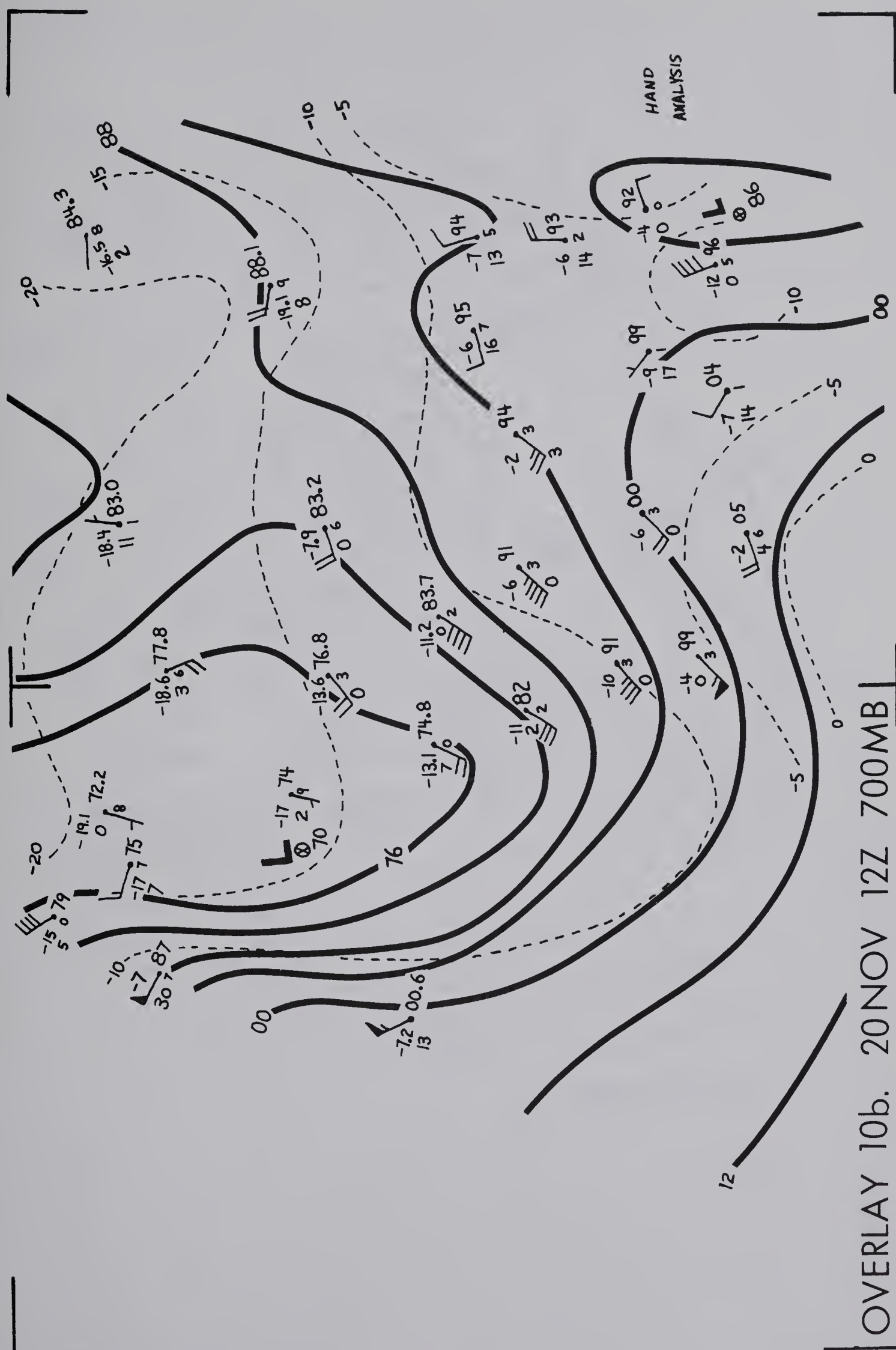


PLATE 9b. 19NOV 73
NOAA SRVIS MOSAIC



OVERLAY 10c: 20 NOV 12Z 500MB





OVERLAY 10a. 20NOV 18Z SFC

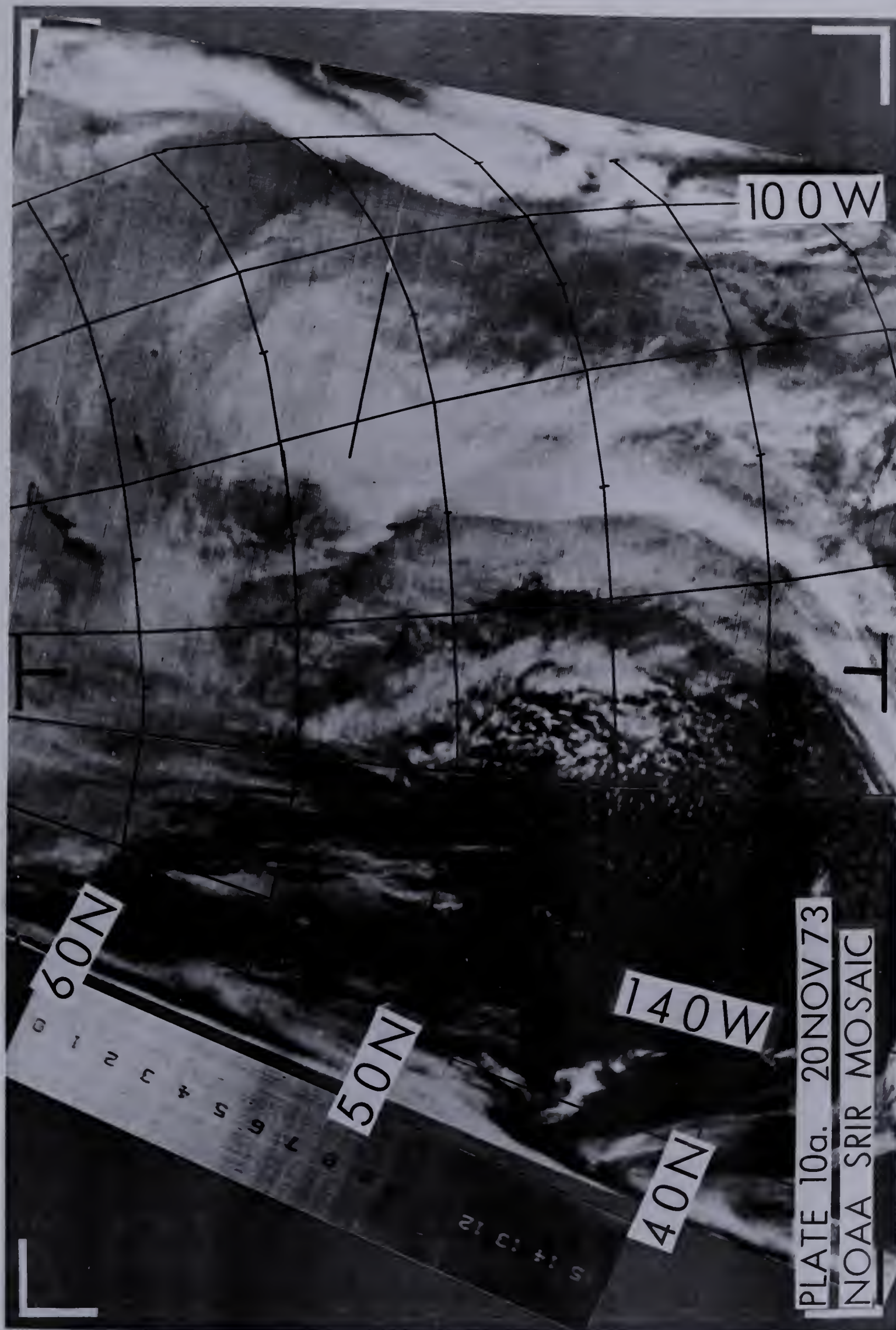




PLATE 10b. 20 NOV 73

NOAA SRVIS MOSAIC

CHAPTER H

SUMMARY AND CONCLUSIONS

Frontal cloud bands generated by Pacific storms undergo complex modifications when approaching and traversing the Cordillera. Over the Pacific Ocean, in the warm sector ahead of the cold front, a broad line of BKN AC/AS with CI plumes frequently parallels the southwesterly flow in the mid-troposphere (700 to 500 mb). Along the frontal cloud band the ceilings lower rapidly in BKN CF/SC and precipitation.

Behind the cold front, SCT/BKN open-cell SC/CU/TCU is observed over the ocean. This "clear" zone is associated with cold air advection (CAA) and subsidence in the lower and mid-troposphere. The vertical motion field shows maximum descent near the center of maximum CAA, and the convective cells are smallest at this location; only SCT CU is normally present. The clear slot is usually followed by SCT CU/SC+TCU, with showers caused by convective instability in the cold surface air moving over warmer water. Deeper in the cold air, behind the zone of CAA, BKN/OVC closed-cell cumulus is found with scattered showers. Even when the cold air begins to shallow, the layer below 700 mb continues to cool. The near-surface layer is colder than the ocean and

thus subject to remaining convectively unstable.

Over the ocean, large clear areas are often maintained by subsidence in an upper ridge, combined with low-level divergence from surface highs. Dew-point depressions throughout the troposphere are then generally greater than 10°C . Low-level off-shore flows of warm, dry continental air also produce clear areas over the ocean.

The sequence of cloud associated with frontal passages on the coast is as follows: streamers of CI increasing to OVC CS, followed by the appearance of lower BKN AC just ahead of the front; then sudden thickening and lowering at the front to OVC/BKN SC with cloud bases of less than 3 kft, more typically, less than 1 kft in ST/SC, and a period of precipitation. Because of the low cloud, the amount and type of middle and high clouds is difficult to determine, but in the clearing after the frontal band, only low-level SC is usually present.

Frequently, when supported by orographic ascent on the Coast Mountains, the frontal cloud will extend throughout the troposphere; rain will then fall for several hours and post-frontal clearing is slower, leading to BKN SC rather than SCT/CLR.

The frontal passage on the West Coast will be slow if the frontal cloud band and frontal zone lie nearly parallel to a southwesterly 700-mb flow. When the 700-mb winds are southwesterly and the surface gradient is northwesterly, the blocking by the mountains produces southerly winds, and

the surface air converges at the front.

Decks of OVC low-level cloud over the ocean are entirely blocked by the Coast Mountains: as a rule only SCT SC is reported to the lee. SCT open-cell SC/TCU forming in the cold air over the ocean will also end along the Coast Mountains, showing again the blocking effect of the mountain range.

Along the coast, cloud bands will appear much brighter when the Coast Mountains are snow-covered; the presence of orographic clouds produced in ascending onshore flow may also increase the total brightness.

Over the interior plateau of B.C., SCT/BKN cellular AC/ACC forms ahead of the cold front, the moisture and cloud usually being advected northeastward. During a frontal passage the main cloud base lowers only to about 4000 feet, although low stratus may form in areas of precipitation. The Coast Mountains effectively block the low-level cloud and act as a "sink" for any moisture moving over the barrier. Orographic ascent saturates the air, forming clouds which precipitate over the barrier --- thus reducing the moisture content of the air, as well as increasing its temperature by the release of latent heat. Descent to the lee unsaturates the air, evaporating the low-level clouds. An initially saturated cloudy layer on the windward slopes thus becomes cloud-free to the lee.

Aided by subsidence caused by NVA, the air mass along a front past the coastal range is thus usually fairly

dry. With the passage of the upper-level trough, the thickness of the orographic cloud over the Coast Mountains will usually decrease to the point where the dendritic pattern of the snow-covered mountains may be faintly seen through the cloud. Over the Cordillera, a cloud band often is transformed into an area of mid-level lee-wave clouds, with OVC conditions prevailing over the higher mountain ranges. Approximate wavelengths of the lee waves observed in Case 1 are 20 to 25 km. The cloud associated with Pacific TROWALS can sometimes not be discerned among the orographic clouds over the Cordillera.

In the warm months the cloud associated with cold lows over the interior plateau consists mostly of SCT/BKN TCU/CU with some AC, the convective cloud being caused by instability in the cold air mass produced by solar heating at the surface. The western edge of an upper cold low is frequently defined by a cyclonically-curved band of CS or high AS, while a thick overcast of NS cloud is maintained to the north and east of the low, in the region of maximum ascent. Cyclonic, comma-shaped clouds are usually associated with 500-mb troughs, to the west of the surface low center.

Strong cross-barrier flow (i.e. 50 kts at 700 mb) tends to produce a surface ridge upstream of the barrier, and a trough downstream. The low pressure is the result of heating by strong orographic subsidence at low levels, subsidence at upper levels and warm air advection (WAA) at mid-

levels, though the pressure decrease may be partly compensated by a rise caused by negative vorticity advection (NVA). At times the subsidence is so intense that a frontal cloud band will all but dissipate, perhaps to reform later over flatter terrain, where the broadening of the frontal band may indicate the location of a new or redeveloping cyclone.

With cross-barrier flow, the Coast Mountains and the Cascade Range are frequently marked by two north-to-south lines of orographic SC+AC cloud. The orographic cloud on the Coast Range will persist and the clearing after the passage of the frontal band is usually not complete. However, subsidence clearing occurs to the lee of the mountains, especially in the Columbia Basin. To the lee of the Coast Mountains, OVC orographic cloud may reform over the Pelly and Selwyn Mountains, with BKN cloud appearing in the inter-mountain valleys. When a 500-mb ridge has flattened, the NVA diminishes and the 700-mb flow will weaken and heating due to subsidence will be less.

The cloud time-sections to the lee of the Rockies show similar frontal cloud features:

(a) Daytime heating produces SCT CU/TCU by mid-afternoon. If the surface air is very dry (dew-point depressions 15 to 30°C), the cloud bases will be high. Overnight, the convective cloud becomes SCT AC/ACC with cloud bases rising to 8 kft or higher.

(b) Patches of SCT AC/ACC may be present above the

CU/TCU.

(c) Ahead of the cold front, the cloud will increase to BKN/OVC AC, with the two cloud layers merging into one layer based at about 10 kft.

(d) At the front, low-level BKN/OVC CB/TCU/SC will give rise to showers and thunderstorms, the height of the cloud base (averaging about 4 kft) depending on the moisture content of the air. The position and orientation of the upper trough determines the amount of frontal cloud and the existence of a post-frontal rain band.

(e) The cloud will then break up and become SCT/BKN CU/TCU in daytime heating, with SCT AC above 10 kft. Surface dew-point depressions will increase again to 15-20°C.

Individual stations will show differences as a result of

(a) the time of frontal passage: A passage during the early afternoon will halt the development of convective cloud;

(b) nearness to the upper trough: Stations distant from the trough may exhibit a post-frontal band of showers, while stations to the east, along the trough line, may be missed by the line of CB/TCU;

(c) moisture content of the air mass: The surface air may be too dry for convective cloud to form. On the other hand, advection of moisture aloft may lead to the formation of convective types of middle cloud;

(d) effects of the mountains: These vary a great deal from station to station and depend strongly on the local topography and wind direction.

Low-level subsidence to the lee of the Mackenzie Mountains frequently clears or prevents cloud forming along the cold front, although BKN AC may reform immediately beyond the lee clearing. If thermal advection at 700 mb and vorticity advection at 500 mb are weak, the vertical motion field will also be very weak, so that cloud formation is largely due to convective instability.

Subsidence clearing will not occur to the lee of the Mackenzie Mountains if the 700-mb wind speeds are less than 20 kts, and the easterly surface flow produces orographic clouds.

To the lee of the Rocky Mountains, a narrow clear zone caused by subsidence in the westerly flow at 700 mb (and frictional divergence in the northwesterly low-level flow) is usually followed by a band of SCT/BKN AC/ACC+CI with streamers of AC downwind.

With low-level easterly circulations, orographic ascent over the plains intensifies along the east slope of the Rocky Mountains, broadening any cloud bands and giving up-slope precipitation over the barrier, while at the same time CI plumes may be carried eastward in the westerly flow at high levels. A surface ridge and trough may be present across the barrier but, because of the easterly flow, their

locations would be reversed from the usual order in that the ridge would now be on the eastern slopes. The westward advection of low-level moisture may extend the cloud band as far west as the coastal mountains.

Cloud vortices do not normally coincide with the position of the surface low center. The cloud spirals are formed by advection of middle cloud, and the 700-mb center of the spiral lags behind the surface low.

Small dew-point depressions at 700 mb indicate middle cloud. If the cloud is very thin, it may not appear on the APT images. Only the thicker, more reflective cloud will show up readily against the background of the dark ocean surface. Over land, SCT CU reported by surface stations cannot be detected on the satellite mosaic when the cloud elements are small and thin, and the area will thus appear CLR.

The dendritic pattern of the Coast, Rocky, and Cassiar Mountains is usually observable in the CLR area underneath the upper ridge. Ridge intensification may be caused by the advection of a warm and fairly dry mT air mass to the north of the ridge across northern B.C.

Change in cloud brightness, i.e. thickness, may reflect the change in surface pressure pattern when the high-pressure center and surface ridge are behind front rather than ahead. In such a situation the surface flow ahead of the front would be northwesterly rather than south to southwesterly, and the flow of potentially unstable air

from the south would have ceased.

BKN CU/TCU is often found downwind of a 500-mb trough line. Such troughs correspond to the maximum depth of the cold air mass or, alternatively, to the leading edge of a warm front in the upper levels of the troposphere. The cloud in the cold air mass (over land in summer) is formed by convective instability from solar heating of the moist air at the surface and by PVA ahead of the trough.

Satellite images are invaluable in correctly positioning fronts, occlusions, TROWALS, squall lines, vortex centers, trough lines, and comma clouds, especially over data-sparse areas such as the Pacific Ocean and the Arctic, where map analysis based on surface observations alone are frequently in error. The images show cloud on the sub-synoptic scale at a much greater resolution than synoptic data (typically 10 times greater for APT and 100 times for VHRR). Thus, cloud organization on the photograph --- mountain waves, bands, shields, and convective cellular patterns --- can be observed which is often not obvious from surface observations. Cloud-top height can be estimated using IR data; cloud "thickness", from the VIS image. Since clouds are observed from above, the images are also useful in determining cloud above OVC ST/SC or AS layers. In reverse, surface observations must be used for lower clouds underneath OVC AS or CS. The images must be used in conjunction with other available data and charts.

REFERENCES

- Austin, Pauline M., and R.A. Houze, Jr., 1972: Analysis of the structure of precipitation patterns in New England. J. Appl. Meteor., 11(6), 926-935.
- Barr, S., M.B. Lawrence, and F. Sanders, 1966: Tiros vortices and large scale vertical motion. Mon. Wea. Rev., 94(12), 675-696.
- Barrett, E.C., 1974: Climatology from Satellites. London, Methuen & Co Ltd, 418 pp.
- Beran, D.W., 1967: Large amplitude lee waves and chinook winds. J. Appl. Meteor., 6(5), 865-877.
- Bonner, W.D., 1965: A program for computer gridding of satellite photographs for mesoscale research. SRMP Research Paper No. 43, University of Chicago, 31 pp.
- _____, 1969: Gridding scheme for APT satellite pictures. J. Geophys. Res., 74(18), 4581-4587.
- Broderick, H.J., and E.P. McClain, 1969: Synoptic/dynamic diagnosis of a developing low-level cyclone and its satellite-viewed cloud patterns. ESSA Technical Report NESG 49, U.S. Dept. of Commerce, 26 pp.
- Charney, J.G., and A. Eliassen, 1949: A numerical method for predicting the perturbations of the middle latitude westerlies. Tellus, 1(2), 38-54.

Chung, Yong-Seung, 1972: Cyclogenesis in the lee of the Canadian Rocky Mountains. M.Sc. thesis, Dept. of Geography, University of Alberta, 156 pp.

Conover, J.H., 1964: The significance of orographically induced clouds observed by TIROS satellites. J. Appl. Meteor., 3(3), 226-234.

_____, W.S. Lanterman, and V.J. Schaefer, 1969: Major cloud systems. World Survey of Climatology Volume 4: Climate of the Free Atmosphere, Edited by D.F. Rex, Amsterdam and New York, Elsevier Publishing Co., 205-246.

Corby, G.C., 1954: The airflow over mountains; a review of the state of current knowledge. Quart. J. Roy. Meteor. Soc., 80(346), 491-521.

_____, 1957: Preliminary study of atmospheric waves using radiosonde data. Quart. J. Roy. Meteor. Soc., 83(355), 49-60.

_____, and J.S. Sawyer, 1958: The air flow over a ridge -- the effects of the upper boundary and high level conditions. Quart. J. Roy. Meteor. Soc., 84(359), 25-37.

Danielsen, E.F., and R. Bleck, 1970: Tropospheric and stratospheric ducting of stationary mountain lee waves. J. Atmos. Sci., 27(5), 758-772.

DeMandel, R.E., and J.R. Scoggins, 1967: Mesoscale wave motions as revealed by improved wind profile measurements. J. Appl. Meteor., 6(4), 617-620.

Döös, B.R. 1962: The influence of exchange of sensible heat with the earth's surface on the planetary flow. Tellus, 14(2), 133-147.

Elliot, R.D., and E.L. Hovind, 1964: On convection bands within Pacific coast storms and their relation to storm structure. J. Appl. Meteor., 3(2), 143-154.

- Egger, J., 1974: Numerical experiments on lee cyclogenesis. Mon. Wea. Rev., 102(12), 847-860.
- Endlich, R.M., and R.C. Singleton, 1969: Spectral analysis of detailed vertical wind speed profiles. J. Atmos. Sci., 26(5, part 2), 1030-1041.
- Frenzen, P., 1955: Westerly flow past an obstacle in a rotating hemispherical shell. Bull. Am. Meteor. Soc., 36(5), 204-210.
- Fritz, S., 1965: The significance of mountain lee waves as seen from satellite pictures. J. Appl. Meteor., 4(1), 31-37.
- Glahn, H.R., and G.W. Hollenbaugh, 1969: An operationally oriented small-scale 500-millibar height analysis program. ESSA Technical Memorandum WBTM TDL 19, U.S. Dept. of Commerce, 18 pp.
- Hage, K.D., 1961: On summer cyclogenesis in the lee of the Rocky Mountains. Bull. Am. Meteor. Soc., 42(1), 20-33.
- Haltiner, G.J., 1971: Numerical Weather Prediction. New York & Toronto, John Wiley & Sons, Inc., 317 pp.
- Hayden, C.M., 1968: The utility of satellite cloud photographs in the objective analysis of the 500-mb height field. Final Report, Contract CWB-11377, University of Michigan, College of Engineering, 147 pp.
- Hess, S.L., 1959: Introduction to Theoretical Meteorology. New York, Holt, Rinehart and Winston, 362 pp.
- Hobbs, P.V., R.A. Houze, Jr. and T.J. Matejka, 1973: Air motions and cloud structure in a frontal system in the Pacific Northwest. Conference on Cloud Physics of the Am. Meteor. Soc. October 21-24, 1974, Tucson, Arizona, 418-423.

- _____, _____, and _____, 1974: The dynamical and microphysical structure of an occluded front and its modification by orography. Res. Rept. 9, Cloud Physics Group, University of Washington, 119 pp.
- Hume, W.D., 1975: Development of a quasi-geostrophic prediction model for weather systems over Western Canada. M.Sc. thesis, Dept. of Geography, Univ. of Alberta, 123 pp.
- Kasahara, A., 1966: The dynamical influence of orography on the large-scale motion of the atmosphere. J. Atmos. Sci., 23(3), 259-271.
- _____, and W.M. Washington, 1969: Thermal and dynamical effects on the general circulation of the atmosphere. Proc. Symp. Numerical Weather Prediction, Tokyo, 1968. Tech. Rept. No. 67, Japan Meteor. Agency, IV-47 to IV-56.
- Kaveney, W.J., R.G. Feddes, and Kuo-Nan Liou, 1977: Statistical inference of cloud thickness from NOAA 4 scanning radiometer data. Mon. Wea. Rev., 105(1), 99-107.
- Khandekar, M.L., 1972: A numerical study of the influence of orography on synoptic-scale atmospheric motion. Presented at the Sixth Annual Congress of the Canadian Meteorological Society, May 31 to June 2, 1972, Edmonton, 15 pp.
- Lahey, J.F., R.A. Bryson, E.W. Wahl, L.H. Horn, and V.D. Henderson, 1958: Atlas of 500mb Wind Characteristics for the Northern Hemisphere. Madison, The University of Wisconsin Press.
- Lamb, D., K.W. Nielsen, and J. Hallett, 1974: Aircraft investigations of winter orographic cloud systems over the Sierra Nevada. Conference on Cloud Physics of the Am. Meteor. Soc. October 21-24, 1974, Tucson, Arizona, 333-338.

- _____, _____, H.E. Klieforth, and J. Hallett, 1976:
Measurements of liquid water content in winter cloud
systems over the Sierra Nevada. J. Appl. Meteor., 15(7),
763-775.
- Landers, H., 1956: Vorticity distribution and advection in
the lower and middle troposphere. J. Meteor., 13(6),
511-520.
- Lesse, J.A., 1962a: The role of advection in the formation of
vortex cloud patterns. Tellus, 14(4), 409-421.
- _____, 1962b: The role of advection in the formation of
vortex cloud patterns. GRD Research Notes No. 78
(AFCRL-62-286), Air Force Cambridge Research
Laboratories, Bedford, Massachusetts, 47 pp.
- Lester, P.F., 1976: Evidence of long lee waves in southern
Alberta. Atmosphere, 14(1), 28-35.
- Long, R.R., 1955: Some aspects of the flow of stratified
fluids. III. Continuous density gradients. Tellus, 7(3),
341-357.
- _____, 1970: Blocking effects in flow over obstacles. Tellus,
22(5), 471-480.
- Ludlam, F.H., 1952: Orographic cirrus clouds. Quart. J. Roy.
Meteor. Soc., 78(338), 554-562.
- Madden, R., and C. Parsons, 1973: A technique for real-time,
quantitative display of APT scanning radiometer data. J.
Appl. Meteor., 12(2), 381-385.
- Manabe, S., and T.B. Terpstra, 1974: The effects of
mountains on the general circulation of the atmosphere
as identified by numerical experiments. J. Atmos. Sci.,
31(1), 3-42.

- McClain, E.P., 1960: Some effects of the western cordillera of North America on cyclonic activity. J. Meteor., 17(2), 104-115.
- _____, Mary A. Ruzecki, and H.J. Broderick, 1965: Experimental use of satellite pictures in numerical prediction. Mon. Wea. Rev., 93(7), 445-452.
- Miller, D.B., and R.G. Feddes, 1971: Global atlas of relative cloud cover 1967-70 based on data from meteorological satellites. National Environmental Satellite Service, National Oceanic and Atmospheric Administration, U.S. Department of Commerce and Air Weather Service (MAC), United States Air Force.
- Morris, R.M., 1971: A case study of the spectacular developments and movement of a February storm. Meteor. Mag., 100(1182), 14-27.
- Nagle, R.E., and S.M. Serebreny, 1962: Radar precipitation echo and satellite cloud observations of a maritime cyclone. J. Appl. Meteor., 1(3), 279-295.
- _____, J.R. Clark, and M.M. Holl, 1966: Tests of the diagnostic-cycle routine in the interpretation of layer-cloud evolution. Mon. Wea. Rev., 94(2), 55-66.
- _____, and C.M. Hayden, 1971: The use of satellite-observed cloud patterns in northern hemisphere 500-mb numerical analysis. NOAA Technical Report NESS 55, U.S. Dept. of Commerce, 47 pp.
- Namias, J., and P.F. Clapp, 1949: Confluence theory of the high-tropospheric jet stream. J. Meteor., 6(5), 330-336.
- NESC (National Environmental Satellite Center), 1969a: ESSA Direct Users Transmission System Users Guide. Environmental Science Services Administration, U.S. Dept. of Commerce, Washington, D.C., 148 pp.

- _____, 1969b: Application of meteorological satellite data in analysis and forecasting. ESSA Technical Report NES-51 (with Supplement No. 1, Chapter 6, Infrared, 1971), National Oceanic and Atmospheric Administration, U.S. Dept. of Commerce, Authored by R.K. Anderson and A.H. Smith, 260 pp.
- Newton, C.W., 1956: Mechanisms of circulation change during a lee cyclogenesis. J. Meteor., 13(6), 528-539.
- Palm, E., and A. Foldvik, 1959: Contribution to the theory of two-dimensional mountain waves. Geoph. Publ., 21, No. 6, Oslo, Norske Videnskaps Akad., 30 pp.
- Panofsky, H.A., 1946: Methods of computing vertical motions in the atmosphere. J. Meteor., 3(2), 45-49.
- Park, S.U., D.N. Sidkar, and V.E. Suomi, 1974: Correlation between cloud thickness and brightness using Nimbus 4 THIR (11.5 channel) and ATS 3 digital data. J. Appl. Meteor., 13(3), 402-410.
- Petterssen, S., 1955: A general survey of factors influencing development at sea level. J. Meteor., 12(1), 36-42.
- _____, 1956: Weather Analysis and Forecasting (2nd ed.), Volume I. New York, McGraw-Hill, 428 pp.
- _____, and S.J. Smebye, 1971: On the development of extratropical cyclones. Quart. J. Roy. Meteor. Soc., 97(414), 457-482.
- Queney, P., 1947: Theory of perturbations in stratified currents with application to airflow over mountain barriers. Misc. Rep. No. 23, Dept. of Meteorology, University of Chicago.
- Reinelt, E.R., 1970: On the role of orography in the precipitation regime of Alberta. The Albertan Geographer, 6, 45-58.

- _____, P. Hof, D. Oracheski, and J. Broszkowski, 1975: Research studies of numerical enhancement of APT scanning radiometer data for application to arctic weather and ice prediction. Final Report, DDS (AES) Contract OSV4-0183, Univ. of Alberta, 116-145.
- Rogers, C.W., and P.E. Sherr, 1966: Toward the dynamical interpretation of satellite-observed extratropical vortical cloud patterns. Final report, Contract No. Cwb-11123, ARACON Geophysics Division, Allied Research Associates, Inc., 125 pp.
- _____, and _____, 1967: A study of dynamical relationships between cloud patterns and extratropical cyclogenesis. Final Report, Contract No. E-47-67(N), Allied Research Associates, Inc., 74 pp.
- Ruff, I., R. Koffler, S. Fritz, J.S. Winston, and P.K. Rao, 1968: Angular distribution of solar radiation reflected from clouds as determined from TIROS IV radiometer measurements. J. Atmos. Sci., 25(2), 323-332.
- Sankar-Rao, M., and B. Saltzman, 1969: On a steady-state theory of global monsoons. Tellus, 21(3), 308-330.
- Sawyer, J.S., 1960: Numerical calculation of the displacements of a stratified airstream crossing a ridge of small height. Quart. J. Roy. Meteor. Soc., 86(369), 326-345.
- Schallert, W.L., 1962: An investigation of Colorado cyclones. Sci. Report No. 7, Contract No. AF 19(604)-7230, Univ. of Chicago, 68 pp.
- Schram, G.R., 1974: The influence of orography and surface friction on synoptic scale vertical motions over Western Canada. M.Sc. thesis, Dept. of Geography, Univ. of Alberta, 83 pp.
- Schwalb, A., 1972: Modified version of the improved TIROS operational satellite (ITOS D-G). NOAA Technical Memorandum NESS 35, National Environmental Satellite Service, National Oceanic and Atmospheric Administration, U.S. Dept. of Commerce, Washington, D.C., 48 pp.

- Scoggins, J.R., 1967: Sphere behavior and measurement of wind profiles. NASA Technical Note D-3994, U.S. National Aeronautics and Space Administration, 53 pp.
- Scorer, R.S., 1949: Theory of waves in the lee of mountains. Quart. J. Roy. Meteor. Soc., 75(323), 41-56.
- _____, and H. Klieforth, 1959: Theory of mountain waves of large amplitude. Quart. J. Roy. Meteor. Soc., 85(364), 131-143.
- Shenk, W.E., and V.V. Solomonson, 1972: A simulation study exploring the effects of sensor spacial resolution on estimates of cloud cover from satellites. J. Appl. Meteor., 11(1), 214-220.
- Srinivasan, V., 1970: Errors in the operational gridding of APT pictures. Indian J. of Meteor. and Geophys., 21(4), 643-646.
- Stephens, G.L., 1976: An improved estimate of the IR cooling in the atmospheric window region. J. Atmos. Sci., 33(5), 806-809.
- Timchalk, A., and L.F. Hubert, 1961: Satellite pictures and meteorological analysis of a developing low in central United States. Mon. Wea. Rev., 89(11), 429-445.
- Vergeiner, I., 1971: An operational linear lee wave model for arbitrary basic flow and two dimensional topography. Quart. J. Roy. Meteor. Soc., 97(411), 30-60.
- _____, and Y. Ogura, 1972: A numerical shallow-fluid model including orography with a variable grid. J. Atmos. Sci., 29(2), 270-284.
- Wallington, C.E., and Janet Portnall, 1958: A numerical study of the wavelength and amplitudes of lee waves. Quart. J. Roy. Meteor. Soc., 84(359), 38-45.

Widger, W.K., Jr., 1964: A synthesis of interpretations of extratropical vortex patterns as seen by TIROS. Mon. Wea. Rev., 92(6), 263-282.

_____, 1966: Orbits, altitudes, viewing geometry, coverage, and resolution pertinent to satellite observations of the earth and its atmosphere. Proceedings of the Fourth Symposium on Remote Sensing of Environment 12, 13, 14 April 1966, University of Michigan, Ann Arbor, Michigan, Revised Edition, December 1966, 489-537.

Wiin-Nielsen, A., 1959: On a graphical method for an approximate determination of the vertical velocity in the mid-troposphere. Tellus, 11(4), 432-440.

Wilson, H.P., 1974: A note on meso-scale barriers to surface flow. Atmosphere, 12(3), 118-120.

WMO, 1960: The airflow over mountains. WMO, Technical Note, No. 34, (WMO-No. TP.43), Edited by M.A. Alaka. Geneva, World Meteorological Organization, 135 pp.

WMO, 1966: The use of satellite pictures in weather analysis and forecasting. WMO, Technical Note, No. 75, (WMO-No. 190.TP.96), Compiled by R.K. Anderson, E.W. Ferguson, and V.J. Oliver, 184 pp.

WMO, 1973a: The use of satellite pictures in weather analysis and forecasting. WMO, Technical Note, No. 124, (WMO-No. 333), Edited by R.K. Anderson and N.F. Veltishchev, 275 pp.

WMO, 1973b: The airflow over mountains -- research 1958-1972. WMO, Technical Note, No. 127, (WMO-No. 355), Compiled by J.M. Nicholls, 73 pp.

Young, M.J., 1967: Variability in estimating total cloud cover from satellite pictures. J. Appl. Meteor., 6(3), 573-579.

APPENDIX 1

LIST OF SYMBOLS

c_p	specific heat at constant pressure = $1004 \text{ J} \cdot \text{kg}^{-1} \cdot \text{K}^{-1}$ (dry air)
D	horizontal divergence [s^{-1}]
F	Froude number (equation A.15)
f	Coriolis parameter = $2 \Omega \sin \phi$ [s^{-1}]
g	acceleration of gravity = $9.806 \text{ m} \cdot \text{s}^{-2}$
$k^2(z)$	Scorer parameter (see equation A.10)
L	latent heat of vaporization = $2.5 \cdot 10^6 \text{ J} \cdot \text{kg}^{-1}$ (water at 0°C)
N	Brunt-Vaisala frequency = $\left(\frac{g}{\theta} \frac{\partial \theta}{\partial z}\right)^{1/2}$ [s^{-1}]
p	pressure [mb, 1 mb = 0.1 kPa]
q	relative vorticity [s^{-1}]
Q	absolute vorticity = $f + q$ (equation B.9) [s^{-1}]
r	mixing ratio of water vapor [gm water/kgm dry air]
R	gas constant = $287.04 \text{ J} \cdot \text{kg}^{-1} \cdot \text{K}^{-1}$ (dry air)
R_E	radius of the Earth = 6371 km (mean value)
T	temperature [$^\circ\text{C}$ or K]
V	wind speed [$\text{m} \cdot \text{s}^{-1}$]
\vec{V}	wind velocity = $u \hat{i} + v \hat{j} + w \hat{k}$ [$\text{m} \cdot \text{s}^{-1}$] = $u \hat{i} + v \hat{j} + \omega \hat{p}$
z	height above sea level of a constant pressure surface [m]
$\hat{i}, \hat{j}, \hat{k}, \hat{p}$	unit vectors along coordinate axes in the x, y, z , and pressure directions, respectively

α specific volume = ρ^{-1} [$\text{m}^3 \cdot \text{kg}^{-1}$]

β Rossby parameter = $(2\Omega \cos \phi) / R_E$

γ = c_p / c_v = 1.40 (dry air)

Γ lapse rate = dT/dp (in pressure coordinates)
= $-dT/dz$ [$^{\circ}\text{C} \cdot \text{km}^{-1}$]

Γ_a adiabatic lapse rate
= $\Gamma_d - \frac{L}{c_p} \frac{dr}{dp}$ (in pressure coordinates)

Γ_d dry adiabatic lapse rate
= g/c_p = $9.76^{\circ}\text{C} \cdot \text{km}^{-1}$

θ potential temperature [K]

θ_e equivalent potential temperature (equation D.2) [K]

κ = R/c_p = $(c_p - c_v)/c_p$ = 0.286 (dry air)

ρ density of air [$\text{kg} \cdot \text{m}^{-3}$]

σ_s stability parameter (see equation B.12)

ϕ latitude

ω dp/dt , vertical motion in pressure coordinates
[$\mu\text{b} \cdot \text{s}^{-1}$]

ω_T vertical motion due to thermal advection

ω_v vertical motion due to vorticity advection

Ω angular velocity of Earth's rotation
= $7.292 \cdot 10^{-5} \text{ rad} \cdot \text{s}^{-1}$

∇ = ∇_3 = $\hat{i} \frac{\partial}{\partial x} + \hat{j} \frac{\partial}{\partial y} + \hat{k} \frac{\partial}{\partial z}$
= $\hat{i} \frac{\partial}{\partial x} + \hat{j} \frac{\partial}{\partial y} + \hat{p} \frac{\partial}{\partial p}$ (in pressure coordinates)

∇_2 = $\hat{i} \frac{\partial}{\partial x} + \hat{j} \frac{\partial}{\partial y}$

$$\nabla_p = \hat{i} \left(\frac{\partial}{\partial x} \right)_p + \hat{j} \left(\frac{\partial}{\partial y} \right)_p$$

Subscripts

g	geostrophic
p	on constant pressure surface
s	at Earth's surface
1000	1000-mb surface

APPENDIX 2







LIST OF ABBREVIATIONS

PVA	positive vorticity advection
NVA	negative vorticity advection
CAA	cold air advection
WAA	warm air advection
kts	knots, nautical miles per hour (1 kt = 0.51 m·s ⁻¹)
nmi	nautical mile (1 nmi = 1.852 km)
kft	thousand feet (1 kft = 0.30480 km)
mT	maritime tropical (air mass)








Cloud Amount

CLR	clear, less than 2/10 cloud
SCT	scattered cloud, 2/10 to 5/10
BKN	broken cloud, 6/10 to 9/10
OVC	overcast, \geq 9/10



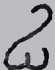
Low Cloud and Symbol

SC		stratocumulus
ST		stratus
SF		stratus-fractus
CU		cumulus
TCU		towering cumulus
CB		cumulonimbus

Middle Cloud and Symbol

AC		(thick) altocumulus
		(thin)
		(banded)
		(patchy)
ACC		altocumulus castellanus
AS		altostratus
NS		nimbostratus (thick altostratus)

High Cloud and Symbol

CI		cirrus
CS		cirrostratus
CC		cirrocumulus

B30203